EXPERIMENTAL STUDIES ON FIBER-MESH REINFORCED
ELASTOMERIC BEARINGS

A THESIS SUBMITTED TO
THE GRADUATE SCHOOL OF NATURAL AND APPLIED SCIENCES
OF
MIDDLE EAST TECHNICAL UNIVERSITY

BY

ALI KARIMZADEH NAGHSHINEH

IN PARTIAL FULFILLMENT OF THE REQUIREMENTS
FOR
THE DEGREE OF DOCTOR OF PHILOSOPHY
IN
CIVIL ENGINEERING

DECEMBER 2013

Approval of the thesis:

**EXPERIMENTAL STUDIES ON FIBER-MESH REINFORCED
ELASTOMERIC BEARINGS**

submitted by **ALI KARIMZADEH NAGHSHINEH** in partial fulfillment of the requirement for the degree of **Doctor of Philosophy in Civil Engineering Department, Middle East Technical University** by,

Prof. Dr. Canan Özgen   _____
Dean, Graduate School of **Natural and Applied Sciences**

Prof. Dr. Ahmet Cevdet Yalçınar   _____
Head of Department, **Civil Engineering**

Prof. Dr. Uğurhan Akyüz   _____
Supervisor, **Civil Engineering Dept., METU**

Examining Committee Members:

Prof. Dr. Murat Dicleli   _____
Engineering Science Dept., METU

Prof. Dr. Uğurhan Akyüz   _____
Civil Engineering Dept., METU

Assoc. Prof. Dr. Seval Pınarbaşı   _____
Civil Engineering Dept., Kocaeli University

Assoc. Prof. Dr. Alp Caner   _____
Civil Engineering Dept., METU

Prof. Dr. Ahmet Yakut   _____
Civil Engineering Dept., METU

                             Date   _____

I hereby declare that all information in this document has been obtained and presented in accordance with academic rules and ethical conduct. I also declare that, as required by these rules and conduct, I have fully cited and referenced all material and results that are not original to this work.

Name, Last Name: Ali Karimzadeh Naghshineh

Signature:

ABSTRACT

EXPERIMENTAL STUDIES ON FIBER MESH REINFORCED ELASTOMERIC BEARINGS

Karimzadeh Naghshineh, Ali

Ph.D., Department of Civil Engıneering

Supervisor: Prof. Dr. Uğurhan Akyüz

December 2013, 191 pages

New types of fiber reinforced rubber based bearings have been a research interest for a number of engineers in the past decade. These new type of bearings can have similar performance compared to the conventional ones. In most of the previous researches, the fiber reinforced rubber based bearings are usually manufactured with placing fiber sheets between pre-cut rubber layers with use of a bonding agent. This research differs from the previous researches in terms of manufacturing process and use of fiber mesh instead of fiber sheets. The aim of this research is to compare the fundamental response characteristics of fiber mesh reinforced elastomeric bearings and conventional steel reinforced bearings. In this scope, ten pairs of fiber mesh reinforced elastomeric bearings and ten pairs of steel reinforced elastomeric bearings were subjected to various levels of compression and cyclic shear strains under constant vertical pressure. The tested types of bearings are fiber mesh reinforced elastomeric bearings and steel reinforced elastomeric bearings. There is not any analytical study which considers the effect of fiber flexural flexibility on horizontal

stiffness of bearings. In this study, the results of horizontal shear tests were used to study the effect of fiber flexibility on horizontal stiffness of bearings. Furthermore results of compression test were used to evaluate the effect of fiber flexibility on vertical stiffness of bearings. Stress distributions in the bearings were studied by modeling two of the bearings in commercial finite element software called ABAQUS. Results of pressure solution were used to study the performance of bearings in vertical direction and compare them with the results of finite element study and experimental tests. To evaluate the performance of bearings in low temperature, some of the specimens were also subjected to low temperature shear test. The major advantage for fiber mesh reinforced bearings observed during the tests was that these bearings developed a considerable low horizontal stiffness compared to the conventional steel reinforced bearings. It is also observed that damping characteristics of the new and conventional types were similar to each other.

Keywords: bearing, steel reinforced bearing, fiber reinforced bearing, pressure solution

ÖZ

FİBER TAKVİYELİ ELASTOMER MESNETLER ÜZERİNE DENEYSEL ÇALIŞMALAR

Karimzadeh Naghshineh, Ali

Doktora, İnşaat Mühendisliği Bölümü

Tez Yöneticisi: Prof. Dr. Uğurhan Akyüz

Aralık 2013, 191 sayfa

Yeni tip elyaf takviyeli kauçuk yastıklar, son yıllarda birçok mühendis için ilgi çekici bir araştırma konusu olmuştur. Bu yeni tip yastıkların performansları geleneksel çelik plakalılara benzer olabilir. Önceki araştırmaların çoğunda, fiber takviyeli kauçuk esaslı yastıklar yapıştırıcı yardımıyla önceden kesilmiş lastik tabakalar arasına yerleştilerek üretilmiştir. Bu araştırma; gerek üretim ve gerekse elyaf levhalar yerine fiber ağı kullanımı ile daha önceki araştırmalardan farklıdır. Bu araştırmanın amacı, yeni tip fiber ağ takviyeli mesnetler ile geleneksel mesnetlerin özelliklerini karşılaştırmaktır. Bu kapsamda, on çift fiber takviyeli ve on çift çelik takviyeli elastomer mesnet, çeşitli düşey basınç seviyelerinde sabit basınç altında tersinir kayma yer değiştirmesine maruz bırakılmıştır. Deneylerde kullanılan mesnet tipleri ise; fiber takviyeli ve çelik takviyeli olarak belirlenmiştir. Lif esnekliğinin mesnetlerin yatay rijitliğine etkisini dikkate alan herhangi bir analitik çalışma bulunmamaktadır. Bu çalışmada yatay kesme test sonuçları kullanılarak, lif

esnekliğinin mesnetlerin yatay rijitliği üzerindeki etkisi incelenmiştir. Ayrıca, basınç test sonuçları, lif esnekliğinin mesnetlerin düşey rijitliği üzerindeki etkisini değerlendirmek için kullanılmıştır. Mesnetlerdeki gerilme dağılımı; ABAQUS ticari yazılımı yardımıyla oluşturulan sonlu elemanlar modeliyle incelenmiştir. Sonlu elemanlar analizlerinin, deneysel sonuçlarla karşılaştırılmasıyla mesnetlerin düşey yöndeki performansı incelenmiştir. Ayrıca, mesnetlerin düşük sıcaklıktaki performanslarını değerlendirmek amacıyla, bazı numuneler kesme testine tabi tutulmuştur. Gerçekleştirilen deneyler neticesinde; fiber takviyeli mesnetlerin diğer mesnet tiplerine göre daha düşük yatay rijitliğe sahip olduğu gözlemlenmiştir. Yeni ve geleneksel tiplerin sönümleme özelliklerinin birbirine benzer olduğu gözlenmiştir.

Anahtar Kelimeler: mesnet, çelik takviyeli mesnet, elyaf takviyeli mesnet

To my family and my wife …..

ACKNOWLEDGEMENTS

TABLE OF CONTENTS

LIST OF TABLES

LIST OF FIGURES

FIGURES

CHAPTER 1

INTRODUCTION

1.1 Base Isolation

Design and use of base isolation systems to protect the structures from devastating effects of earthquakes have been increased rapidly within the past few years. Advantages of base isolation systems in seismic prone areas have been proven within the past earthquakes. As a result, this relatively new design methodology has been incorporated in many structures which also prove their reliability. Rubber bearings are the most commonly used seismic isolation systems and due to their effectiveness designers use them in most of their projects.

It is seen that conventionally constructed buildings with seismic protection have been crumbled under the tremendous destructive strength of earthquake in many parts of the world. Conventional design approach to earthquake resistance design of buildings has found to be followed all over world. This conventional design method mostly depends upon providing building with strength, stiffness and inelastic deformation capacity which are great enough to withstand a given level of earthquake-generated force. This is generally accomplished through selection of an appropriate structural configuration and careful detailing of structural members, such as beams, columns and shear walls, and connections between them. As an alternative to this method, seismic base isolation can be used to save human lives.

In general buildings with foundation fixed to the super structure are known as fixed base, and buildings with isolation between the base foundation and structure are known as base isolated buildings. The philosophy of base isolation is to separate the structure and base of the building and also isolate the structure and its movements from foundation. Variety of different types of base isolation bearings has been developed. A base isolated structure is supported by a series of bearings, which are usually placed between the foundation and superstructure.

These rubber based bearings are manufactured by vulcanization; elastomers used are either natural rubber or neoprene. Conventional elastomeric bearings consist of alternating thin layers of rubber and steel which provide orthotropic properties, where the rubber layers achieve the desired low horizontal stiffness while reinforcing steel plates maintain a relatively high level of vertical stiffness necessary to support structure. These bearings are very stiff in vertical direction and very flexible in horizontal direction. Under seismic loading, bearing layers isolate building from the horizontal components of ground movements, while the vertical component transmitted to the structure remains relatively unchanged. Although vertical accelerations do not affect the buildings, the bearings also isolate building from unwanted high-frequency vertical vibrations produced by underground railways and local traffic [1].

Rubber based isolation gives structure a fundamental frequency that is much lower than its fixed-base frequency and also much lower than predominant frequencies of ground motion. The first dynamic mode of isolated structure involves deformation only in isolation system and structure above remains rigid. The higher modes that produce deformation in the structure are orthogonal to the first mode and consequently to the ground motion. These higher modes do not participate in motion, so that if there is high energy due to ground motion at these higher frequencies, this energy will not be transmitted into structure [1]. Figure 1.1 depicts a schematic view of a structure with a base isolation system. Note that during an earthquake event, the ground moves while the superstructure remains rigid [2].
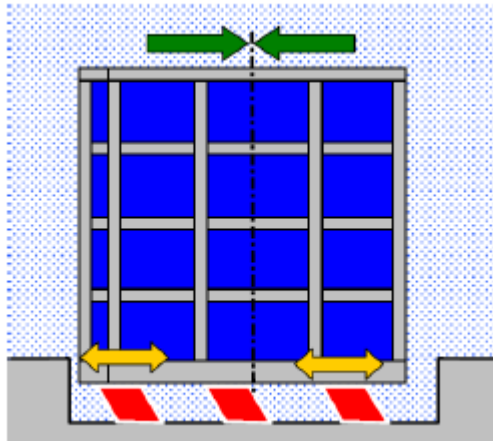
Figure 1.1 First Dynamic Mode of Structure: Horizontal Deformation of Isolation System and Superstructure Remains Rigid [3]

1.2 History of Base Isolation

Dating back to 1876 and continuing through 1895, John Milne, a mining engineer and a professor at the University of Tokyo, conducted significant seismological research and was the first to propose an isolation technique. His structure was supported by 6.35 millimeter diameter balls in cast-iron plates with saucer-like edges on the heads of piles. Above the balls and attached to the building were slightly concave, cast-iron plates [4].

In 1909 Dr. Johannes A. Calantarients, a physician from Scarborough, England proposed the isolation of a building from its foundation by means of a layer of fine sand, mica, or talc that would allow the building to slide during an earthquake, ultimately reducing seismic forces acting upon the structure [4].

In 1921, the Imperial Hotel in Tokyo was built utilizing a design developed by Frank Lloyd Wright. This structure was built on top of hard soil strata of about 2.4 meter in depth. The hard soil strata was located above a layer of soft mud, for which Wrights' reasoning was "…a good cushion to relieve the terrible shocks. Why not float the building above it?" In this fashion, the building was designed to be

supported by several closely spaced short piles that would penetrate only the hard soil strata, allowing the building to float on the soft mud sub-strata. The Imperial Hotel successfully resisted the devastating earthquake of 1923 in Tokyo. It was unfortunately demolished in the 1960's due to the degradation of building materials and economic concerns [5].

In 1959 in the city of Ashkhabad, Turkmenistan, a building was constructed supported by suspending it by cables. The system was designed to allow the structure to mimic a pendulum under the action of ground motion [6].

In 1969 rubber was utilized in base isolation systems for the first time. This particular system was designed and built by a Swiss engineer and was used to isolate the Pestalozzi Elementary School in Skopje, Yugoslavia. The superstructure of the three story building was made of concrete and was designed to rest on large unreinforced blocks of natural rubber positioned between the foundation and superstructure. The lack of reinforcement on the rubber blocks was the cause of large lateral bulging. In addition, the lack of reinforcement in the rubber blocks resulted in the back-and-forth bouncing of the structure [2].

The concept of using steel laminated rubber bearings also referred to as elastomeric bearings, used to isolate buildings, began in England in the 1960's, after decades of experience in applying this technique to bridge bearings (Kuntz and Tanner, 1999). In 1967, Ivan Skinner and his associates conducted extensive research on base isolation devices at the Physics and Engineering Laboratory of the Department of Scientific and Industrial Research (PEL, DSIR) in New Zealand, which contributed significantly to the study and development of base isolators and the seismic control systems that exist today [7].

The first building in the United States utilizing a base isolation system was the Foothill Communities Law and Justice Center (FCLJC), completed in 1985. The building is four stories high with a base isolation system that consists of 98 elastomeric bearings (Kelly 1998). Although the completion of FCLJC project

4

clearly demonstrated the reliability and economic feasibility of the use of base isolation systems for buildings, there was not an immediate continuation of isolation projects, due largely in part to the lack of official building code provisions governing the design of isolated structures [8].

Base isolation technology continues to advance along with other techniques to prevent seismic damage to structures.

The focus of the present study is to manufacture and analyze the performance parameters of fiber reinforced bearings and compare them with conventional steel reinforced ones. In this study performance parameters of elastomeric bearings, such as vertical and horizontal stiffness, and energy dissipation capacity were studied.

1.3 Current Practice in Base Isolation

The basic approach underlying advanced techniques for earthquake resistance is not to strengthen building, but to reduce the earthquake-generated forces acting upon it by choosing the right and appropriate base isolation system. Today, there are two main types of passive base isolation system: elastomeric bearings and sliding systems.

Sliding systems work by limiting the transfer of shear across the isolation interface through sliding and friction. Many sliding systems have been proposed and some have been used. The friction-pendulum system is a sliding system using a special interfacial material sliding on stainless steel and has been used for several projects in the United States, both new and retrofit construction.

Another type of isolation systems is elastomeric bearings. Elastomeric bearings have several benefits; one major benefit is that the vertical stiffness of the bearing can be sufficiently high, while its horizontal stiffness can be much lower. Elastomeric bearings have inherent restorative forces to replace the structure to its original position after the effect of an earthquake. Elastomeric bearings also have an inherent damping property that can be quite beneficial during an earthquake.

As discussed previously, elastomeric bearings that are not reinforced can cause the building to bounce and rock back and forth. Because of this, an effective system has been incorporated to increase the vertical stiffness of the bearing while keeping the horizontal stiffness low. Reinforcement is usually done by means of steel shim plates between the individual layers of rubber. The rubber is then bonded to the steel plates forcing the steel and rubber to work together. As rubber is subjected to a vertical load, it has a tendency to bulge. In the above described configuration, the steel plates keep the rubber from expanding at free surfaces, effectively creating high stiffness in vertical direction while still allowing the bearing to deflect horizontally as though it were unreinforced.

1.4 Fiber Reinforced Elastomeric Bearings

The current practice of using steel plates to reinforce the bearing has proved to be effective, but is also one of the main reasons that such bearings are so expensive and heavy and therefore, limited to only certain types of applications. Within the past few years, alternative methods of developing effective elastomeric bearings have been studied. One very promising alternative is to use carbon fibers to serve as the reinforcing layers. The tensile strength of the fibers can be comparable to steel while the weight can be drastically reduced. An abstract of a seminar given by James Kelly at the University of Illinois states that in order for base isolation in the form of elastomeric bearings to become more widely used, especially for housing in developing countries, "the cost and weight of the isolators must be reduced" [9]. Kelly then explains that the majority of the weight in a bearing comes from the steel reinforcing plates. He also explains that the high cost comes from the labor involved in preparing the steel plates and rubber layers for vulcanization. During this preparation process, steel plates are cut, sand-blasted, acid-cleaned, and then coated with bonding compound. By replacing the steel layers with fiber reinforcement, the weight reduction is possible because fiber materials have elastic stiffness of the same order as steel. Thus the reinforcement needed to provide the vertical stiffness may be

obtained by using a much lighter material. Eliminating the process of preparation the steel and rubber layers may also reduce the labor, and as a result, the cost [10].

1.5 Literature Survey

Steel reinforced elastomeric bearings have been used widely throughout the world [1]. In an attempt to decrease the weight and cost of these bearings, Kelly [11] introduced a certain type of fiber reinforced rubber specimens and showed that these isolators can provide adequate vertical and tilting stiffness for base isolation. At later stages, the fiber-reinforced bearings have been tested to identify various seismic characteristics such as damping and horizontal stiffness (Kelly 2001, Moon 2002, Ashkezari 2008 And Toopchi-Nezhad 2008). Moon et al. [12] designed and manufactured some specimens of multilayer elastomeric isolator using different kinds of fibers such as carbon, glass, Nylon and polyester. They concluded that it has high possibility to replace steel reinforcements in isolators with fiber reinforcement. Ashkezari et al. [13] manufactured some specimens of multilayer elastomeric seismic isolators reinforced by layers of woven carbon and steel. They concluded that 'steel like fiber reinforced elastomeric isolators' (SLFREI) can be used in seismic isolation of structures. Toopchi-Nezhad et al. [14&15] evaluated the lateral response of fiber reinforced seismic isolators using shake table testing method. Kelly and Calabrese [16] had an overview on the mechanical properties of fiber-reinforced bearings. They compared the theoretical solution with the results of finite element analysis.

The fiber reinforced bearings can have similar seismic performance compared to other rubber based isolators. On the other hand, it has been known that the vertical stiffness of fiber-reinforced bearings can be low compared to the other classes of rubber-based isolators [13]. The accuracy of theoretical approach predicting the vertical stiffness is only supported with limited amount of tests conducted on fiber reinforced strip isolators [10].

Studying the global behavior of multilayer reinforced rubber bearing by means of finite element analysis have been the concern of several studies within the past years;

Simo and Kelly [17] considered the stability of multilayer elastomeric bearings within the framework of two-dimensional finite elasticity. Seki et al. [18] investigated the principal strain distribution in an elastomeric bearing and denoted the rubber-steel interface as the most likely failure region. Takayama et al. [19] studied the principal strain and stress distributions under different values of the mean vertical pressure. Mordini and Strauss [20] presented an innovative isolation system using fiber-reinforced rubber bearing and verified analytical models for these new isolation devices using finite element analysis. Kelly and Calabrese [16] investigated the load-displacement behavior and stress state of fiber-reinforced bearings.

Modeling the ultimate behavior of fiber-reinforced bearings subjected to large shear strains with the current computational recourses is challenging due to the material and geometric non-linearity, change of contact condition, large strain (elastomeric behavior) and near-incompressibility of the rubber. The so-called mixed methods are used in modern finite element treatments of incompressible and near compressible materials.

1.6 Research Objective and Scope

The purpose of this study is to investigate the performance parameters of a new type of fiber reinforced elastomeric bearings, namely, fiber mesh reinforced bearings, and to verify whether it is possible to produce an effective fiber-reinforced bearing which is cheap, and light. To accomplish this aim, different forms of fiber reinforced elastomeric bearings have been designed and manufactured. Reinforcement of these bearings in the vertical direction has been done by means of carbon fiber reinforced polymer (CFRP) or in short term carbon fiber. Use of carbon fiber instead of normally used steel plates was done to make the bearings lighter and if mass-produced more economical.

Experimental studies including compression, combined compression and shear and low temperature shear tests were carried out to determine the mechanical properties of multi-layer fiber mesh reinforced elastomeric bearings. The influence of

the fiber flexibility on the mechanical properties of fiber mesh reinforced elastomeric bearing, such as the vertical and horizontal stiffness, was studied. Several samples of fiber and steel reinforced bearings with different geometry and size were manufactured and tested. Then the results obtained for fiber mesh reinforced bearings were compared with the corresponding results of steel-reinforced bearings. It is important to note that in all tests, size of the bearings for both reinforcement types were identical. Details of these bearings are given in Chapter 3.

To calculate and compare the mechanical properties of fiber mesh reinforced elastomeric bearings with steel reinforced ones, different tests were performed in the Structural Laboratory of Civil Engineering Department of Middle East Technical University.

Experimental research includes;

1. *Compression test*: The aim of this test is to calculate the average vertical stiffness of the bearings during the vertical load controlled cyclic loadings.

2. *Combined compression and shear test*: Results of this test are used to calculate the average and effective horizontal stiffness and other performance parameters of the bearings during the horizontal displacement controlled cyclic loadings.

3. *Low temperature shear test*: This test is necessary for bridge bearings which are going to be used in a bridge constructed in cold climates. The results of this test are compared by the corresponding values given in AASHTO M251-97 specifications.

After accomplishing these tests and analyzing the experimental data to obtain performance parameters of both types of bearings, comparison is done to verify the viability of producing a fiber mesh reinforced elastomeric bearing that resembles the behavior of steel reinforced one. Then, according to these comparisons, parameters which are important in designing the fiber mesh reinforced elastomeric bearings are determined.

This study also investigates the vertical stiffness (load-displacement behavior) and stress state of fiber and steel reinforced circular bearings by means of commercial finite element program named 'ABAQUS'. Furthermore, the results of the pressure solution are verified by comparing with the results of finite element analysis.

1.7 Organization of the Dissertation

This dissertation is composed of six main chapters. Every chapter includes the following brief contents:

Chapter 1: Introduction

General overview of the seismic isolation and previous studies about the seismic base isolation as well as the objective and scope of the dissertation

Chapter 2: Theory of Seismic Base Isolation

Theoretical background of seismic isolation and calculation of vertical stiffness for bearings with rigid reinforcement and also a brief summary of compression stiffness of bearings with flexible reinforcement

Chapter 3: Fiber Reinforced Elastomeric Bearing Tests

Geometrical and material properties of test bearings along with the description of the tests

Chapter 4: Horizontal Shear Test Results

Results of different experimental study in tabular format along with the hysteresis loops of bearings and comparison of test results for fiber and steel reinforced bearings

Chapter 5: Finite Element Analysis of Elastomeric Bearings

Finite element modeling of elastomeric bearing in a computer based software and their analysis and comparison of test results with the results of finite element analysis and pressure method

Chapter 6: Conclusion

A brief summary, conclusions and recommendations for future studies

CHAPTER 2

THEORY OF SEISMIC BASE ISOLATION

2.1 Introduction

In this chapter a brief overview of dynamic theory for earthquakes is given. This theory attempts to explain the performance of structural and mechanical systems which are subjected to vibrations. It seeks to form the equation of motion for the system, generally results in a second order, non-homogeneous differential equation. The solution for the equation of motion predicts the response of the system subjected to dynamic load. After obtaining equation of motion and solving the differential equation, concept of base isolation and transmissibility (TR) is introduced. Then the impact of frequency ratio which is an important factor in determining the response of structure subjected to earthquake stimulation is discussed.

In order to model an elastomeric bearing's behavior two components are required; vertical stiffness and horizontal stiffness. Therefore, the next part of this chapter covers calculation of vertical and horizontal stiffness for elastomeric bearings whose reinforcement is considered rigid. In fiber reinforced elastomeric bearings reinforcement is not rigid and effect of fiber flexibility should be considered. By considering fiber's flexibility, second set of equation for calculating vertical stiffness is derived in this chapter.

2.2 Dynamic Theory for Earthquakes

In theory of vibration, a mathematical model of the structure and also source of vibration is studied. This model is formulated by engaging the mass, stiffness, and damping of the structural system.

The after-mentioned analysis follows closely the work of Kelly [2] and incorporates items discussed in the book Mechanical Vibrations, by Singiresu S. Rao [21].

The entire system can be modeled using the mass, stiffness, and damping of the system. Figure 2.1 shows a simplified model of a single degree of freedom system (SDOF) representing a structure. For the figure shown, **m** is the mass of the structure, **c** is the damping coefficient of the structure, **k** is the spring constant representing the structure's stiffness, and **x** and **u_g** are the displacements of the structure and the ground respectively.
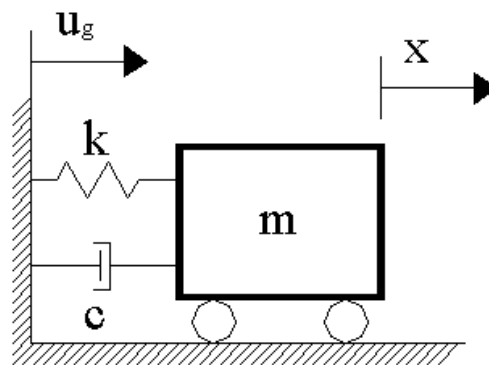
Figure 2.1 Single Degree of Freedom System [21]

Replacing the system with a free body diagram, with only forces acting on the mass, results in
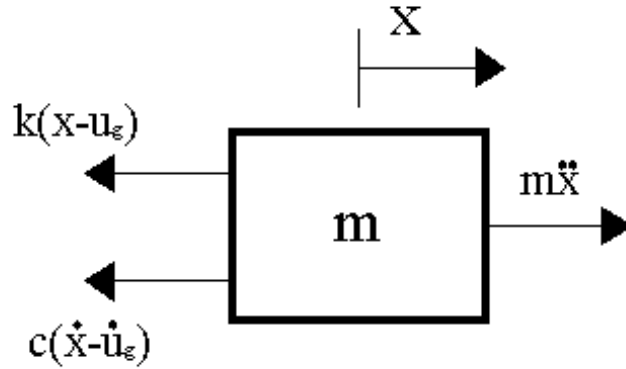
Figure 2.2 Free Body Diagram for SDOF System [21]

It is important to note that the forces acting on the left side of the mass incorporate the relative displacements and relative velocities of the mass and the ground. The force acting on the right side of the mass incorporates the acceleration of the input motion, in this case stemming from an earthquake. Thus, one obtains

$$m\ddot{x} = -k[x - u_g] - c[\dot{x} - \dot{u}_g] \tag{2.1}$$

Dividing both sides of the equation by the mass yields the following equation;

$$\ddot{x} = -\frac{k}{m}[x - u_g] - \frac{c}{m}[\dot{x} - \dot{u}_g] \tag{2.2}$$

The following variable definitions can be used in the analysis of the SDOF system;

$$\frac{k}{m} = \omega_n^2 \tag{2.3}$$

where ω_n is the natural frequency of the undamped system.

$$\frac{c}{m} = 2\omega_n\beta \tag{2.4}$$

where β is the damping ratio given by

$$\beta = \frac{c}{c_{cr}}$$

where

c = Viscous Damping Coefficient

c_{cr} = Critical Damping Coefficient = $2m\omega_n$

substituting the above variables simplifies Equation 2.2 into the following equation.

$$\ddot{x} = -\omega_n^2[x - u_g] - 2\omega_n\beta[\dot{x} - \dot{u}_g] \qquad (2.5)$$

Transmissibility (TR) is defined as the ratio of the displacement of the mass to the ground and is written in the following form.

$$TR = \frac{\tilde{x}}{\tilde{u}_g} = \frac{\max \ displacement \ of \ structure}{\max \ displacement \ of \ ground} \qquad (2.6)$$

It is assumed that the input motion is harmonic described in complex notation, and the resulting motion of the structure is written in the same form as shown below

$$u_g(t) = \tilde{u}_g e^{i\omega t} \quad \text{(ground motion)} \qquad (2.7)$$

$$x(t) = \tilde{x} e^{i\omega t} \quad \text{(response of the structure)}$$

Taking the first and second derivatives of both motion equations yields the following set of equations.

$$\dot{u}_g(t) = i\omega \tilde{u}_g e^{i\omega t} \qquad \ddot{u}_g(t) = i^2 \omega^2 \tilde{u}_g e^{i\omega t} \qquad (2.8)$$

$$\dot{x}(t) = i\omega \tilde{x} e^{i\omega t} \qquad \ddot{x}(t) = i^2 \omega^2 \tilde{x} e^{i\omega t}$$

Substituting Equations 2.8 back into Equation 2.5 gives the following equation

$$i^2 \omega^2 \tilde{x} e^{i\omega t} = -\omega_n^2[\tilde{x} e^{i\omega t} - \tilde{u}_g e^{i\omega t}] - 2\omega_n\beta[i\omega \tilde{x} e^{i\omega t} - i\omega \tilde{u}_g e^{i\omega t}]$$

(2.9)

and dividing both sides by $e^{i\omega t}$ gives

$$i^2 \omega^2 \tilde{x} = -\omega_n^2[\tilde{x} - \tilde{u}_g] - 2\omega_n\beta[\tilde{x} i\omega - \tilde{u}_g i\omega] \qquad (2.10)$$

Recognizing that $i^2 = -1$, multiplying through and collecting terms yields

$$\tilde{x}(-\omega^2 + \omega_n^2 + 2\omega_n\beta i\omega) = \tilde{u}_g(\omega_n^2 + 2\omega_n\beta i\omega) \qquad (2.11)$$

The transmissibility then becomes

$$TR = \frac{\tilde{x}}{\tilde{u}_g} = \frac{(2\omega_n\beta i\omega + \omega_n^2)}{(-\omega^2 + \omega_n^2 + 2\omega_n\beta i\omega)} \qquad (2.12)$$

Dividing top and bottom by ω_n^2 gives

$$TR = \frac{\tilde{x}}{\tilde{u}_g} = \frac{(1 + i2\beta\dfrac{\omega}{\omega_n})}{\left[(1 - \dfrac{\omega^2}{\omega_n^2}) + i2\beta\dfrac{\omega}{\omega_n}\right]} \qquad (2.13)$$

and using the identity

$$\left|\frac{a + ib}{c + id}\right| = \frac{(a^2 + b^2)^{1/2}}{(c^2 + d^2)^{1/2}}$$

Equation 2.13 can be written as

$$TR = \frac{\tilde{x}}{\tilde{u}_g} = \frac{\left[1 + 4\beta^2\left(\dfrac{\omega}{\omega_n}\right)^2\right]^{1/2}}{\left\{\left[1 - \left(\dfrac{\omega}{\omega_n}\right)^2\right]^2 + 4\beta^2\left(\dfrac{\omega}{\omega_n}\right)^2\right\}^{1/2}} \qquad (2.14)$$

Introducing the frequency ratio as

$$\Omega = \frac{\omega}{\omega_n}$$

the transmissibility can be simplified to

$$TR = \frac{\widetilde{x}}{\widetilde{u}_g} = \frac{(1+4\beta^2\Omega^2)^{1/2}}{\left[(1-\Omega^2)^2 + 4\beta^2\Omega^2\right]^{1/2}} \qquad\qquad (2.15)$$

Figure 2.3 shows the transmissibility versus frequency ratio for different values of the damping coefficient β.
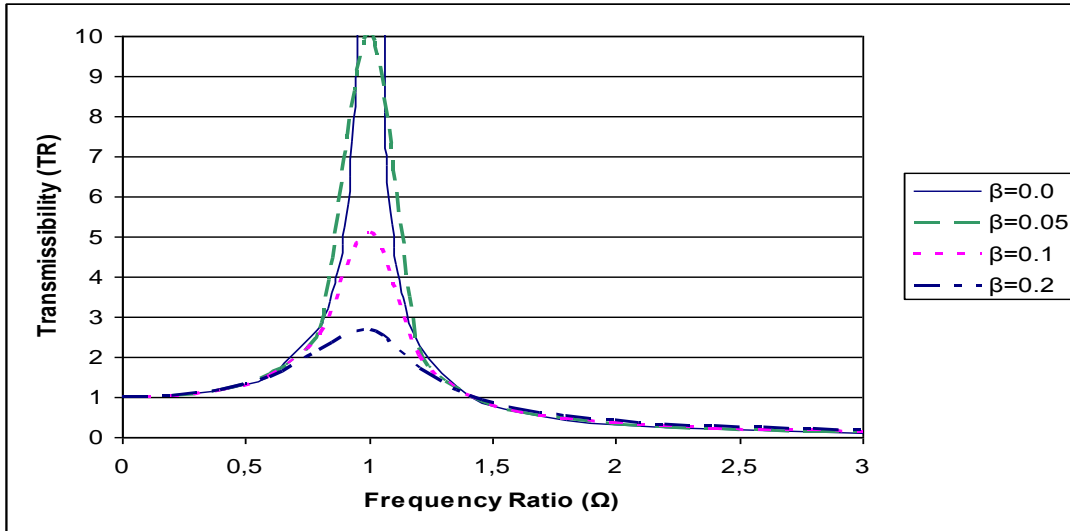
Figure 2.3 Transmissibility vs. Frequency Ratio (Ω)

Figure 2.3 gives the ratio $\widetilde{x}/\widetilde{u}_g$ as a function of frequency ratio. If the excitation frequency ω is much smaller than the natural frequency ω_n of the system, $\widetilde{x} \cong \widetilde{u}_g$ representing static displacement (i.e., the mass moves rigidly with the ground, both undergoing the same displacement). If the excitation frequency ω is much higher than the natural frequency ω_n of the system, $\widetilde{x} \cong 0$ (i.e., the mass stays still while the ground beneath it moves). There is a value for Ω (Ω = $\sqrt{2}$) at which point transmissibility for all values of β is equal to 1, and beyond that value the transmissibility is less than 1 for all values of β. This is the basic concept underlying isolation of a mass from a moving base by using a very flexible support system. The goal of base isolation is to have the transmissibility less than 1 [22].

In seismic base isolation, the stiffness and damping properties of the building are replaced by those of the base isolation system in the above analysis. For that reason, the stiffness of the bearing becomes extremely important in understanding the behavior and response of a structure in the event of an earthquake.

2.3 Mechanical Properties of Elastomeric Bearings

In vertical direction there is a need for relatively high vertical stiffness in order to support the weight of the structure and also in horizontal direction there should be a relatively lower horizontal stiffness to allow the foundation to move relative to the structure. By using reinforcing plates between the rubber layers, an orthotropic system with different stiffness values in the vertical and horizontal directions can be achieved. Vertical stiffness of these bearings is several times larger than their horizontal stiffness due to reinforcing plates which prevent the bulging of the rubber layers under the weight of the structure. Reinforcement of the bearings in vertical direction can be done by means of either steel plates which is a custom method or fiber meshes as an alternative. In this study, fiber meshes are also used for reinforcing the bearings to manufacture and produce fiber reinforced bearings which are much lighter than their steel reinforced ones and also if mass produced can lead to less costly manufacturing process. In comparison to steel reinforcement, fiber reinforcement is considered to be flexible and therefore the effect of fiber flexibity in calculating the compression stiffness of these bearings should be considered. In order to develop these systems, it is necessary to determine the stiffness of the bearing in both directions. Before discussing bearings with flexible reinforcement, a review of rigid reinforced bearings is presented.

2.3.1 Horizontal Stiffness of Bearing

Elastomeric bearing's horizontal frequency is a parameter which controls the response of an isolated structure. Horizontal frequency of bearings depends on the horizontal stiffness of bearing and weight of the structure above it. Recalling Equation (2.3)

$$\omega_n = \sqrt{\frac{k}{m}}$$

it becomes evident that undamped natural frequency, and structure's response is a function of the horizontal stiffness. In order to determine the horizontal stiffness of a bearing, a linear analysis is adequate. Considering only small shear deformations of the bearings, the following model is studied in both reinforcement conditions.
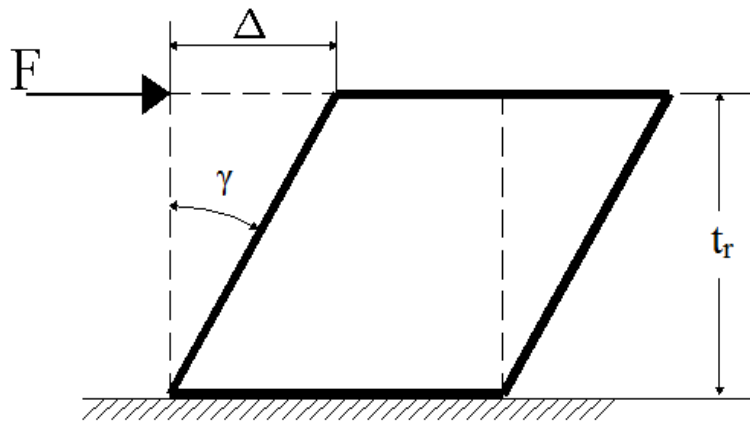
Figure 2.4 Bearing under Shear

Shearing strain γ, for small displacement can be defined as

$$\gamma = \frac{\Delta}{t_r} \tag{2.16}$$

Using Hook's law for linear deformations, the shear modulus, G, can be defined as

$$G = \frac{\tau}{\gamma} \tag{2.17}$$

where

$$\tau = \frac{F}{A}$$

Substitution into Equation 2.17 yields

$$G = \frac{Ft_r}{A\Delta} \tag{2.18}$$

Rearranging the above equation yields

$$F = \frac{AG}{t_r}\Delta \tag{2.19}$$

Knowing that $F = k_H\Delta$, k_H can be defined as

$$k_H = \frac{AG}{t_r} \tag{2.20}$$

where

Δ: Horizontal displacement

F: Horizontal force

A: Full cross sectional area of the bearing

t_r: Total thickness of the rubber

k_H: Horizontal stiffness

2.3.2 Vertical Stiffness of Bearing

Vertical stiffness of a bearing is dependent upon the compression modulus E_c, for the bearing as a whole. The following equation for vertical stiffness, k_v, results from mechanics of materials.

$$k_V = \frac{E_c A}{t_r} \tag{2.21}$$

where

E_c : Compression modulus of the bearing under specified level of vertical load

A: Area in which the load is applied

Although the vertical stiffness is important in determining the stability of the bearing and ensuring sufficient vertical support, the horizontal stiffness is what a structure's

response depends upon in the event of an earthquake. The compression modulus of the elastomeric bearings, E_c, depends on the compression properties of the shims and the rubber. The following section presents a theoretical analysis of the elastomeric bearings and their mechanical characteristics under compressive forces where the reinforcing shims are assumed to behave rigidly. After that a brief summary of stiffness analysis for fiber-reinforced bearings, whose reinforcing shims are not rigid but flexible, is given.

2.3.2.1 Behavior of Elastomeric Bearings with Rigid Reinforcement under Compression

Before discussing bearings with flexible reinforcement, a review of rigid reinforced bearings is presented. The following theory follows the simplified version found in Kelly [2] and Kelly and Takhirov [23]. Kelly's simplified version results from the analysis of Rocard [24], Gent and Lindley [25], and Gent and Meinecke [26] and is applicable to bearings with shape factors greater than five. Several assumptions are used for this simplified version being:

1. Points on a vertical line before deformation lie on a parabola after loading.

2. Horizontal planes remain horizontal.

3. The material is incompressible.

Considering an arbitrarily shaped pad of thickness t shown in Figure 2.5, with a Cartesian coordinate system located in the middle surface of the pad, $u, v,$ and w are the displacements in directions $x, y,$ and $z,$ respectively.
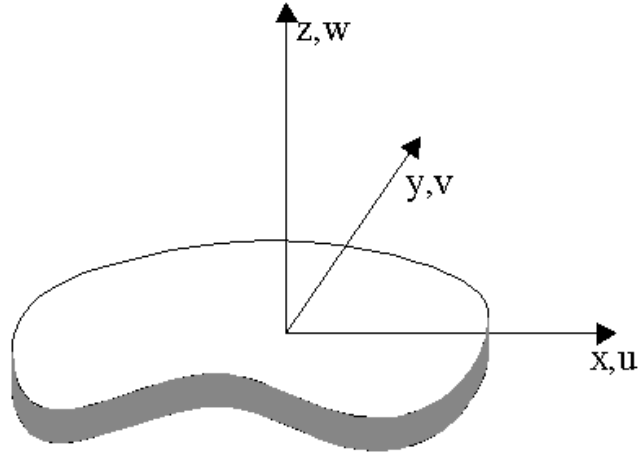
Figure 2.5 Arbitrarily Shaped Pad with Cartesian coordinate system

Establishing displacement equations for the system gives

$$u(x, y, z) = u_0(x, y)\left(1 - \frac{4z^2}{t^2}\right)$$

$$v(x, y, z) = v_0(x, y)\left(1 - \frac{4z^2}{t^2}\right) \tag{2.22}$$

$$w(x, y, z) = w(z)$$

In the first and second equation, terms u_0 and v_0 represent the kinematic assumption of quadratically varied deformation of the vertical lines in the elastomer and the third equation represents the assumption that horizontal plane remain planar after deformation in the elastomer.

Setting the boundary conditions which satisfy the displacement Equation 2.22 as

$$u(x, y, \pm\frac{t}{2}) = v(x, y, \pm\frac{t}{2}) = 0 \tag{2.23}$$

Using the assumption that the material is incompressible, a strain compatibility equation may been written as

$$\varepsilon_{xx} + \varepsilon_{yy} + \varepsilon_{zz} = 0 \tag{2.24}$$

Strains in the *x, y,* and *z* directions are given as

$$\varepsilon_{xx} = \frac{\partial u}{\partial x} \qquad \varepsilon_{yy} = \frac{\partial v}{\partial y} \qquad \varepsilon_{zz} = \frac{\partial w}{\partial z} \qquad (2.25)$$

Substituting Equations 2.25 and 2.22 into Equation 2.24 results in

$$\frac{\partial u_0(x, y)}{\partial x}(1 - \frac{4z^2}{t^2}) + \frac{\partial v_o(x, y)}{\partial y}(1 - \frac{4z^2}{t^2}) + \frac{\partial w}{\partial z} = 0 \qquad (2.26)$$

Simplifying Equation 2.26 yields

$$(u_{0,x} + v_{0,y})(1 - \frac{4z^2}{t^2}) + w_{,z} = 0 \qquad (2.27)$$

where the commas imply partial differentiation with respect to the indicated coordinate. Integrating through the thickness in the following form

$$\int_{-t/2}^{t/2} [(u_{0,x} + v_{0,y})(1 - \frac{4z^2}{t^2}) + w_{,z}]dz = 0$$

yields

$$[(u_{0,x} + v_{0,y})(z - \frac{4z^3}{3t^2}) + w(z)]_{-t/2}^{t/2} = 0$$

which reduces to

$$\frac{2}{3}t(u_{0,x} + v_{0,y}) + w(t/2) - w(-t/2) = 0 \qquad (2.28)$$

Compressive strain ε_c, where $\varepsilon_c > 0$ in the direction of the load, can be defined as

$$\varepsilon_c = -\frac{\Delta t}{t} = -\left[\frac{w(t/2) - w(-t/2)}{t}\right] \qquad (2.29)$$

Rearranging Equation 2.28 and substituting into Equation 2.29 yields

$$(u_{0,x} + v_{0,y}) = -\frac{3}{2}\left[\frac{w(t/2) - w(-t/2)}{t}\right] = \frac{3}{2}\varepsilon_c = -\frac{3\Delta t}{2t} \qquad (2.30)$$

24

By considering a three-dimensional general state of stress at a point as shown in Figure 2.6:
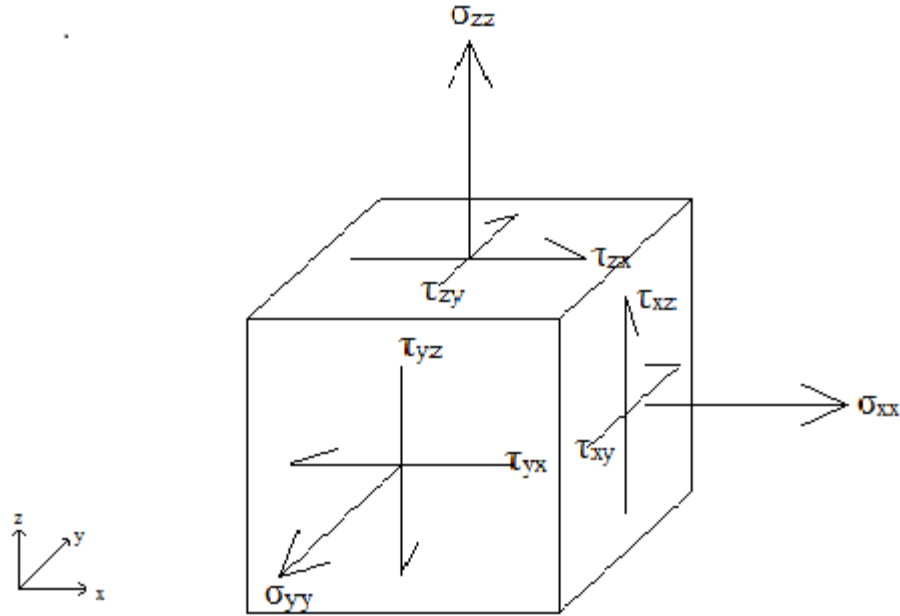
Figure 2.6 Stress Block for assumed Cartesian coordinate system

the following equilibrium equations are obtained.

$$\sigma_{xx,x} + \tau_{yx,y} + \tau_{xz,z} = 0$$

(2.31)

$$\sigma_{yy,y} + \tau_{yx,x} + \tau_{yz,z} = 0$$

The stress state is assumed to be dominated by the internal pressure, p, such that the normal stress components, σ_{xx}, σ_{yy}, σ_{zz}, differ from $-p$ only by terms of order $(t^2/l^2)p$, where l is the typical dimension of the pad. The shear stress components, τ_{xz} and τ_{yz} which are generated by the constraints at the top and bottom of the pad, are assumed to be of order $(t/l)p$. The in-plane shearing stress τ_{xy} is assumed to be of order $(t^2/l^2)p$.

Under these assumptions, the equilibrium equation in the x and y directions for the stresses of the elastomer reduces to

$$\sigma_{xx,x} + \tau_{xz,z} = 0$$

$$\sigma_{yy,y} + \tau_{yz,z} = 0$$

(2.32)

Assuming that the material is linearly elastic, the shear stresses can be related to the shear strains using Hooke's Law.

$$\tau_{xz} = G\gamma_{xz}$$

(2.33)

$$\tau_{yz} = G\gamma_{yz}$$

where G is the shear modulus of the material, leading to

$$\tau_{xz} = -8Gu_0(\frac{z}{t^2})$$

(2.34)

$$\tau_{yz} = -8Gv_0(\frac{z}{t^2})$$

and then substituting into the equilibrium equations,

$$\frac{\partial \sigma_{xx}}{\partial x} = \frac{8Gu_0}{t^2}$$

(2.35)

$$\frac{\partial \sigma_{yy}}{\partial y} = \frac{8Gv_0}{t^2}$$

Inverting Equation 2.35 to obtain u_0 and v_0, and substituting into the incompressibility condition results in

$$\frac{t^2 \partial^2 \sigma_{xx}}{8G \partial x^2} + \frac{t^2 \partial^2 \sigma_{yy}}{8G \partial y^2} = \frac{t^2}{8G}(\frac{\partial^2 \sigma_{xx}}{\partial x^2} + \frac{\partial^2 \sigma_{yy}}{\partial y^2}) = \frac{3\varepsilon_c}{2}$$

(2.36)

which can also be written as

$$\frac{t^2}{8G}\left(\sigma_{xx,xx} + \sigma_{yy,yy}\right) = \frac{3\varepsilon_c}{2} = -\frac{3\Delta t}{2t}$$

(2.37)

26

Identifying $\sigma_{xx} = \sigma_{yy} = -p$ from the principle of hydrostatic equilibrium, Equation 2.37 reduces to

$$(p,_{xx} + p,_{yy}) = \nabla^2 p = -\frac{12G\varepsilon_c}{t^2}$$
(2.38)

Setting the boundary condition, $p = 0$, at the perimeter of the pad, Equation 2.38 is solved for $p(x,y)$ and integrated over the area of the pad, A, to obtain the resultant normal load P, from which the modulus of elasticity, E_c, can be calculated using the following relationship,

$$E_c = \frac{P}{A\varepsilon_c}$$
(2.39)

where E_c is the modulus of elasticity in the direction of the compression.

The value of E_c for a single rubber layer is controlled by the shape factor, S, defined as

$$S = \frac{loaded\,area}{free\,area}$$

which is a dimensionless aspect ratio of a single layer of rubber.

For an infinite strip of width $2a$, and a single layer thickness of t,

$$S = \frac{a}{t}$$
(2.40)

For a circular bearing of radius a and thickness t,

$$S = \frac{a}{2t}$$
(2.41)

For a square bearing of side a and thickness t,

$$S = \frac{a}{4t}$$
(2.42)

The shape of a bearing has direct impact on the modulus of elasticity of the bearing in the vertical direction. The geometrical properties of the bearing in the form of shape factor, is used in predicting the vertical stiffness of the bearing. For the infinite strip, the Poisson Equation given by Equation 2.38 reduces to

$$\frac{\partial^2 p}{\partial x^2} = \nabla^2 p = -\frac{12G\varepsilon_c}{t^2} \qquad (2.43)$$

Applying the boundary conditions that p=0 at $\pm a$ and solving Equation 2.43 yields

$$p = \frac{6G}{t^2}(a^2 - x^2)\varepsilon_c$$

The load, P, per unit length for the strip is given by

$$P = \int_{-a}^{a} p\,dx = \frac{8Ga^3}{t^2}\varepsilon_c$$

Knowing that the area per unit length, A, and shape factor, S, for an infinite strip are given by 2a, and a/t, respectively, Equation 2.39 can be rewritten as

$$E_c = \frac{P}{A\varepsilon_c} = 4GS^2 \qquad (2.44)$$

Following the same approach for other shapes, Equation 2.39 can be rewritten for a circular bearing as

$$E_c = \frac{P}{A\varepsilon_c} = 6GS^2 \qquad (2.45)$$

And for a square bearing as

$$E_c = \frac{P}{A\varepsilon_c} = 6.73GS^2 \qquad (2.46)$$

The derivation of the circular and square bearing configurations can be found in [2]. The same method and equations can be applied to bearings with different shapes to determine the modulus of elasticity of the bearing which is essential in determining the vertical stiffness of the bearing.

2.3.2.2 Behavior of Elastomeric Bearings with Flexible Reinforcement under Compression

The solution for the compression of a pad with rigid reinforcement is algebrically simple enough to be treated in two dimensions and for an arbitrary shape. To calculate the stiffness of a steel-reinforced bearing, an approximate analysis which assumes that each individual layer of elastomer in the bearing deforms in such a way that horizontal planes remain planar and points on a vertical line lie on a parabola after loading, is used. The steel plates are assumed to be rigid to constrain the displacement at the top and bottom of the elastomer. The elastomer is assumed to be strictly incompressible and its normal stress components are approximated by the pressure. This leads to the well-known 'pressure solution' approach [2]. The problem for the pad with flexible reinforcement is more complicated. In [23] the extensional flexibility of the fiber reinforcement has been incorporated into the 'pressure solution' approach, and that prediction of the resulting stiffness is made. As before, the rubber is assumed incompressible and the pressure is assumed to be the dominant stress component. The kinematic assumption of quadratically variable displacement is supplemented by an additional displacement that is constant through the thickness and is intended to accommodate the stretching of the reinforcement. Also, the assumption that horizontal planes remain horizontal is valid. The following theory follows the simplified version found in [10, 27]. Thus

$$u(x,y,z) = u_0(x,y)(1 - \frac{4z^2}{t^2}) + u_1(x,y)$$

$$v(x,y,z) = v_0(x,y)(1 - \frac{4z^2}{t^2}) + v_1(x,y) \qquad (2.47)$$

$$w(x,y,z) = w(z)$$

In Eqs. (2.47), the terms of u_0 and v_0 represent the kinematic assumption of quadratically varied displacements and are supplemented by additional

displacements u_1 and v_1 , respectively, which are constant through the thickness and are intended to accommodate the stretch of the reinforcement. The third equation represents the assumption that horizontal planes remain planar.

The elastomer is assumed to have linearly elastic behavior with incompressibility. The assumption of incompressibility produces a constraint on displacements in the form

$$u_{,x} + v_{,y} + w_{,z} = 0 \tag{2.48}$$

Substituting Eqs. (2.47) into the equation (2.48) and then taking integration through the thickness from $z=-t/2$ to $z=t/2$ lead to

$$\frac{2}{3}(u_{0,x} + v_{0,y}) + u_{1,x} + v_{1,y} = \varepsilon_c \tag{2.49}$$

in which $\varepsilon_c = (w(-t/2) - w(t/2))/t$ is the nominal compression strain.

The stress state in the elastomer is assumed to be dominated by the internal pressure, such that the stress components of the elastomer are

$$\sigma_{xx} \approx \sigma_{yy} \approx \sigma_{zz} \approx -p; \qquad \sigma_{xy} \approx 0 \tag{2.50}$$

The equilibrium equations in the x and y directions for the stresses of the elastomer are then reduced to

$$-p_{,x} + \sigma_{xz,z} = 0 \tag{2.51}$$

$$-p_{,y} + \sigma_{yz,z} = 0 \tag{2.52}$$

Under the displacement assumptions in Eqs. (2.47), the shear stress components of the elastomer are

$$\sigma_{xz} = -\frac{8G}{t^2} z u_0$$
$$\sigma_{yz} = -\frac{8G}{t^2} z v_0 \tag{2.53}$$

and the equilibrium equations become

$$p_{,x} = -\frac{8G}{t^2} u_0 \tag{2.54}$$

$$p_{,y} = -\frac{8G}{t^2} v_0 \tag{2.55}$$

Differentiating Eqs. (2.54) and (2.55) with respect to x and y, respectively, and then adding them up yield

$$p_{,xx} + p_{,yy} = -\frac{8G}{t^2}(u_{0,x} + v_{0,y}) \tag{2.56}$$

The internal forces acting in the reinforcing sheet are related to the shear stresses, σ_{xz} and σ_{yz}, acting on the surfaces of the reinforcing sheet bonded to the top and bottom layers of elastomer through two equilibrium equations in the x and y directions

$$N_{xx,x} + N_{xy,y} + \sigma_{xz}\big|_{z=-\frac{t}{2}} - \sigma_{xz}\big|_{z=\frac{t}{2}} = 0 \tag{2.57}$$

$$N_{yy,y} + N_{xy,x} + \sigma_{yz}\big|_{z=-\frac{t}{2}} - \sigma_{yz}\big|_{z=\frac{t}{2}} = 0 \tag{2.58}$$

where N_{xx} and N_{yy} are the normal forces per unit length in the x and y directions, respectively; N_{xy} is the in-plane shear force per unit length. Figure 2.7 illustrates forces in reinforcing sheet bonded to rectangular layers of elastomers. Substituting Eq. (2.53) into the above equations, and then combining these with the equilibrium equations of the elastomeric layer in Eqs. (2.54) and (2.55) to eliminate u_0 and v_0 give

$$N_{xx,x} + N_{xy,y} = tp_{,x} \tag{2.59}$$

$$N_{yy,y} + N_{xy,x} = tp_{,y} \tag{2.60}$$

Bringing the strain-stress relation of the reinforcement into Eqs. (2.59) and (2.60) leads to

$$\frac{E_f t_f}{1-\upsilon_f{}^2}(u_{1,xx}+\upsilon_f\, v_{1,yx})+\frac{E_f t_f}{2(1+\upsilon_f)}(u_{1,yy}+v_{1,xy})=tp_{,x} \qquad (2.61)$$

$$\frac{E_f t_f}{1-\upsilon_f{}^2}(v_{1,yy}+\upsilon_f\, u_{1,xy})+\frac{E_f t_f}{2(1+\upsilon_f)}(v_{1,xx}+u_{1,yx})=tp_{,y} \qquad (2.62)$$
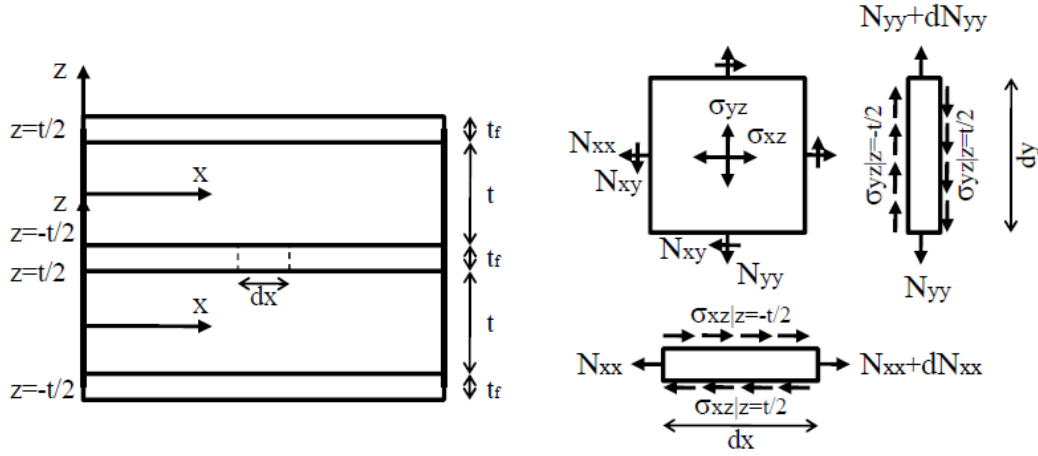
Figure 2.7 Forces in reinforcing sheet bonded to rectangular layers of elastomers[10]

where E_f and v_f are the elastic modulus and Poisson's ratio of the reinforcing material. Differentiating Eqs. (2.61) and (2.62) with respect to x and y, respectively, and then adding them up yield

$$(u_{1,x}+v_{1,y})_{,xx}+(u_{1,x}+v_{1,y})_{,yy}=\frac{t(1-\upsilon_f{}^2)}{E_f t_f}(p_{,xx}+p_{,yy}) \qquad (2.63)$$

Combining Eq. (2.49) with Eq. (2.56) to eliminate the terms of u_0 and v_0 gives

$$u_{1,x}+v_{1,y}=\varepsilon_c+\frac{t^2}{12G}(p_{,xx}+p_{,yy}) \qquad (2.64)$$

Substitution of this into Eq. (2.63) leads to

$$p_{,xxxx}+2p_{,xxyy}+p_{,yyyy}-\alpha^2(p_{,xx}+p_{,yy})=0 \qquad (2.65)$$

in which α is defined as

32

$$\alpha = \sqrt{\frac{12G(1-\upsilon_f{}^2)}{E_f t_f t}} \tag{2.66}$$

The pressure p can be solved by satisfying the boundary conditions that the pressure in the elastomer and the normal force in the reinforcement vanish at the edges of the pad.

The compression stiffness of a bearing is determined by the effective compressive modulus E_c defined as

$$E_c = \frac{P}{A\varepsilon_c} \tag{2.67}$$

where A is the area of the pad in the x-y plane and the resultant compression load P has the form

$$P = -\int_A \sigma_{zz} dA \approx \int_A p(x,y) dA \tag{2.68}$$

For infinitely long strip pads, the deformation is in a plane strain state, so that displacement component in y direction vanishes and the governing equation of the pressure becomes a ordinary differential equation of x. If the strip pad has a width of *2a*, the effective compressive modulus has the form

$$E_c = GS^2 \frac{12}{(\alpha a)^2}(1 - \frac{\tanh \alpha a}{\alpha a}) \tag{2.69}$$

in which $S = a/t$ is the shape factor of the infinitely long strip pad.

For rectangular pads, the pressure can be solved by using the approximate boundary conditions [27]. If the aspect of the rectangular pad is *2a* by *2b*, the effective compressive modulus has the form

$$E_c = GS^2 \frac{24}{\pi^2 (\alpha a)^2} (1 + \frac{a}{b})^2$$

$$\sum_{n=1}^{\infty} \frac{1}{(n-\frac{1}{2})^2} (\frac{\tanh \gamma_n b}{\gamma_n b} - \frac{\tanh \beta_n b}{\beta_n b} + \frac{\tanh \overline{\gamma}_n a}{\overline{\gamma}_n a} - \frac{\tanh \overline{\beta}_n a}{\overline{\beta}_n a}) \qquad (2.70)$$

in which $S = \dfrac{ab}{t(a+b)}$ is the shape factor of the rectangular pad, and

$$\begin{aligned} \gamma_n &= (n-\frac{1}{2})\frac{\pi}{a} & \beta_n &= \sqrt{\gamma_n^2 + \alpha^2} \\ \overline{\gamma}_n &= (n-\frac{1}{2})\frac{\pi}{b} & \overline{\beta}_n &= \sqrt{\overline{\gamma}_n^2 + \alpha^2} \end{aligned} \qquad (2.71)$$

Assuming that the value of E_c is linearly varied between a/b = 0 and a/b = 1, an empirical formula for the effective compressive modulus of rectangular reinforced layers is derived (by author) from Eq. (2.69)

$$E_c = GS^2 \frac{12}{(\alpha a)^2} (1 - \frac{\tanh \alpha a}{\alpha a})$$

$$\left\{ 1 + \frac{a}{b} \left[0.657 + 0.125(\alpha a) + 0.279(\alpha a)^2 - 0.085(\alpha a)^3 + 0.0073(\alpha a)^4 \right] \right\} \qquad (2.72)$$

with $a/b \leq 1$. Because the range of the values used in the regression analysis is between 0 and 5, the effective compressive modulus in Eq. (2.72) is only applicable to the range of $0 \leq \alpha a \leq 5$. The maximum error in this range is smaller than 4 percent.

If one denotes a to be the length of short side and b to be the length of long side, the value of aspect ratio *a/b* is between 0 and 1. When the aspect ratio *a/b* tends to zero, $\gamma_n b \to \infty, \beta_n b \to \infty, \overline{\beta}_n a \to \alpha a$ and $\overline{\gamma}_n a \to 0$ which makes

$$\frac{\tanh \overline{\gamma}_n a}{\overline{\gamma}_n a} = 1$$

Using the following series equation

$$\sum_{n=1}^{\infty} \frac{1}{(n-\frac{1}{2})^2} = \frac{\pi^2}{2} \qquad (2.73)$$

Eq. (2.70) is reduced to

$$E_c = \frac{12GS^2}{(\alpha a)^2}(1 - \frac{\tanh\alpha a}{\alpha a}) \qquad (2.74)$$

which is the effective compressive mudulus of the infinitely long strip isolator. Furtheremore, when the stiffness of the reinforcement becomes rigid, $\alpha \to 0$ and using the following Taylor series

$$\tanh\alpha a = \alpha a - \frac{(\alpha a)^3}{3} \qquad (2.75)$$

in Eq. (2.74) the compressive modulus of infinitely long strip with rigid reinforcement is obtained

$$E_c = 4GS^2 \qquad (2.76)$$

which has the same form as the one in equation (2.44).

To calculate the compressive modulus of the rectangular layer of elastomer bonded to rigid reinforcement, according to reinforcement rigidity, $\alpha \to 0$. β_n defined in Eq. (2.64) can be approximated as a series of α

$$\beta_n \approx \gamma_n \left[1 + \frac{1}{2}(\frac{\alpha}{\gamma_n})^2 \right] \qquad (2.77)$$

and $tanh \; \beta_n b$ becomes

$$\tanh\beta_n b \approx \tanh\gamma_n b + \frac{\gamma_n b}{2Cosh^2 \gamma_n b}(\frac{\alpha}{\gamma_n})^2 \qquad (2.78)$$

Similarly, $\bar{\beta}_n$ defined in Eq. (2.71) can be approximated as

$$\bar{\beta}_n \approx \bar{\gamma}_n \left[1 + \frac{1}{2}(\frac{\alpha}{\bar{\gamma}_n})^2 \right] \qquad (2.79)$$

and *tanh* $\bar{\beta}_n b$ becomes

$$\tanh \bar{\beta}_n b \approx \tanh \bar{\gamma}_n b + \frac{\bar{\gamma}_n b}{2 Cosh^2 \bar{\gamma}_n b}(\frac{\alpha}{\bar{\gamma}_n})^2 \qquad (2.80)$$

Substituting these approximations into Eq. (2.70) and neglecting the high order terms of α,

$$E_c = \frac{12 GS^2}{\pi^4}(1+\frac{a}{b})^2$$
$$\sum_{n=1}^{\infty} \frac{1}{(n-\frac{1}{2})^4} \left[\frac{\tanh \gamma_n b}{\gamma_n b} - \frac{1}{Cosh^2 \gamma_n b} + \frac{b^2}{a^2}\left(\frac{\tanh \bar{\gamma}_n a}{\bar{\gamma}_n a} - \frac{1}{Cosh^2 \bar{\gamma}_n a} \right) \right] \qquad (2.81)$$

which is the effective compressive modulus of the rectangular layer of elastomer bonded to rigid reinforcement. In this case an empirical formula developed (by author) can be used to calculate the compressive modulus

$$E_c = GS^2 \left[2.127(\frac{a}{b})^4 - 4.225(\frac{a}{b})^3 - 0.586(\frac{a}{b})^2 + 5.427(\frac{a}{b}) + 4 \right] \qquad (2.82)$$

As it is clear from Figure 2.8, there is a good agreement between the results of Eq. (2.81) and (2.82).

From Eq. (2.70), it is known that the ratio $E_c/(GS^2)$ is a function of αa and the aspect ratio a/b. The variation of $E_c/(GS^2)$ with αa is plotted in Figure 2.9 for $a/b = 0$, 0.1, 0.2, 0.5 and 1, which shows that the effective compressive modulus decreases with increasing αa [27]. To have a high compressive modulus, the value of αa must be small. The figure also reveals that a larger value of a/b produces a larger value of the effective compressive modulus.
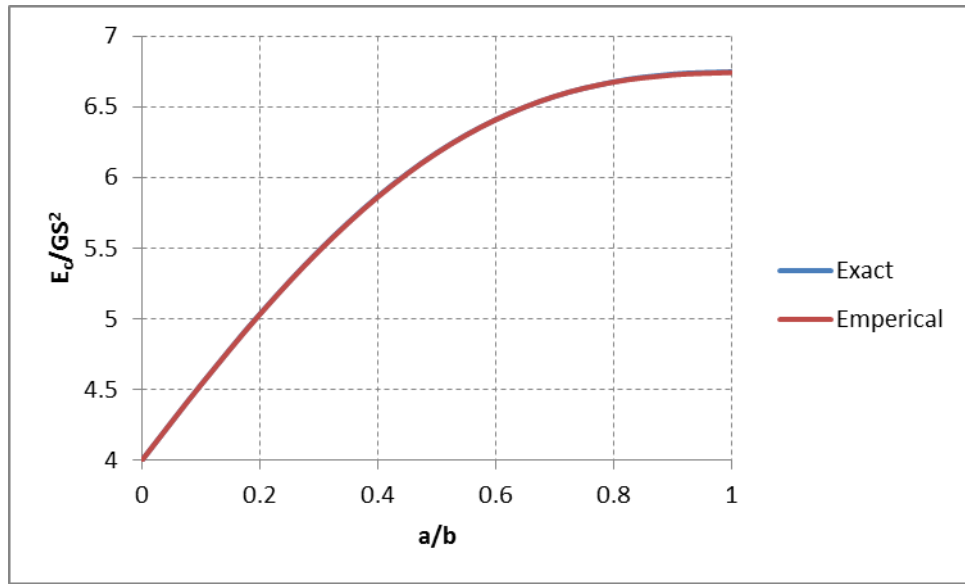
Figure 2.8 Variation of effective compressive modulus in rectangular pad with rigid reinforcement
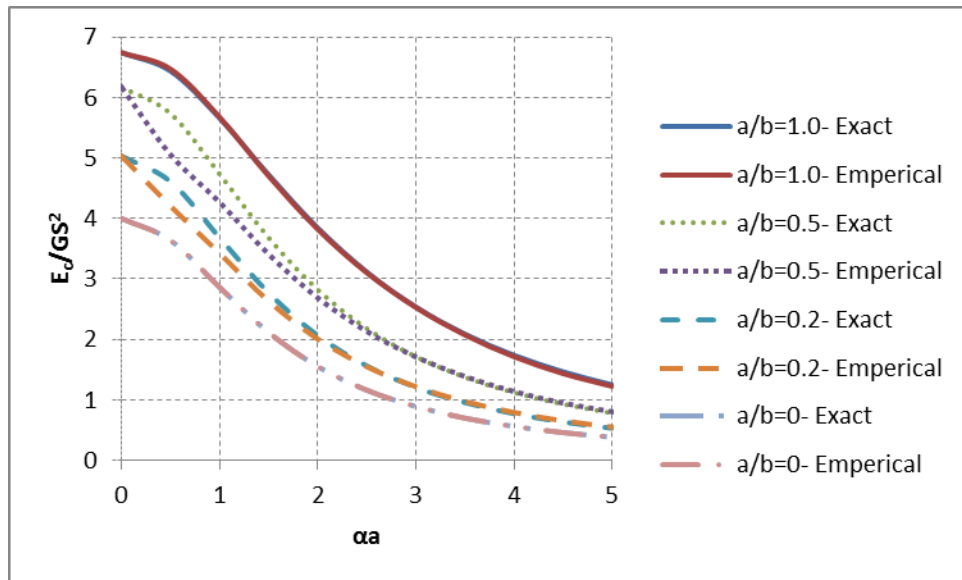
Figure 2.9 Variation of effective compressive modulus with αa in rectangular pad

For circular pads under compression, the deformation is in an axisymmetric state. The governing equation of the pressure can be expressed by the cylindrical coordinate system *(r,z)*. If the circular pad has a radius of *a*, the effective compressive modulus has the form

$$E_c = GS^2 \frac{24(1+\upsilon_f)}{(\alpha a)^2} \left[\frac{I_0(\alpha a) - \dfrac{2}{\alpha a} I_1(\alpha a)}{I_0(\alpha a) - \dfrac{(1-\upsilon)}{\alpha a} I_1(\alpha a)} \right] \tag{2.83}$$

in which *S* is the shape factor of the circular pad and I_n is the modified Bessel function of the first kind of order *n* defined as

$$I_0(\alpha a) \approx 1 + \frac{(\alpha a)^2}{4} \tag{2.84}$$

$$I_1(\alpha a) \approx \frac{\alpha a}{2} + \frac{(\alpha a)^3}{16} \tag{2.85}$$

$$S = \frac{a}{2t} \tag{2.86}$$

when $\alpha \to 0$ as in rigid reinforcement, by substituting Eqs. (2.84) and (2.85) into Eq. (2.83) and neglecting the higher-order terms of *αa*

$$E_c = 6GS^2$$

which is the effective compressive modulus for the circular layer of elastomer bonded to the rigid reinforcement [2].

The ratio $E_c/(GS^2)$ is plotted in Figure 2.10 as a function of *αa* for ν = 0, 0.3 and 0.5, which shows that the effective compressive modulus decreases with increasing *αa* [27]. To have high compressive modulus, one must keep the value of *αa* as low as possible. The figure also reveals that a higher Poisson's ratio of the reinforcement tends to have higher modulus, but the difference becomes negligible when *αa* is small.
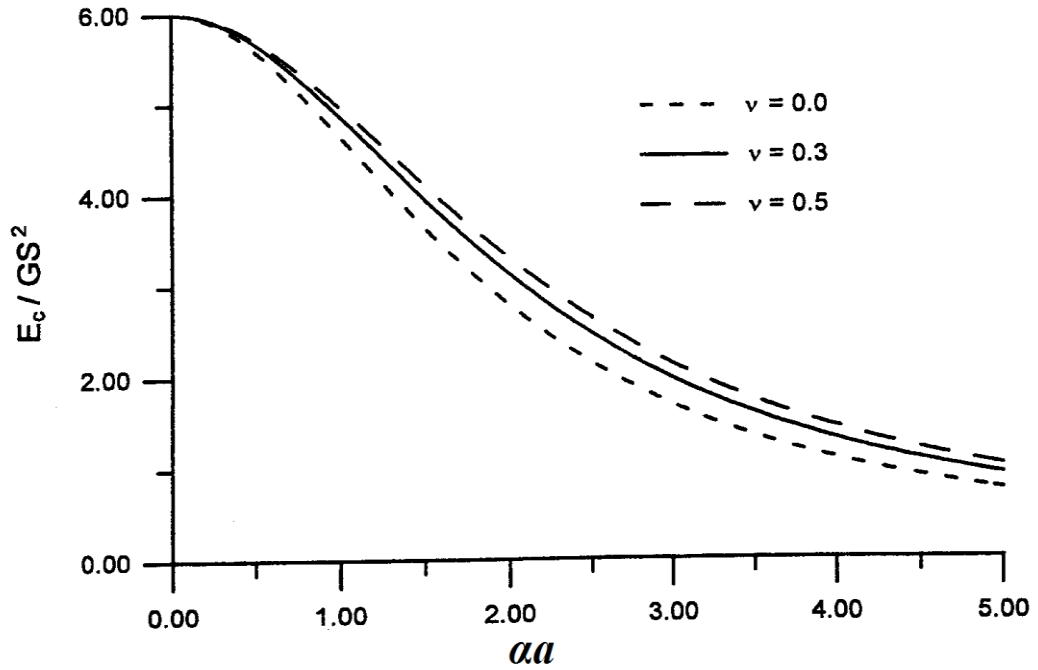
Figure 2.10 Variation of effective compressive modulus with αa in circular pad [27]

By considering the equlibrium of forces in equivalent sheet of reinforcement, stresses in the reinforcement can be calculated. Tangential and radial forces per unit length in reinforcement can be proven to be equal to;

$$N_r(r) = \frac{E_f t_f}{1-v^2} \frac{\Delta}{2t}(1+v)\left[1 - \frac{I_0(\alpha r) - \frac{1-v}{\alpha r}I_1(\alpha r)}{I_0(\alpha a) - \frac{1-v}{\alpha a}I_1(\alpha a)}\right]$$ (2.87)

$$N_\theta(r) = \frac{E_f t_f}{1-v^2} \frac{\Delta}{2t}(1+v)\left[1 - \frac{v I_0(\alpha r) + \frac{1-v}{\alpha r}I_1(\alpha r)}{I_0(\alpha a) - \frac{1-v}{\alpha a}I_1(\alpha a)}\right]$$ (2.88)

where $N_r(r)$ and $N_\theta(r)$ are the radial and tangential force per unit length in reinforcement, respectively and the other parameters are defined as before. The solution presented here is a summary of the work proposed by Kelly and compelete solution can be found in [23].

Stress distribution in elastomeric material of a circular bearing with radius (a) normalized with respect to average pressure is defined as [23]

$$\frac{p}{E_c \varepsilon_c} = \frac{I_0(\alpha a) - I_0(\alpha r)}{I_0(\alpha a) - \frac{2}{\alpha a} I_1(\alpha a)} \quad \& \quad 0 \le r \le a \tag{2.89}$$

where $\sigma_r \approx \sigma_\theta \approx \sigma_z \approx -p$ is the internal stress and $p_{ext} = p_{ave} = E_c \varepsilon_c$ is the applied mean pressure.

Normalized tangential stress $(\sigma_\theta^f t_f / p_{ave} t)$ and normalized radial $(\sigma_r^f t_f / p_{ave} t)$ stress in reinforcing material is given by

$$\frac{\sigma_\theta^f t_f}{p_{ave} t} = \frac{I_0(\alpha a) - \frac{1 - v_f}{\alpha a} I_1(\alpha a) - v_f I_0(\alpha r) - \frac{1 - v_f}{\alpha r} I_1(\alpha r)}{I_0(\alpha a) - \frac{2}{\alpha a} I_1(\alpha a)}$$

$$\frac{\sigma_r^f t_f}{p_{ave} t} = \frac{I_0(\alpha a) - \frac{1 - v_f}{\alpha a} I_1(\alpha a) - I_0(\alpha r) + \frac{1 - v_f}{\alpha r} I_1(\alpha r)}{I_0(\alpha a) - \frac{2}{\alpha a} I_1(\alpha a)} \tag{2.90}$$

In the case of material compressibility, Equation (2.24) becomes

$$\varepsilon_x + \varepsilon_y + \varepsilon_z = \frac{-p}{K} \tag{2.91}$$

where p is the pressure in elastomer and K is the bulk modulus of material. In the case of rigid reinforcement and material compressibility (steel reinforced bearings) Equation (2.45) becames

$$E_c = \frac{P}{A\varepsilon_c} = 48GS^2 \frac{\left[I_0(\beta a) - \frac{2}{\beta a} I_1(\beta a) \right]}{(\beta a)^2 I_0(\beta a)} \tag{2.92}$$

where β is a parameter, which considers the effect of compressibility and is defined as

$$\beta^2 = \frac{12G}{Kt^2} \tag{2.93}$$

where

E_c: Compression modulus (MPa)

G: shear modulus of elastomer (MPa)

a: radius of bearing (mm)

K: Bulk modulus of elastomer (MPa)

t: thickness of the individual elastomer layer (mm)

and I_0 and I_1 are modified Bessel functions of the first kind of order 0 and 1, respectively and are defined as:

$$I_0(\beta a) \approx 1 + \frac{(\beta a)^2}{4} \tag{2.94}$$

$$I\ (\beta a) \approx \frac{\beta a}{2} + \frac{(\beta a)^3}{16} \tag{2.95}$$

In calculating the compression modulus of fiber reinforced bearing with compressible material both the material compressibility and fiber flexibility should be considered. In this case equation (2.83) for compressive modulus becomes

$$E_c = 24GS^2(1+\upsilon_f)\frac{\left[I_0(\lambda a) - \dfrac{2}{\lambda a}I_1(\lambda a)\right]}{(\alpha\lambda)^2\left[I_0(\lambda a) - \dfrac{1-\upsilon_f}{\lambda a}I_1(\lambda a)\right] + (\beta a)^2\dfrac{1+\upsilon_f}{2}I_0(\lambda a)} \tag{2.96}$$

where λ is a parameter defined as;

$$\lambda^2 = \alpha^2 + \beta^2 \tag{2.97}$$

and as before $\alpha^2 = \dfrac{12(1-\upsilon_f^2)G}{E_f t_f t}$ considers the effect of flexibility

where

ν_f : Poisson's ratio of the reinforcing sheet

E_f: Elastic modulus of reinforcing sheet (MPa)

t_f: thickness of the reinforcing sheet (mm)

By considering the material compressibility, stress distribution in elastomeric material is given by

$$\frac{p}{E_c \varepsilon_c} = \frac{I_0(\lambda a) - I_0(\lambda r)}{I_0(\lambda a) - \dfrac{2}{\lambda a} I_1(\lambda a)} \quad \& \quad 0 \leq r \leq a \tag{2.98}$$

Distribution of in-plane stresses in the reinforcement is given by Eq. (2.99). The quantities σ_r^f and σ_θ^f have units of stresses and can be normalized by dividing by the average pressure, $p_{ave} = E_c \varepsilon_c$. The resulting normalized stresses are proportional to t/t_f, so that is convenient to present the stress behavior in forms of $\sigma_r^f t_f / p_{ave} t$ and $\sigma_\theta^f t_f / p_{ave} t$.

By considering the material compressibility, stress distribution in reinforcement is given by

$$
\begin{aligned}
\frac{\sigma_\theta^f t_f}{p_{ave} t} &= \frac{I_0(\lambda a) - \dfrac{1 - \nu_f}{\lambda a} I_1(\lambda a) - \nu_f I_0(\lambda r) - \dfrac{1 - \nu_f}{\lambda r} I_1(\lambda r)}{I_0(\lambda a) - \dfrac{2}{\lambda a} I_1(\lambda a)} \\[2em]
\frac{\sigma_r^f t_f}{p_{ave} t} &= \frac{I_0(\lambda a) - \dfrac{1 - \nu_f}{\lambda a} I_1(\lambda a) - I_0(\lambda r) + \dfrac{1 - \nu_f}{\lambda r} I_1(\lambda r)}{I_0(\lambda a) - \dfrac{2}{\lambda a} I_1(\lambda a)}
\end{aligned}
\tag{2.99}
$$

To sum up, results of these theoretical analyses on different shapes of elastomeric layer bonded to flexible reinforcements and subjected to compression loading show that the compression stiffness of the fiber-reinforced bearing is affected by the shape factor of the elastomer and the flexibility of the reinforcement. Similar to steel-reinforced bearings, the stiffness of fiber-reinforced bearings increases with increasing the shape factor, but the flexibility of the reinforcement can decrease the stiffness of the bearing. It is worth noting that material compressibility is an important parameter which affects the compressive modulus of elastomeric bearings and the stiffness of the bearing in vertical direction.

CHAPTER 3

TESTS OF FIBER MESH REINFORCED ELASTOMERIC BEARING

3.1 Introduction

To evaluate the performance of fiber mesh reinforced elastomeric bearings and compare their performance with steel reinforced ones, a research program which covers the content of this dissertation was conducted in Department of Civil Engineering of Middle East Technical University. In this research program several samples of fiber and steel reinforced bearings were designed and tested. To evaluate the effect of different geometrical parameters such as shape and shape factor on the performance of the bearings, three diffrent geometries (rectangle, circle and square) were examined. To examine the effect of shape factor, each group of bearings was designed with two different thicknesses of elastomer layers. Furthermore, two samples for each bearing type were produced making the total number of the bearings to become 40.

It is important to note that all geometrical properties of compared bearings produced with different reinforcing material were identical. Under these conditions a logical assessment of testing results could be made to verify if the approach was practical. The experimental research was conducted in three stages. During the first stage bearings were tested under compression individually. The specimens were monotonically loaded up to 3.45 and 6.90 MPa vertical pressure and then three fully reversed cycles with amplitudes ±0.35 and ±1.73 MPa were performed. In the second

stage, bearings were tested under combined compression and shear in pairs under a vertical pre-load equivalent to 3.45 and 6.90 MPa. Within the third stage, specimens were tested in low temperature shear test condition.

3.2 Bearing Types

Several samples of fiber mesh reinforced bearings were manufactured and tested. Results of these experimental studies were compared by the results of corresponding steel reinforced bearings. The test bearings consist of natural rubber with nominal stiffness of 60 Shore A.

Each type of bearing (Type w-x-y-z) is specified by four group of characters. The first character in each type shows the bonding condition in a way that "U" is used for unbonded bearings and "B" is used for bonded specimens. The second character in each type shows the reinforcement condition; such that "St" is used for steel reinforced and "Fb" for fiber mesh reinforced bearings. The third character represents the geometry of bearings in a way that "R" is for rectangular, "S300" for square bearing with side length of 300 mm and "S150" for square bearing with side length of 150 mm, "C200" for circular bearings with diameter of 200 mm and "C150" for circular bearings with diameter of 150 mm. The forth character "l" or "h" reflects the magnitude of shape factor such that "l" reffers to bearing with lower shape factor than "h" types in each case. For example "Type U-Fb-C200-l" refers to a unbonded FRP mesh reinforced circular bearing whose shape factor is less than "Type U-Fb-C200-h".

Bearings types "R", "S300" and "C200" were manufactured by Maurer Söhne Group and type "C150" and "S150" were manufactured by Ozdekan Rubber Industry.

Steel reinforced bearings were reinforced by "St 37" steel with technical specifications given in Table 3.1.

Table 3.1 Mechanical properties of "St 37" [28]

Modulus of elasticity (GPa)	200
Poisson ratio	0.3
Density ($\times 1000$ kg/m^3)	7.8
Tensile yield strength (MPa)	250
Tensile ultimate strength (MPa)	400

Fiber mesh reinforced elastomeric bearings used in this research have been manufactured by a similar vulcanization method used to manufacture reinforced steel bearings. It should be noted that during the manufacturing process no adhesives are used to bond the fiber mesh to internal rubber layers. This manufacturing process has also been used by Russo G. et al. [29]. A special type of fiber reinforcement needs to be selected to resist high vulcanization temperatures of 150°C to 200°C. Furthermore, availability of spaces between the wefts and warps of the reinforcing fiber grid are important to accommodate a better bonding between the adjacent rubber layers above and below the reinforcing layer during the vulcanization process. For this purpose, a bidirectional carbon fiber in the mesh form (0/90) and k-12 type is used. The mechanical and physical properties of CFRP are presented in Figure 3.1 and Table 3.2.
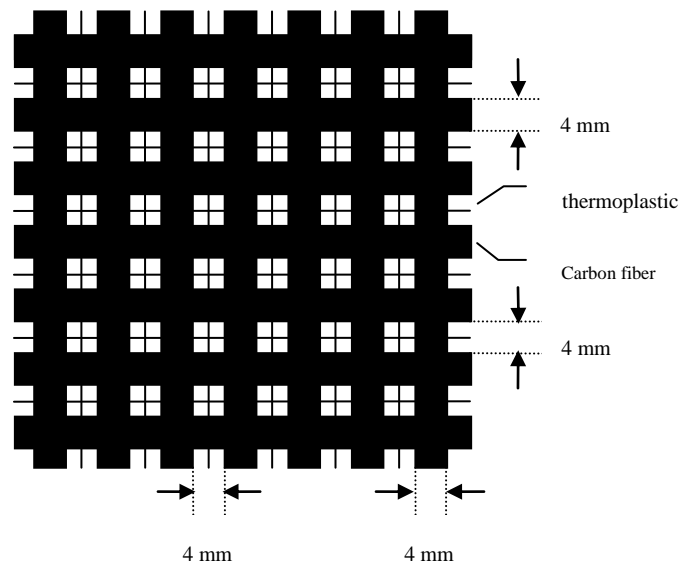
Figure 3.1 Bi-directional carbon fiber mesh

Table 3.2 Mechanical properties of carbon fiber provided by the supplier [30]

Tensile modulus of carbon fibers (GPa)	240
Poisson ratio	0.05
Areal weight (gr/m^2)	236
Net areal weight in carbon fiber (gr/m^2)	208
Weaving style	0/90-Plain
Warp	12K carbon fiber (44%) + thermoplastic (6%)
Weft	12K carbon fiber (44%) + thermoplastic (6%)
Tensile strength (MPa)	4900
Elongation at break (%)	2.0
Thickness (μm)	125 ± 5

Details of both fiber and steel reinforced bearings are presented in Tables 3.3-3.8.

Also, details of bearings in a schematic manner are presented in Appendix A.

Table 3.3 Type "R" test specimens

Type	Length mm	Width mm	Height mm	Shape factor	Reinforcement Layers $n \times t_{f \text{ or } s}$ [I]	Elastomer thickness (mm)		Cover (5 mm)
						Top & Bottom	Middle $n \times t_r$ [II]	
U-Fb-R-l	400	250	56	9.28	6×1	5	5×8	No
U-Fb-R-h	400	250	41	14.85	6×1	5	5×5	No
U-St-R-l	400	250	62	9.28	6×2	5	5×8	Yes
U-St-R-h	400	250	47	14.85	6×2	5	5×5	Yes

[I] n: Number of reinforcing layer & $t_{f \text{ or } s}$: Approximate thickness of reinforcing layer

[II] n: Number of individual middle elastomer layers & t_r: Thickness of individual middle elastomer layer

Table 3.4 Type "S300" test specimens

Type	Length mm	Width mm	Height mm	Shape factor	Reinforcement Layers $n \times t_{f \text{ or } s}$	Elastomer thickness (mm)		Cover (5 mm)
						Top & Bottom	Middle $n \times t_r$	
U-Fb-S300-l	300	300	46	12.08	6×1	5	5×6	No
U-Fb-S300-h	300	300	41	14.5	6×1	5	5×5	No
U-St-S300-l	300	300	52	12.08	6×2	5	5×6	Yes
U-St-S300-h	300	300	47	14.5	6×2	5	5×5	Yes

Table 3.5 Type "C200" test specimens

Type	Diameter mm	Height mm	Shape factor	Reinforcement Layers $n \times t_{f \text{ or } s}$	Elastomer thickness (mm)		Cover (5 mm)
					Top & Bottom	Middle $n \times t_r$	
U-Fb-C200-l	200	43	4.75	3×1	10	2×10	No
U-Fb-C200-h	200	59	9.5	9×1	5	8×5	No
U-St-C200-l	200	46	4.75	3×2	10	2×10	Yes
U-St-C200-h	200	68	9.5	9×2	5	8×5	Yes

Table 3.6 Type "S150" test specimens

Type	Length mm	Width mm	Height mm	Shape factor	Reinforcement Layers $n \times t_{f \text{ or } s}$	Elastomer thickness (mm)		Cover (5 mm)
						Top & Bottom	Middle $n \times t_r$	
U-Fb-S150-l	150	150	59	8.75	11×1	4	10×4	No
U-Fb-S150-h	150	150	59	17.5	19×1	2	18×2	No
U-St-S150-l	150	150	59	8.75	11×1	4	10×4	Yes
U-St-S150-h	150	150	59	17.5	19×1	2	18×2	Yes

Table 3.7 Type "C150" test specimens

Type	Diameter mm	Height[III] mm	Shape factor	Reinforcement Layers $n \times t_{f\ or\ s}$	Elastomer thickness (mm)		Cover (5 mm)
					Top & Bottom	Middle $n \times t_r$	
B-Fb-C150-l	150	79	8.75	11×1	4	10×4	Yes
B-Fb-C150-h	150	79	17.5	19×1	2	18×2	Yes
B-St-C150-l	150	79	8.75	11×1	4	10×4	Yes
B-St-C150-h	150	79	17.5	19×1	2	18×2	Yes

3.3 Performance Parameters of Elastomeric Bearings

Two important parameters of elastomeric bearings are vertical and horizontal stiffness. Vertical stiffnes was obtained from compression test and is defined as the slope of the straight line interpolating the cyclic part of compression test. This vertical stiffness is referred as average stiffness of the specimen or K_{ave}^{v}.

Results of horizontal shear test were used to calculate the horizontal stiffness of the bearings. Two different definitions of horizontal stiffness were used while calculating the horizontal stiffness of bearings in all of the shear tests.

A simple calculation of shear stiffness based on the values of peak force and displacement is defined as [31]:

$$K_{eff}^{h} = \frac{\left|F^{+}\right| + \left|F^{-}\right|}{\left|d^{+}\right| + \left|d^{-}\right|} \tag{3.1}$$

where d^{+} and d^{-} are the maximum positive and maximum negative test displacements, respectively, and F^{+} and F^{-} are the maximum positive and maximum negative forces at instance of displacements d^{+} and d^{-}, respectively. This stiffness is interpreted as the effective or overall stiffness of the bearing during the test. This

---

[III] These values include the thickness of top and bottom steel end plates (2×10 mm)

51

stiffness is used to calculate the stored or elastic energy of the bearings during cyclic tests.

Another stiffness, K_{av}^h, is defined as the slope of the straight line interpolating the hysteresis loops obtained during the tests. This stiffness is referred as the average stiffness of the specimens during cyclic reversals.

The hysteresis loops were also analyzed to obtain the equivalent viscous damping ratio of the bearing for each test. A hysteresis loop represents the plot of force against displacement, and the area contained within such a loop represents the energy dissipated by the bearing.

The equivalent viscous damping ratio exhibited by the bearing is evaluated in the usual structural engineering fashion [32]

$$\xi = \frac{W_d}{4\pi W_s} \tag{3.2}$$

where W_d represents the dissipated energy per cycle which is equal to the enclosed area by hysteresis loop and W_s corresponds to stored or elastic energy defined by the following formula:

$$W_s = K_{eff}^h \frac{d_{max}^2}{2} \tag{3.3}$$

Here, d_{max} is the average of positive and negative maximum displacements and is defined as

$$d_{max} = \frac{\left|d^+\right| + \left|d^-\right|}{2} \tag{3.4}$$

The linear viscous model assumes that the energy dissipated in each cycle is linear with the frequency and quadratic with the displacement [22].

3.4 Experimental Study

To obtain the mechanical properties of the bearings, experimental study was carried out in Structural Engineering Laboratory of Middle East Technical University. The influence of fiber flexibility on mechanical properties of fiber mesh reinforced elastomeric bearings, such as the vertical and horizontal stiffness, was studied to verify if it is possible to produce a fiber mesh reinforced bearing that matches the behavior of a steel-reinforced one.

Experimental testing includes; compression test, horizontal shear test and low temperature shear test

3.4.1 Compression Test (Vertical Test)

This test was performed at two different pre-load magnitudes. At first, specimens were monotonically loaded up to 3.45 MPa vertical pressure, and then three fully reversed cycles with amplitude ±0.35 MPa were performed. In the final stage the specimens were monotonically unloaded. The aim of this test was to evaluate the performance of the bearings under lower values of vertical load and obtain their vertical stiffness. In the second step of the compression test, the specimens were monotonically loaded to 6.90 MPa pre-load and then three fully reversed cycles were applied with amplitude ±1.73 MPa. At the end, the specimens were unloaded. This stage of the compression test studied the vertical stiffness of the bearings at higher values of vertical load.

3.4.2 Combined Compression and Shear Test

In these test, bearings were tested in shear in pairs under a constant vertical load equivalent to a pressure of 6.90 and 3.45 MPa. They were tested in cyclic shear, by applying three fully reversed cycles at three different strain levels: 25%, 50% and 100% defined based on the total rubber thickness. Horizontal stiffness of the bearings and their equivalent viscous damping ratio was calculated by analyzing the hysteresis loops obtained during this test.

3.4.3 Low Temperature Shear Test for Bridge Bearings

Since elastomeric bearings become stiffer as they are subjected to low temperatures, the forces on both bridge piers and bearings increase, which, in turn, may damage the bridge or cause the slip of the bearings and/or girders out of their positions. For this reason, low temperature behavior of bearings that will be used in a bridge constructed in cold climates must be determined before installation. Bridge bearings should be subjected to the low temperature shear tests defined in AASHTO M251-97 specifications [33]. This test requires that at least two pads per lot be tested. The bearing is contained at -29°C for 96 hr. The conditioned bearing is tested in open air with a compressive stress of 3.45 MPa applied. The bearing is then pushed to 25-percent maximum shear strain and held at this strain for 15 min. After this period, the shear stress is measured. The test is required to be completed within 30 min after the specimen is removed from the cold environment. For a bearing constructed with 50 durometer elastomer, the measured stress at 25-percent strain after 15 minutes must be less than 0.35 MPa for neoprene and 0.21 MPa for natural rubber.

3.5 Test Setup

This section summarizes the test setup used in the experimental studies. The tests were carried out in the Structural and Material Research Laboratories of Middle East Technical University, Ankara, Turkey.

3.5.1 Horizontal Shear Test Setup

Seismic isolator testing system available in Structural Engineering Laboratory of METU has been designed to test the bearings in both horizontal and vertical directions. This system is capable of conducting in-plane horizontal cyclic loading tests, as shown in Figure 3.2. This machine can test a pair of elastomeric bearing by applying vertical pressure and keeping it constant at a desired level, then implementing cyclic displacement control loading in horizontal direction. Load

capacity of testing system is about 3000 kN in vertical direction and 600 kN in horizontal direction.

(a)

A: push-pull steel plate

B: bearings to be tested (two bearings are tested)

C: hydraulic cylinder (for application of vertical loads)

D: hydraulic cylinder (for application of horizontal loads)

E: load cell in the vertical direction

F: load cell in the horizontal direction

G: LVDT
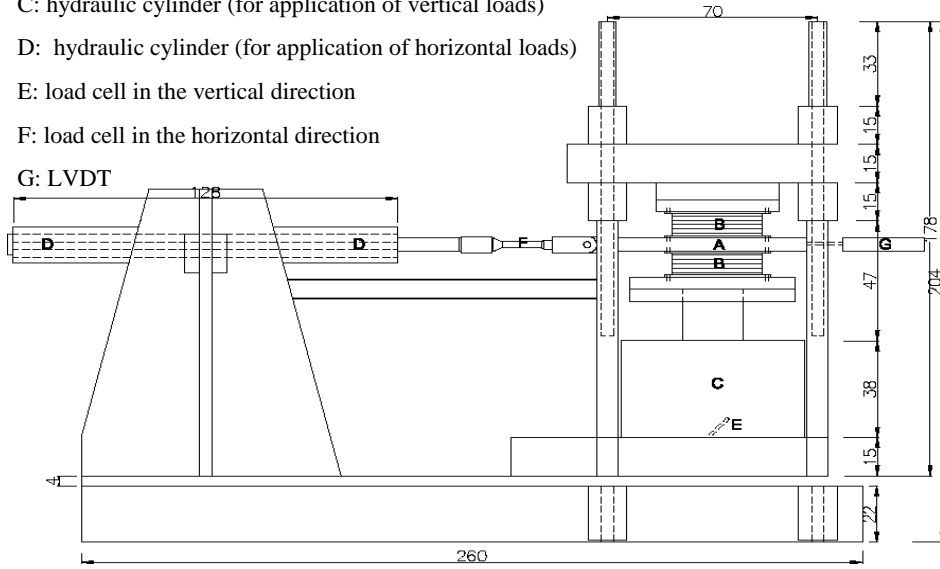
(b)

Figure 3.2 (a) General View of the horizontal shear Test Equipment

(b) Schematic Layout (Dimensions: cm) [34]

As it is clear from the Figure 3.2 experimental setup is composed of two distinct main loading systems in horizontal and vertical directions; loading system in vertical direction is used for applying the desired level of pressure and loading system in horizontal direction is capable of doing displacement control tests. Loading system in vertical direction with its adjustable upper plate, provides testing opportunity for different type and size of bearings. Horizontal loading system is capable of sliding on rails located on vertical support plates to adjust the inserted horizontal load in accordance with the bearing's height. Also, horizontal loading system can be relocated on bottom support plates to increase the horizontal loading capacity.

3.5.1.1 Instrumentation

Figure 3.3 shows the loading and measuring systems used for testing of the bearings. Two LVDTs placed on middle sliding plate were used to measure the horizontal displacement of the bearing during the shear test. Total displacement in vertical direction was measured by means of four electronic comparators inserted in the four corners of the bottom plate of the testing system.

Figure 3.3 Loading and measuring systems

3.5.1.2 Data Acquisition

Data acquisition system were run by a PC Windows-based control and acquisition program called StrainSmart 6000 developed by Vishay Precision Group, Wendell, USA. System 6000 features data acquisition rates of up to 10,000 samples per second per channel. This system accepts up to 20 plug-in input cards (one channel per card and up to 20 channels per unit) and supports software identification and setup of each type of plug-in card. In all tests StrainSmart data acquisition system was used to monitor and force-feedback signals [35]. Figure 3.4 shows this acqusition system connected to testing machine.

(a)

(b)

Figure 3.4 (a) Data aquisition system

(b) Data aquisition system connected to testing system

3.5.2 Vertical Compression Test Setup

Vertical tests have been performed by dynamic tension and compression test machine named MTS Landmark Servo-Hydraulic Test System as shown in Figure 3.5. By integrating the latest in MTS servo-hydraulic technology, Flex Test controls, MTS software and a complete selection of accessories, these systems can be easily configured for a range of static and dynamic tests — everything from fatigue life and fracture growth studies to tension, bending and compression tests. This machine can impose a maximum force of 250 kN and tests can be conducted either force control or displacement control. The data acquisition and control of the machine are run by a PC Windows-based control and acquisition program called Flex Test 40 Digital Controller developed by MTS Systems Corporation, Minnesota, USA [36].

Figure 3.5 Vertical compression test setup

3.5.3 Data Processing

Vertical load and vertital displacement between top and bottom end plates were used to characterize the behavior of the specimens during the compression test. In the case of horizontal test, horizontal load and the horizontal displacement of the middle sliding plate were used to characterize the behavior of bearings.

A linear regression analysis was used to calculate the average stiffness of the bearing during cyclic reversals. The average stiffness was calculated for the vertical and horizontal directions. For both directions the data from the corresponding cyclic test were used.

A set of program for the MATLAB 7.11.0.584 (R2010 b) environment and also Microsoft Office Excel 2010 were created to process the data and to plot results in accordance with the procedure described above.

CHAPTER 4

RESULTS OF COMBINED COMPRESSION AND SHEAR TESTS

4.1 Introduction

In this chapter, results of combined compression and shear tests along with testing process are presented. Evaluation of the results is also given in the foregoing sections. Before discussing the tests conducted on bearings, it is important to determine the mechanical properties of materials. Therefore, the next part of this section covers the experimental test on fiber reinforcement mesh.

4.2 Material Test

Typical properties of Carbon Fiber Reinforced Polymer (CFRP) mesh provided by supplier is only for guidance and general information. It is recommended by supplier not to use these data for design purposes. Tensile properties of carbon fiber mesh were determined in accordance with the method described in 'standard test method for tensile properties of polymer matrix composite materials under the jurisdiction of ASTM committee [37]'. Five specimens were tested under tension using displacement control method. Tensile strains measured by two bonded strain gages and applied loads were recorded. Elastic modulus of carbon fiber under the test condition described in this standard was determined to be 238 GPa (the value given by manufacturer was 240 GPa). Figure 4.1 illustrates the specimens and strain gages used in this test. In deriving the vertical stiffness formulation of fiber reinforced bearing by J.Kelly a homogeneous reinforcing fiber sheet with an equivalent

thickness of t_f and elastic modulus of E_f was assumed [27]. The theoretical equations for vertical stiffness were developed [27] for fiber sheet applications. However, in this research fiber mesh openings are filled and bonded with rubber during vulcanization to have a composite behavior. Therefore, tensile tests have been conducted on composite sections consisting of fiber mesh and rubber. 300 x 50 x 3-mm-thick plaque specimens of rubber reinforced by carbon fiber mesh were used to determine the elastic modulus of this composite section. These plaques were manufactured with the same vulcanization process as used in manufacturing of bearings. Elastic modulus of this specimen was determined to be 35 GPa. A schematic view of this reinforced rubber compound is shown in Figure 4.2.
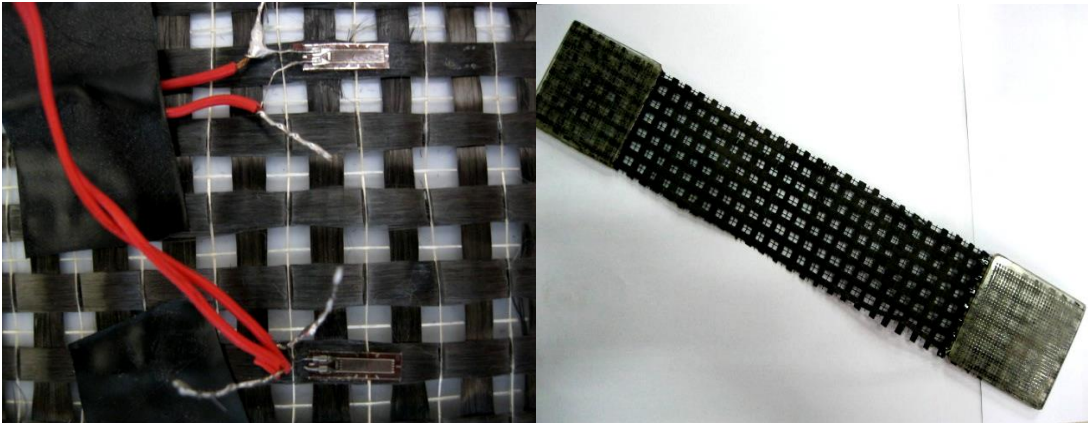
Figure 4.1 Carbon fiber mesh specimens
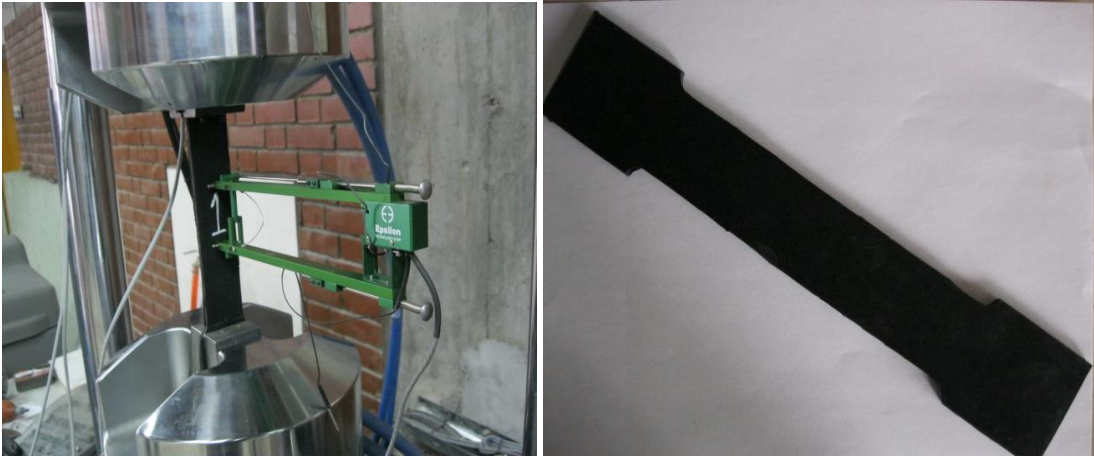
Figure 4.2 Composite rubber sections under tensile test

According to the method described in [37], tensile chord modulus of elasticity is defined as

$$E^{chord} = \Delta\sigma / \Delta\varepsilon \qquad (4.1)$$

where

E^{chord} [GPa]: tensile chord modulus of elasticity

$\Delta\sigma$ [MPa]: difference in applied tensile stress between the two strain points given in Table 3 of [37] as

ε_1=1000 με (start point)

ε_2=3000 με (end point)

$\Delta\varepsilon$: difference between the two strain points given above (nominally 2000 με)

Figures 4.3 and 4.4 present the strain-stress diagrams for carbon mesh and composite plaque, respectively.
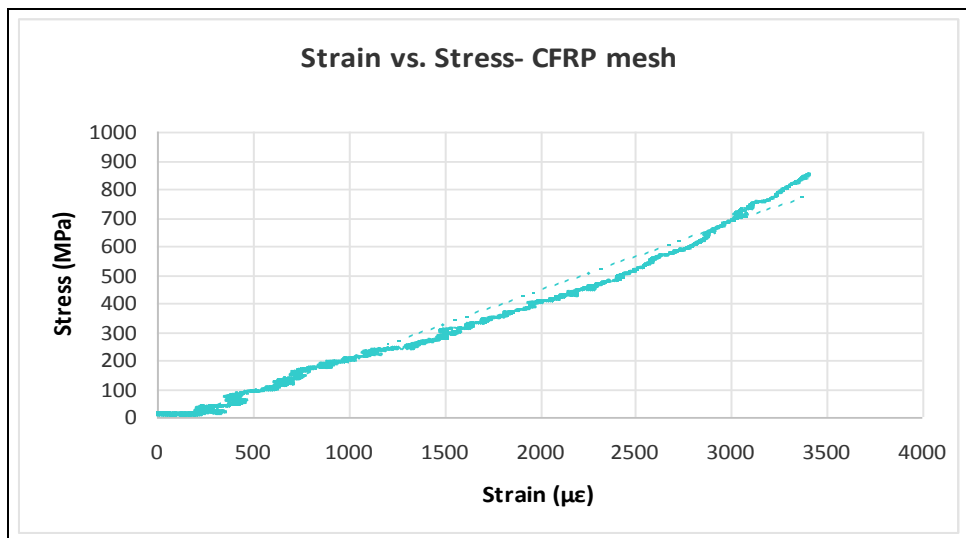
Figure 4.3 Tensile stress vs. strain diagram for CFRP mesh
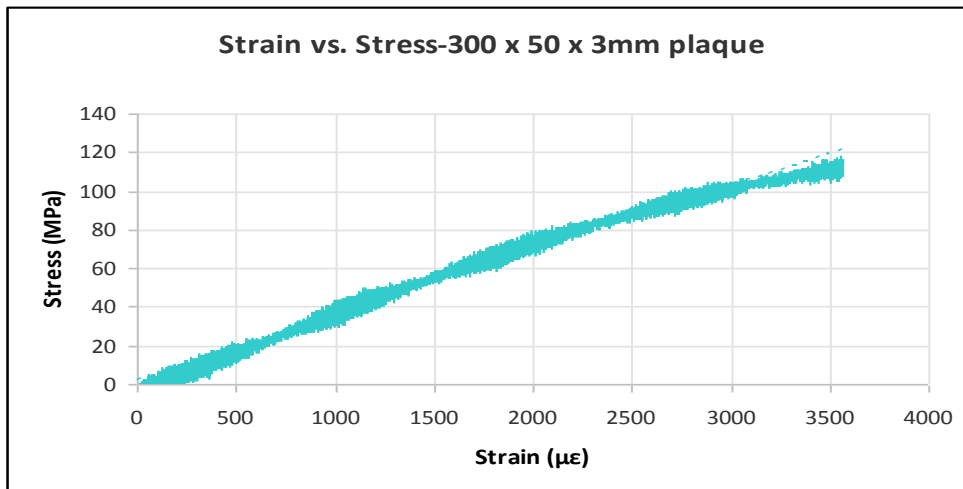
Figure 4.4 Tensile stress vs. strain diagram for 300*50*3 mm plaque

4.3 Combined Compression and Shear Test

This test was conducted in Structural Engineering Labratory of Middle East Technical University. Specimens were subjected to three reverse cyclic loading at

1. 25% t_r

2. 50% t_r

3. 100% t_r

where t_r is total thickness of the elastomer in each bearing. Effective and average horizontal stiffness of bearings and also other parameters such as energy dissipated per cycle, stored energy per cycle, equivalent viscous damping coefficient were calculated from the hysteresis loops obtained during this test. Two full size specimens were inserted in seismic base isolation testing system and vertical pressure at target level was applied. During the first step 3.45 MPa vertical pressure was applied and kept constant until the end of the test. Then 9 cycles of horizontal loading according to target horizontal displacements were performed. This test is a displacement control test and also a constant value of vertical pressure is applied throughout the test. The next level of vertical pressure is 6.90 MPa and all the

64

specimens were tested under this pressure. The loading history of the horizontal test for type "R" and "S300" bearing is presented in Figure 4.5. Figure 4.6 depicts the input signal for type "C200", "S150" and "C150" bearings. The average speed of loading in type "R" and "S300" bearings was approximately 4 mm/sec and speed of loading for other bearings was around 6 mm/sec. Different seismic isolation systems have also been tested using the same setup by Ozkaya et al. [38] and Pinarbasi et al. [39]. The functions of the testing system are also defined in BS EN 1337-3:2005 [40]. Results of these tests for both fiber and steel reinforced bearings under two levels of vertical pressure are given in Appendix B.

It is important to note that the mechanical properties of an elastomeric bearing depend on its loading history. During the first several cycles, the bearing has higher effective horizontal stiffness and damping (scragging effect). By the third cycle, however, the response of the bearing stabilized [41] and the responses presented in this study are stablized response of bearing.
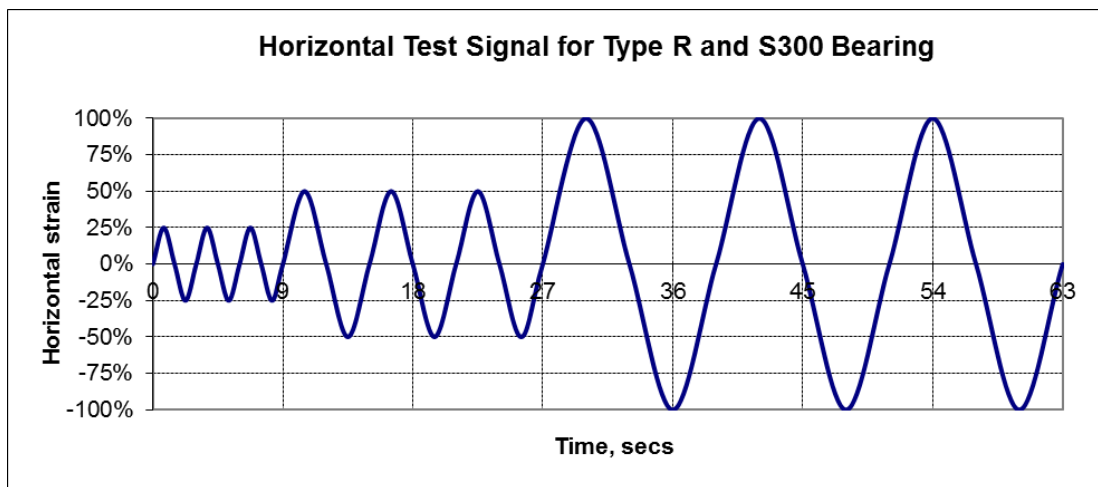
Figure 4.5 Input signal for horizontal shear test with 3.45 MPa and 6.90 MPa vertical pre-load
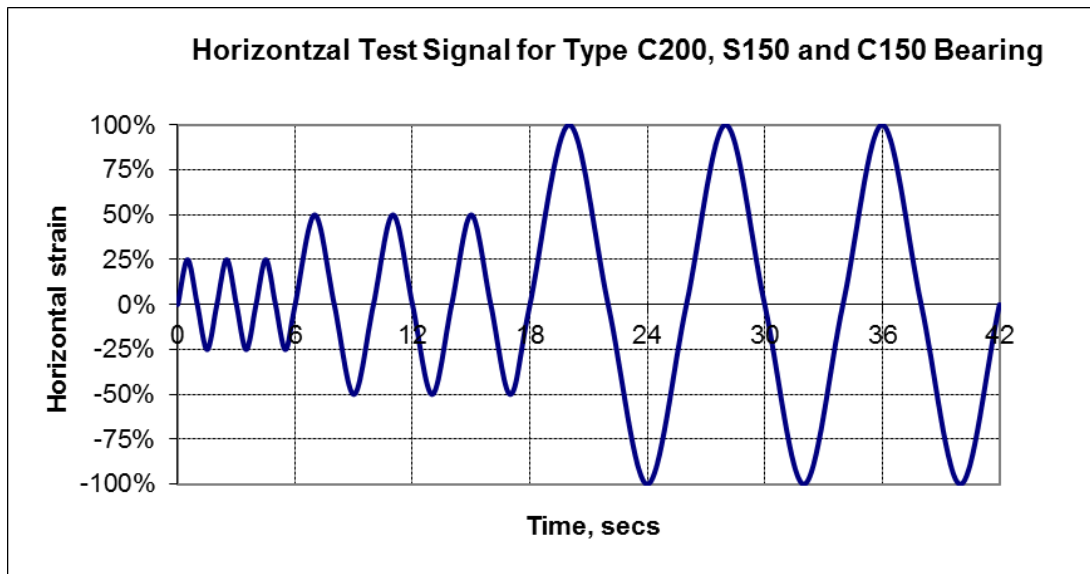
Figure 4.6 Input signal for horizontal shear test with 3.45 MPa and 6.90 MPa vertical pre-load

In unbonded specimens, according to [40], metal strips were used to prevent the slippage of the bearings during the testing whereas in bonded specimens anchorage plates were screwed to testing system. Figure 4.7a shows the deformed shape of fiber-reinforced bearing at 100% strain level. Figure 4.7b and 4.8 illustrates the insertion of unbonded and bonded specimens in testing machine, respectively. Figure 4.9 displays a view of "B-St-C150-l" under 100% shear strain level and action of 6.90 MPa vertical pre-load.
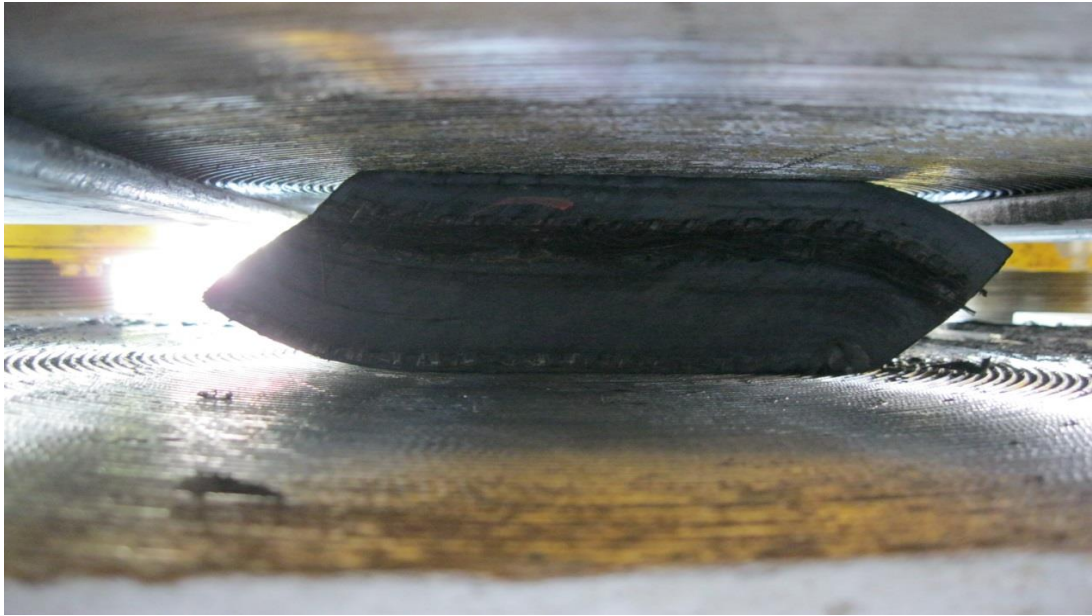
(a)
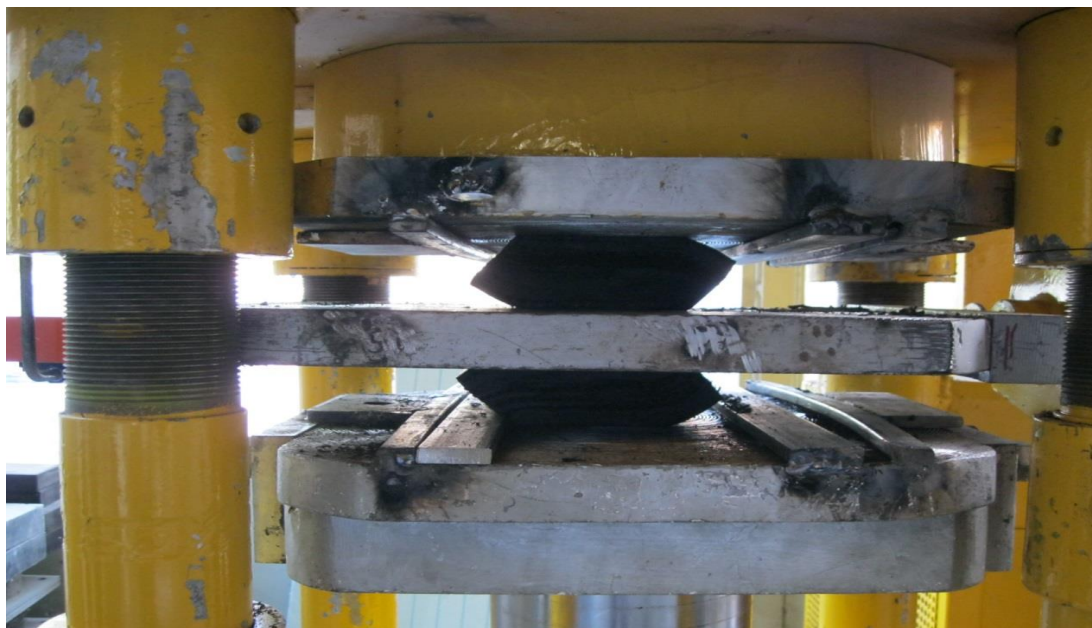
(b)

Figure 4.7 Horizontal shear test in progress, a) U-Fb-S150-l under 100% shear strain, b) U-Fb-S150-l and metal strips to prevent slippage in unbonded specimens
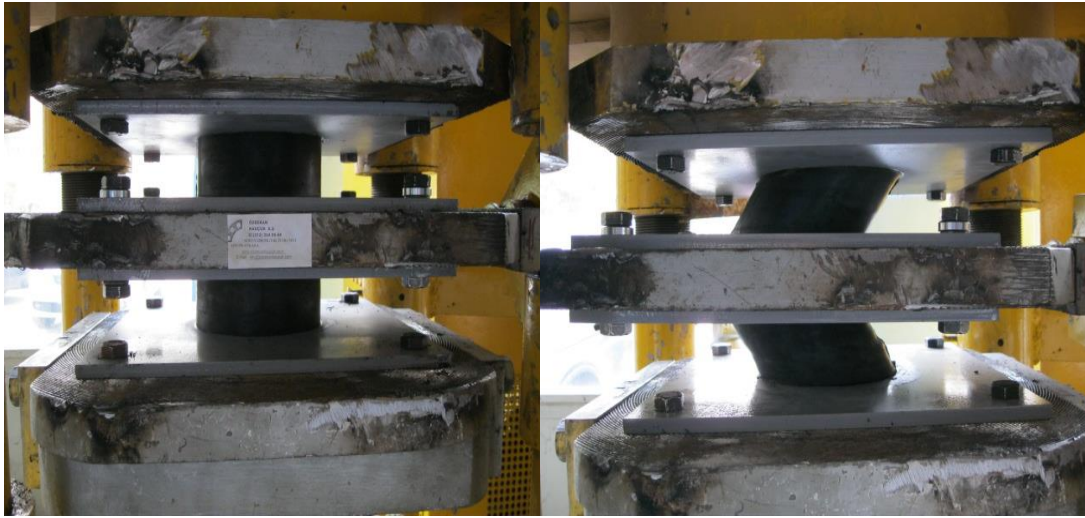
(a)   (b)

Figure 4.8 Horizontal shear test in progress, a) B-Fb-C150-l under vertical pressure,
b) B-Fb-C150-l under vertical pressure and 100% shear strain

Figure 4.9 B-St-C150-l under vertical pressure and 100% shear strain

Results of horizontal shear test are used to calculate the shear modulus of the bearings. There is no analytical study to investigates the effects of fiber flexibility on horizontal stiffness of the bearing. In this dissertation results of experimental tests were used to investigate this effect. Shear modulus of both fiber and steel reinforced bearings under different strain levels are compared. These comparisons reveals the effect of fiber flexibility on horizontal stiffness of the bearings.

4.3.1 Horizontal Behavior of Bearing

Summary of the horizontal test results is presented in Tables 4.1-4.4. Some of the hysteresis loops obtained during the tests are presented in Figure 4.10 as horizontal force versus horizontal displacement curves for two different levels of vertical pressure. Horizontal shear test results revealed that horizontal stiffness of bearings is affected by the amplitude of lateral displacement as well as vertical pre-load. Bearings subjected to higher levels of lateral displacements have significantly low lateral stiffness compared to the bearing subjected to lower levels of lateral displacements. Furthermore, decrease in vertical pre-load also results in decrease in the lateral stiffness. In general, elastic bending of reinforcing plates would decrease the lateral stiffness of the bearing. An increase in compression due to vertical pre-load would decrease the elastic bending of reinforcing layers and an increase in lateral displacement amplitude would amplify this effect.

4.3.1.1 Effect of Fiber Flexibility on Equivalent Viscous Damping of Bearings

Table 4.1 presents the values of damping ratios for both types of bearings. The main source of energy dissipation in elastomeric bearing without lead core is the inherent properties of rubber compounds. Since there is not any other source of energy dissipation in bearing without lead core, the damping values in these bearings depends mostly on the rubber properties. As it was expected, there is not that much of difference between the damping values of fiber and steel reinforced bearings and these values are more or less equal.

Figures 4.11-4.15 display the equivalent viscous damping ratios of steel reinforced bearings over the fiber reinforced ones in different strain levels. The fourth column in these charts presents the ratio of average equivalent viscous damping (average of equivalent viscous damping in three strain levels) of steel reinforced bearings over the fiber reinforced ones. The maximum difference in average damping of bearings is about 22%. Thus, it can be concluded that there is not that much of difference in damping capacities of fiber mesh and steel reinforced bearings and damping capacity in these types of bearings mostly depends on the inherent properties of rubber compound.

(a) (b)
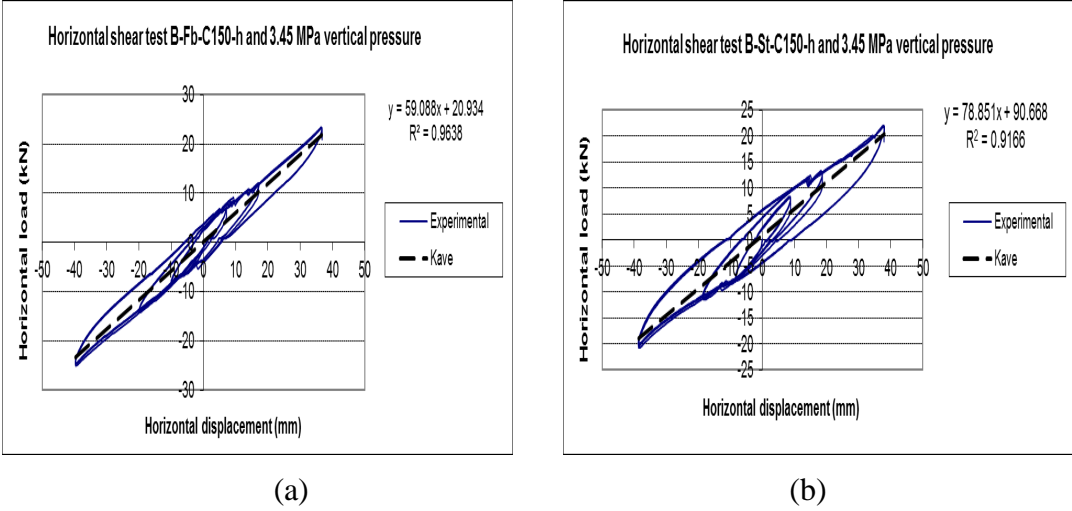
Figure 4.10 Horizontal vs. displacement cyclic curves for some of bearings
(a) B-Fb-C150-l under 3.45 MPa vertical load and **(b)** B-St-C150-l under 3.45 MPa vertical load

70

Table 4.1 Equivalent Viscous Damping Values

Type & Damping Ratio	Equivalent Viscous Damping, ξ%							
	Vertical Pressure (MPa)							
	3.45				6.90			
	Strain Level (%)				Strain Level (%)			
	25	50	100	Average	25	50	100	Average
U-St-R-l	11.6	10.8	13.6	12	8.6	10	9.6	9.4
U-Fb-R-l	10.7	10.7	10.9	10.8	7.5	8.2	9.8	8.5
ξ_s / ξ_f	**1.09**	**1.01**	**1.25**	**1.11**	**1.15**	**1.23**	**0.98**	**1.11**
U-St-R-h	10.2	13.2	12.5	11.97	6.7	9.2	10.9	8.93
U-Fb-R-h	13.4	16.6	15.0	15.0	7.4	12.1	13.2	10.9
ξ_s / ξ_f	**0.76**	**0.79**	**0.83**	**0.80**	**0.91**	**0.76**	**0.83**	**0.82**
U-St-S300-l	8.4	11.6	13.2	11.07	5.8	8.8	8.7	7.7
U-Fb-S300-l	11.7	10.1	8.7	10.2	6.5	10.9	7.9	8.4
ξ_s / ξ_f	**0.72**	**1.15**	**1.51**	**1.09**	**0.90**	**0.81**	**1.09**	**0.92**
U-St-S300-h	7.4	11.3	14.3	11.0	5.3	7.8	12.4	8.5
U-Fb-S300-h	9.4	10.4	8.9	9.6	6	9.1	7.6	7.6
ξ_s / ξ_f	**0.79**	**1.09**	**1.59**	**1.15**	**0.88**	**0.86**	**1.62**	**1.12**
U-St-C200-l	5.8	8.5	10.2	8.2	5.2	6.3	7.8	6.4
U-Fb-C200-l	6.9	8.5	9.2	8.2	5	5.8	7.2	6.0
ξ_s / ξ_f	**0.84**	**1.00**	**1.11**	**1.00**	**1.04**	**1.09**	**1.09**	**1.07**
U-St-C200-h	8.5	6.9	7.7	7.7	5.1	5	6.3	5.5
U-Fb-C200-h	6	7.8	8	7.3	5.7	5.5	7.5	6.2
ξ_s / ξ_f	**1.42**	**0.89**	**0.97**	**1.06**	**0.88**	**0.90**	**0.84**	**0.88**
U-St-S150-l	10.1	11.4	10.5	10.7	9.9	8.8	9.9	9.5
U-Fb-S150-l	9.8	9.3	8.4	9.2	9.8	8.6	8	8.8
ξ_s / ξ_f	**1.03**	**1.23**	**1.26**	**1.16**	**1.01**	**1.02**	**1.23**	**1.08**
U-St-S150-h	9.7	10.3	8.8	9.6	9.7	8.1	9.5	9.1
U-Fb-S150-h	10.8	10.1	9.7	10.2	10	8.7	8.4	9.0
ξ_s / ξ_f	**0.90**	**1.02**	**0.91**	**0.94**	**0.98**	**0.93**	**1.14**	**1.01**
B-St-C150-l	9.9	9.6	9.2	9.6	9.2	8.4	9	8.9
B-Fb-C150-l	10.8	9.6	7.4	9.3	9.5	7.4	7.7	8.2
ξ_s / ξ_f	**0.91**	**1.00**	**1.24**	**1.03**	**0.97**	**1.13**	**1.17**	**1.08**
B-St-C150-h	11.9	11.6	10	11.2	10.1	8.2	10.5	9.6
B-Fb-C150-h	11.6	11.4	10.3	11.1	10.1	8.1	10.3	9.5
ξ_s / ξ_f	**1.04**	**1.02**	**1.20**	**1.01**	**1.00**	**1.01**	**1.02**	**1.01**
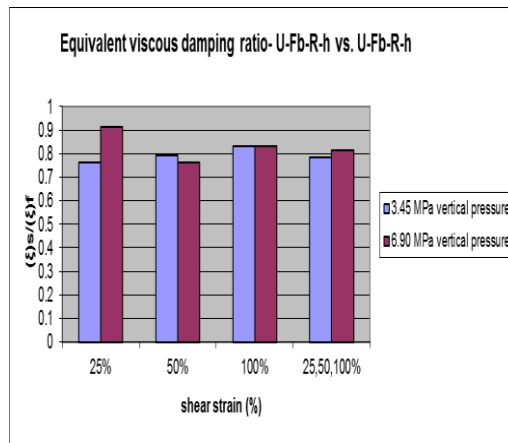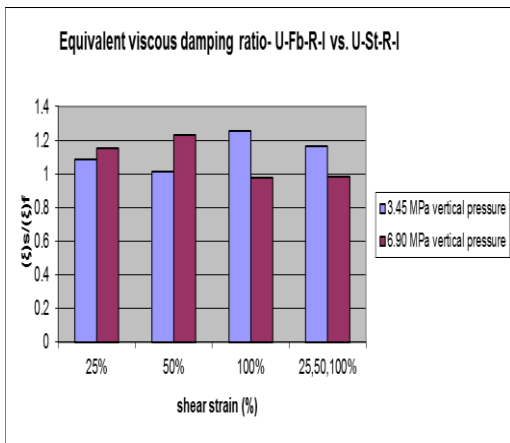
Figure 4.11 Comparison of equivalent viscous damping-Type R bearings
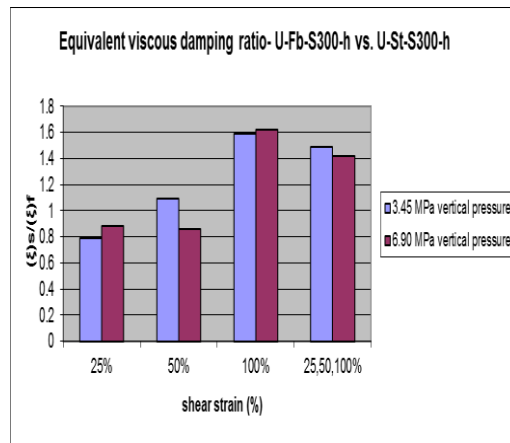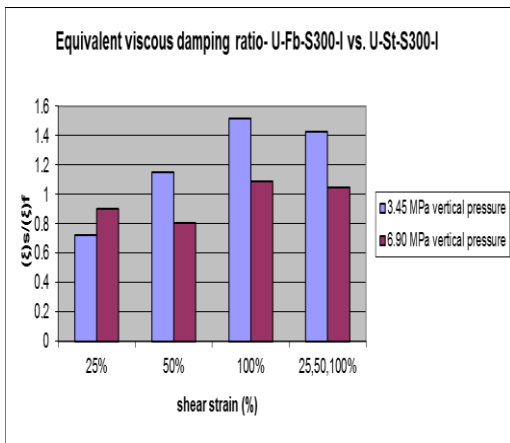
Figure 4.12 Comparison of equivalent viscous damping-Type S300 bearings
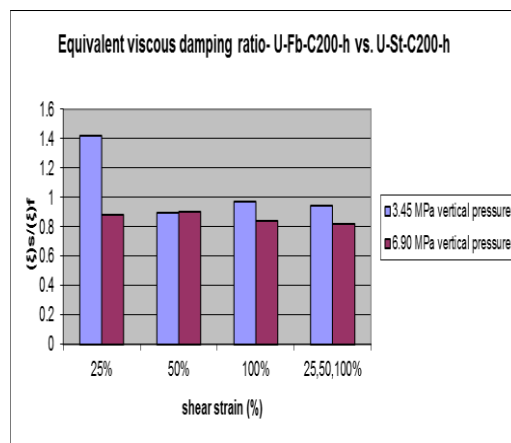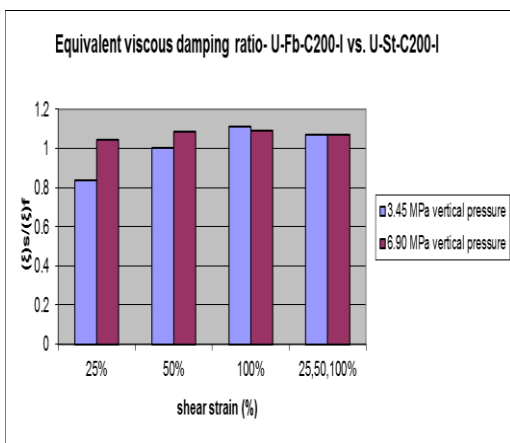
Figure 4.13 Comparison of equivalent viscous damping-Type C200 bearings
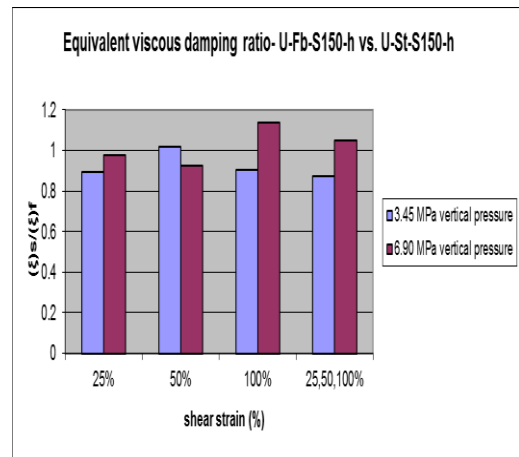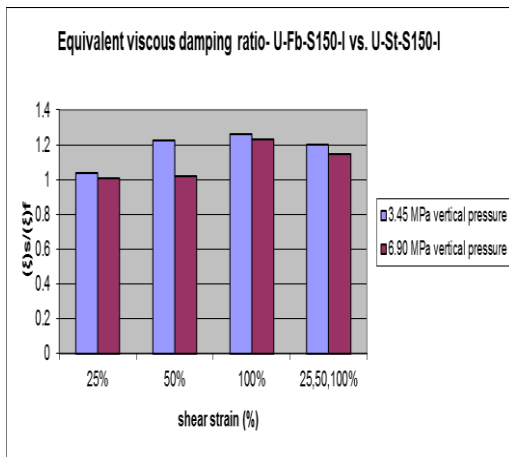
Figure 4.14 Comparison of equivalent viscous damping-Type S150 bearings
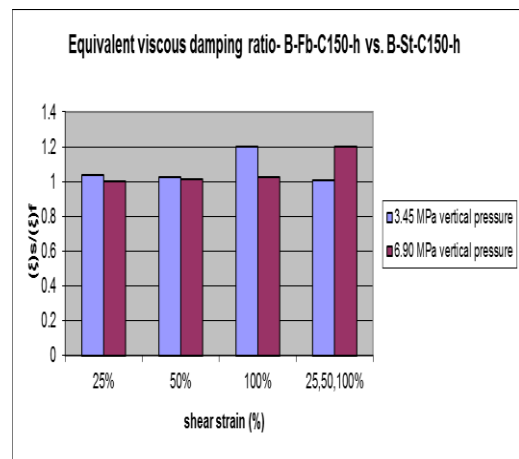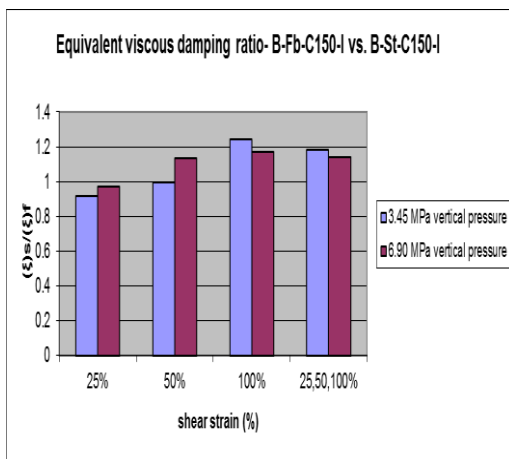
Figure 4.15 Comparison of equivalent viscous damping-Type C150 bearings

4.3.1.2 Effect of Fiber Flexibility on Horizontal Stiffness of Bearings

As discussed in Chapter 3, two different definitions of horizontal stiffness were used to evaluate the shear behavior of bearings. Average horizontal stiffness of bearings is used to calculate the shear modulus of bearings in different strain levels. Effective stiffness of bearings (calculated from horizontal shear test results) is used to calculate the energy dissipation capacity and shear stress in tested specimens.

There are different test methods for calculating the shear modulus of the bearings in different standards. In this dissertation conventional shear modulus of bearing is calculated from the measured average stiffness in each strain level. The average shear modulus of the test specimens during the 9 cycles are also determined and compared. Tables 4.2-4.3 present and compare the values of effective and average horizontal stiffness. Furthermore, shear modulus of specimens in different strain levels are presented and compared in Table 4.4. Figures 4.16-4.35 compare the values of shear modulus and shear stress in bearings. It can be concluded from the figures that an increase in vertical pre-load resulted in an increase in shear modulus. Also as strain level increases, shear modulus of bearings decreases. It should be noted that elastic bending of reinforcing fibers may occur and that, in this case, the calculated modulus would be lower than the corresponding value in steel reinforced ones.

Table 4.2 Effective Stiffness Values

Type & Stiffness Ratio	Effective Stiffness K^h_{eff} (kN/m)					
	Vertical Pressure (MPa)					
	3.45			6.90		
	Strain Level(%)			Strain Level(%)		
	25	50	100	25	50	100
U-St-R-l	2221	1866	1619	2363	1995	1822
U-Fb-R-l	2383	1931	1633	2730	2187	1827
K_s/K_f	**0.93**	**0.97**	**0.99**	**0.86**	**0.91**	**0.99**
U-St-R-h	3438	2725	2387	3787	3005	2633
U-Fb-R-h	3674	2708	2278	4164	3326	2663
K_s/K_f	**0.94**	**1.01**	**1.05**	**0.91**	**0.90**	**0.99**
U-St-S300-l	2519	2086	1784	2772	2307	2133
U-Fb-S300-l	2347	2053	1865	2757	2296	2080
K_s/K_f	**1.07**	**1.02**	**0.96**	**1.01**	**1.01**	**1.02**
U-St-S300-h	2962	2420	2035	3270	2755	2420
U-Fb-S300-h	2737	2256	2135	3180	2602	2374
K_s/K_f	**1.08**	**1.07**	**0.95**	**1.03**	**1.06**	**1.02**
U-St-C200-l	944	762	657	918	793	707
U-Fb-C200-l	811	656	548	898	751	617
K_s/K_f	**1.16**	**1.16**	**1.20**	**1.02**	**1.06**	**1.15**
U-St-C200-h	669	559	507	716	609	562
U-Fb-C200-h	582	472	371	615	508	395
K_s/K_f	**1.15**	**1.18**	**1.37**	**1.16**	**1.20**	**1.42**
U-St-S150-l	570	440	429	595	472	445
U-Fb-S150-l	464	358	306	485	375	321
K_s/K_f	**1.23**	**1.23**	**1.40**	**1.22**	**1.25**	**1.39**
U-St-S150-h	725	581	558	769	612	537
U-Fb-S150-h	543	414	313	535	415	323
K_s/K_f	**1.33**	**1.40**	**1.78**	**1.44**	**1.47**	**1.6**
B-St-C150-l	458	362	311	476	384	328
B-Fb-C150-l	373	303	269	426	339	285
K_s/K_f	**1.23**	**1.19**	**1.16**	**1.12**	**1.13**	**1.15**
B-St-C150-h	547	456	410	581	492	420
B-Fb-C150-h	442	349	313	484	393	324
K_s/K_f	**1.24**	**1.30**	**1.31**	**1.20**	**1.25**	**1.30**

Table 4.3 Average Stiffness Values

Type & Stiffness Ratio	Average Stiffness K^h_{ave} (kN/m)							
	Vertical Pressure (MPa)							
	3.45				6.90			
	Strain Level(%)				Strain Level(%)			
	25	50	100	25, 50, 100	25	50	100	25, 50, 100
U-St-R-l	2141	1812	1539	1493	2319	1976	1790	1775
U-Fb-R-l	2219	1880	1584	1556	2640	2158	1770	1750
K_s/K_f	**0.96**	**0.96**	**0.97**	**0.95**	**0.87**	**0.91**	**1.01**	**1.01**
U-St-R-h	3201	2482	2181	2194	3737	2918	2592	2544
U-Fb-R-h	3353	2396	2068	2044	3924	3239	2549	2481
K_s/K_f	**0.95**	**1.03**	**1.05**	**1.07**	**0.95**	**0.90**	**1.01**	**1.02**
U-St-S300-l	2425	2025	1650	1647	2656	2262	2048	2005
U-Fb-S300-l	2228	1941	1749	1677	2653	2234	1962	1913
K_s/K_f	**1.08**	**1.04**	**0.94**	**0.98**	**1.00**	**1.01**	**1.04**	**1.04**
U-St-S300-h	2853	2337	1917	1858	3159	2705	2373	2336
U-Fb-S300-h	2547	2138	1999	1889	3021	2550	2260	2207
K_s/K_f	**1.12**	**1.09**	**0.95**	**0.98**	**1.04**	**1.06**	**1.05**	**1.05**
U-St-C200-l	908	742	612	611	888	786	668	648
U-Fb-C200-l	771	638	521	507	865	745	599	600
K_s/K_f	**1.17**	**1.16**	**1.17**	**1.20**	**1.02**	**1.05**	**1.11**	**1.08**
U-St-C200-h	644	554	475	471	690	602	521	539
U-Fb-C200-h	565	470	379	382	602	512	405	412
K_s/K_f	**1.14**	**1.17**	**1.25**	**1.23**	**1.14**	**1.17**	**1.28**	**1.30**
U-St-S150-l	525	417	371	379	555	451	389	402
U-Fb-S150-l	431	346	283	292	450	363	297	308
K_s/K_f	**1.21**	**1.20**	**1.31**	**1.29**	**1.23**	**1.24**	**1.30**	**1.30**
U-St-S150-h	666	543	489	508	710	582	484	472
U-Fb-S150-h	505	396	304	310	498	401	315	320
K_s/K_f	**1.31**	**1.37**	**1.60**	**1.63**	**1.42**	**1.45**	**1.53**	**1.47**
B-St-C150-l	433	349	284	298	450	372	302	315
B-Fb-C150-l	349	289	248	256	404	327	265	271
K_s/K_f	**1.24**	**1.20**	**1.14**	**1.16**	**1.11**	**1.13**	**1.14**	**1.16**
B-St-C150-h	527	434	385	394	558	459	396	401
B-Fb-C150-h	414	325	286	295	456	376	306	320
K_s/K_f	**1.27**	**1.33**	**1.34**	**1.33**	**1.22**	**1.22**	**1.29**	**1.25**

76

Table 4.4 Shear Modulus Values

Type & Shear Modulus Ratio	Shear Modulus G (MPa)							
	Vertical Pressure (MPa)							
	3.45				6.90			
	Strain Level (%)				Strain Level (%)			
	25	50	100	25, 50, 100	25	50	100	25, 50, 100
U-St-R-l	1.07	0.91	0.77	0.75	1.16	0.99	0.89	0.89
U-Fb-R-l	1.11	0.94	0.79	0.78	1.32	1.08	0.88	0.87
G_s/ G_f	**0.96**	**0.96**	**0.97**	**0.96**	**0.88**	**0.91**	**1.01**	**1.01**
U-St-R-h	1.12	0.87	0.76	0.77	1.31	1.02	0.91	0.89
U-Fb-R-h	1.17	0.84	0.72	0.65	1.37	1.13	0.89	0.87
G_s/ G_f	**0.95**	**1.04**	**1.05**	**1.07**	**0.95**	**0.90**	**1.02**	**1.02**
U-St-S300-l	1.08	0.90	0.73	0.73	1.18	1.00	0.91	0.89
U-Fb-S300-l	0.99	0.86	0.78	0.74	1.18	0.99	0.87	0.85
G_s/ G_f	**1.09**	**1.04**	**0.94**	**0.98**	**1.00**	**1.01**	**1.04**	**1.05**
U-St-S300-h	1.11	0.91	0.74	0.72	1.23	1.05	0.92	0.91
U-Fb-S300-h	0.99	0.83	0.78	0.73	1.17	0.99	0.88	0.86
G_s/ G_f	**1.12**	**1.09**	**0.96**	**0.98**	**1.04**	**1.06**	**1.05**	**1.06**
U-St-C200-l	1.16	0.94	0.78	0.78	1.13	1.00	0.85	0.82
U-Fb-C200-l	0.98	0.81	0.66	0.64	1.10	0.95	0.76	0.76
G_s/ G_f	**1.18**	**1.16**	**1.17**	**1.20**	**1.03**	**1.05**	**1.11**	**1.08**
U-St-C200-h	1.02	0.88	0.75	0.75	1.10	0.96	0.83	0.86
U-Fb-C200-h	0.90	0.75	0.60	0.61	0.96	0.81	0.64	0.65
G_s/ G_f	**1.14**	**1.18**	**1.25**	**1.23**	**1.15**	**1.18**	**1.29**	**1.31**
U-St-S150-l	1.12	0.89	0.79	0.81	1.18	0.96	0.83	0.86
U-Fb-S150-l	0.92	0.74	0.60	0.62	0.96	0.77	0.63	0.66
G_s/ G_f	**1.22**	**1.20**	**1.31**	**1.30**	**1.23**	**1.24**	**1.31**	**1.30**
U-St-S150-h	1.18	0.96	0.87	0.90	1.26	1.03	0.86	0.84
U-Fb-S150-h	0.90	0.70	0.54	0.55	0.88	0.71	0.56	0.57
G_s/ G_f	**1.32**	**1.37**	**1.61**	**1.64**	**1.42**	**1.45**	**1.54**	**1.47**
B-St-C150-l	1.18	0.95	0.77	0.81	1.22	1.01	0.82	0.85
B-Fb-C150-l	0.95	0.78	0.67	0.69	1.10	0.89	0.72	0.74
G_s/ G_f	**1.24**	**1.21**	**1.14**	**1.16**	**1.11**	**1.14**	**1.14**	**1.16**
B-St-C150-h	1.19	0.98	0.87	0.89	1.26	1.04	0.90	0.91
B-Fb-C150-h	0.94	0.73	0.65	0.67	1.03	0.85	0.69	0.72
G_s/ G_f	**1.27**	**1.33**	**1.35**	**1.33**	**1.22**	**1.22**	**1.29**	**1.25**
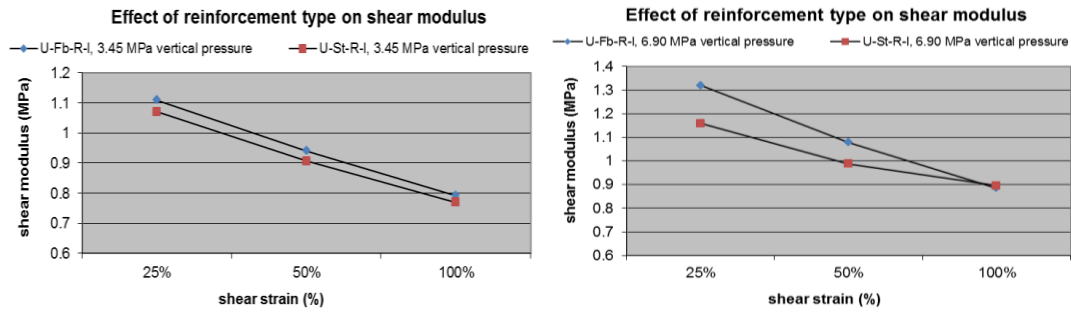
(a)
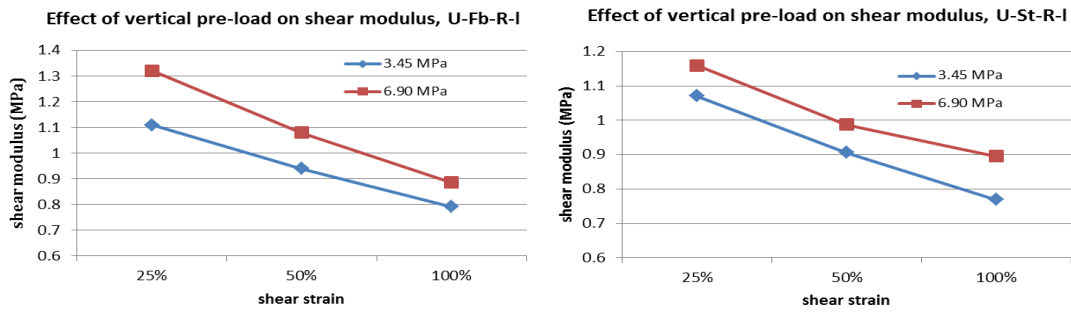
(b)
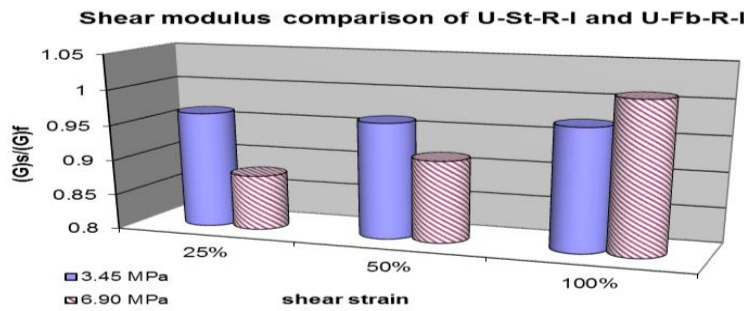
(c)

Figure 4.16 Comparison of shear modulus-Type U-R-l bearings; a) fiber and steel reinforced bearings, b) effect of vertical pre-load, c) ratio of shear modulus of S.R.B. over F.R.B.

78
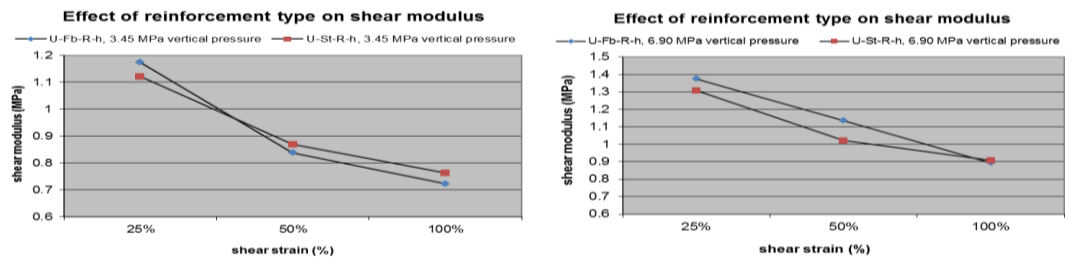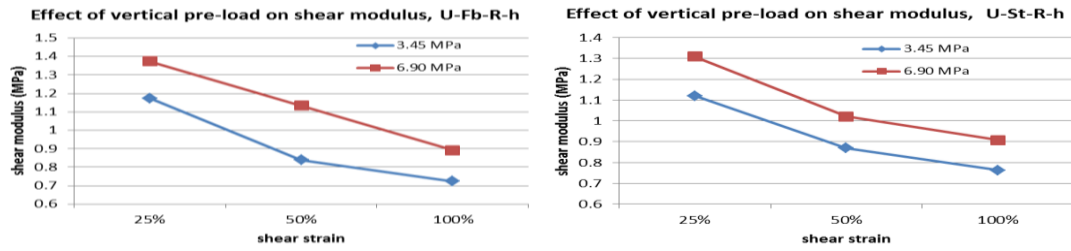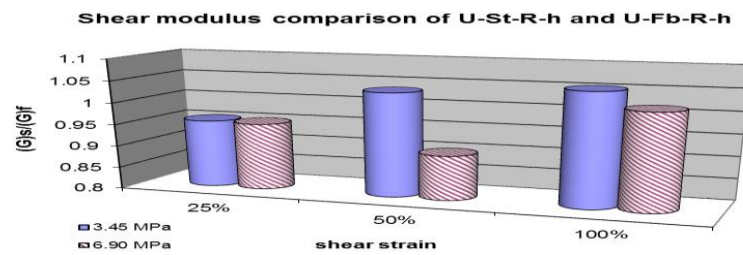
Figure 4.17 Comparison of shear modulus-Type U-R-h bearings*;* a) fiber and steel reinforced bearings, b) effect of vertical pre-load, c) ratio of shear modulus of S.R.B. over F.R.B.

Type R bearings were tested in shear direction and according to the geometry and size of these bearings, elastic bending of reinforcing plates did not affect the performance of bearings in tested strain levels. According to Figures 4.17 & 4.18 the maximum difference in shear modulus of bearings was about 13%. It can be concluded that shear modulus of Type U-R bearings was not affected by fiber flexibility due to geometrical properties of these bearings.

There was not that much of difference between the shear modulus of type 'a' and 'b' bearings. In this case shape factor had no impact on shear modulus of the bearings.
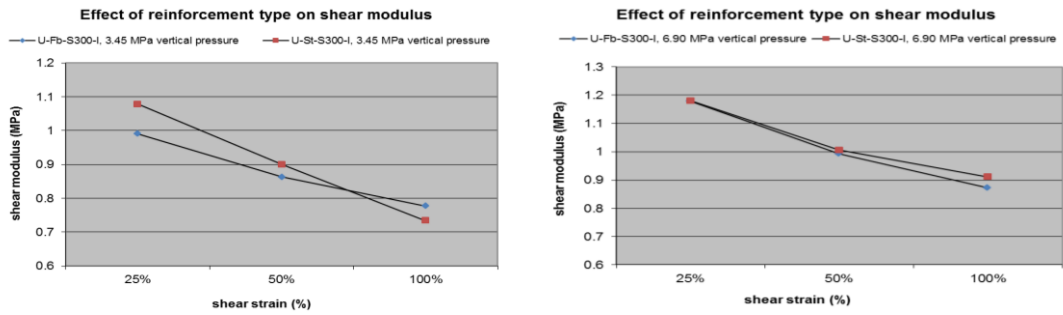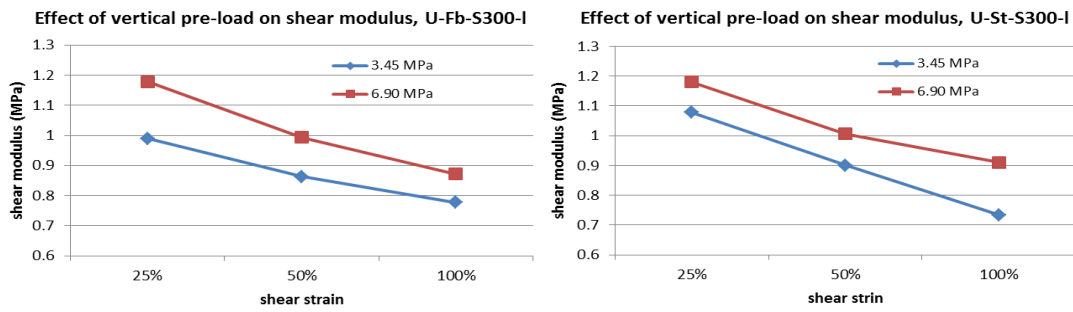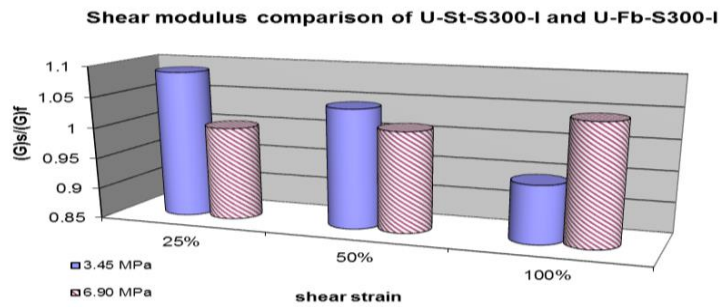
Figure 4.18 Comparison of shear modulus-Type U-S300-l bearings; a) fiber and steel reinforced bearings, b) effect of vertical pre-load, c) ratio of shear modulus of S.R.B. over F.R.B.
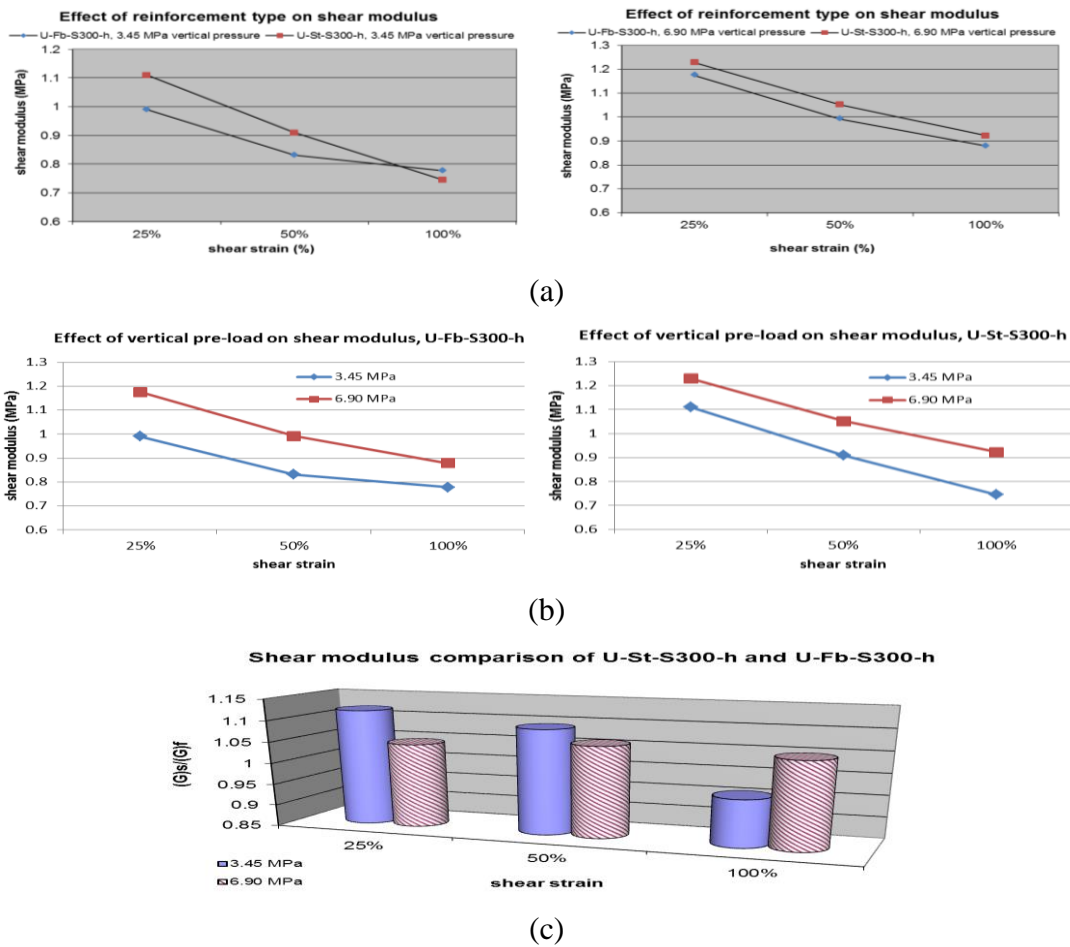
Figure 4.19 Comparison of shear modulus-Type U-S300-h bearings; a) fiber and steel reinforced bearings, b) effect of vertical pre-load, c) ratio of shear modulus of S.R.B. over F.R.B.

Elastic bending of reinforcing plates did not affect the performance of these square bearings in tested strain levels. According to Figures 4.19 & 4.20 the maximum difference in shear modulus of bearings was about 12%. It can be concluded that shear modulus of type 2 bearings was not affected by fiber flexibility due to geometrical properties of these bearings.

While shape factor of type 'h' bearings is greater than type 'l', shear modulus of these types of bearings was almost equal and value of shape factor had almost no effect on shear modulus of bearings in this case.
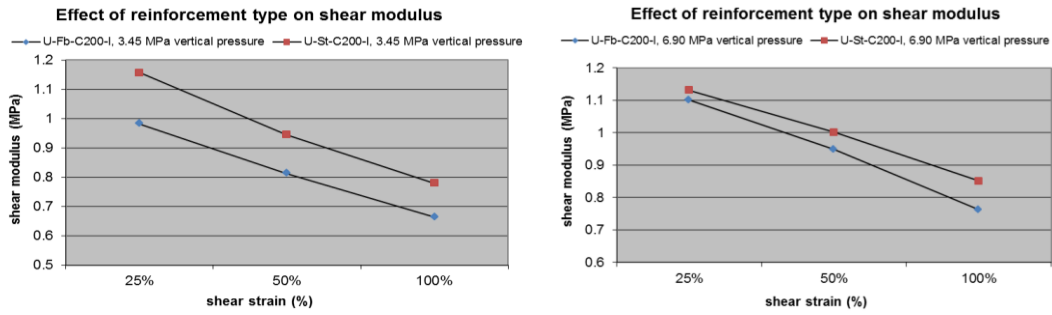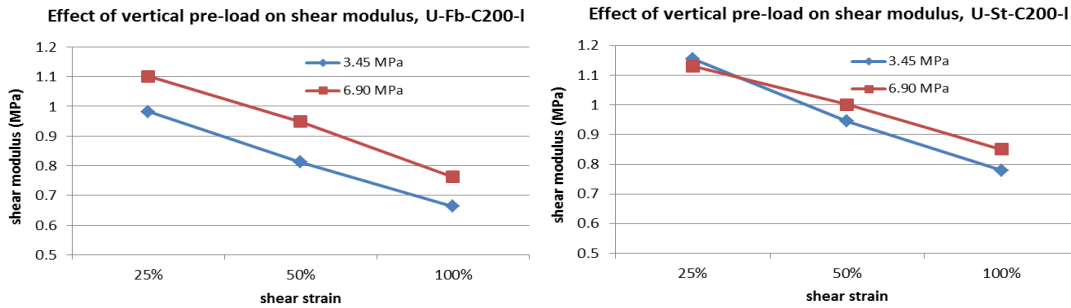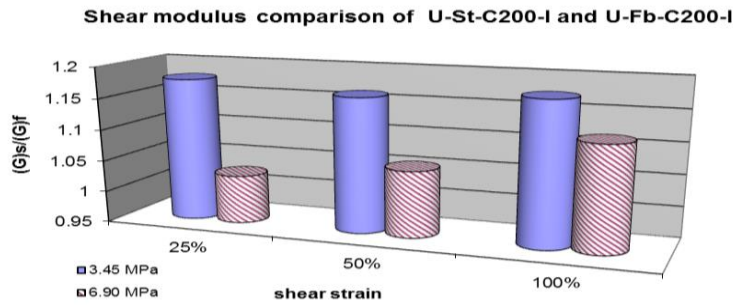
Figure 4.20 Comparison of shear modulus-Type U-C200-l bearings; a) fiber and steel reinforced bearings, b) effect of vertical pre-load, c) ratio of shear modulus of S.R.B. over F.R.B.
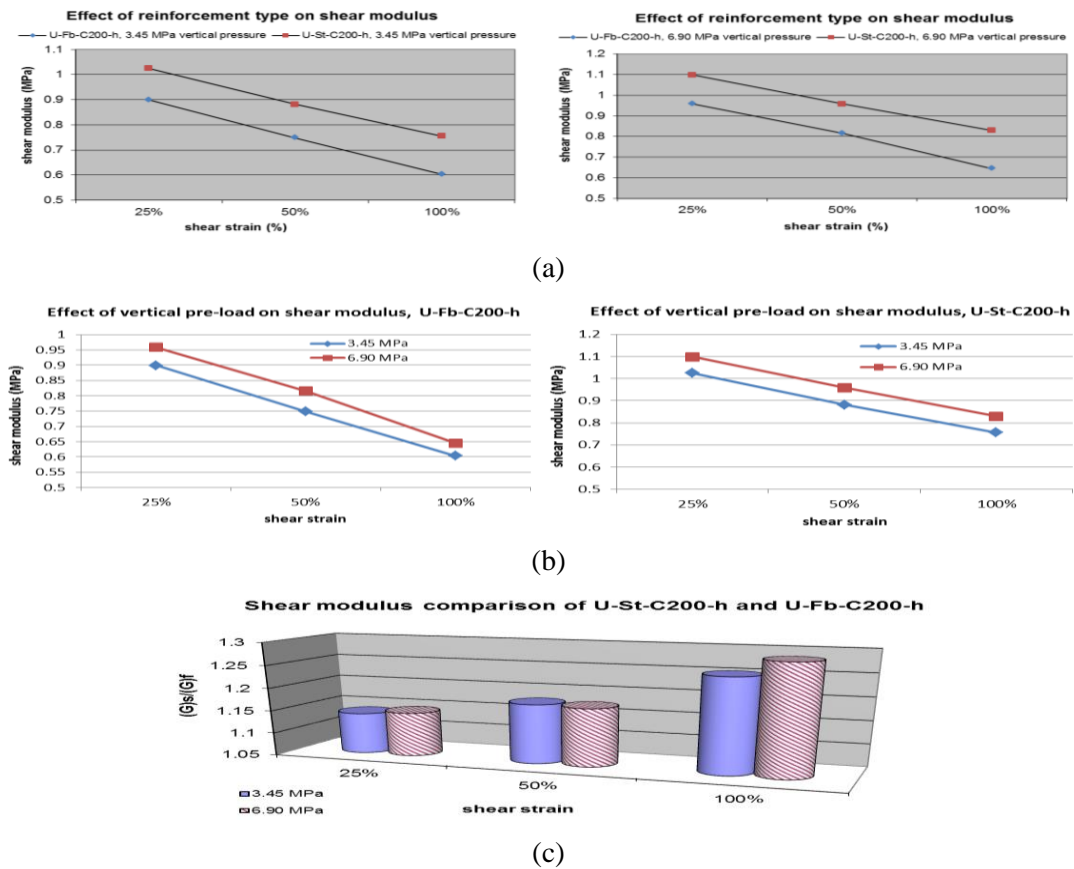
Figure 4.21 Comparison of shear modulus-Type U-C200-h bearings; a) fiber and steel reinforced bearings, b) effect of vertical pre-load, c) ratio of shear modulus of S.R.B. over F.R.B.

In Type U-C200 bearings which are unbounded and in circular form, fiber flexibility affects the performance of the bearings in horizontal direction. In this case as strain level increases difference between the shear modulus of steel and fiber-reinforced bearings increases, too. This difference stems from the roll-out property of fiber-reinforced bearing which occurs at higher levels of strain. Maximum difference between the shear modulus of steel and fiber-reinforced bearings was about 30% in this type of bearings. Again there is not any considerable trend between the shear modulus and shape factor of the bearings in this type. It is worth noting that shear modulus of fiber-reinforced bearings have decreased in comparison to Type R and S300 bearings due to geometry and elastic bending of reinforcement material.
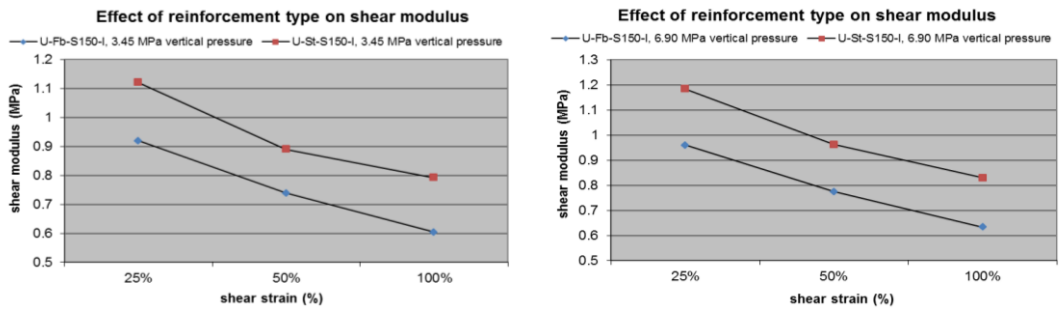
(a)
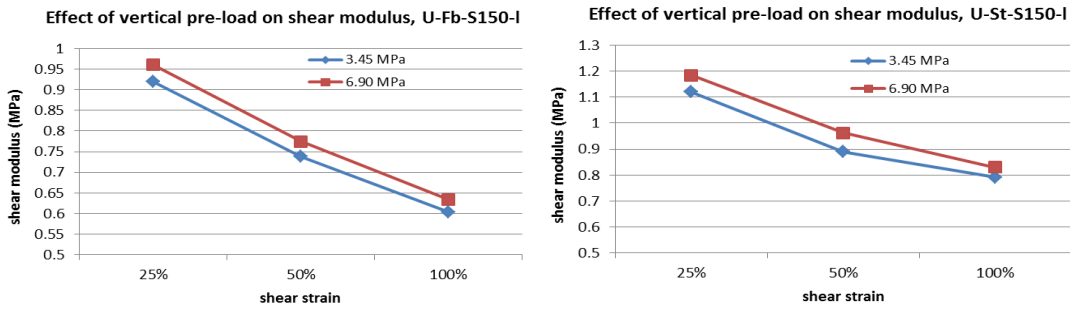
(b)
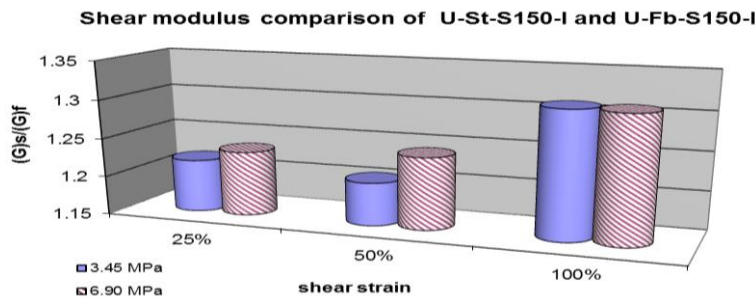
(c)

Figure 4.22 Comparison of shear modulus-Type U-S150-l bearings; a) fiber and steel reinforced bearings, b) effect of vertical pre-load, c) ratio of shear modulus of S.R.B. over F.R.B.
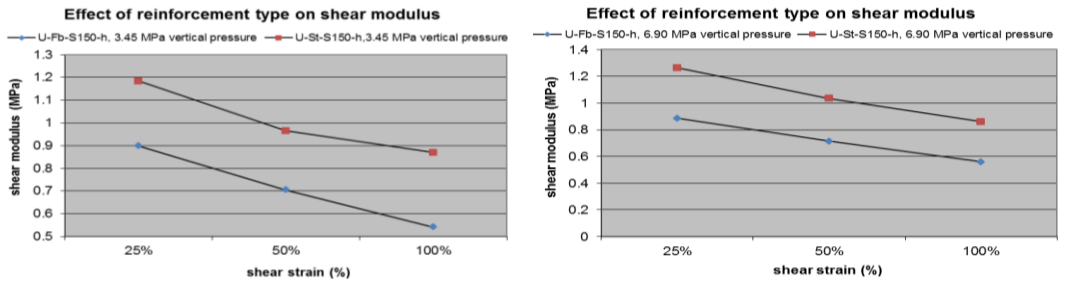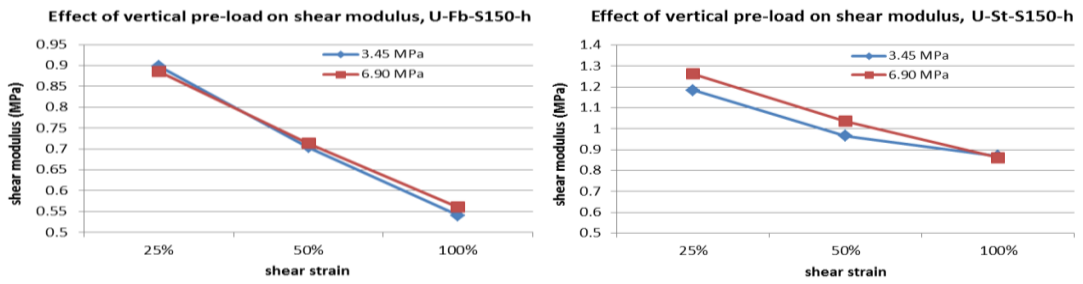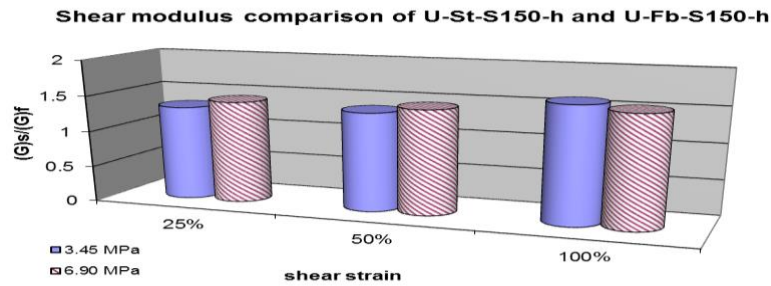
Figure 4.23 Comparison of shear modulus-Type U-S150-h bearings; a) fiber and steel reinforced bearings, b) effect of vertical pre-load, c) ratio of shear modulus of S.R.B. over F.R.B.

In Type U-S150 bearings which are unbounded and in square form, shear modulus of steel reinforced bearings was at least 22% greater than the shear modulus of fiber reinforced bearings. In this case maximum difference in mentioned value reached to 64% at 100% strain level. The experimental test results showed that Type U-S150 bearings were prone to roll-out and as roll-out occurred shear modulus of fiber reinforced bearings decreased drastically. Shape factor had almost no effect on shear modulus of the bearings in this case.
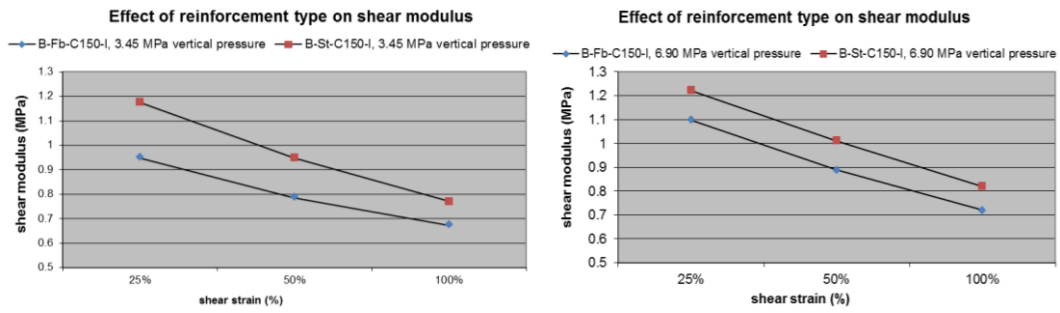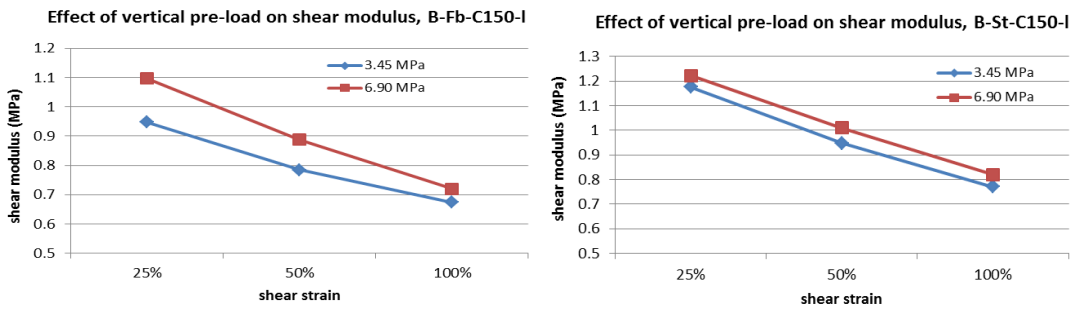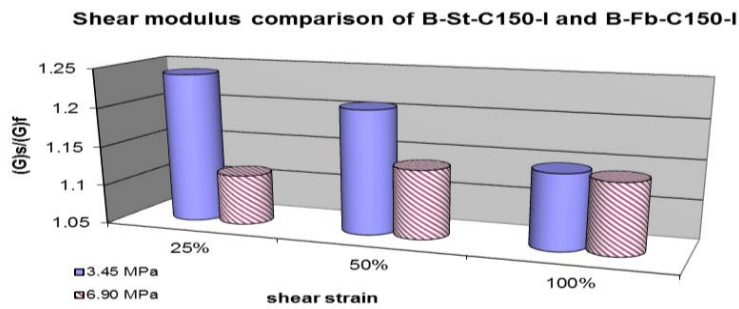
Figure 4.24 Comparison of shear modulus-Type B-C150-l bearings; a) fiber and steel reinforced bearings, b) effect of vertical pre-load, c) ratio of shear modulus of S.R.B. over F.R.B.
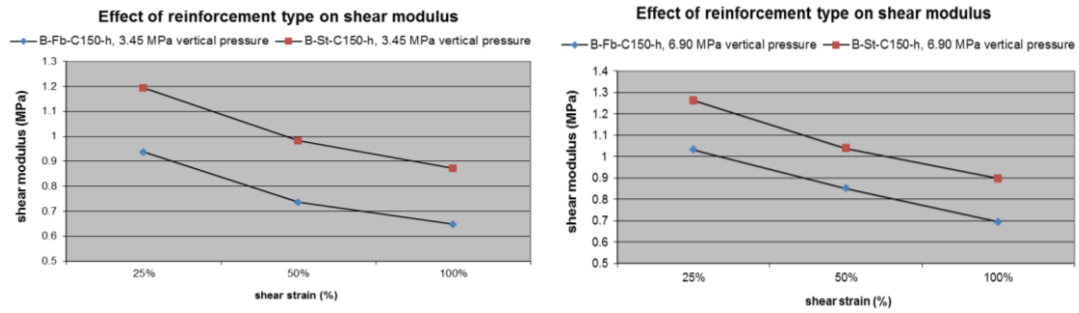
(a)
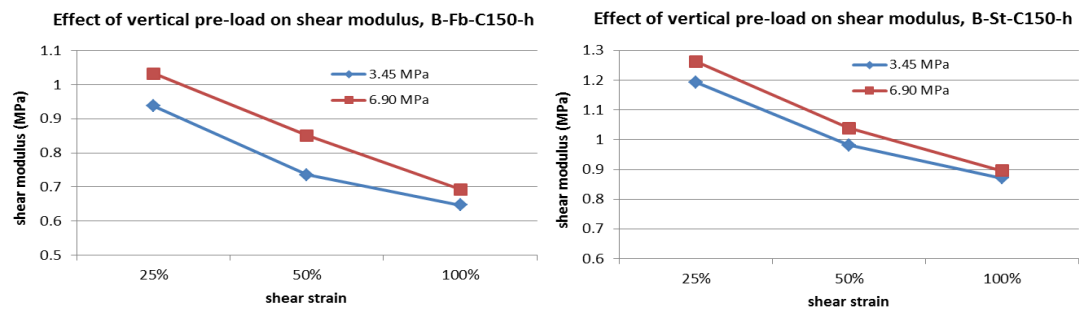
(b)
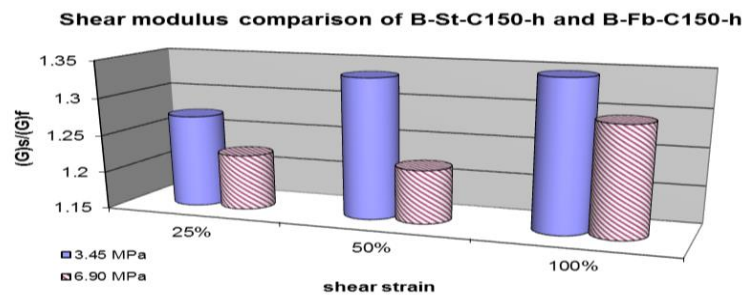
(c)

Figure 4.25 Comparison of shear modulus-Type B-C150-h bearings; a) fiber and steel reinforced bearings, b) effect of vertical pre-load, c) ratio of shear modulus of S.R.B. over F.R.B.

In Type B-C150 bearings which are bonded and in circular form, shear modulus of fiber reinforced bearigs was less than corresponding value in steel reinforced bearings. The maximum difference was about 35% which reflects the elastic bending of reinforcing material. Due to anchorage condition of this type, shear modulus did not decreased as much as Type U-S150 bearings.
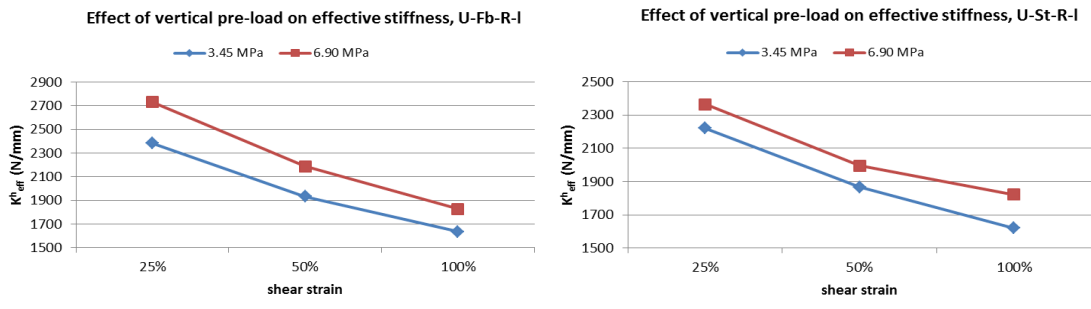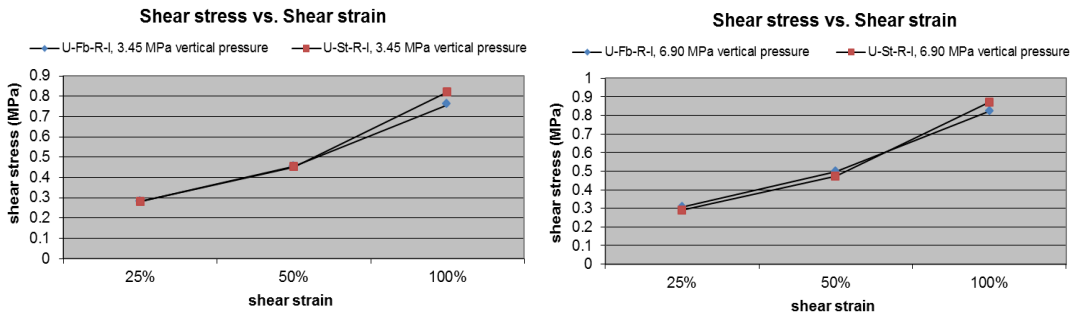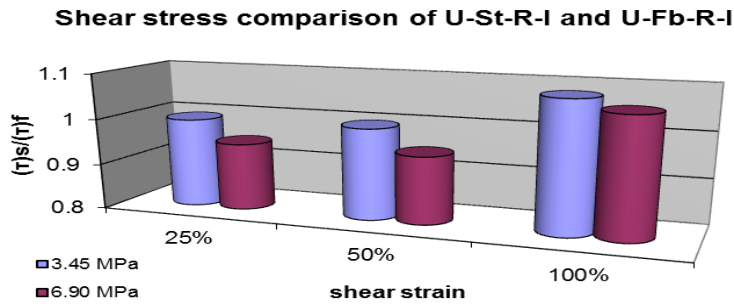
Figure 4.26 Comparison of effective stiffness-Type U-R-l bearings; a) effect of vertical pre-load, b) fiber and steel reinforced bearings, c) ratio of effective stiffness of S.R.B. over F.R.B.

(a)

(b)

(c)
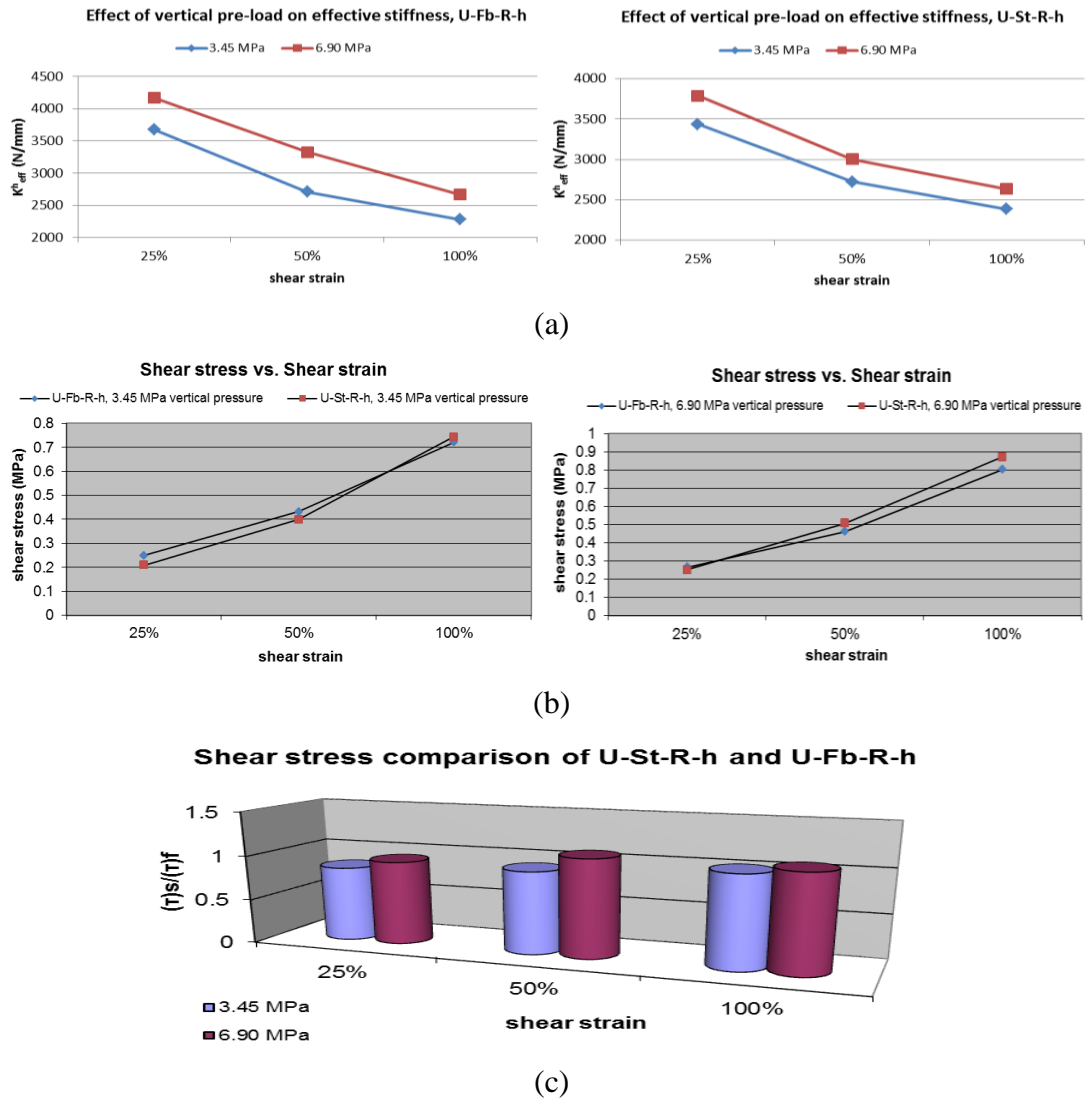
Figure 4.27 Comparison of effective stiffness-Type U-R-h bearings; a) effect of vertical pre-load, b) fiber and steel reinforced bearings, c) ratio of effective stiffness (shear stress) of S.R.B. over F.R.B.

As vertical pre-load increased, horizontal stiffness of the bearings increased, too. Horizontal stiffness of Type U-R bearings in both reinforcement conditions were almost equal. Horizontal stiffness of bearings decreased as shear strain level increased. As expected, shear stress in both types of bearings increased with an increase in strain level.

(a)

(b)
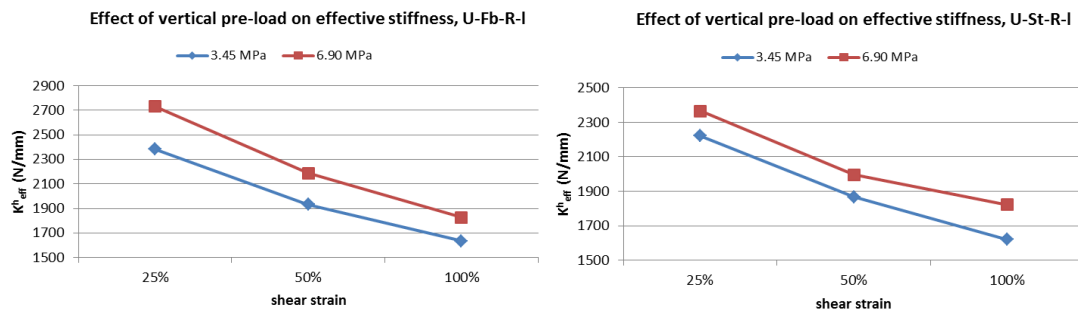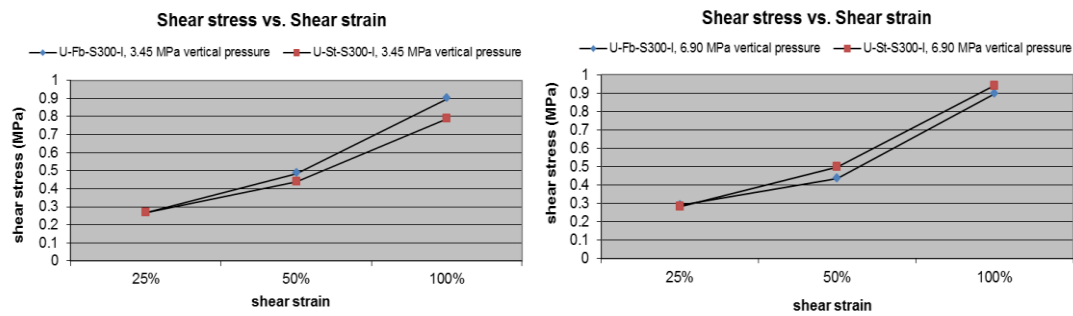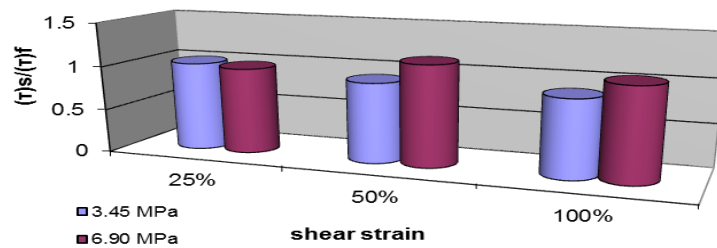
(c)

Figure 4.28 Comparison of effective stiffness-Type U-S300-l bearings; a) effect of vertical pre-load, b) fiber and steel reinforced bearings, c) ratio of effective stiffness of S.R.B. over F.R.B.

(a)

(b)

(c)

Figure 4.29 Comparison of effective stiffness-Type U-S300-h bearings; a) effect of vertical pre-load, b) fiber and steel reinforced bearings, c) ratio of effective stiffness of S.R.B. over F.R.B.

In Type U-S300 bearings, effective stiffness of steel and fiber-reinforced bearings were almost equal. The same trend for strain level and shear stress and also effective stiffness was considered in this type of bearings, too.

(a)

(b)

(c)

Figure 4.30 Comparison of effective stiffness-Type U-C200-l bearings; a) effect of vertical pre-load, b) fiber and steel reinforced bearings, c) ratio of effective stiffness of S.R.B. over F.R.B.

(a)

(b)

(c)

Figure 4.31 Comparison of effective stiffness-Type U-C200-h bearings; a) effect of vertical pre-load, b) fiber and steel reinforced bearings, c) ratio of effective stiffness of S.R.B. over F.R.B.

In Type U-C200 bearings, horizontal stiffness of fiber-reinforced bearings was less than steel reinforced bearings. The maximum difference was about 42% in 100% shear strain level . Again elastic bending of reinforcing material decreases the effective stiffness of the bearings in this case. As strain level increases difference between the horizontal stiffness of steel and fiber reinforced bearings increases, too.
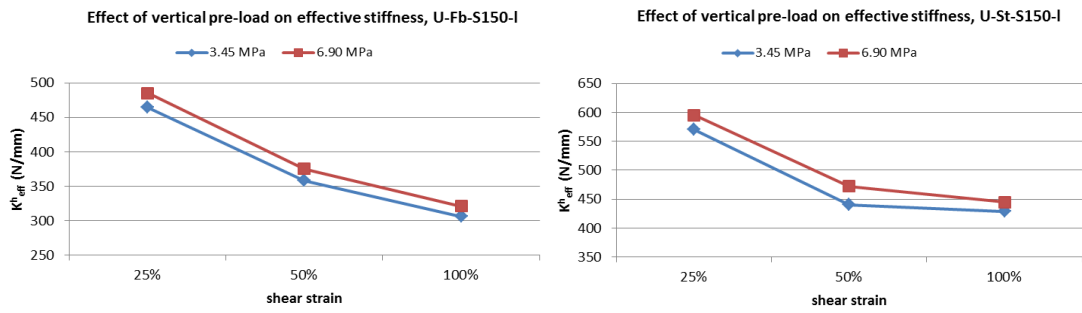
(a)
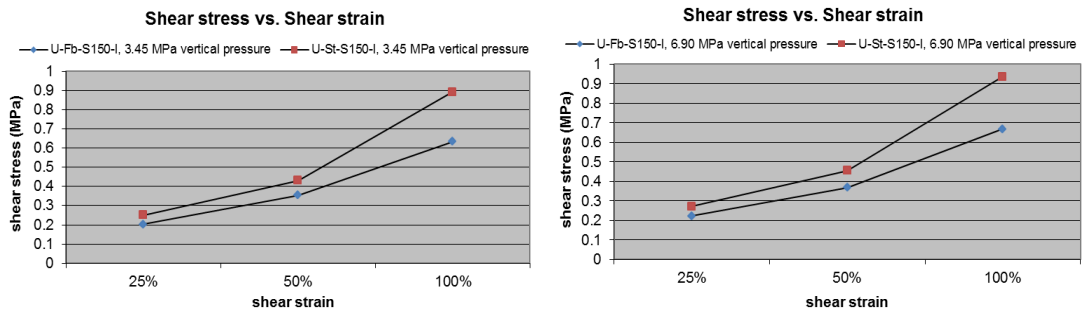
(b)
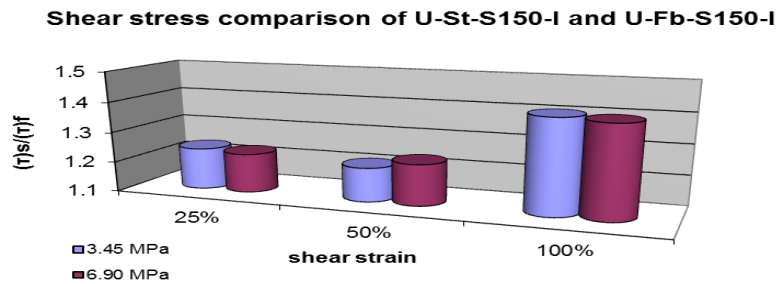
(c)

Figure 4.32 Comparison of effective stiffness-Type U-S150-l bearings; a) effect of vertical pre-load, b) fiber and steel reinforced bearings, c) ratio of effective stiffness of S.R.B. over F.R.B.

Effect of vertical pre-load on effective stiffness, U-Fb-S150-h

Effect of vertical pre-load on effective stiffness, U-St-S150-h

(a)

Shear stress vs. Shear strain

Shear stress vs. Shear strain

(b)

Shear stress comparison of U-St-S150-h and U-Fb-S150-h

(c)
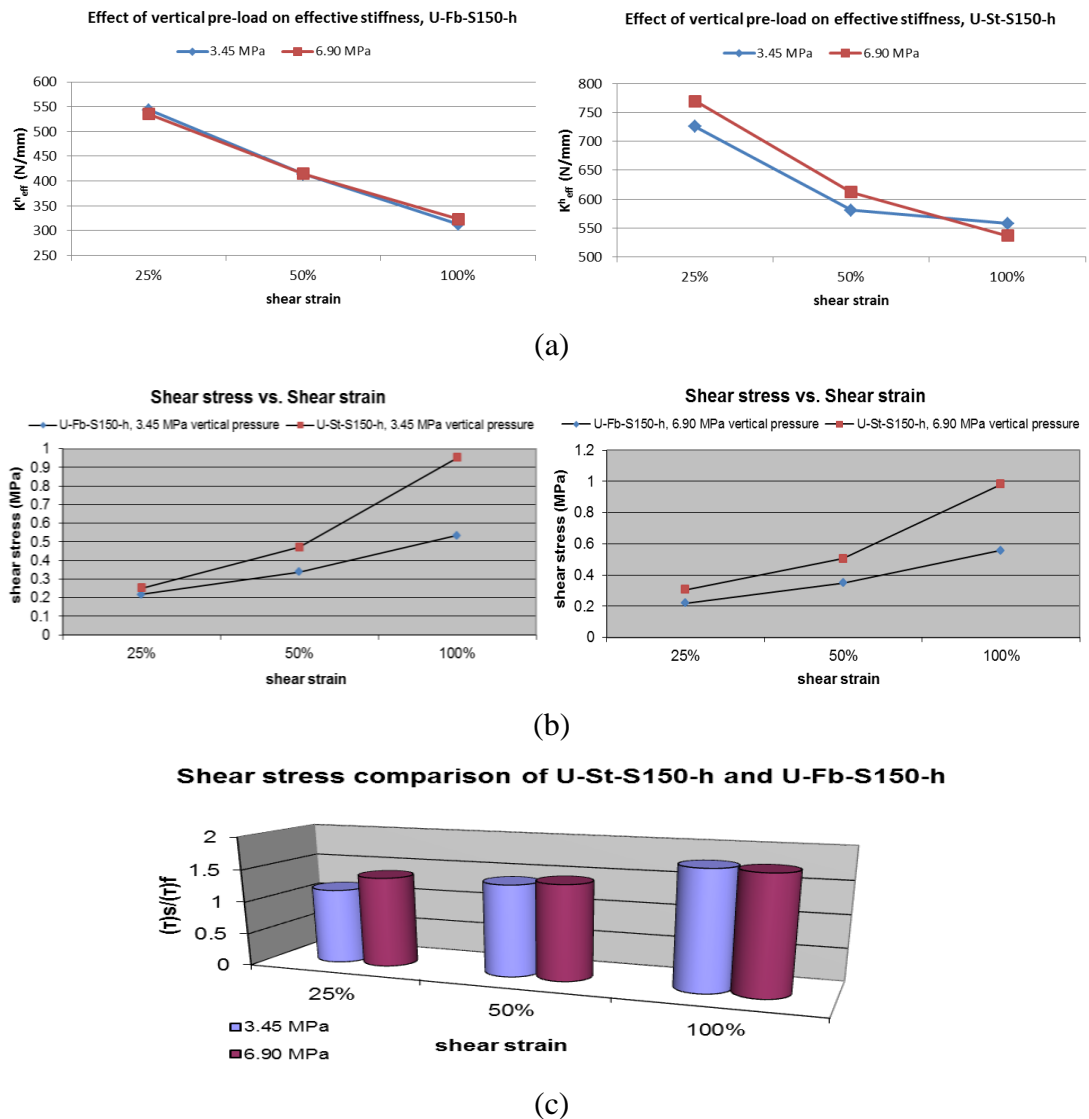
Figure 4.33 Comparison of effective stiffness-Type U-S150-h bearings; a) effect of vertical pre-load, b) fiber and steel reinforced bearings, c) ratio of effective stiffness of S.R.B. over F.R.B.

In Type U-S150 bearings the maximum difference between the horizontal stiffness of the bearings was considered to occure at 100% strain level. In this case the maximum difference is about 78% . As this type of bearings were unbonded, roll-out of fiber-reinforced bearings at higher strain levels occures and decreases the stiffness drastically.
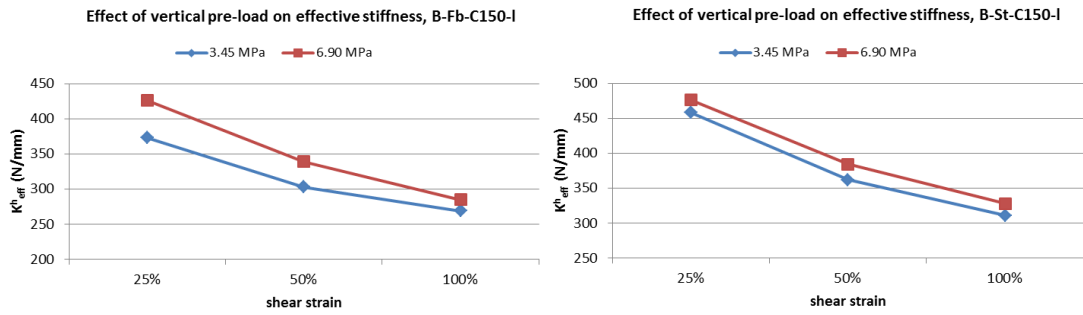
(a)
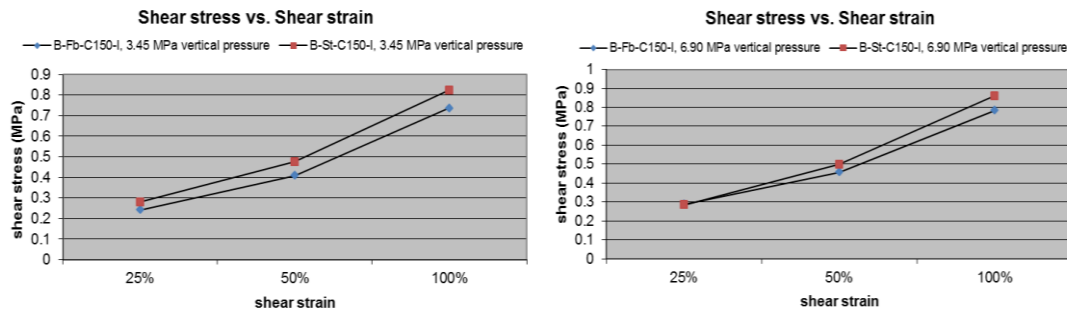
(b)
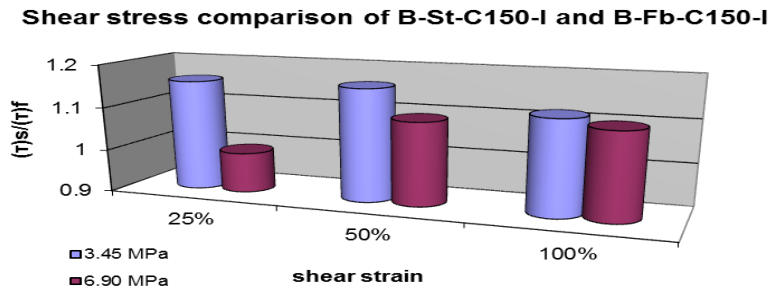
(c)

Figure 4.34 Comparison of effective stiffness-Type B-C150-l bearings; a) effect of vertical pre-load, b) fiber and steel reinforced bearings, c) ratio of effective stiffness of S.R.B. over F.R.B.

(a)

(b)

(c)
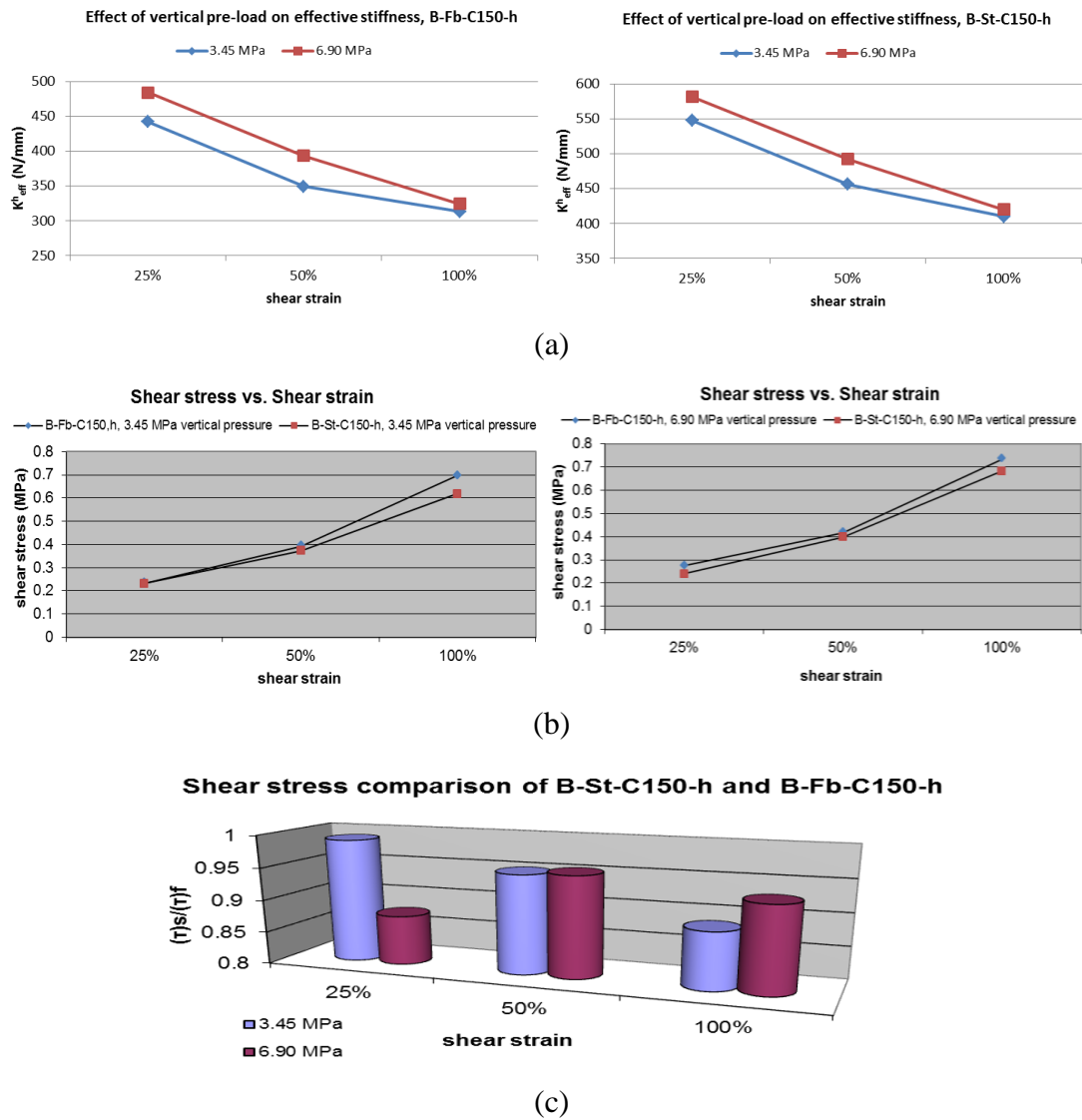
Figure 4.35 Comparison of effective stiffness-Type B-C150-h bearings; a) effect of vertical pre-load, b) fiber and steel reinforced bearings, c) ratio of effective stiffness of S.R.B. over F.R.B.

Anchorage condition in this type (Type B-C150) of bearings decreased the difference between the horizontal stiffness of fiber and steel reinforced bearings in comparison to Type U-S150 bearings. The maximum difference is about 31% and steel reinforced bearings has higher horizontal stiffness.

4.4 Low Temperature Shear Test

According to inherent property of elastomer, as temperature decreases elastomer becomes stiffer. This temperature dependent behavior of elastomer is shown in Figure 4.36 [42]. As it is clear from the figure, shear modulus of elastomer increases in low temperatures. This increase in shear modulus depends on several parameters such as velocity of loading, temperature, ingredients of elastomer's material and etc.
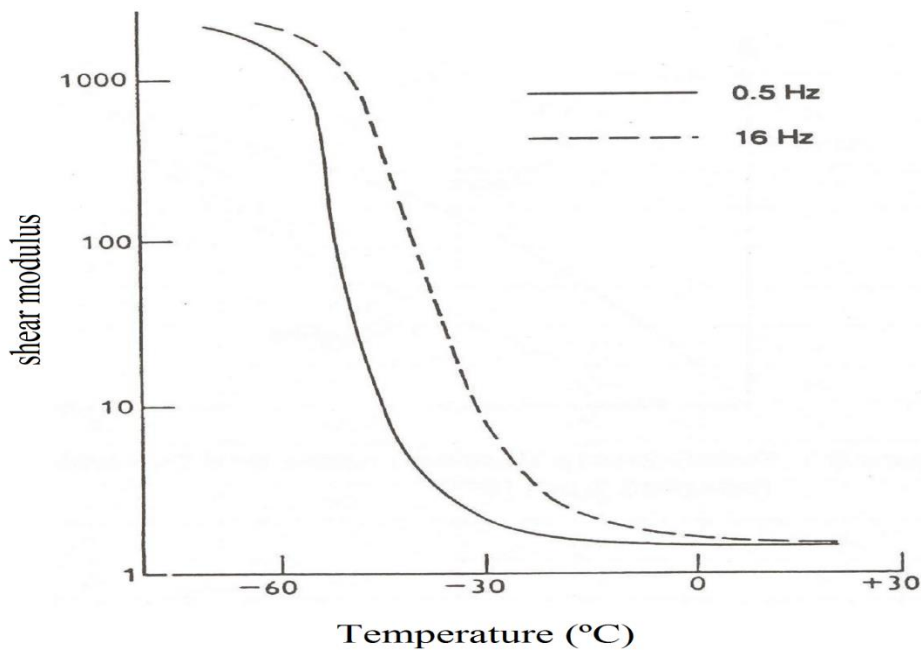
Figure 4.36 Temperature's effect on elastomer's property [42]

Behavior of elastomer in low temperatures is completely different from that of normal room temperatures. As temperature decreases, elastomer becomes stiffer. But this behavior is reversible and as temperature increases, elastomer can gain all its properties again [43].

This behavior of elastomer would affect the performance of bearing in an unwanted manner. An increase in bearings stiffness could increase the shear loads in bearings and as a result the horizontal loads transferred [43]. So, in this case the bridge's piers

98

should be designed to withstand higher level of horizontal load or other mechanisms should be used to decrease the horizontal loads transferred to the piers.

Another solution to this problem is to construct the bearings with a more resistant elastomer compound. This will improve the bearings behavior in cold climates [44].

As each rubber supplier has its own compound and there is not any standard specification for elastomer compounding, current codes on bridge bearings require the testing of the developed compounds to verify their mechanical characteristics by specifying several test procedures. Here in this study, rectangular and square shaped bearings are subjected to low temperature shear test defined in AASHTO[IV] M251-97 [32]. This test procedure was described in Chapter 3 and here in this section the result of experimental test are given in a graphical manner.

All the tests were accomplished in Structure Engineering Laboratory of Middle East Technical University. Table 4.5 summarizes the test results and shear stresses of specimens during the different steps of test are presented in this table. Figure 4.37 displays the different test steps from the beginning until the end of the test and Figures 4.38-4.43 present the strain versus stress curves for this test.

[IV] American Association of State Highway and Transportation Officials

Table 4.5 Low temperature shear test results

Specimen	Shear Stress (MPa)			Shear Modulus (MPa)		τ_{L0}/τ_R	τ_{L15}/τ_R
	Low Temperature		Room Temperature	Low Temperature	Room Temperature		
	$\tau_{L0}{}^1$	$\tau_{L15}{}^2$	$\tau_R{}^3$	$G_{L0}{}^4$	$G_R{}^5$		
U-St-R-l	0.35	0.21	0.27	1.4	1.08	1.30	0.81
U-Fb-R-l	0.45	0.17	0.28	1.8	1.12	1.61	0.61
U-St-R-h	0.29	0.18	0.24	1.16	0.96	1.21	0.75
U-Fb-R-h	0.31	0.12	0.25	1.24	1	1.24	0.48
U-St-S300-l	0.32	0.16	0.26	1.28	1.04	1.23	0.61
U-Fb-S300-l	0.33	0.16	0.25	1.32	1	1.32	0.64
U-St-S300-h	0.34	0.18	0.28	1.36	1.12	1.21	0.64
U-Fb-S300-h	0.35	0.18	0.26	1.4	1.04	1.35	0.69
U-St-S150-l	0.74	0.19	0.25	2.96	1	2.96	0.76
U-Fb-S150-l	0.63	0.14	0.2	2.52	0.8	3.15	0.7
U-St-S150-h	0.75	0.29	0.25	3	1	3	1.16
U-Fb-S150-h	0.62	0.16	0.22	2.48	0.88	2.82	0.73

Note:

[1] shear stress of the conditioned bearing subjected to 25% shear strain at the beginning of test

[2] shear stress of the conditioned bearing subjected to 25% shear strain at the end of test

[3] shear stress of the bearing subjected to 25% shear strain at room temperature

[4] shear modulus of the conditioned bearing subjected to 25% shear strain at the beginning of test

[5] shear modulus of the bearing subjected to 25% shear strain at room temperature

(a)   (b)

(c)   (d)

Figure 4.37 Low temperature shear test in progress, a) Conditioning the specimens in refrigerator, b) applying the shear strain along with vertical pressure, c) test in progress, d) unloading the specimens after 15 minutes
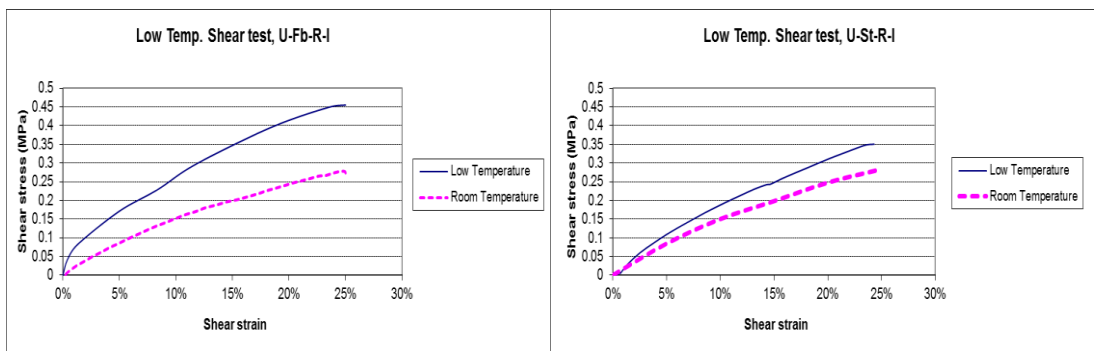
Figure 4.38 Stress vs. strain in low temperature shear test for Type U-R-l
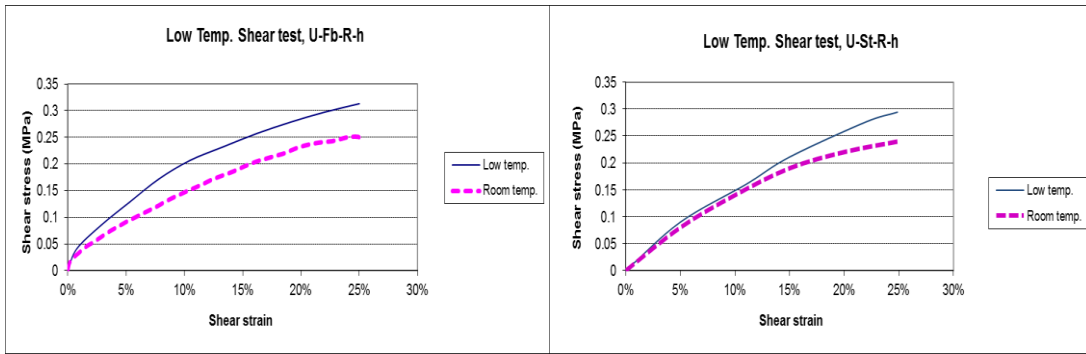
Figure 4.39 Stress vs. strain in low temperature shear test for Type U-R-h
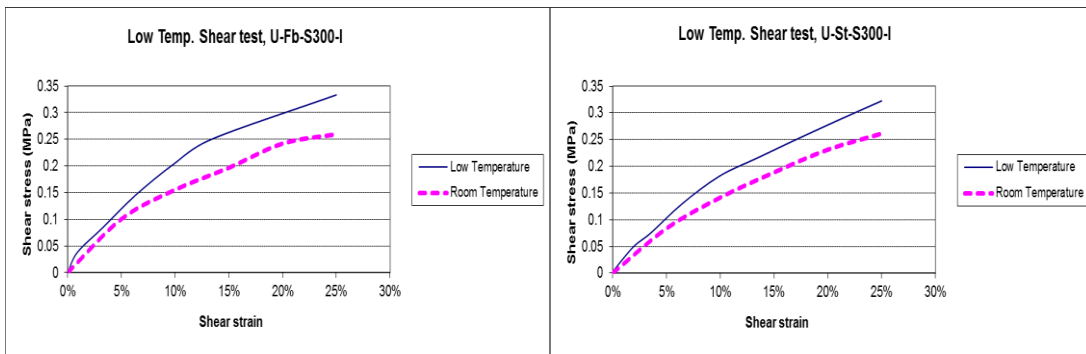
Figure 4.40 Stress vs. strain in low temperature shear test for Type U-S300-l
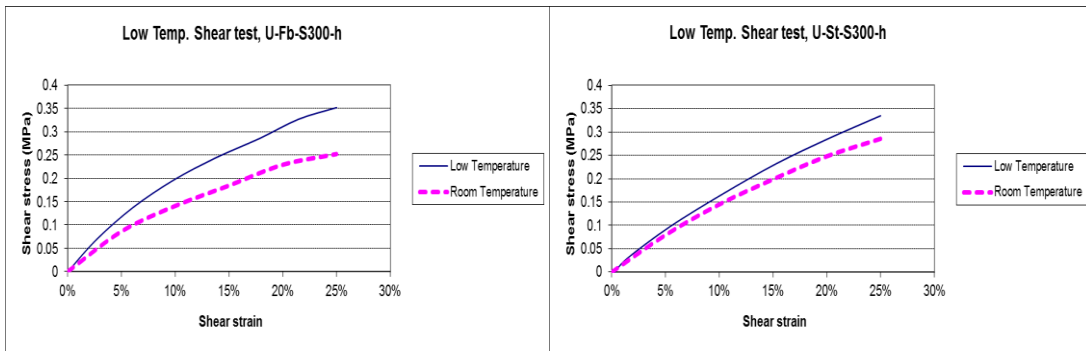
Figure 4.41 Stress vs. strain in low temperature shear test for Type U-S300-h
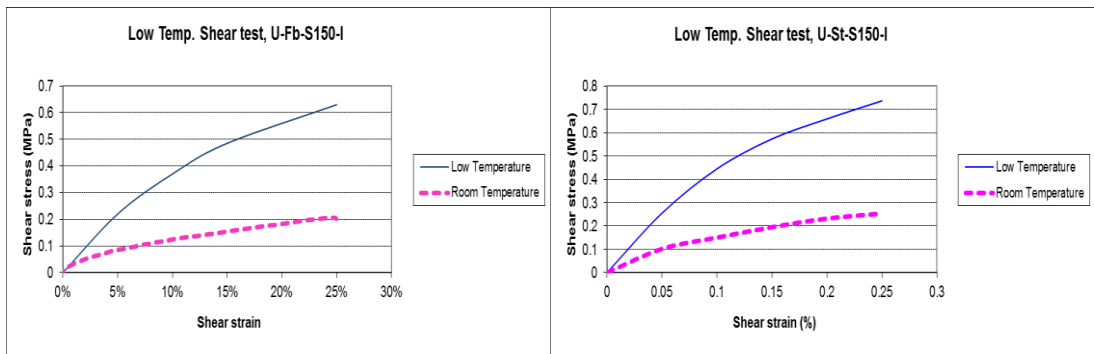
Figure 4.42 Stress vs. strain in low temperature shear test for Type U-S150-l
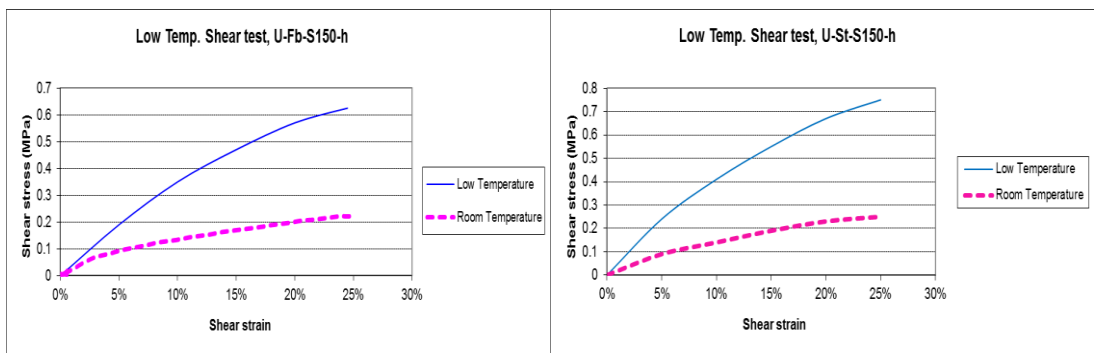
Figure 4.43 Stress vs. strain in low temperature shear test for Type U-S150-h

The stress levels described in AASHTO M251-97 give maximum permissible low temperature secant shear moduli of 1.38 MPa (200 psi) and 0.83 MPa (120 psi) for neoprene and natural rubber, respectively. This test does not appear to have a rational performance criterion because there are no requirements for bearings with a durometer hardness greater than 50 [42].

As stated, there are no limits specified for the bearings constructed with 60 durometer elastomer in AASHTO M251-97. Hence, the test results are compared with the limits given for 50 durometer elastomer. Figures 4.44-4.46 show the shear stress developed in bearing at three different stages.
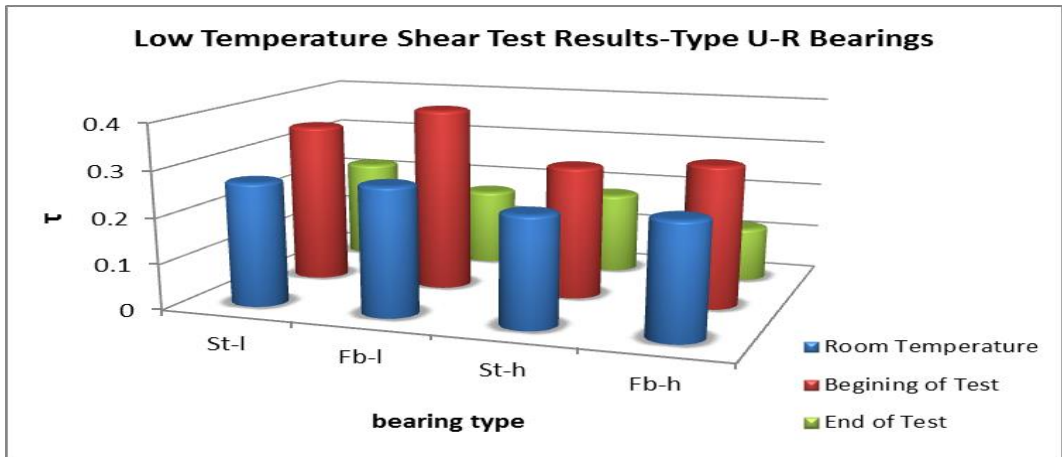
Figure 4.44 Comparison of low temperature shear test results with
AASHTO M251-97-Type U-R bearings

As it can be seen from Figure 4.44, Type U-R bearings satisfy the AASHTO M251-97, level I shear test requirement. The shear stress developed in fiber-reinforced bearings at the beginning of the test was higher than the corresponding values in steel reinforced ones. After 15 minutes, the stress values in fiber-reinforced bearings showed a drastic decrease and at the end of test, the stress level in fiber-reinforced bearings was lower than steel reinforced ones.
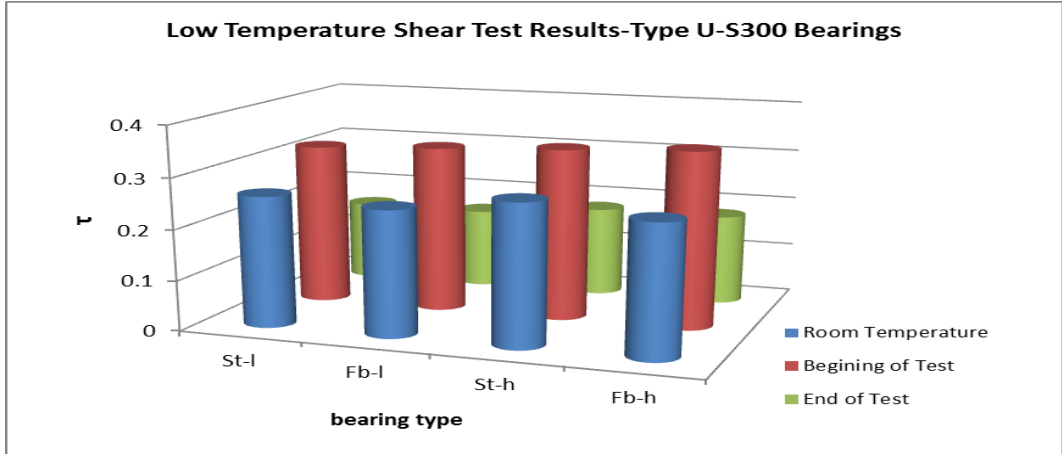
Figure 4.45 Comparison of low temperature shear test results with
AASHTO M251-97-Type U-S300 bearings

Type U-S300 bearings satisfied the stress requirement of AASHTO and the stress values developed in bearings at the begining and end of the test was almost equal in both reinforcement conditions.
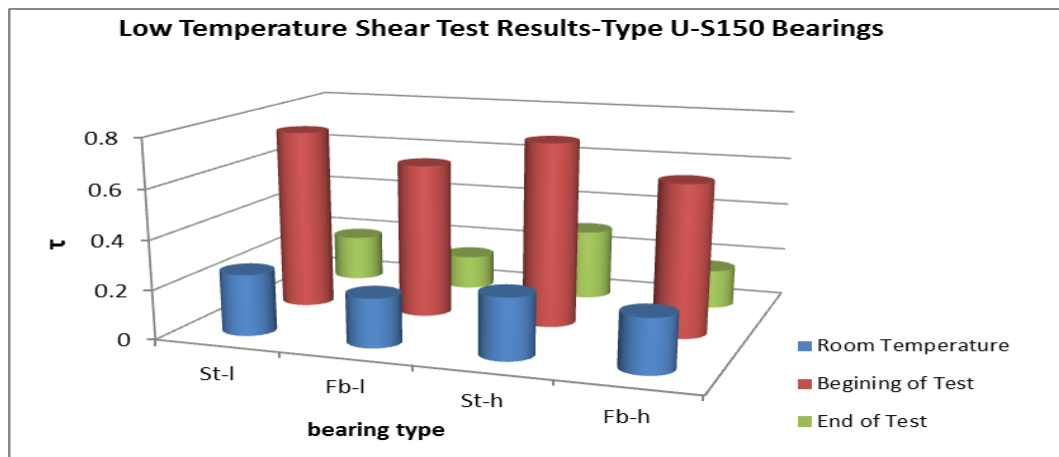
Figure 4.46 Comparison of low temperature shear test results with
AASHTO M251-97-Type U-S150 bearings

Shear stress developed in Type U-S150 bearings at the begining of the test was almost three times higher than the stress developed in room temperature. At the end of the test, except for U-St-S150-h, all the other bearings satisfied the AASHTO limit. The high levels of stress in bearings at the beginning of the test can be attributed to the inherent properties of elastomer.

It was observed that the performance of the bearings subjected to low temperature shear test depends on the inherent properties of elastomer and fiber flexibility has almost no effect.

CHAPTER 5

VERTICAL STIFFNESS AND FINITE ELEMENT ANALYSIS OF ELASTOMERIC BEARINGS

5.1 Introduction

In this chapter result of pressure solution [16], finite element analysis and experimental tests for the vertical stiffness of bearings are presented. To investigate the stress distribution in bearings, finite element model of bearings under pure compression is studied and the results of finite element analysis are compared by the results of pressure solution.

To investigate the effect of fiber flexibility on vertical stiffness of the bearings, vertical stiffness of both fiber and steel reinforced bearings are compared. Results of pressure solution for vertical stiffness of bearings with both compressible and incompressible material are presented and compared with the results of finite element analysis and experimental tests.

5.2 Finite Element Analysis of Bearings

To investigate the stress distribution in elastomeric bearings and reinforcing material, bearing Type B-Fb-C150-l and B-St-C150-l are modeled in ABAQUS commercial finite element software. Next, the results of finite element modeling and pressure solution are compared and conclusions are made.

5.2.1 Overview of Incompressible Material in ABAQUS/STANDARD

The rubber is modeled by using the hyperelastic material model. The hyperelastic material model:

- is isotropic and nonlinear;
- is valid for materials that exhibit instantaneous elastic response up to large strains (such as rubber, solid propellant, or other elastomeric materials); and
- requires that geometric nonlinearity be accounted for during the analysis step, since it is intended for finite-strain applications [45].

5.2.1.1 Isotropy Assumption

In Abaqus, all hyperelastic models are based on the assumption of isotropic behavior throughout the deformation history. Hence, the strain energy potential can be formulated as a function of the strain invariants.

5.2.1.2 Strain Energy Potentials

Hyperelastic materials are described in terms of a "strain energy potential," $U(\varepsilon)$, which defines the strain energy stored in the material per unit of reference volume (volume in the initial configuration) as a function of the strain at that point in the material. There are several forms of strain energy potentials available in Abaqus to model approximately incompressible isotropic elastomers; the Arruda-Boyce form, the Marlow form, the Mooney-Rivlin form, the neo-Hookean form, the Ogden form, the polynomial form, the reduced polynomial form, the Yeoh form, and the Van der Waals form. The reduced polynomial and Mooney-Rivlin models can be viewed as particular cases of the polynomial model; the Yeoh and neo-Hookean potentials, in turn, can be viewed as special cases of the reduced polynomial model. Thus, these models are referred collectively as "polynomial models." Generally, when data from multiple experimental tests are available (typically, this requires at least uniaxial and equibiaxial test data), the Ogden and Van der Waals forms are more accurate in

fitting experimental results. If limited test data are available for calibration, the Arruda-Boyce, Van der Waals, Yeoh, or reduced polynomial forms provide reasonable behavior. When only one set of test data (uniaxial, equibiaxial, or planar test data) is available, the Marlow form is recommended. In this case a strain energy potential is constructed that will reproduce the test data exactly and that will have reasonable behavior in other deformation modes [45]. In this study rubber is modeled by using the Neo-Hookean form with strain energy function described in next part.

5.2.1.3 Strain Energy in Neo-Hookean Form

The form of the neo-Hookean strain energy potential is

$$U = C_{10}(\bar{I}_1 - 3) + \frac{1}{D_1}(J^{el} - 1)^2 \tag{5.1}$$

where U is the strain energy per unit of reference volume; C_{10} and D_1 are temperature-dependent material parameters; $\bar{I}_1$ is the first deviatoric strain invariant defined as

$$\bar{I}_1 = \bar{\lambda}_1^{\ 2} + \bar{\lambda}_2^{\ 2} + \bar{\lambda}_3^{\ 2}, \tag{5.2}$$

where the deviatoric stretches $\bar{\lambda}_i = J^{-\frac{1}{3}}\lambda_i$; J is the total volume ratio; J^{el} is the elastic volume ratio and λ_i are the principal stretches. The initial shear modulus and bulk modulus are related to C_{10} and D_1 by equation (5.11);

$$G = 2C_{10} \qquad\qquad K_0 = \frac{2}{D_1} \tag{5.3}$$

Using the results of horizontal shear test, shear modulus of rubber can be determined. On the other hand, the bulk modulus of rubber in elastomeric bearing can be assumed to be in the range of 1800-2000 MPa [40]. Knowing these two parameters, the Neo-Hookean material form is used to model the rubber in ABAQUS.

5.2.1.4 Element Type and Integration Method

For the three-dimensional modeling of bearings, rubber is described by the 20-node quadratic brick elements with reduced integration and 3D stress family (C3D20R). The fiber layers are modeled with the 8-node quadrilateral membrane elements with reduced integration (M3D8R) sharing their nodes with the rubber elements. Perfect bond is assumed between rubber and fiber layer as done in the work of Mordini and Strauss [20]. Fiber is defined as an elastic material with Young's modulus E=35000 Mpa and Poisson ratio equal to 0.05. In addition, steel is defined as an elastic material with the mechanical property given in Table 3.1. Steel plates are described by 20-node 3D solid elements (C3D20R) and perfect bond between rubber layers and steel plates is considered.

5.2.2 Finite Element Model of B-Fb-C150-l

Finite element model of B-Fb-C150-l with top and bottom anchorage plates was defined. Geometrical properties of this bearing was presented in Chapter 3 and the finite element discretization is shown in Figure 5.1. This model consists of 21141 elements and each element is a twenty-node quadratic brick element with side length of 4 mm. It is important to note that due to symmetry half of the model is studied.
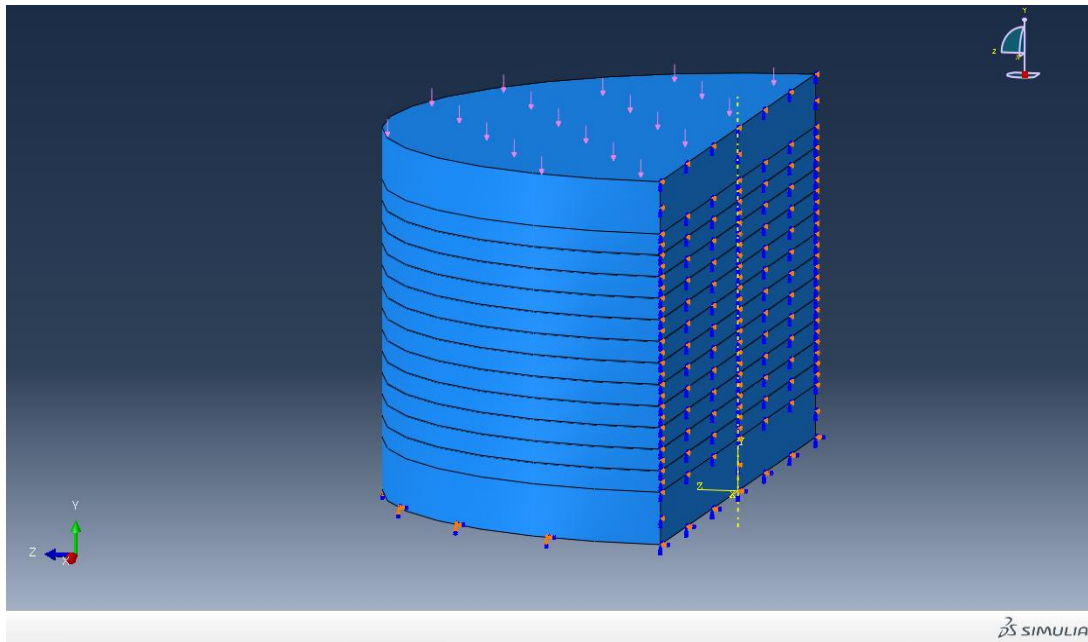
Figure 5.1 Layout of B-Fb-C150-l in Abaqus

The goal of this section is to verify the validity of the results provided by pressure solution by comparing them with results of FE analysis. Experimental test results for the vertical stiffness of the bearings are used to have a comparison between the results of FE analysis, pressure solution and experimental tests. All the figures presented in this part show the contour maps of the equivalent stress obtained from analysis with ABAQUS for B-Fb-C150-l, under pure compression of 6.90 Mpa. The plots show the results on half of the bearing in a cylindrical coordinate system.

Figures 5.2-5.4 illustrate the stress distribution in rubber layers and confirm the validity of $\sigma_r \approx \sigma_\theta \approx \sigma_z \approx -p$, which is one of the main assumptions in pressure solution. It is important to note that (1,2,3) in local coordinate system corresponds to (r,θ,z) and matches the cylindrical coordinate system which was used in pressure solution. In addition, Figure 5.5 and 5.6 compares the results of pressure solution and finite element analysis for internal stress distribution in rubber. As it is clear from the figures, results of finite element analysis are in good agreement with pressure solution.
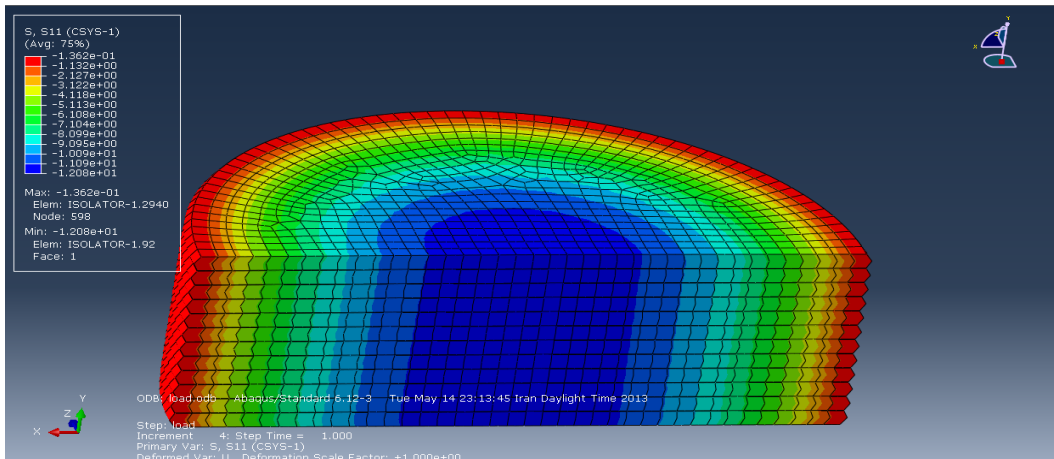
Figure 5.2 Distribution of σ_r in rubber layers
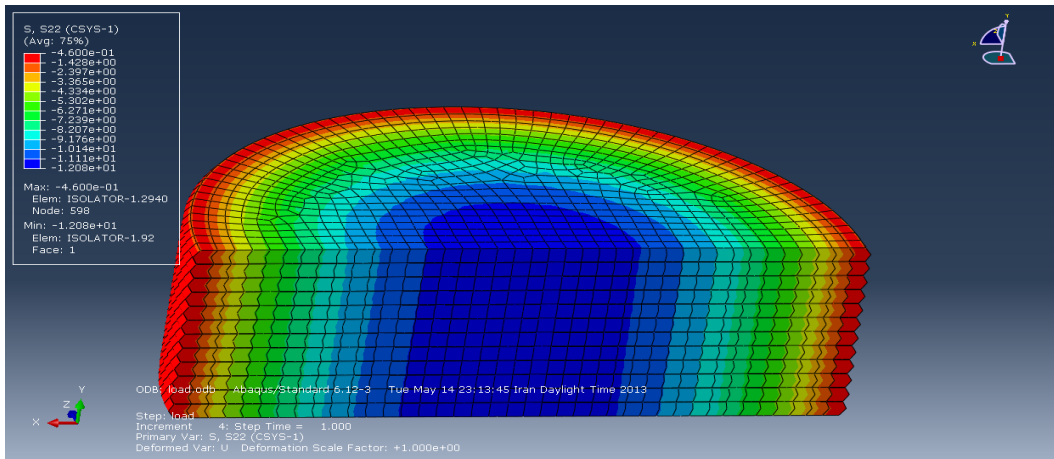
Figure 5.3 Distribution of σ_θ in rubber layers
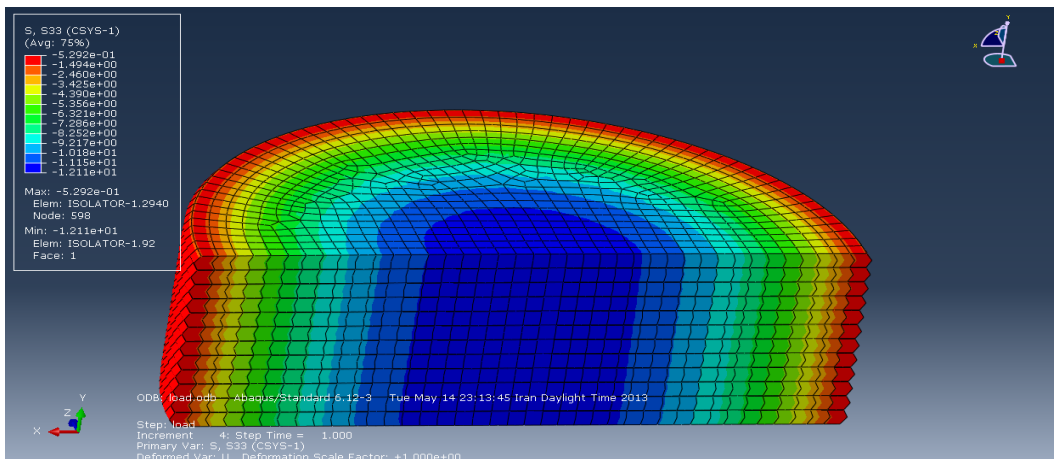
Figure 5.4 Distribution of σ_z in rubber layers

112
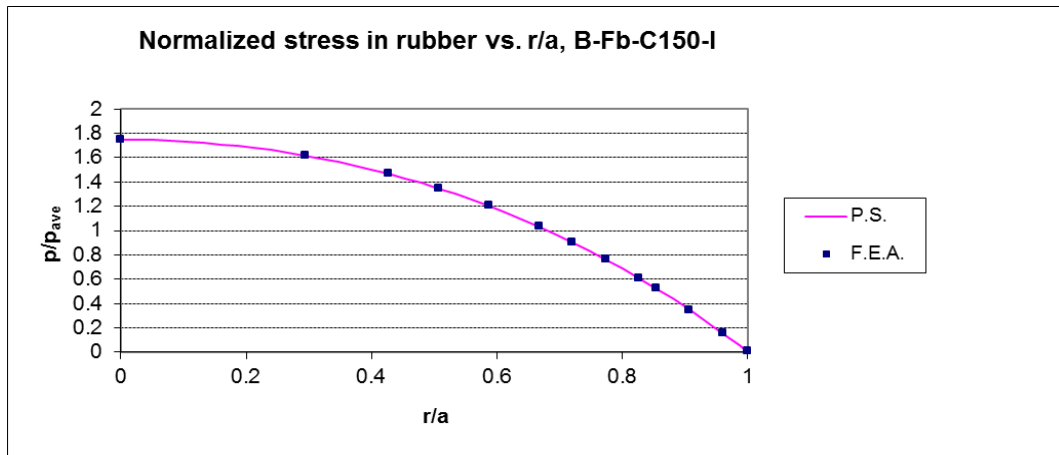
Figure 5.5 Normalized stress distribution in B-Fb-C150-l with respect to average external pressure
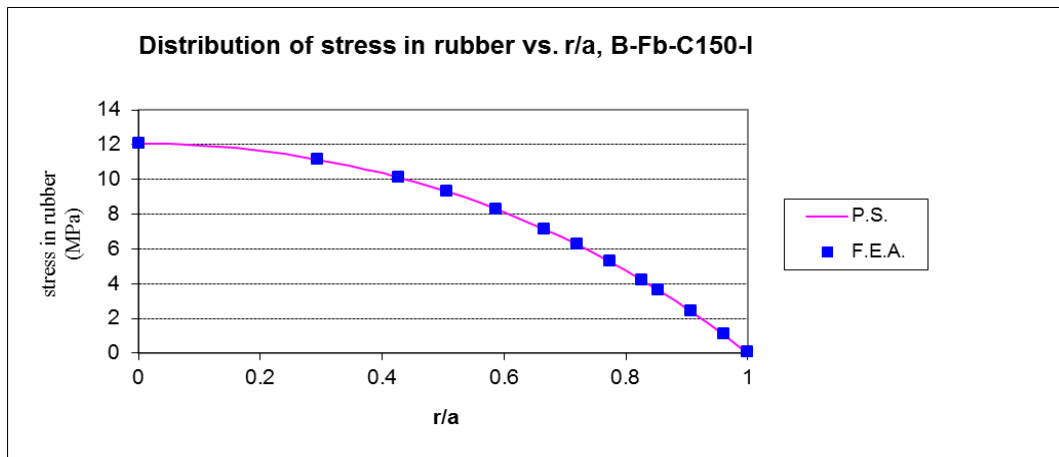
Figure 5.6 Distribution of stress in B-Fb-C150-l

Results of finite element analysis were used to calculate the vertical stiffness of the bearing. According to compression analysis of bearing in considered range of load, the force-displacement behavior in the vertical direction was obtained to be linear. Figure 5.7 shows the load-deflection curve for B-Fb-C150-l obtained from finite element analysis.
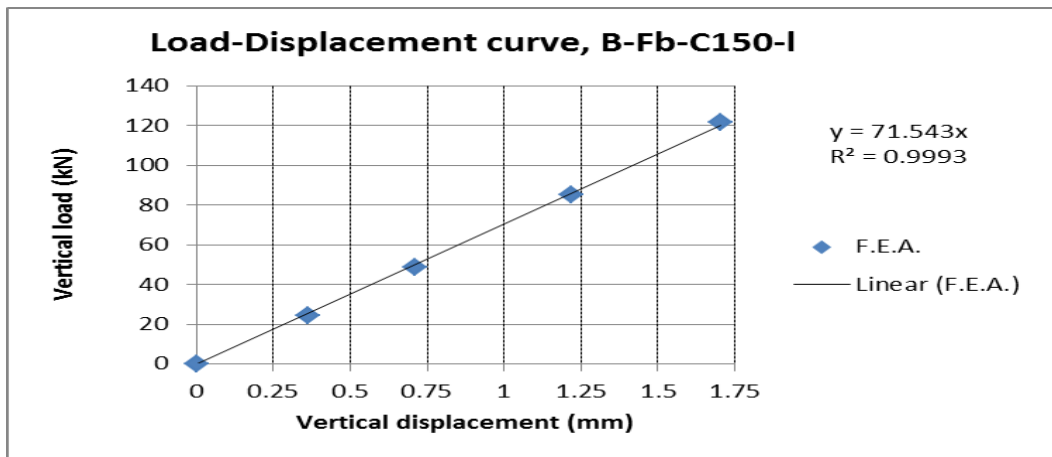
Figure 5.7 Load-deflection curve in vertical direction for B-Fb-C150-l

Figure 5.8 shows the vertical displacement of the bearing under constant pressure.
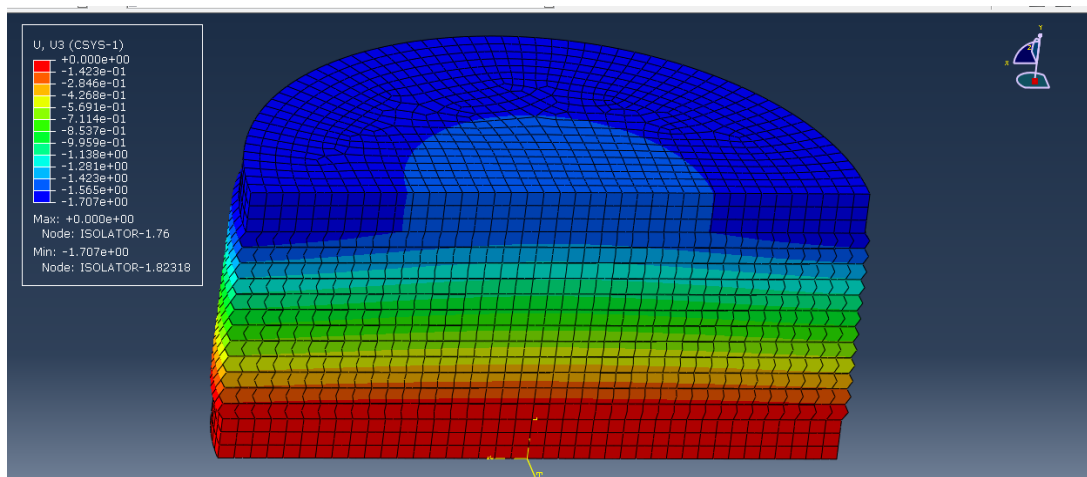
Figure 5.8 Displacement of B-Fb-C150-a in the direction of applied load

In pressure solution for fiber reinforced bearings, the kinematic assumption of quadratically varible displacement is supplemented by an additional displacement that is constant through the thickness and is intended to accommodate the stretching of the reinforcement. Figure 5.9 shows the deformation of the bearing in radial direction and complies with the pressure solution assumption. Figure 5.10 depicts the deformed and undeformed shape of the B-Fb-C150-l under compression and it is in

114

good agrement with the mentioned assumption of pressure solution. Figure 5.11 shows the elongation of fiber reinforcement under compression and this elongation is constant throughout the layers.
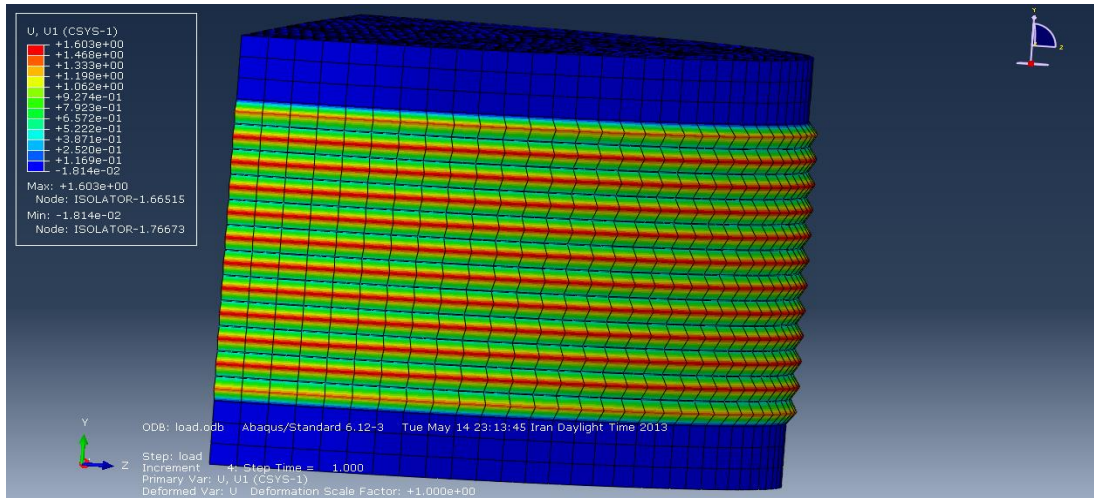
Figure 5.9 Deformation of bearing in radial direction
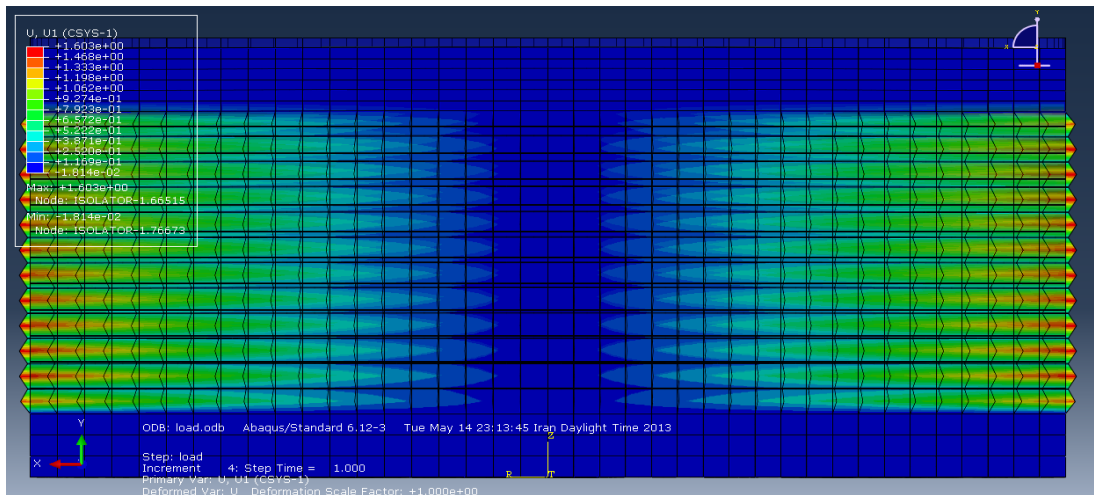
Figure 5.10 Deformed and undeformed shape of B-Fb-C150-l under compresion
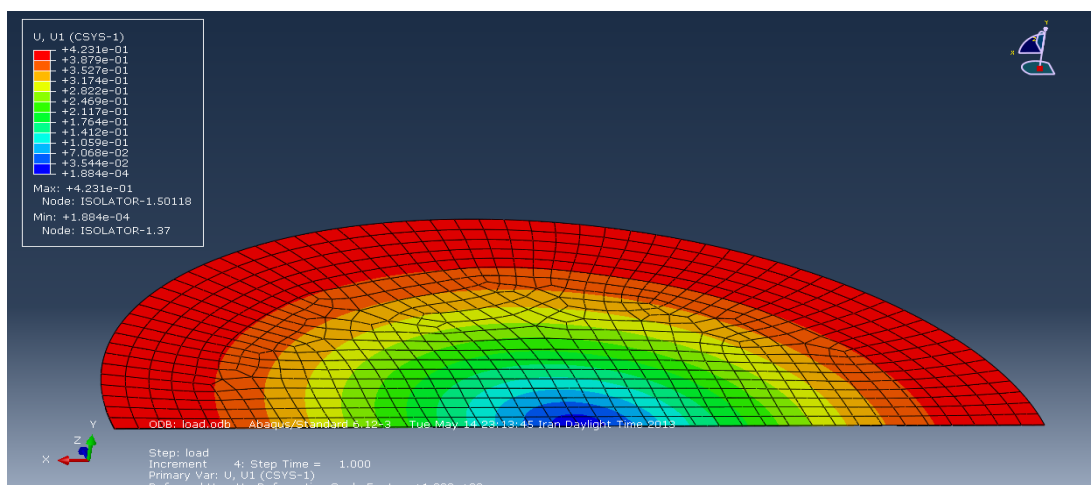
Figure 5.11 Radial elongation of fiber layers under compression

Figures 5.12 and 5.13 show the radial and tangential stress distribution in fiber reinforcement, respectively. As it can be seen from the figures the stress distribution is almost uniform throughout the layers. Figure 5.14 and 5.15 show the tangantial and radial stress distribution in an individual reinforcement layer and these results are compared by the results of pressure solution in Figures 5.16 and 5.17. As it is clear from Figures 5.16 and 5.17 there is a good agreement between the results of finite element analysis and pressure solution. Also Figures 5.18 and 5.19 depicts the normalized stress distribution in reinforcing layers of B-Fb-C150-l predicted by pressure solution and obtained from finite element analysis. The results of finite element analysis complies with the results of pressure solution. As it can be seen from these figures the values of tangential and radial stress in the center of reinforcing layer are equal and this was predicted by pressure solution. According to pressure solution when r/a is equal to 1 (perimeter of reinforcement), radial stress tends to zero but this is not the case for tangential stress. The results of finite element analysis confirm the pressure solution's prediction.

116
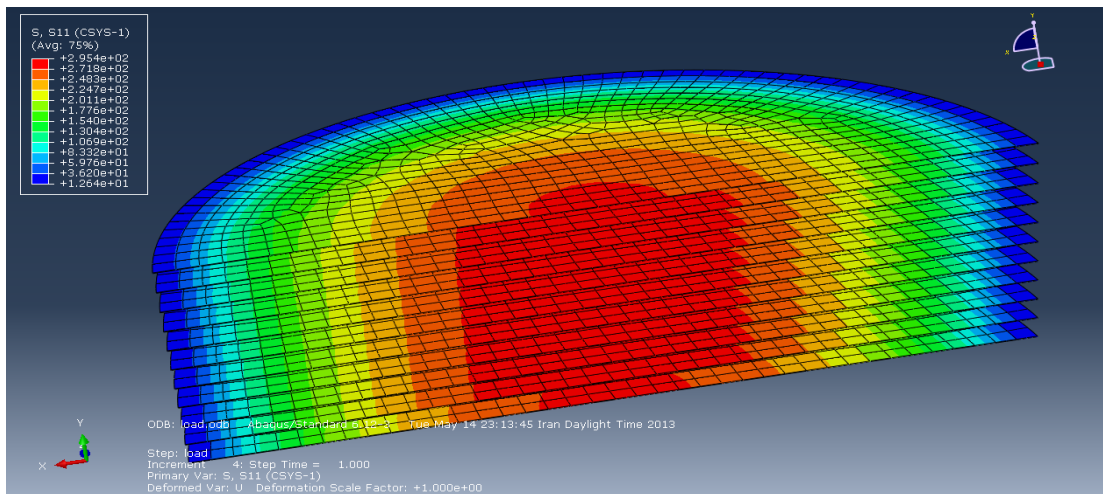
Figure 5.12 Radial stress distribution in reinforcing layers of B-Fb-C150-l
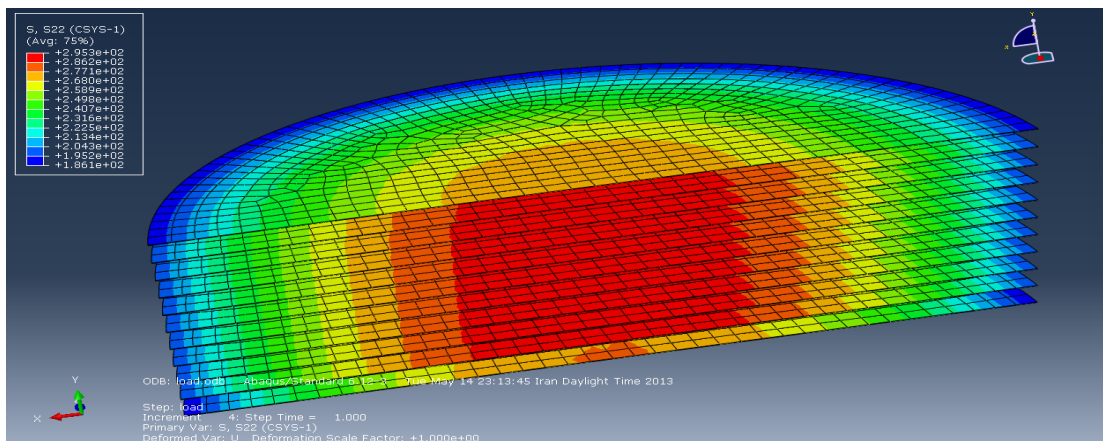
Figure 5.13 Tangential stress distribution in reinforcing layers of B-Fb-C150-l
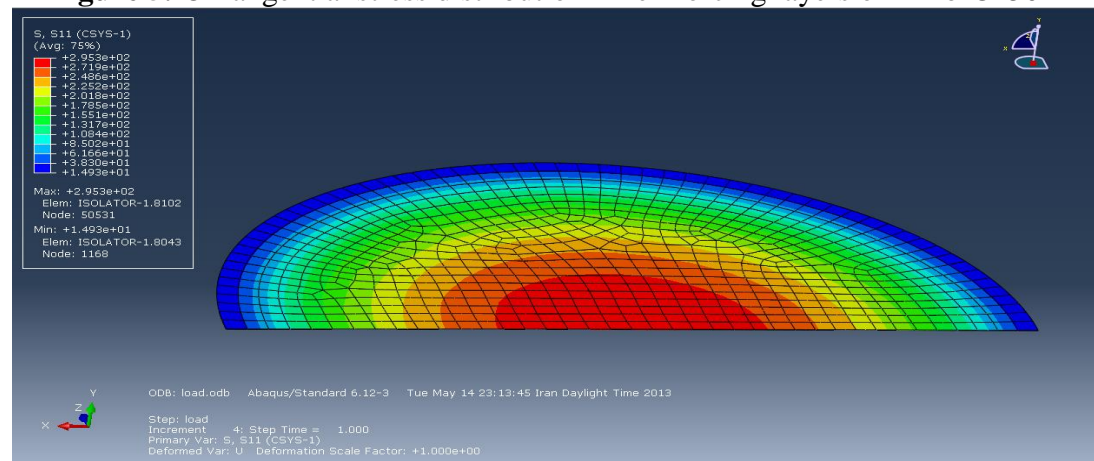
Figure 5.14 Radial stress distribution in an individual reinforcement layer of B-Fb-C150-l
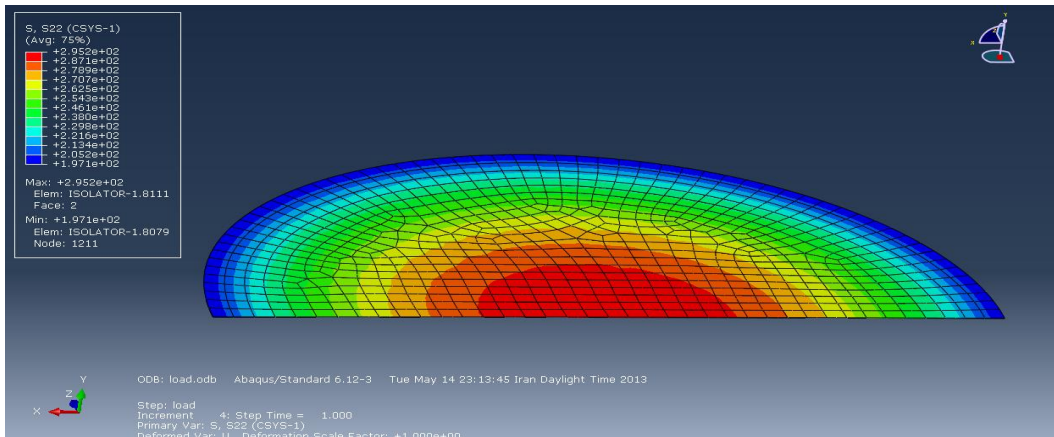
Figure 5.15 Tangential stress distribution in an individual reinforcement layer of B-Fb-C150-l
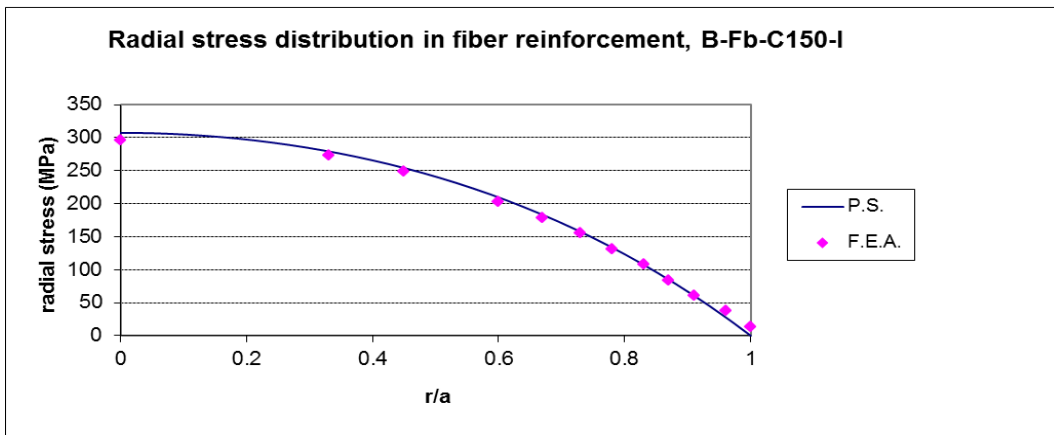
Figure 5.16 Radial stress distribution in reinforcement, B-Fb-C150-l
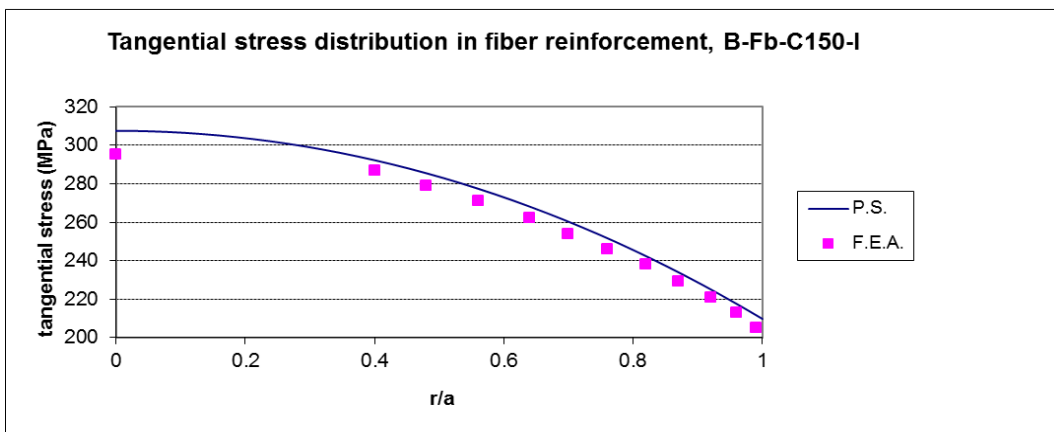
Figure 5.17 Tangential stress distribution in reinforcement, B-Fb-C150-l

118
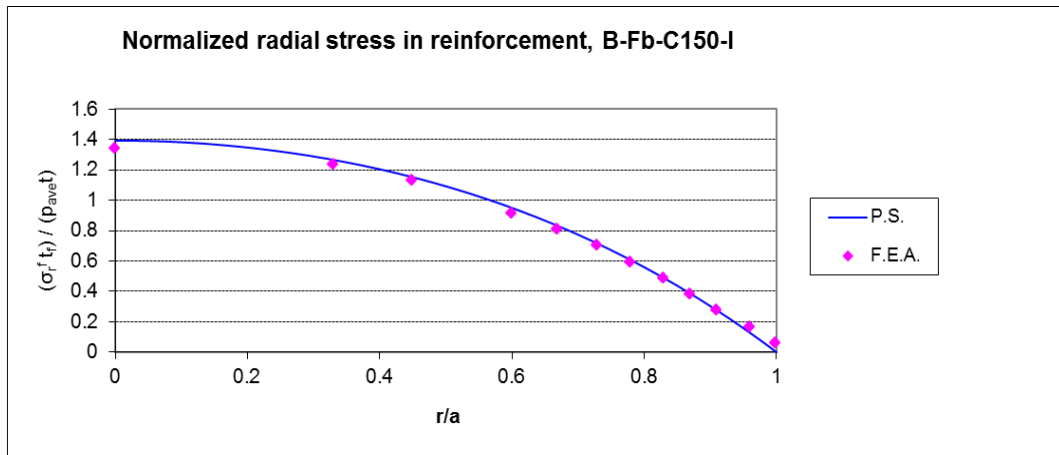
Figure 5.18 Normalized radial stress in reinforcement, B-Fb-C150-l
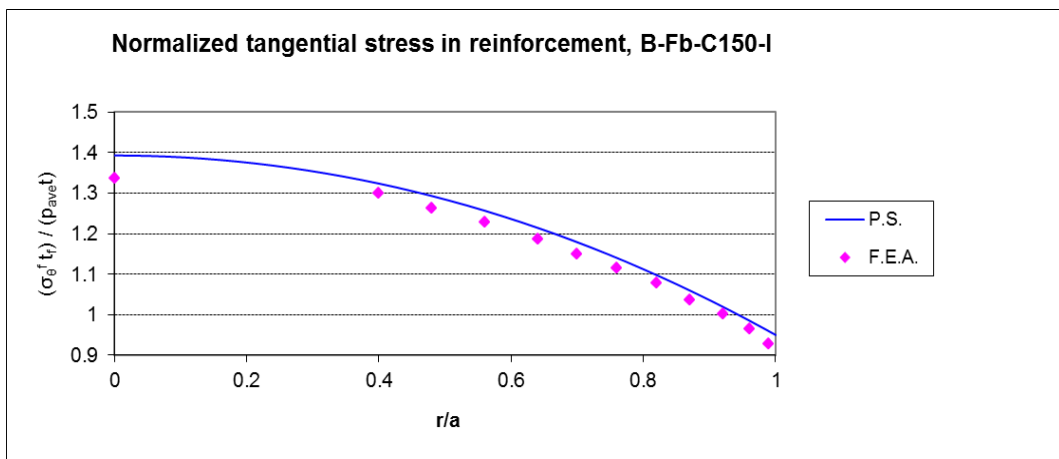
Figure 5.19 Normalized tangential stress in reinforcement, B-Fb-C150-l

Due to symmetry of model, the only non-zero component of shear stress in pressure solution is τ_{rz} and the other two components of shear stress are equal to zero. Figures 5.20-5.22 present the shear stress distribution in rubber layers of B-Fb-C150-l. It can be easily concluded from these figures that the only non-zero component of shear stress is τ_{rz} and this conclusion confirms the validity of pressure solution.

Accordingly, results of finite element analysis of B-Fb-C150-l in ABAQUS comply with the results of pressure solution for predicting the stress distribution in elastomeric material and fiber reinforcement and validate the pressure solution.

119
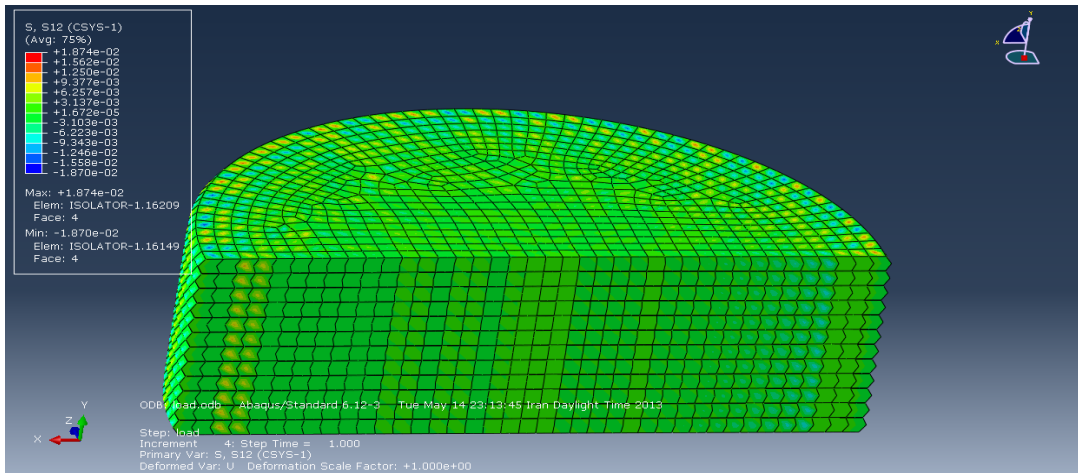
Figure 5.20 Distribution of $\tau_{r\theta}$ in elastomer layers of B-Fb-C150-l
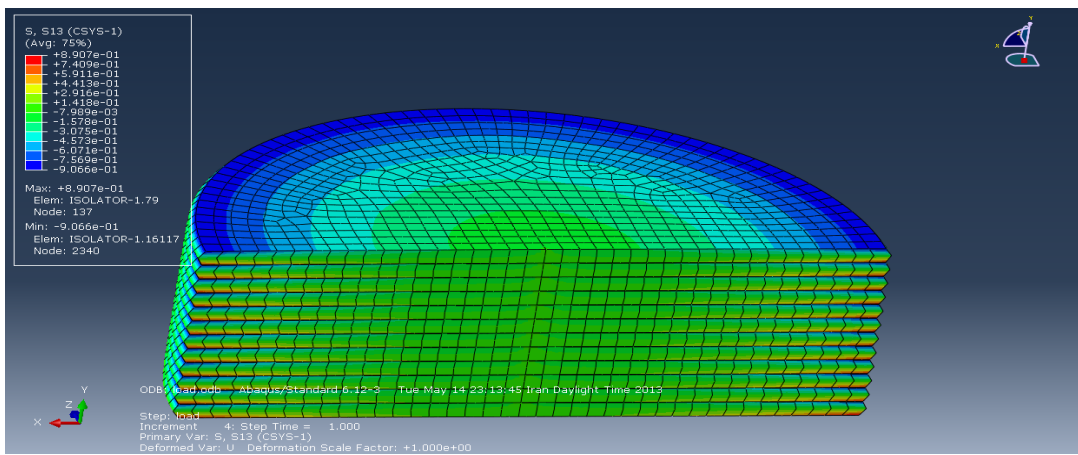
Figure 5.21 Distribution of τ_{rz} in elastomer layers of B-Fb-C150-l
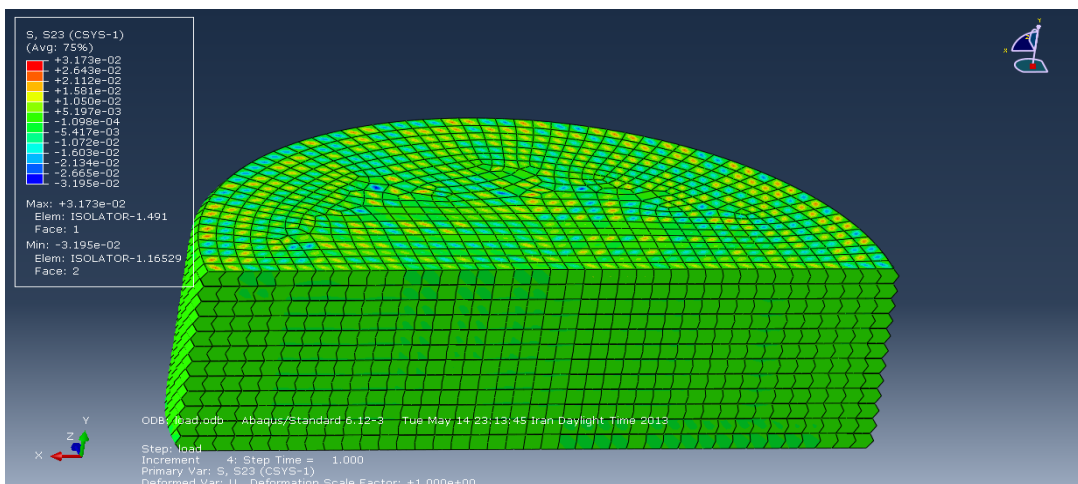
Figure 5.22 Distribution of $\tau_{\theta z}$ in elastomer layers of B-Fb-C150-l

5.2.3 Finite Element Model of B-St-C150-l

Finite element model of B-St-C150-l with top and bottom anchorage plates was defined. Geometrical properties of this bearing was presented in Chapter 3 and the finite element discretization is shown in Figure 5.23. This model consists of 21141 elements and each element is a twenty-node quadratic brick element with side length of 4 mm. Figure 5.24 shows the model mesh of this bearing which was created in ABAQUS.
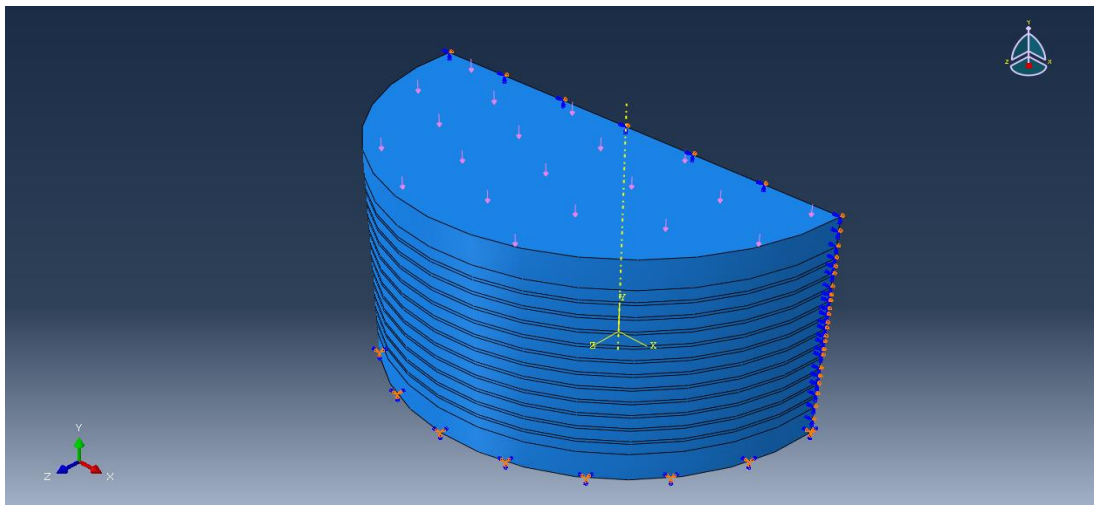
Figure 5.23 Layout of B-St-C150-l in Abaqus
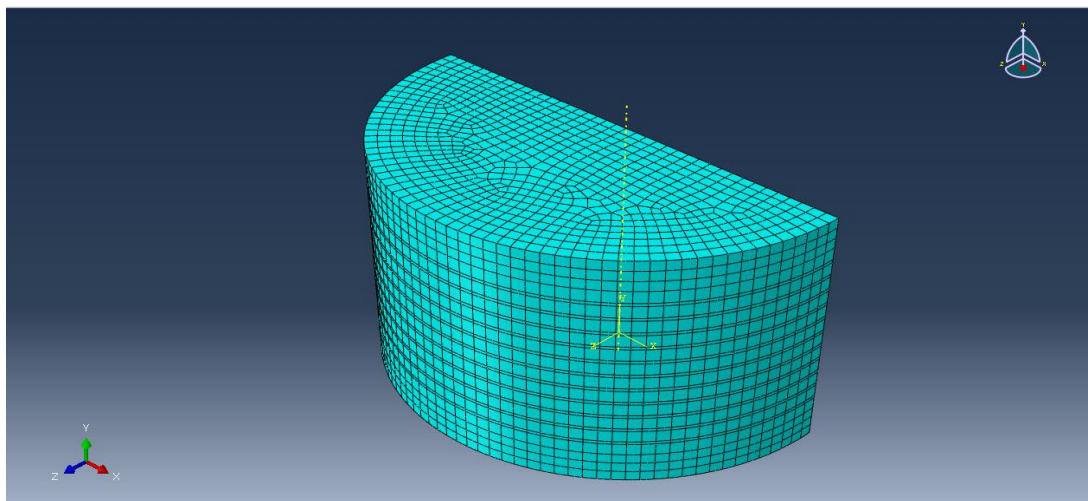
Figure 5.24 Model mesh of B-St-C150-l in Abaqus

The dominant stress components in elastomeric material under pure compression are equal in three main directions. Figure 5.25-5.27 show the pressure distribution in elastomer layers of B-St-C150-l and Figures 5.28-5.29 compare the results of finite element analysis with presssur solution. As before $\sigma_r \approx \sigma_\theta \approx \sigma_z \approx -p$ and the results of finite element analysis and pressure solution are in good agreement.
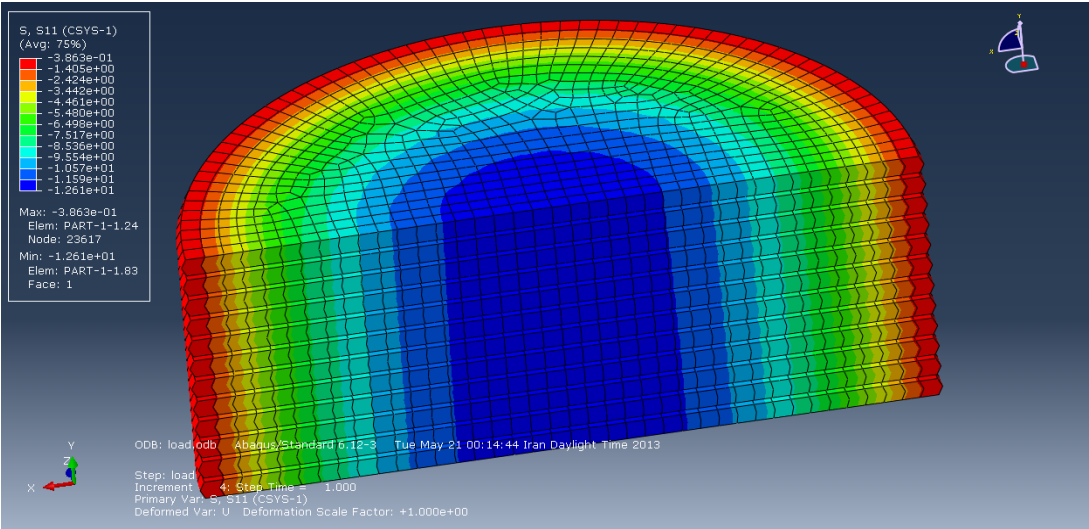
Figure 5.25 Distribution of σ_r in rubber layers
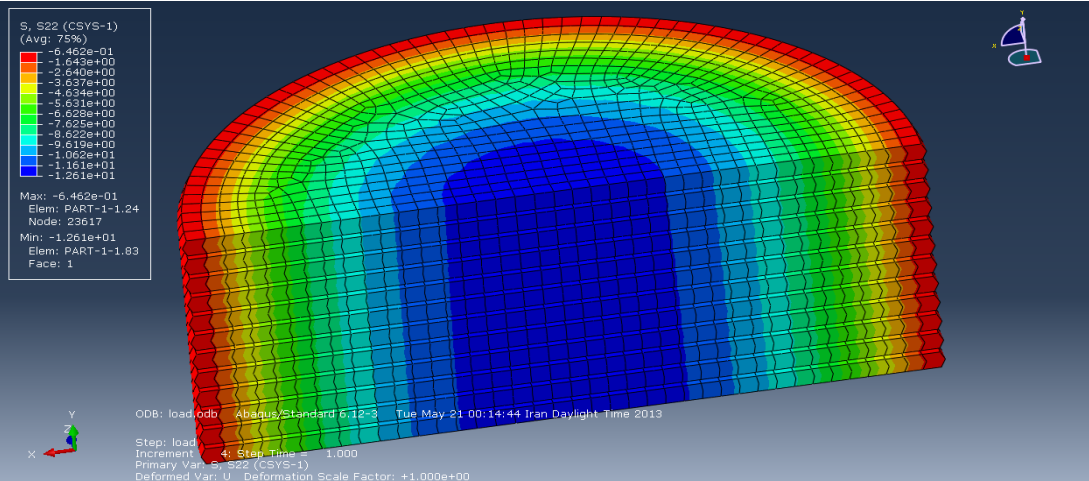
Figure 5.26 Distribution of σ_θ in rubber layers
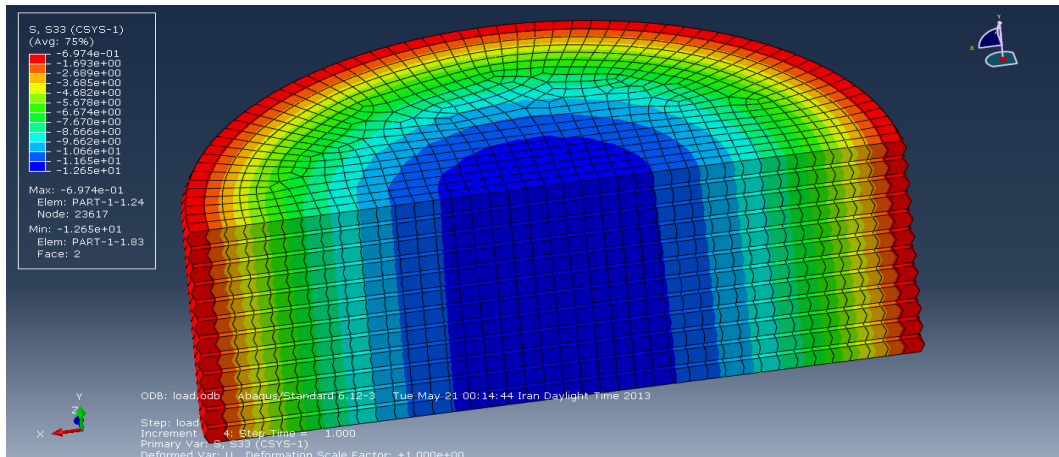
Figure 5.27 Distribution of σ_z in rubber layers
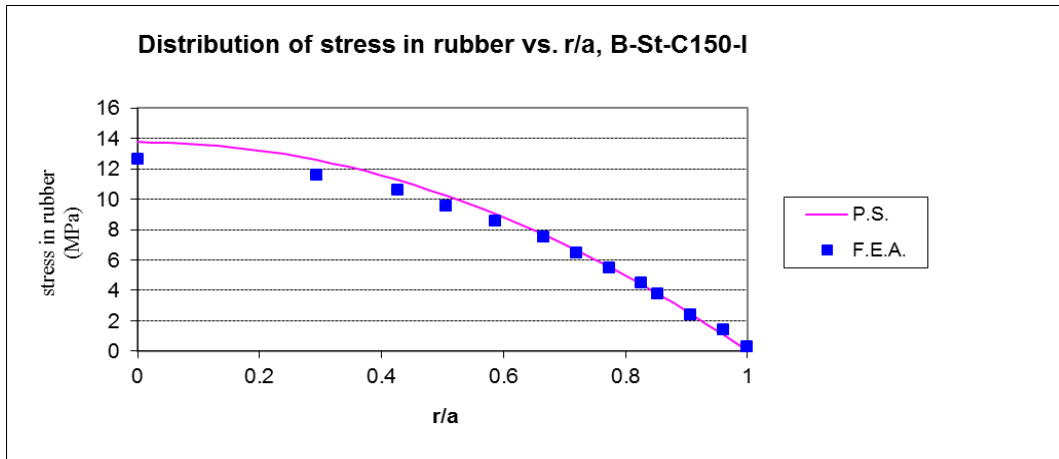
Figure 5.28 Distribution of stress in B-St-C150-l
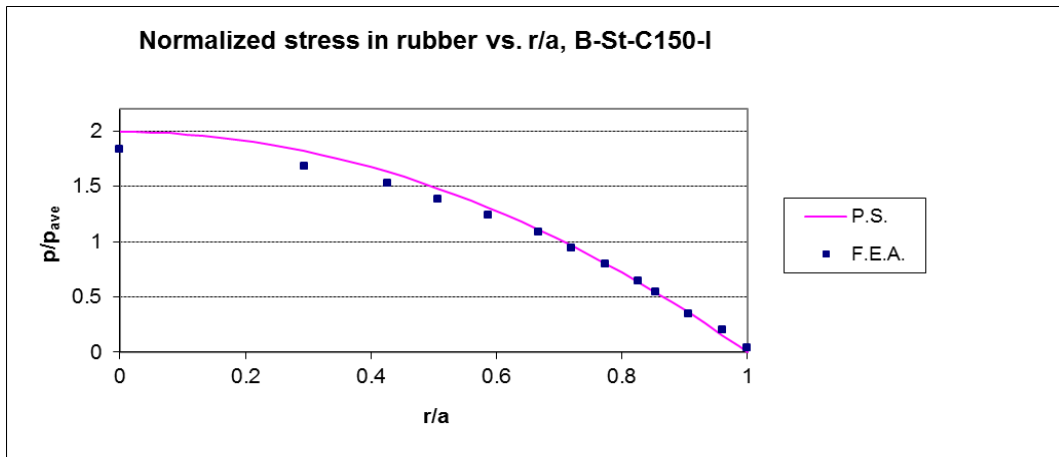
Figure 5.29 Normalized stress distribution in B-St-C150-l with respect to average external pressure

To obtain the vertiacal stiffness of the bearing, the load-deflection relationship of bearing was studied. In the considered range of load and under pure compression (average pressure = 6.90 MPa) the force displacement behavior was obtained to be linear. The value of vertical stiffness is shown in Figure 5.30 and Figures 5.31 and 5.32 illustrate the displacement of the bearing in the direction of applied load.

Figures 5.31 and 5.32 depict the deformation mode of bearing under pure compression. As it can be seen from the figures, displacement of elastomer layers comply with the kinematic assumption of quadratically variable displacement.

In deriving the vertical stiffness of steel reinforced bearing by pressure solution, elongation of steel reinforcing plates was assumed to be zero. This assumption is supported by Figure 5.33 in which the elongation of steel plates tends to be zero.
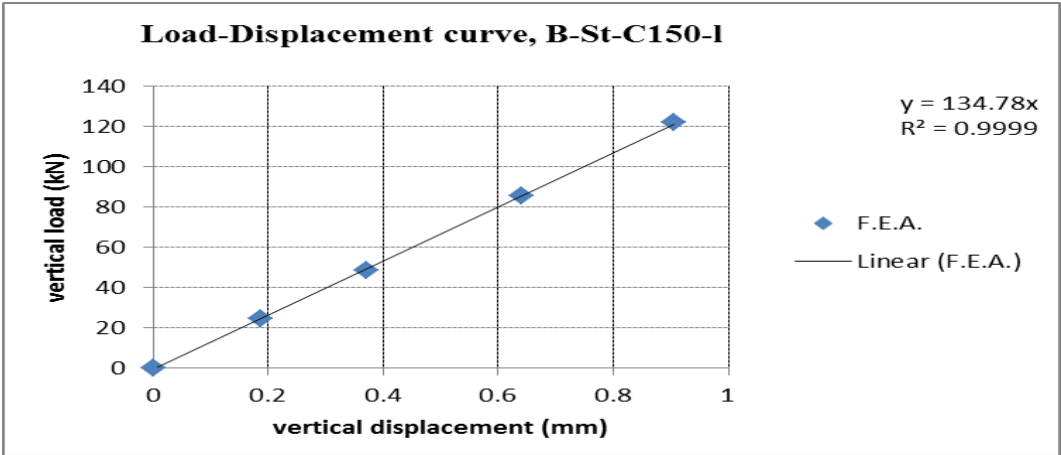
Figure 5.30 Load-deflection curve in vertical direction for B-St-C150-l
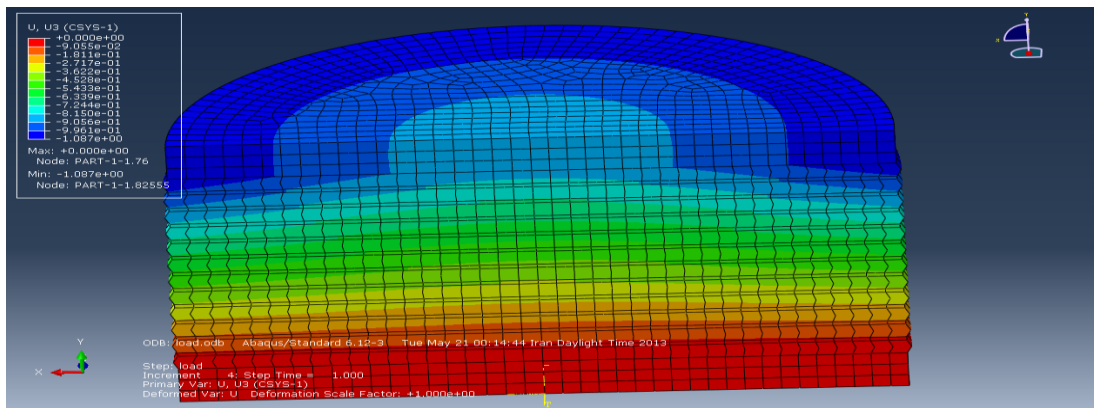
Figure 5.31 Displacement of B-St-C150-l in the direction of applied load
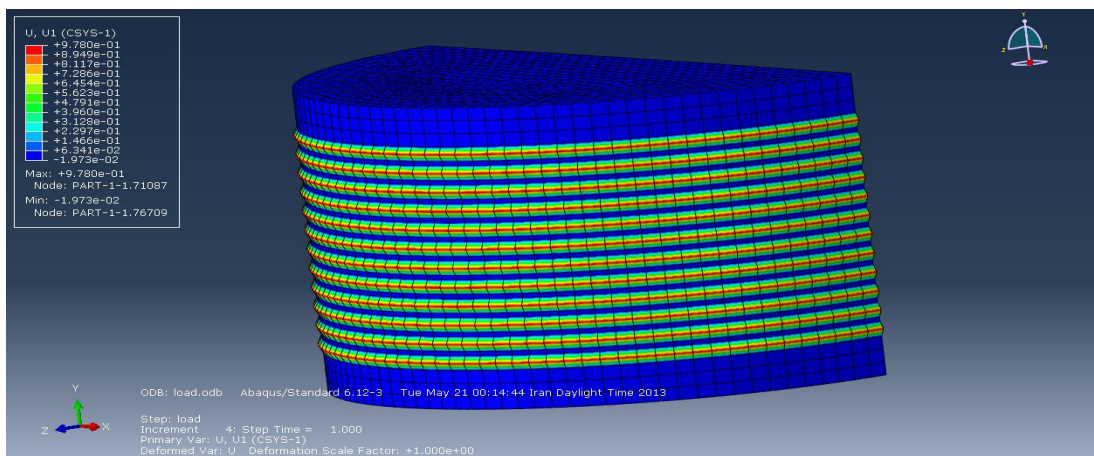
Figure 5.32 Deformation of bearing in radial direction
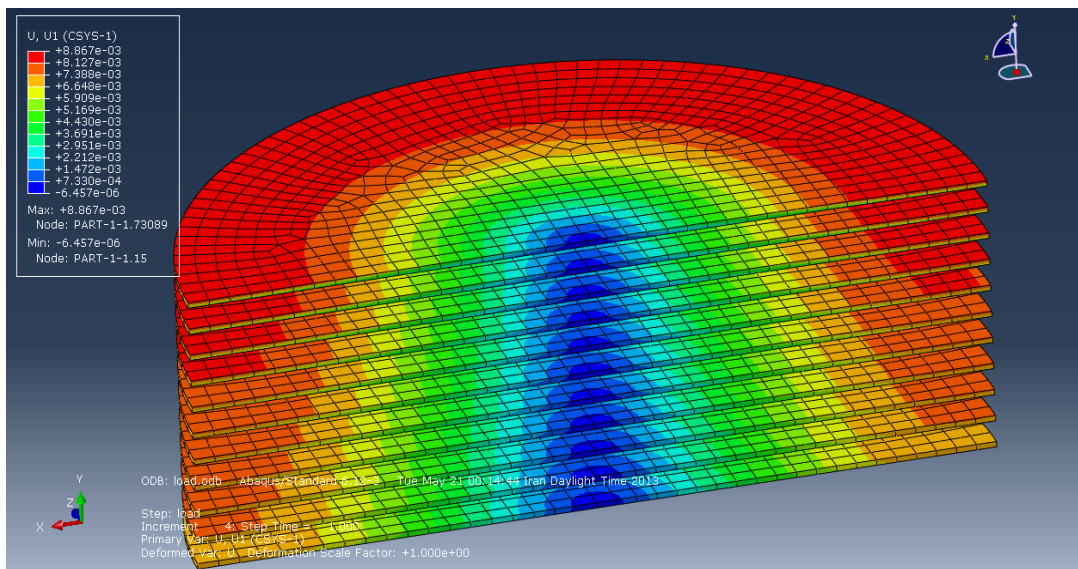
Figure 5.33 Displacement of steel plates under compression in radial directon

Figures 5.34 and 5.35 display the radial and tangential stress distribution in steel plates of B-St-C150-l. Figures 5.36 and 5.37 present the pressure solution results for radial and tangential stress distribution in steel plates. As it can be seen from Figures 5.34-5.35 the maximum value of stress occurs in upper reinforcing plates. Moving downward this maximum stress decreases and tends to the values predicted by pressure solution. The values of radial and tangential stress at the core of the bearing are equal and this is consistent with pressure solution. Figures 5.38 and 5.39 show the normalized radial and tangential stress in reinforcement plates of B-St-C150-l. The radial stress tends to zero at the perimeter of bearing but this is not the case for tangential stress and finite element analysis results support this stress distribution in reinforcing plates.
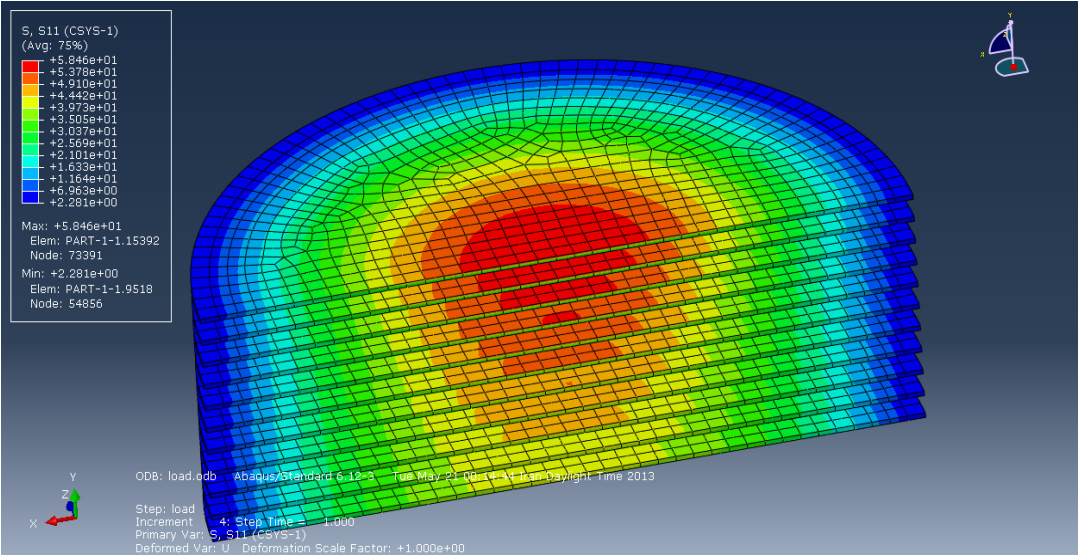
Figure 5.34 Radial stress distribution in steel plates of B-St-C150-l
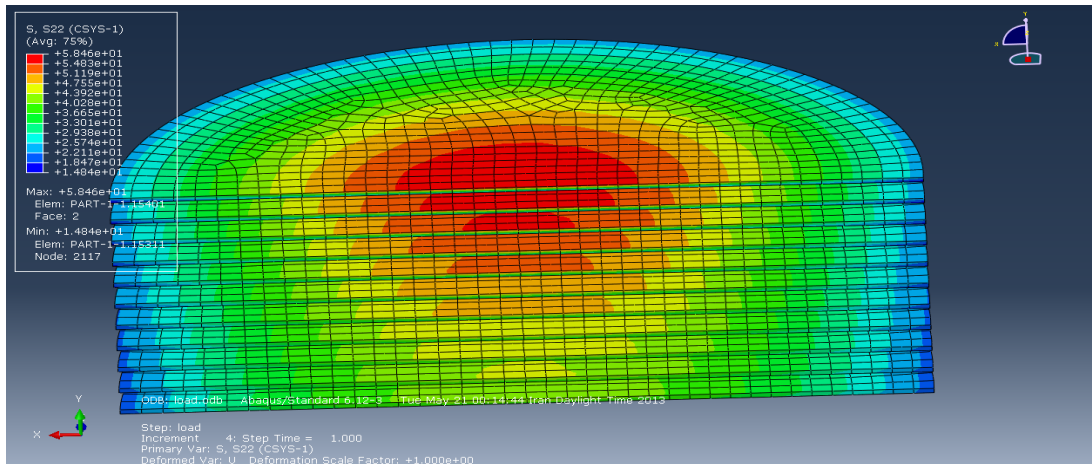
Figure 5.35 Tangential stress distribution in steel plates of B-St-C150-l
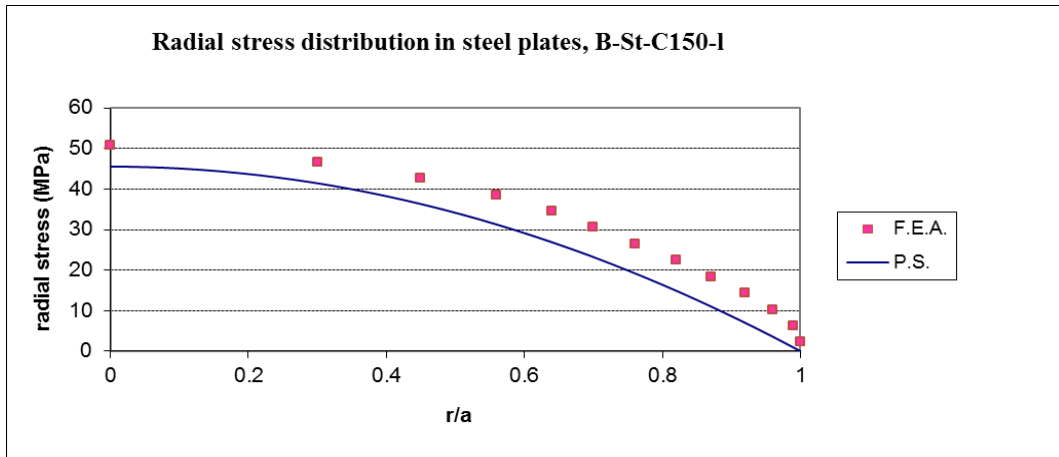
Figure 5.36 Radial stress distribution in reinforcement plates- B-St-C150-l
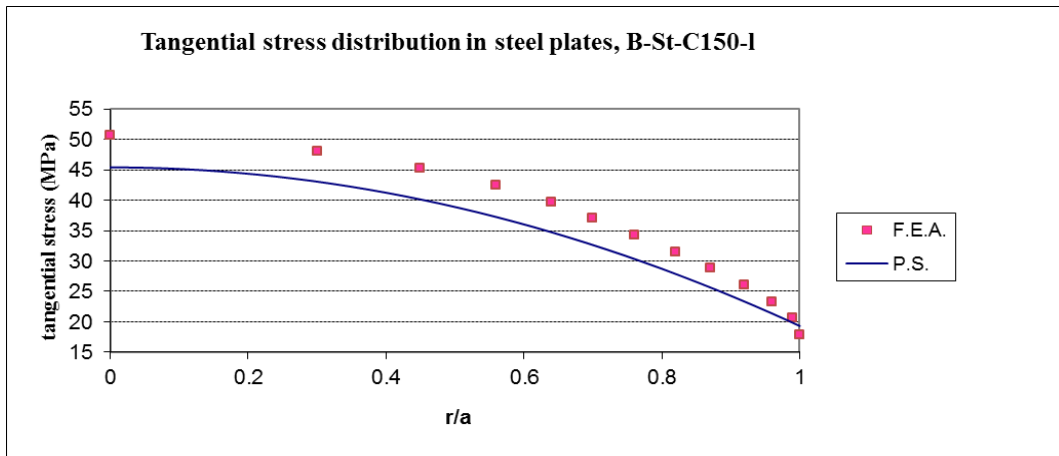
Figure 5.37 Tangential stress distribution in reinforcement plates- B-St-C150-l
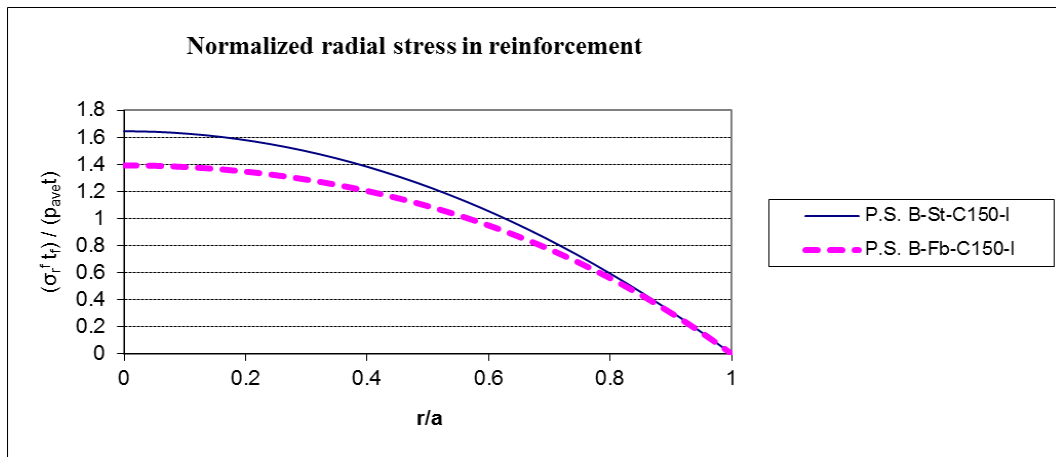
Figure 5.38 Normalized radial stress in reinforcement plates- B-St-C150-l & B-Fb-C150-l
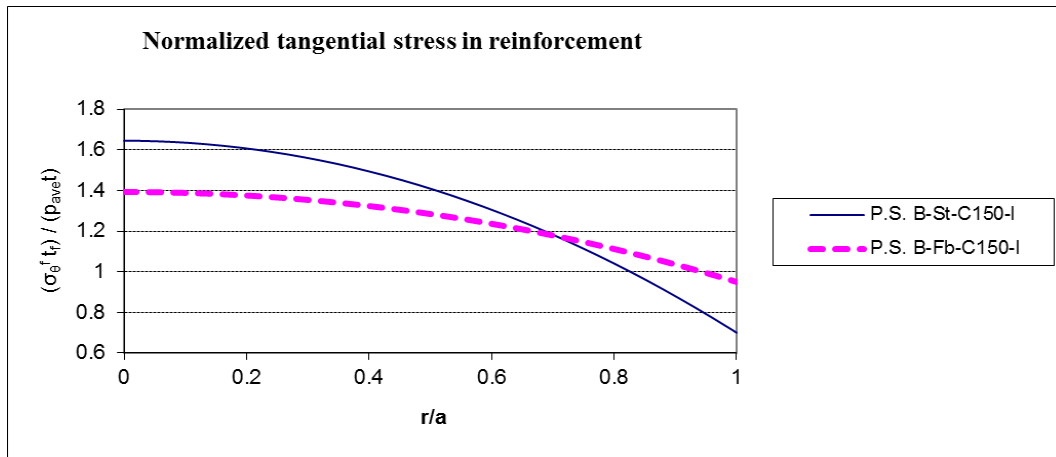
Figure 5.39 Normalized tangential stress in reinforcement plates- B-St-C150-l & B-Fb-C150-l

Figures 5.40-5.42 show the shear stress distribution in elastomeric layers of B-St-C150-l. These figures reveal that the only non-zero component of shear stress is τ_{rz} and this was predicted by theoretical solution.

To sum up, results of finite element analysis of B-Fb-C150-l and B-St-C150-l in ABAQUS complies with the results of pressure solution for predicting the stress distribution in elastomeric material and reinforcement material and validates the pressure solution.

At the core of the bearing with rigid reinforcement, the maximum value of p/p_{ave} in elastomeric material is equal to two. As the reinforcement rigidity decreases this value decreases too and tends to be one as there is no reinforcement and in this case the pressure tends to be uniform with the value p_{ave} . Results of finite element analysis of B-Fb-C150-l and B-St-C150-l comply with this pressure distribution and support the theory. It can be concluded that the effect of the flexibility of the reinforcement is to make the pressure more uniform and decrease the maximum value.

Normalized radial and tangential stress for fiber and steel reinforcement are approximately of the same order. Nevertheless, as the thickness of fiber reinforcement is several times smaller than steel reinforcement, fiber reinforcement undergoes a stress level that is several times greater than the stress level of steel plates.
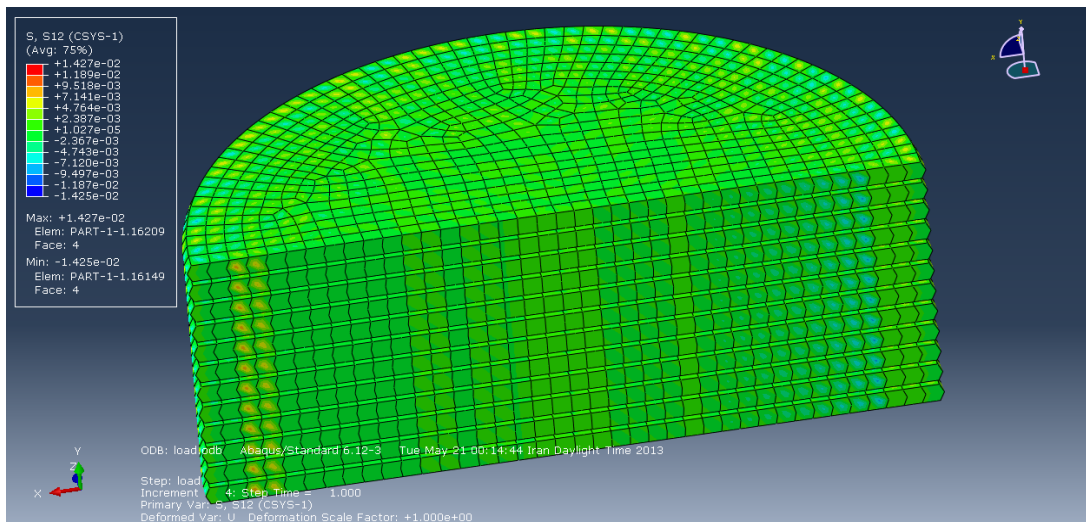
Figure 5.40 Distribution of $\tau_{r\theta}$ in elastomer layers of B-St-C150-l
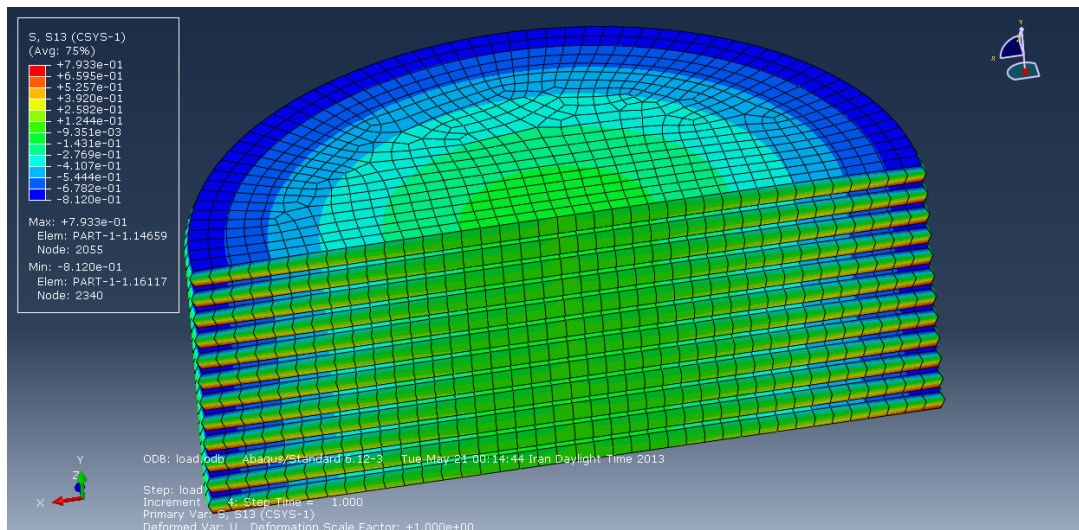
Figure 5.41 Distribution of τ_{rz} in elastomer layers of B-St-C150-l
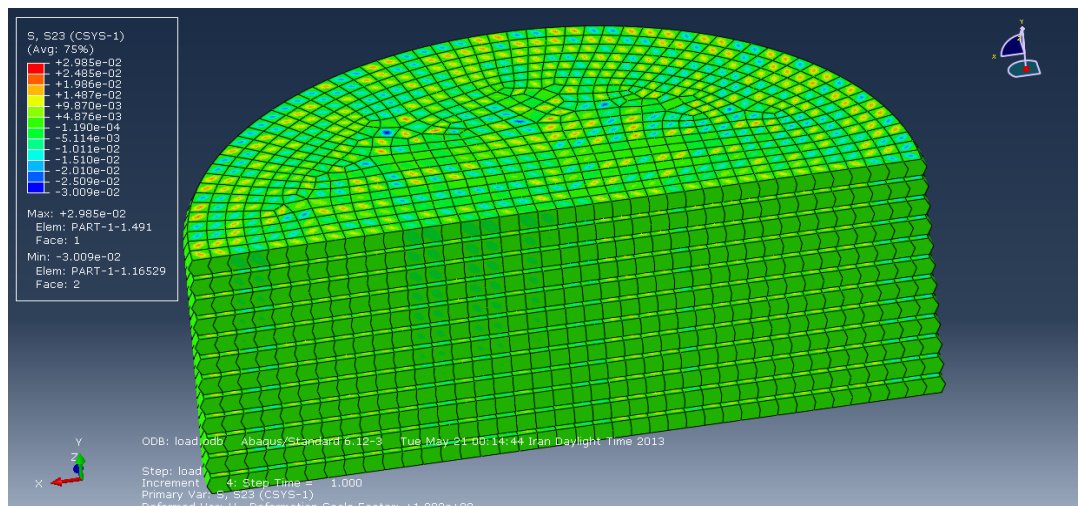
Figure 5.42 Distribution of $\tau_{\theta z}$ in elastomer layers of B-St-C150-l

5.3 Vertical Compression Test

The average vertical stiffness of bearings was obtained from a compression test conducted in Civil-Material Engineering Laboratory of Middle East Technical University. Test specimens were monotonically loaded up to the target value of vertical pressure and then three cycles of vertical loading with small amplitude about this target value were performed. According to the loading capacity of the testing

130

machine only small size bearings were subjected to this test. It is important to note that fulfillment of this test requires a testing system which is capable of doing load control tests in vertical direction. It is worth noting that vertical stiffness of an elastomeric isolation bearing is always a difficult measurement to make, since the displacements at the vertical loads corresponding to practical use are extremely small and a great deal of scatter is to be expected [10]. During this test, at first specimens were subjected to 3.45 MPa vertical pressure and then three fully reversed cycles with the amplitude of 0.35 MPa were applied. After doing first step and unloading the specimens, second step of the test was done. During the second step, specimens were monotonically loaded up to 6.90 MPa vertical pressure and then three fully reversed cycles with the amplitude of 1.73 MPa were applied. The average vertical stiffness of the bearing under 3.45 MPa and 6.90 MPa vertical loads was obtained from the cyclic part of the load-displacement curve of the bearing. In fact, slope of the inclined line interpolating the cyclic part of the load-displacement curve corresponds to the average stiffness of the specimens during the cyclic part of testing. The loading history of the vertical test is presented in Figure 5.43.
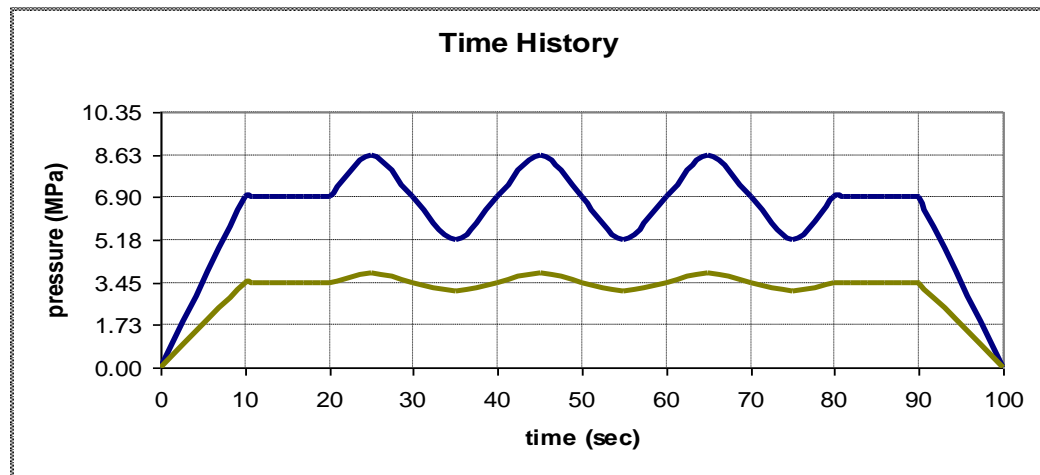
Figure 5.43 Vertical loading history of bearings during test

Bearing type B-St-C150-l, B-Fb-C150-l, B-St-C150-h and B-Fb-C150-h were subjected to this test. Figure 5.44 shows B-St-C150-l under compression test.
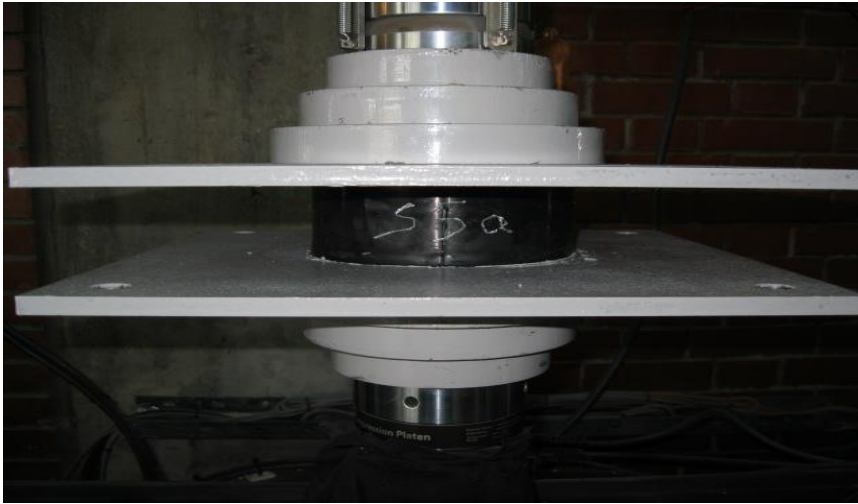
Figure 5.44 Vertical compression test in progress

Results of vertical compression test are presented in Appendix C as vertical load versus vertical displacement. Some of the compression test results are presented in Figure 5.45 and the expression for K_{ave} is presented in these figures. Also in these figures y represent the force and x represent the displacement and coefficient of x in equation y=ax+b represent the average vertical stiffness. The related value of R (Correlation Coefficient) is a measure of the degree of linear relationship between two variables (force-displacement). In correlation, the emphasis is on the degree to which a linear model may describe the relationship between two variables.
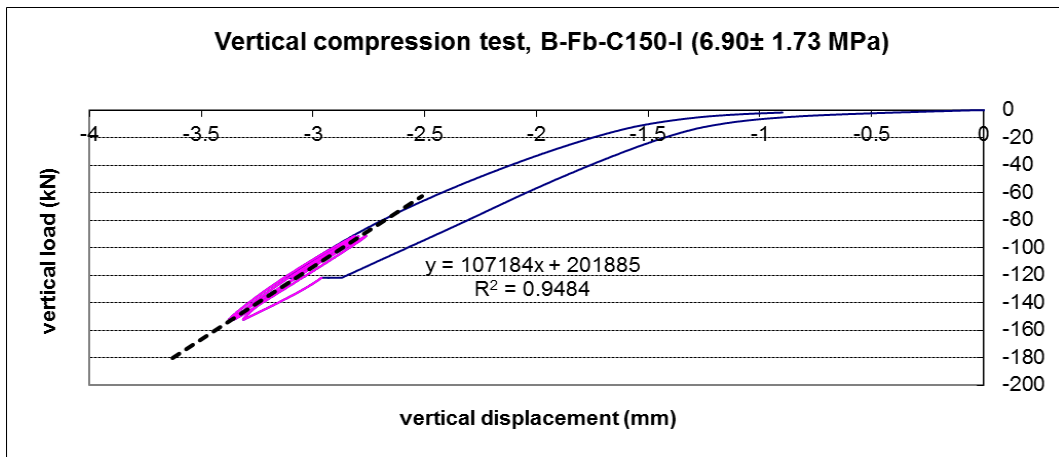
(a)
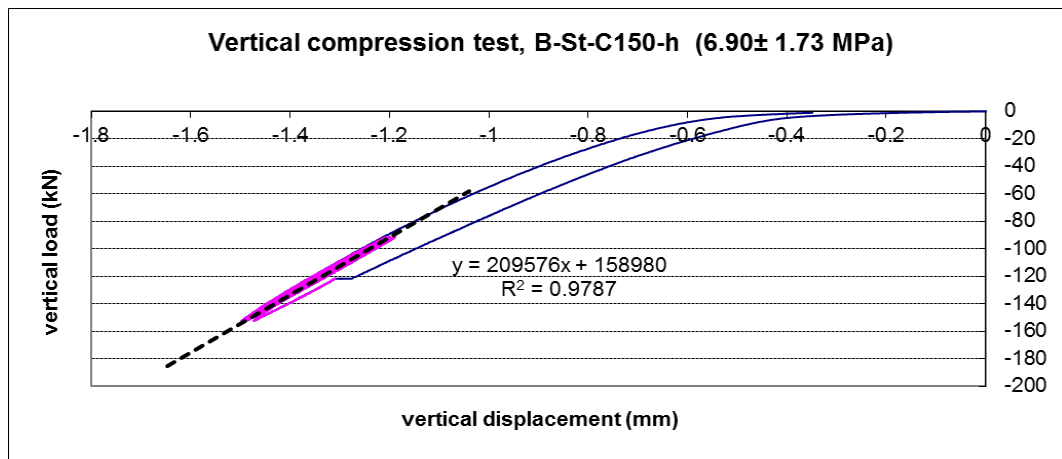
(b)

Figure 5.45 Vertical Load vs. vertical displacement curves for some of bearings: **(a),(b)** B-Fb-C150-h and B-St-C150-h under 6.90 MPa vertical load, respectively

5.3.1 Effect of Fiber Flexibility on Vertical Stiffness

Table 5.1 presents the results of the vertical compression test along with the pressure solution (with and without considering the effect of compressibility) and finite element analysis for the vertical stiffness of the bearings. In calculating the vertical stiffness of bearings, closed form solutions presented in section 2.3.2.2 were used. According to experimental results, it is considered that vertical stiffness of type B-C150-l bearings is close to theoretical values of incompressible material, but this is not the case in type B-C150-h bearings. This means that as thickness of individual

elastomer layer decreases or shape factor increases, the effect of incompressibility in determining the vertical stiffness becomes vital. To consider this effect in type B-C150-h bearings, Bulk modulus of elastomer was assumed to be 1800 MPa. For type B-C150-l bearings theoretical values of vertical stiffness with incompressible material is considered. In Figure 5.46a the ratios of both theoretical and experimental vertical stiffness of steel reinforced bearing over fiber reinforced ones are depicted. As it is seen there is not that much of difference between the theoretical and experimental stiffness ratios in bearings. Figure 5.46b compares the theoretical and experimental stiffness of bearings. Experimental values of stiffness are lower than theoretical values. Fig. 5.46c shows the effects of both fiber flexibility and elastomer compressibility on compression modulus of tested circular bearings. In general, the compression modulus of circular bearing is equal to αGS^2. α is a coefficient which depends on reinforcement rigidity and material compressibility. In the case of rigid reinforcement and incompressible material, this coefficient equals to six. In steel reinforced bearings and in larger shape factors effects of compressibility decreases this coefficient. In fiber-reinforced bearings, effect of fiber flexibility and material compressibility (bearing with larger shape factors) decreases this coefficient drastically.

Results of finite element analysis, experimental tests and pressure solution for vertical stiffness of type B-C150-l bearings are compared in Figure 5.47. It is clear that in steel reinforced bearings there is not that much of difference between the results of three methods and vertical stiffness of steel reinforced bearings can be estimated by one of the mentioned methods. In fiber reinforced bearing, the values predicted by finite element analysis are higher than the other methods. This can be attributed to the stiffening contribution of quadratic mesh. Also experimental values of vertical stiffness in both types of bearings are less than the values predicted by pressure solution. The difference between the experimental stiffness and pressure solution's stiffness increases as the shape factor of bearings incurrences. This can be explained as a result of compressibility.

Table 5.1 Vertical stiffness of bearings

Specimens (B-C150)	Compressive pressure								
	3.45±0.35 (MPa)				6.90±1.73 (MPa)				6.90 (MPa)
	Theoretical K_v^* (kN/mm)		Experimental		Theoretical K_v (kN/mm)		Experimental		F.E.A.
	K=1800MPa	K=infinity	K_v(kN/mm)	E_c(MPa)	K=1800MPa	K=infinity	K_v(kN/mm)	E_c(MPa)	K_v(kN/mm)
Fb-l	49.43	59.65	57.13	155.17	50.61	61.37	60.66	164.76	71.54
St-l	92.85	136.89	132.09	358.78	96.38	144.72	142.1	385.97	134.78
Fb-h	122.34	189.15	103.73	234.79	124.53	194.45	107.18	242.60	-
St-h	226.01	650.47	194.55	440.37	229.67	681.71	209.57	474.36	-
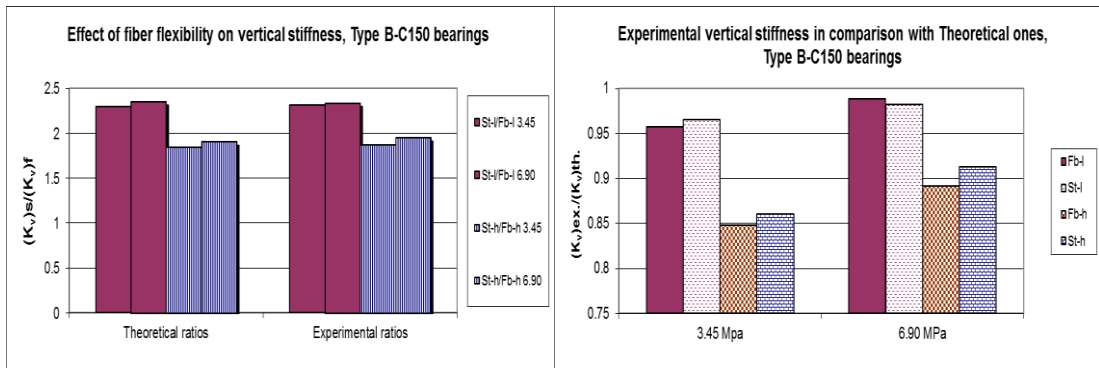
(a)

(b)
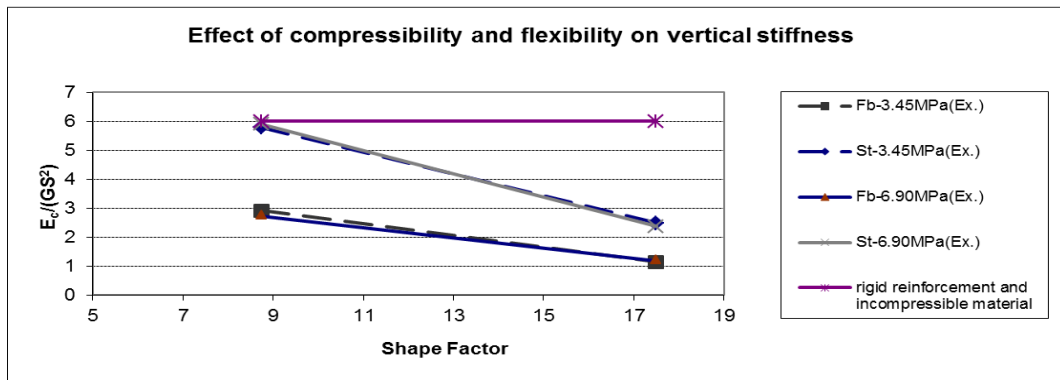
(c)

Figure 5.46 Comparison of vertical test results; **(a)** effect of fiber flexibility (ratios of vertical stiffness of steel reinforced bearings over fiber reinforced ones) **(b)** Ratios of experimental vertical stiffness over the theoretical stiffness **(c)** Experimental values of $E_c/(GS^2)$ versus shape factor
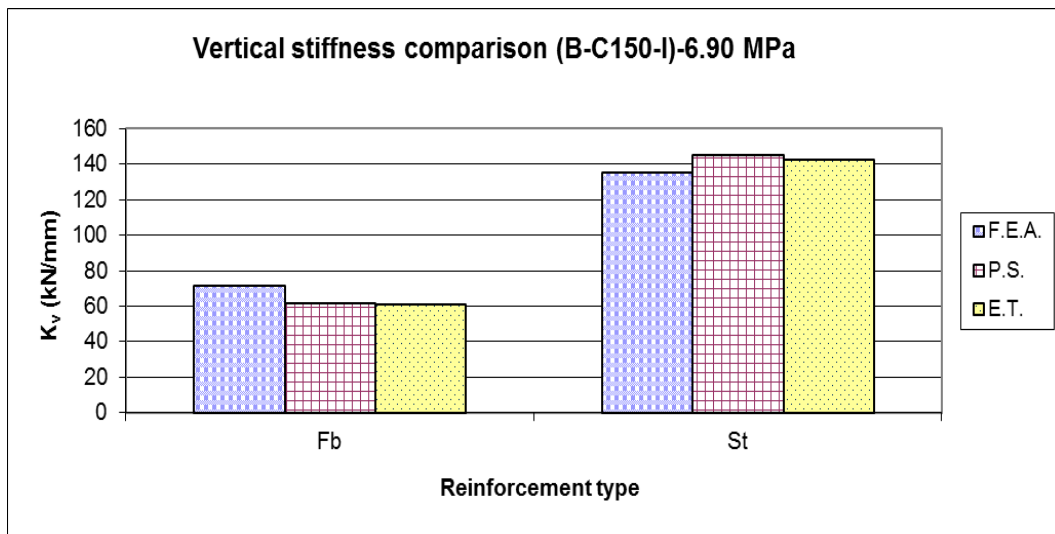
Figure 5.47 Comparison of vertical stiffness of bearings (finite element analysis, pressure solution and experimental test); B-Fb-C150-l & B-St-C150-l

CHAPTER 6

SUMMARY AND CONCLUSION

6.1 Summary

In this dissertation, performance parameters of fiber and steel reinforced bearings were investigated and compared. All of the bearings were produced with the same manufacturing process and twelve pair of each type of bearings were manufactured and tested. To determine the effect of fiber flexibility on vertical stiffness of the bearings, some of the bearings were subjected to vertical compression test. Pressure solution was used to calculate the vertical stiffness of the bearings and comparisons have been made between the pressure solution and test results. To study the stress distribution under pure compression and compare the result with pressure solution, finite element models of both fiber and steel reinforced bearing were created in ABAQUS. Stress distribution in both types of bearings were studied and compared.

According to the results of theoretical and experimental studies, deformation of fiber and steel reinforced bearings are depicted in Figure 6.1. In this figure, part (a) shows the deformation of fiber-reinforced bearing during the horizontal shear test. This deformation mode is accompanied by bending of reinforcing fibers that leads to lower effective stiffness of the bearings. Part (b) illustrates the deformation mode of the fiber-reinforced bearing in vertical compression test. This mode of deformation is along with elongation of fiber reinforcement and deformation of elastomer layer in the form of parabola, which is consistent with theory. Part (c) and (d) illustrate the horizontal and vertical mode shapes of steel reinforced bearings. In part (d) deformation of elastomer layer is parabolic and there is no elongation in steel reinforcement.

Performance of bearings in horizontal direction was investigated by horizontal shear test. In this test, at first a constant vertical pre-load was applied and kept constant throughout the test. Then bearings were subjected to different levels of shear strain and their performance parameters under each strain level were studied. To study the effect of vertical pre-load on horizontal stiffness of the bearings, two different levels of vertical pre-load were applied.

Results of horizontal shear test were used to compare the performance parameters of both types of bearings at different strain levels and according to the results of these comparisons effect of each parameter on performance of bearings were determined.

To investigate the performance of the bearings in cold climates, some of the specimens were subjected to low temperature shear test defined in AASHTO M251-97. Results of low temperature shear test were compared by the recommendations of mentioned standard.
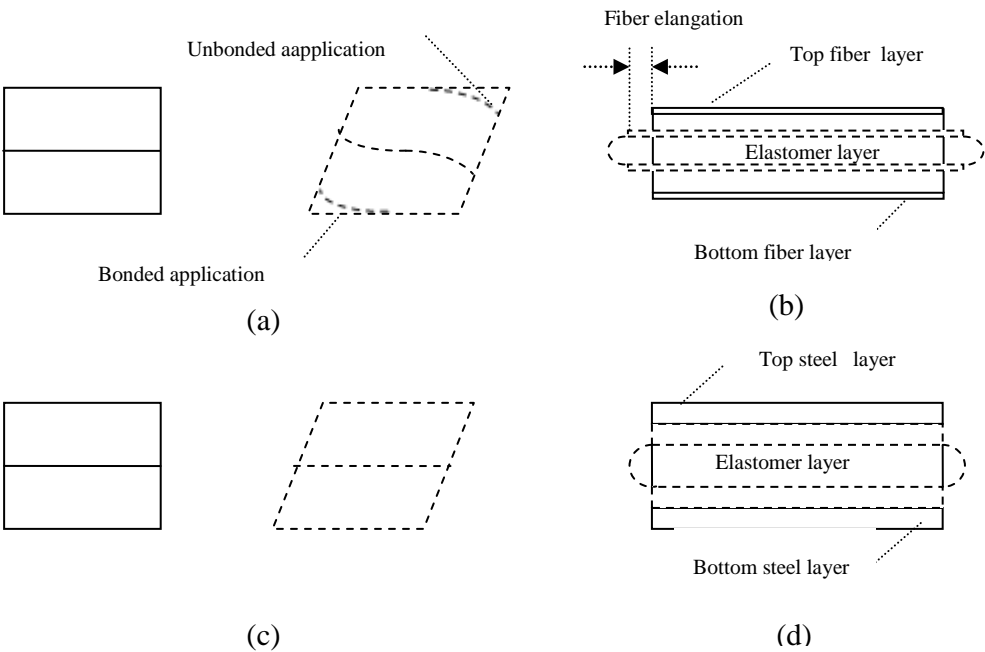
Figure 6.1 Deformation mode shapes of fiber and steel reinforced bearings in bonded and unbounded application

6.2 Conclusion

Test results of fiber mesh reinforced elastomeric bearings and conventional bearings are compared. The following conclusions are made based on the test results;

- The tested fiber mesh reinforced bearings (Type U-Fb-C200, U-Fb-S150 and B-Fb-C150) have a significant reduction in terms of horizontal stiffness compared to the conventional bearings at high levels of vertical load and at high levels of shear strain. This is due to rollover response of fiber mesh reinforced bearings which occurs at higher strain levels.

- Damping values in both Fb and St type bearings are pretty much comparable, as when no lead core is inserted, damping is mostly provided by the elastomer material.

- In all tested cases, high level of vertical load results in high horizontal stiffness as expected. It is believed that an increase in compression, increases the bonding between the molecules and this leads to an increased stiffness.

- In all tested case, vertical stiffness of the fiber-reinforced bearings are significantly low compared to the steel ones and this observation is consistent with the previous research results. In fiber reinforced bearings, elongation of fibers in each reinforcing layer increases the total displacement of the bearing in vertical direction and as displacement of bearing increases, stiffness decreases. There is no elongation of reinforcing material in steel reinforced bearings and as a result their vertical stiffness is higher than fiber reinforced ones. Vertical stiffness of fiber-reinforced bearings as steel reinforced ones is affected by magnitude of shape factor. Shape factor is an important parameter in designing fiber-reinforced bearing for high levels of vertical loads in low to mid rise buildings.

- The theoretical equations developed in the previous research [16] for fiber sheet reinforced bearings are determined to be satisfactory when compared

the test results of the fiber mesh reinforced bearings presented in this dissertation.

- It is believed that the vulcanization of fiber mesh is more effective than vulcanization of steel plate to rubber since the rubber not only bonds to the surface of the fiber but also provides a positive connection between the adjacent layers through the openings of the mesh.

- Results of finite element analysis or pressure solution predict well the vertical stiffness of both types of bearings. Results of these methods match the experimental test results for vertical stiffness of bearings.

- Performance of bearing in low temperature depends mostly on rubber compound and fiber reinforcement has not any considerable effects.

6.3 Recommendations for Further Researches

In the light of the studies conducted in this dissertation, the following recommendations can be made for further research on the subject.

- All of the previous studies including this one considered small sizes of fiber-reinforced bearings. However larger specimens may be tested and studied in detail for further development of this type of bearings.

- Although Pinarbasi [46] and Kelly [10] derived the closed form solutions of infinitely long strip bearings subjected to pure compression, there is not any closed form solution for vertical stiffness of rectangular fiber-reinforced bearings with considering the effect of compressibility. These closed form solutions may be developed and their validity may be examined by tests.

- Effect of fiber flexibility on horizontal stiffness of the bearings may be studied analytically and the results of analytical study may be validated by testing.

-   Application of fiber reinforced bearings in prototype tests are required to investigate the performance of fiber-reinforced elastomeric bearings in vertical and horizontal directions.

REFERENCES

[1] Kelly, J. M. (1991). "Base Isolation: Origins and Development." EERC News, Vol. 12, No. 1.

[2] Kelly, J. M. (1997). "Earthquake Resistance Design with Rubber." Second Edition, Spronger-Verlag London Ltd, Great Britain.

[3] http://www.maurer.co.uk/doc/SEISMIC-isolation.pdf, last visited on December 2013.

[4] Naeim, F., Kelly, J. M. (1999). "Design of Seismic Isolated Structures: From Theory to Practice." John Wiley & Sons, Inc. New York.

[5] Kuntz, R. J., Tanner, D.L. (1992). "Earthquake Mitigation Technology Life, Safety, Structures, Contents, and function." Disaster Recovery Journal, 5(4).

[6] Eisenberg, J. M., et al. (1992). "Application of Seismic Isolation in the URSS." Proceeding of the Tenth World Conference on Earthquake Engineering, A.A. Balkema, Rotterdam, 4, 2039-2044.

[7] Skinner, R. I., et al. (1993). "An Introduction to Seismic Isolation." John Wiley & Sons, Inc. Chichester, England.

[8] Taylor, A. W., and Igusa, T. (2004). "Primer on Seismic Isolation." American Society of Civil Engineering (ASCE), Reston, Virginia.

[9] Kelly, J. M. (2001). "Structural Control in Developing Countries." SLC Seminar Series, MAE Center, University of Illinois.

[10] Kelly, J. M., Takhirov, Sh. M. (2002). "Analytical and Experimental Study of Fiber-Reinforced Strip Isolators." PEER Report, University of California, Berkeley.

[11] Kelly, J. M. (1999). "Analysis of fiber-reinforced elastomeric isolators." J. Seismol. Earthquake Eng., 2(1), 19-34.

[12] Moon, B. Y., Kang, G. J., Kang, B. S., Kelly, J. M. (2002). "Design and manufacturing of fiber reinforced elastomeric isolator for seismic isolation" J. Mater. Process., 130–131, 145–150.

[13] Ashkezari, Gh., Aghakouchak, A., Kokabi, M. (2007). "Design, manufacturing and evaluation of the performance of steel like fiber reinforced elastomeric seismic isolators." J. Mater. Process. Technol., 197, 140-150.

[14] Toopchi-Nezhad, H., Tait, M., Drysdale, R. (2008). "Lateral response evaluation of fiber-reinforced neoprene seismic isolators utilized in an unbonded application." J. Struct. Eng., 134, 1627-1637.

[15] Toopchi-Nezhad, H., Tait, M., Drysdale, R. (2009). "Shake table study on an ordinary low rise building seismically isolated with SU-FREIs (stable unbonded-fiber reinforced elastomeric isolators)." J. Earthquake Eng. & Structural Dynamics, 38, 1335–1357.

[16] Calabrese, A., Kelly, J. M. (2012). "Mechanics of Fiber Reinforced Bearings." PEER Report, University of California, Berkeley.

[17] Simo J. C., Kelly J. M. (1984). "Finite element analysis of the stability of multilayer elastomeric bearings." J. Eng. Struct., 6(3), 162−174.

[18] Seky, W., Fukahori, Y., Iseda, Y., and Matsunaga, T. (1987). "A large deformation finite element analysis for multilayer elastomeric bearings." Rubber Chem. Tech., 60, 856−869.

[19] Takayama, M., Tada, H., Tanaka, R. (1994). "Finite element analysis of laminated rubber bearings used in base-isolation system." J. Rubber Chem. Tech., 65, 46−62.

[20] Mordini, A., Strauss, A. (2008). "An innovative earthquake isolation system using fibre reinforced rubber bearings." J. of Eng. Struct., 30, 2739–275

[21] Rao, Singiresu S. (1995). "Mechanical Vibrations." 3rd Edition, Addison-Wesley Publishing Company, Inc.

[22] Chopra, Anil K. (2012). "Dynamics of Structures: Theory and Applications to Earthquake Engineering" Second Edition, Prentice Hall, Upper Saddle River, New Jersey.

[23] Kelly, J. M., Takhirov, Sh. M. (2001). "Analytical and Experimental Study of Fiber-Reinforced Elastomeric Isolators." PEER Report, University of California, Berkeley.

[24] Rocard, Y. (1937), "Note sur le calcul des properietes elastique des supports en caoutchoue adherent." Journel de Physique et de Radium, 8, 197.

[25] Gent, AN., Lindley, PB. (1959). "The Compression of Bonded Rubber Blocks." J. Proceedings Institution of Mechanical Engineers., 173, 324.

[26] Gent, AN., Meinecke, EA. (1970). "Compression, Bending and Shear of Bonded Rubber Blocks." J. Engineering Mechanics., 10(2), 48-53.

[27] Tsai, H. Ch., Kelly, J. M. (2001). "Stiffness Analysis of Fber-Reinforced Elastomeric Isolators." PEER Report, University of California, Berkeley.

[28] http://www.steelss.com/Carbon-steel/st37-3u.html, last visited on December 2013

[29] Russo, G., Pauletta, M. (2012). "Sliding instability of fiber-reinforced elastomeric isolators in unbonded applications." J. Engineering Structures., Doi: 10.1016/j.engstruct.

[30] http://www.fibermaxcomposites.com/shop/-p-1032.html, last visited on December 2013

[31] AASHTO (2000). "Guide Specification for Seismic Isolation Design." Second Edition, INTERIM 2000, p. 49.

[32] Clough, WR., Penzien, J. (1975). "Dynamics of Structures." 2nd ed., McGraw-Hill, New York.

[33] AASHTO M251-97 (1997). "Standard Specifications for Plane and Laminated Elastomeric Bridge Bearings."

[34] Ozkaya, C. (2010). "Development of a New Seismic Isolator Named 'Ball Rubber Bearing'. " Ph.D. Dissertation, Middle East Technical University.

 [35] http://www.vishaypg.com/docs/11270/syst6000.pdf, last visited on December 2013

[36] http://www.upc.edu/pct/documents_equipament/d_55_id-373.pdf, last visited on December 2013

[37] D 3039 /D 3039 M – 00 (Reapproved 2006). "Standard Test Method for Tensile Properties of Polymer Matrix Composite Materials."

[38] Ozkaya, C., Akyuz, U., Caner, A., Dicleli, M., and Pinarbasi, S. (2011). "Development of a new rubber seismic isolator: 'Ball Rubber Bearing'." J. Earthquake Eng. & Structural Dynamics, 40(12), 1337–1352.

 [39] Pinarbasi, S., Akyüz, U., and Ozdemir, G. (2007). "An Experimental Study on Low Temperature Behavior of Elastomeric Bridge Bearing." 10th world conference on seismic isolation, energy dissipation and active vibrations control of structures, Istanbul, Turkey

[40] European Standard BS EN 1337-3:2005

[41] Constantinou, M. C., Whittaker, A. S., Kalpakidis, Y., Fenz, D. M., and Warn, G. P. (2007). "Performance of seismic isolation hardware under service and seismic loading." MCEER-07-0012, Multidisciplinary Center for Earthquake Engineering Research, State University of New York, Buffalo, NY.

[42] Yakut, A. (2000). "Performance of Elastomeric Bridge Bearings at Low Temperatures." Ph.D. Dissertation, The University of Texas at Austin.

[43] Stanton, J. F., Roeder, C. W. (1982). "Elastomeric Bearings, Design, Construction and Materials." NCHRP Report 248, Washington, D.C.

[44] Roeder, C. W., Stanton, J. F., and Taylor A. W. (1987). "Performance of Elastomeric Bearings." NCHRP Report 298, Washington, D.C.

[45] ABAQUS analysis user's manuel, Materials (2013). "Hyperelastic behavior of rubberlike materials," Section 21.5.1

[46] Pinarbasi, S. (2007). "A New Formulation for the Analysis of Bonded Elastic Layers." Ph.D. Dissertation, Middle East Technical University.

APPENDIX A

BEARINGS SCHAMETIC VIEW
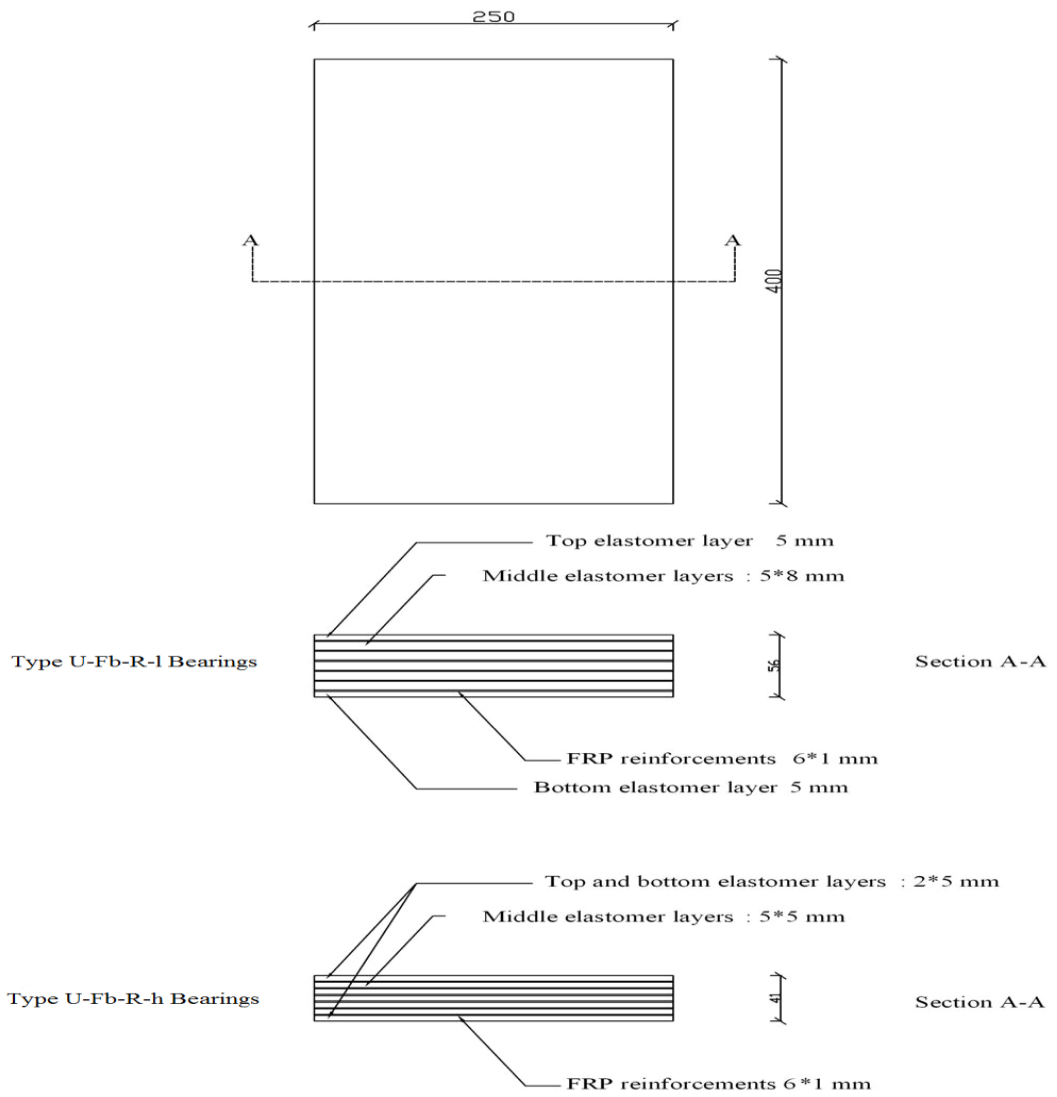
Figure A.1 Schematic view of Type U-Fb-R bearings
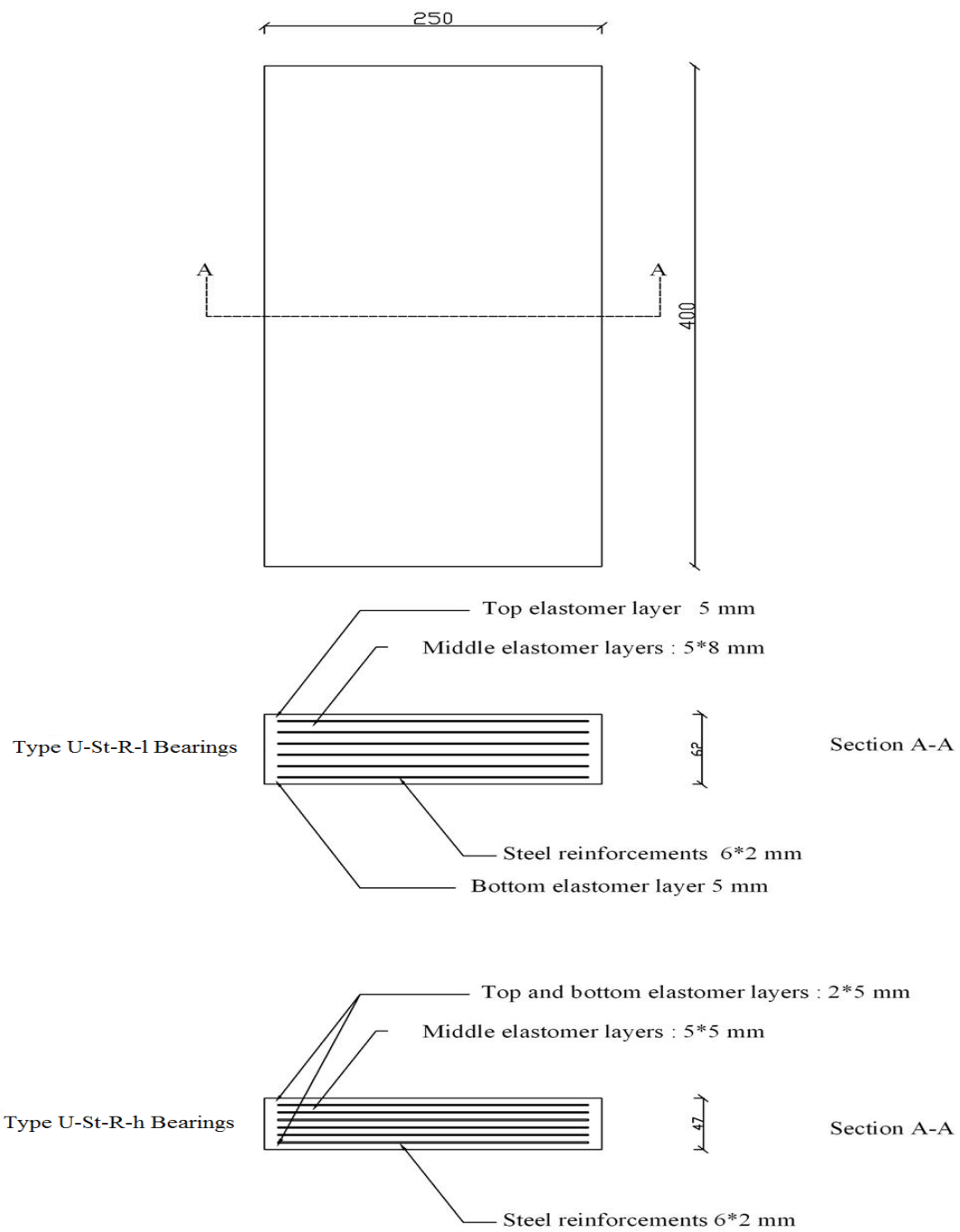
Figure A.2 Schematic view of Type U-St-R bearings
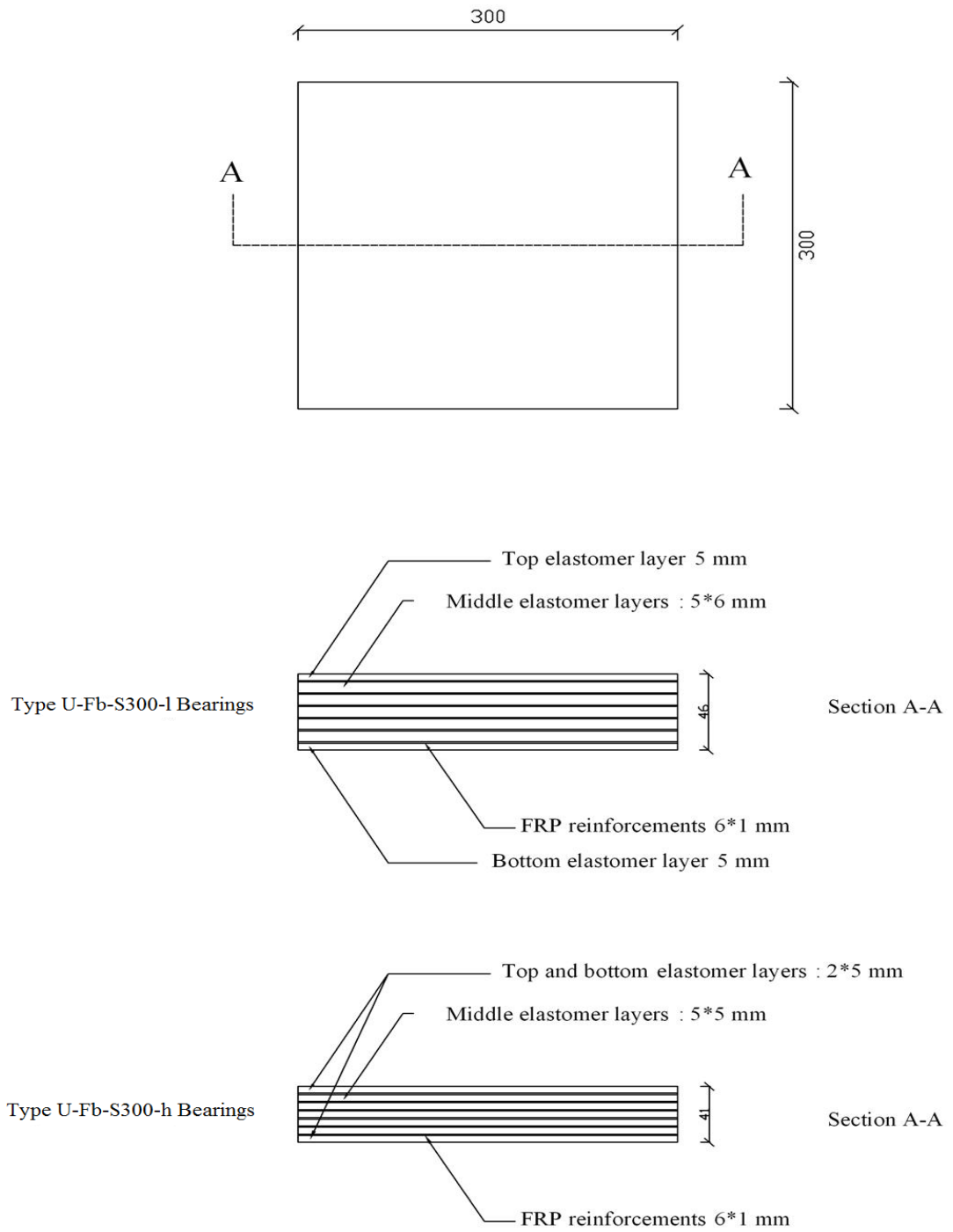
Figure A.3 Schematic view of Type U-Fb-S300 bearings
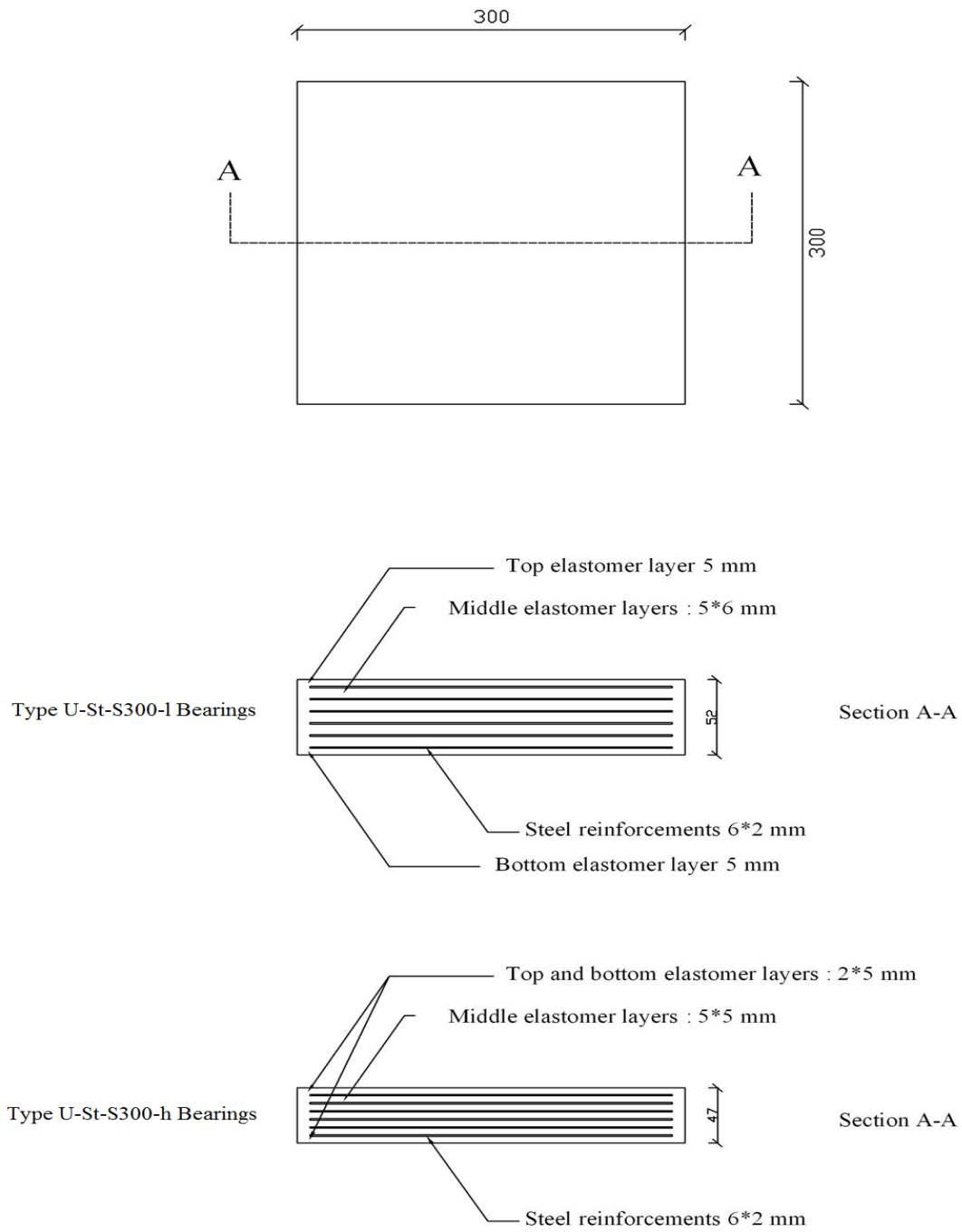
Figure A.4 Schematic view of Type U-St-S300 bearings
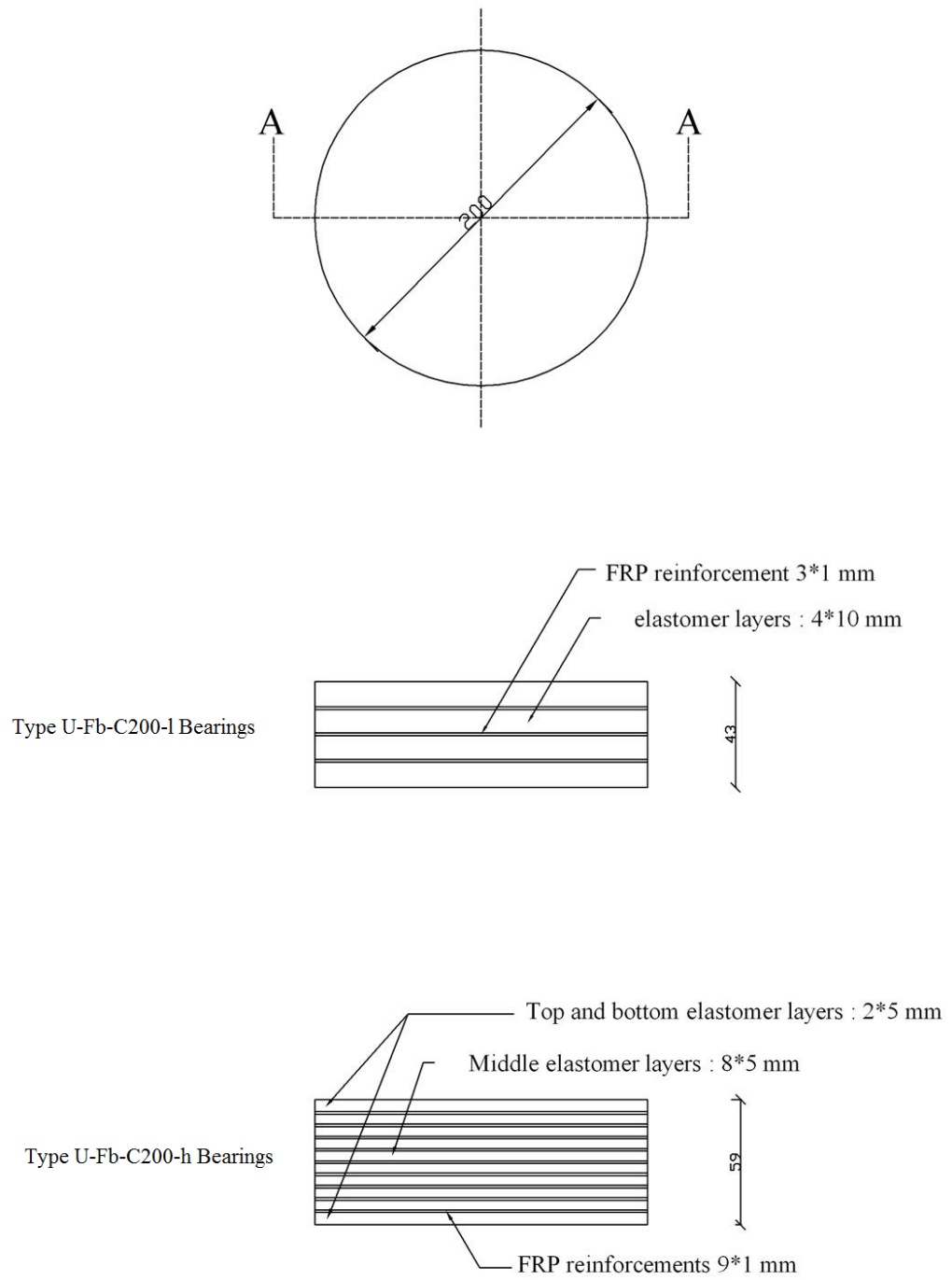
Figure A.5 Schematic view of Type U-Fb-C200 bearings
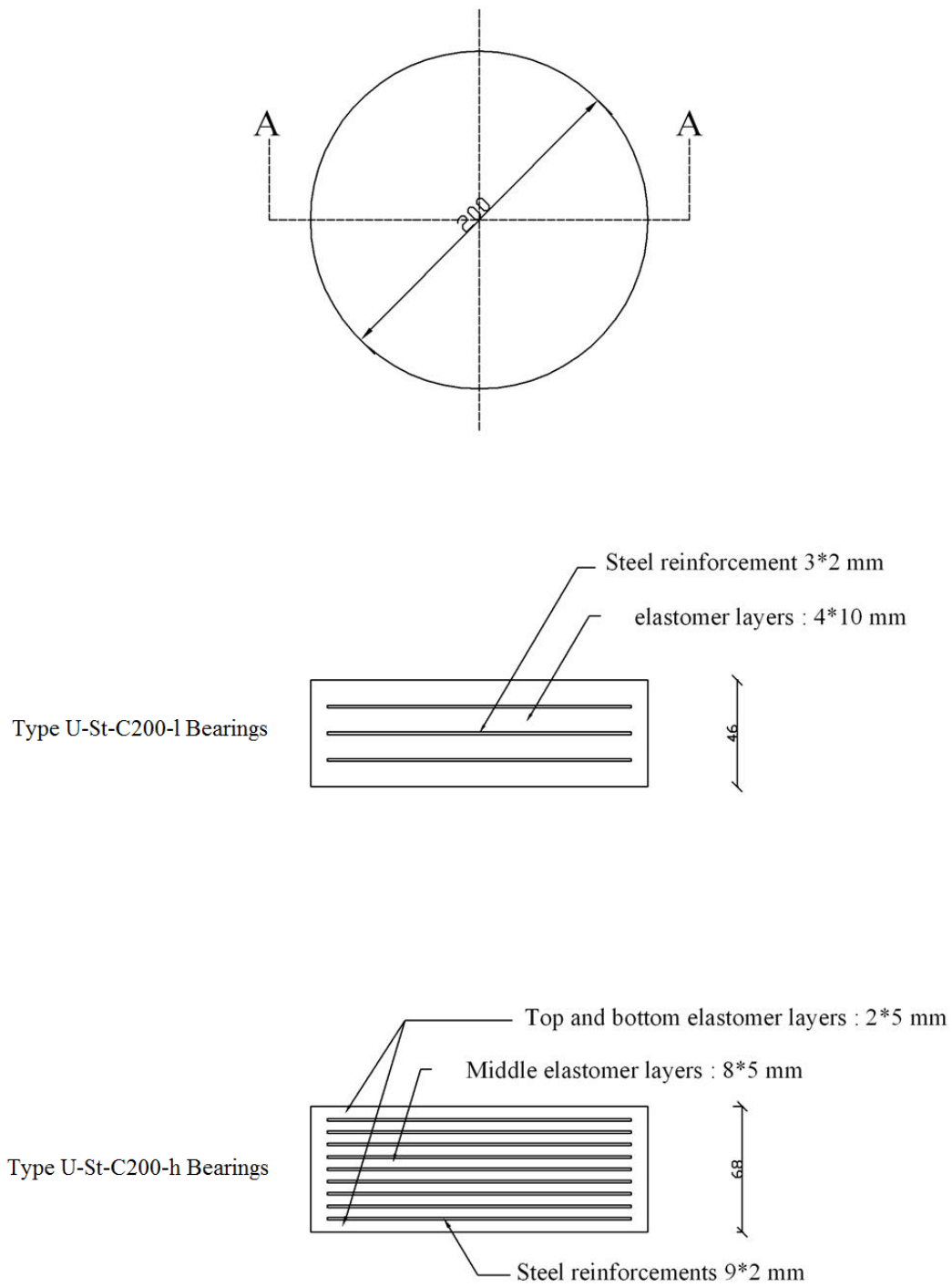
Figure A.6 Schematic view of Type U-St-C200 bearings

154
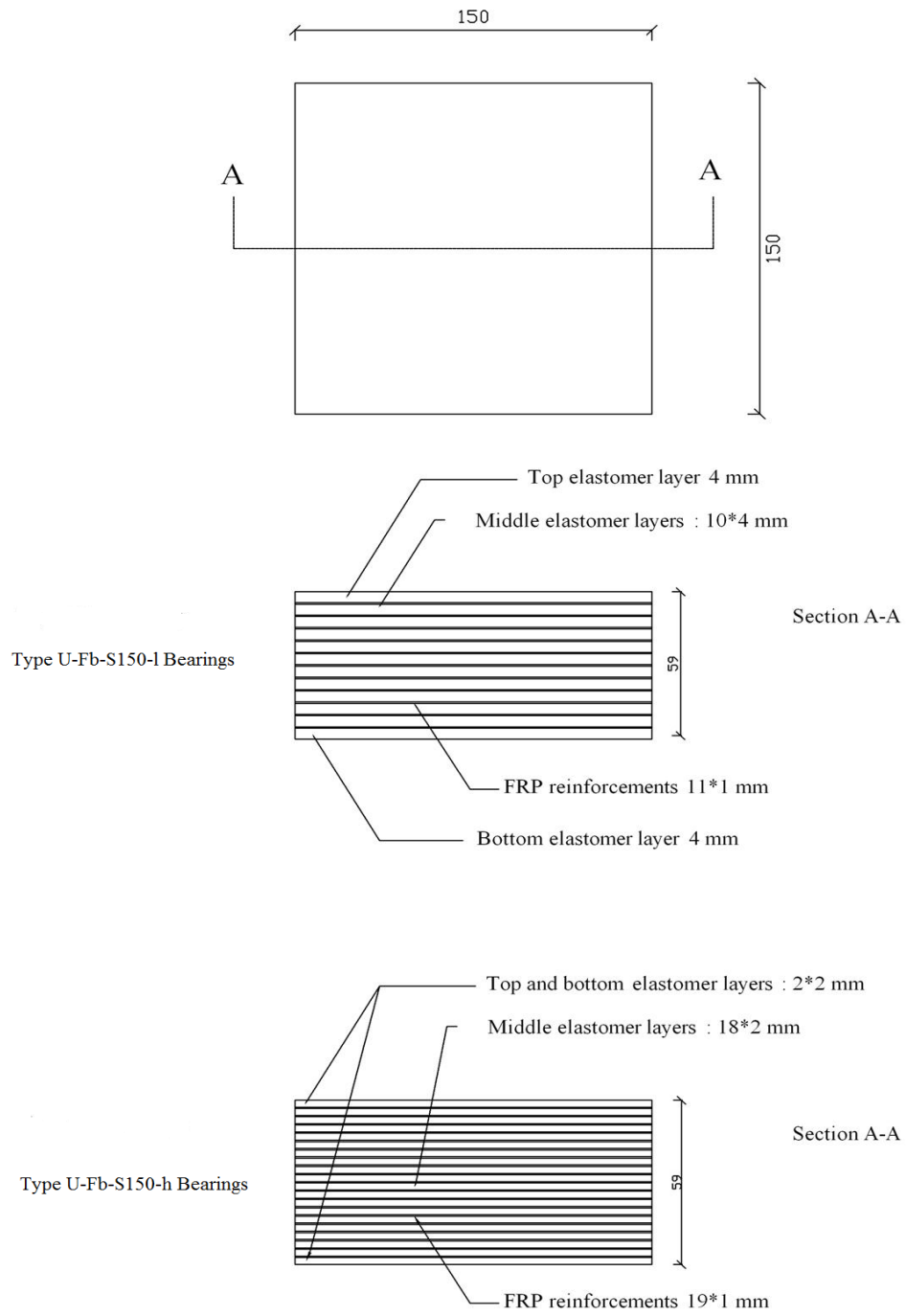
Figure A.7 Schematic view of Type U-Fb-S150 bearings

150

150

Top elastomer layer 4 mm

Middle elastomer layers : 10*4 mm

Section A-A

Type U-St-S150-l Bearings

59

Steel reinforcements 11*1 mm

Bottom elastomer layer 4 mm

Top and bottom elastomer layers : 2*2 mm

Middle elastomer layers : 18*2 mm

Section A-A

Type U-St-S150-h Bearings

59

Steel reinforcements 19*1 mm
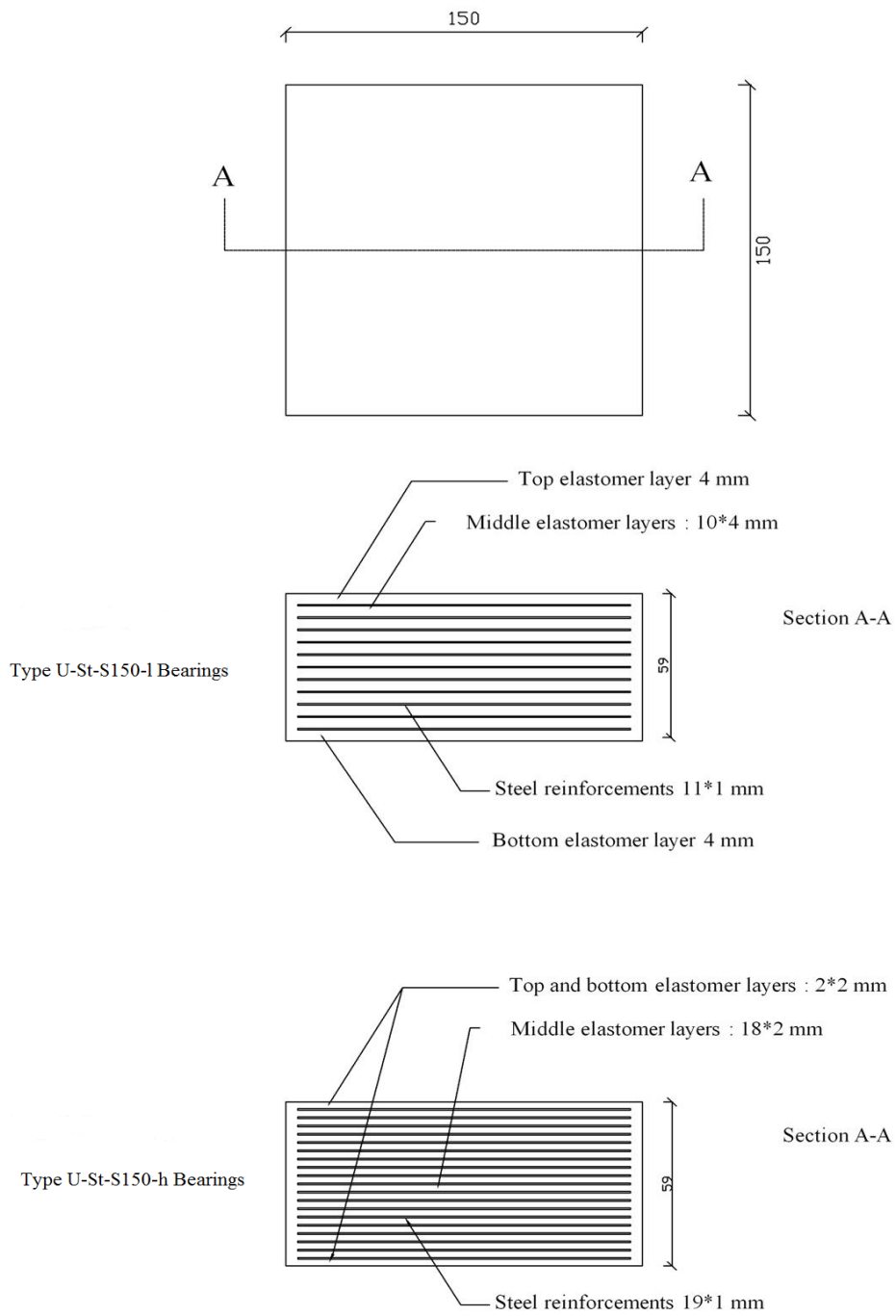
Figure A.8 Schematic view of Type U-St-S150 bearings
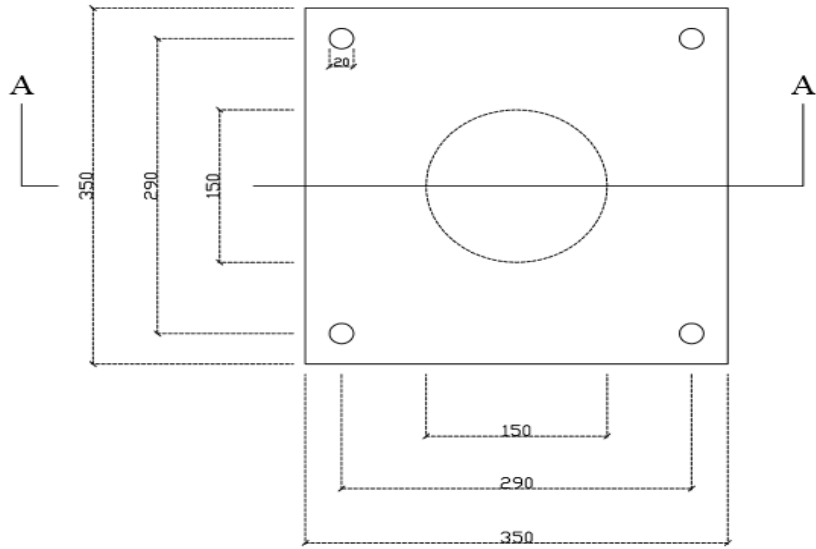
Type B-Fb-C150-l Bearings
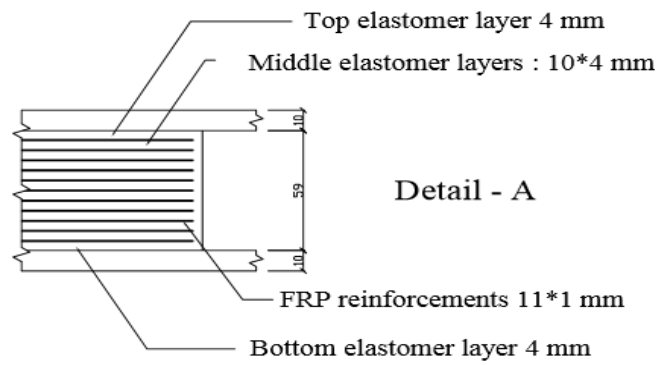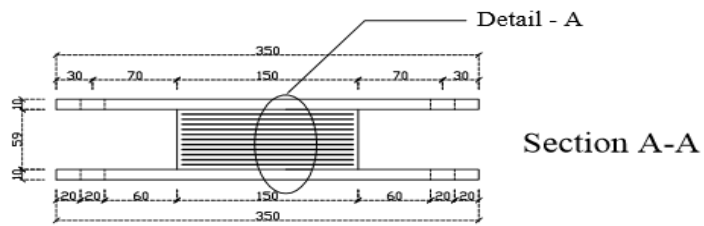
Figure A.9 Schematic view of Type B-Fb-C150-l bearings

157
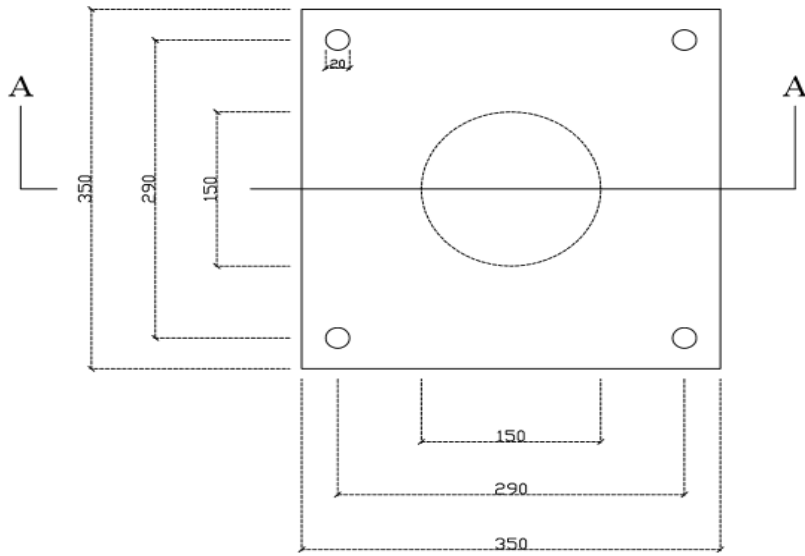
Type B-Fb-C150-h Bearings

Section A-A

Detail - A

Top elastomer layer 2 mm

Middle elastomer layers : 18*2 mm

FRP reinforcements 19*1 mm

Bottom elastomer layer 2 mm
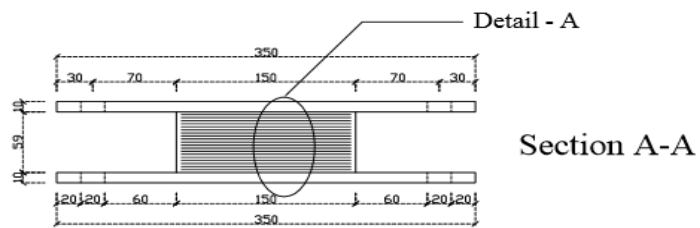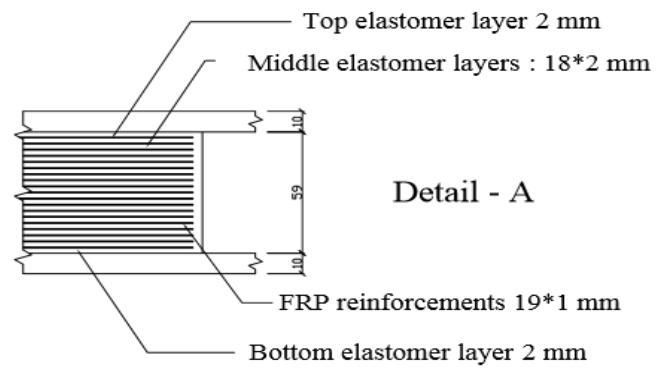
Figure A.10 Schematic view of Type B-Fb-C150-h bearings
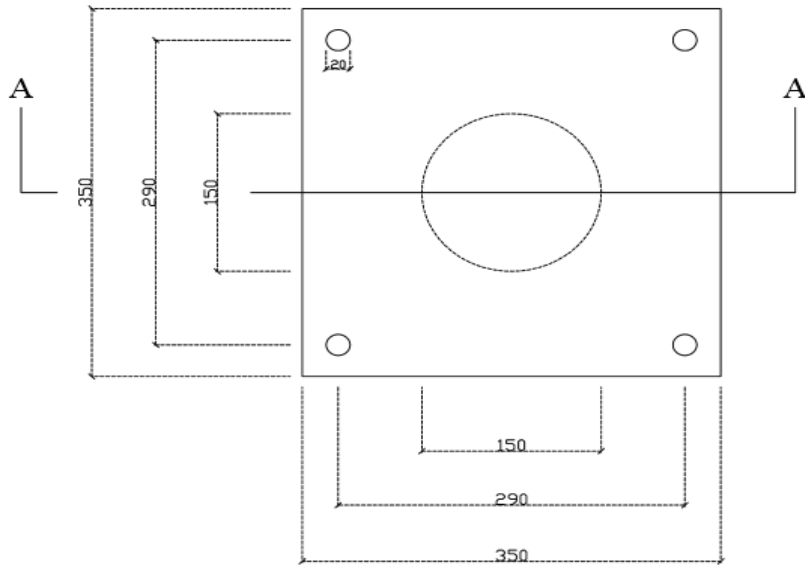
Type B-St-C150-l Bearings
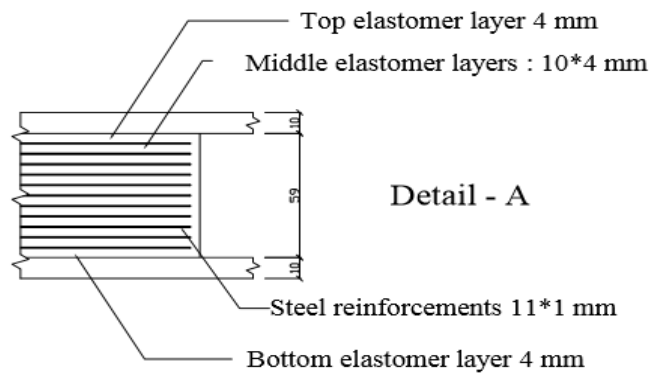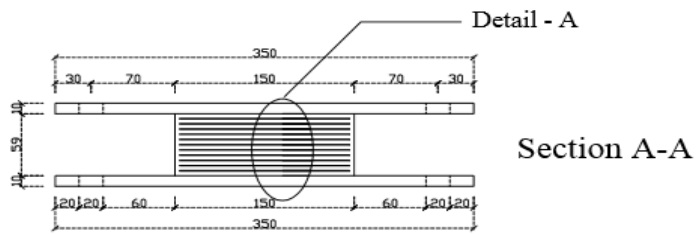
Figure A.11 Schematic view of Type B-St-C150-l bearings
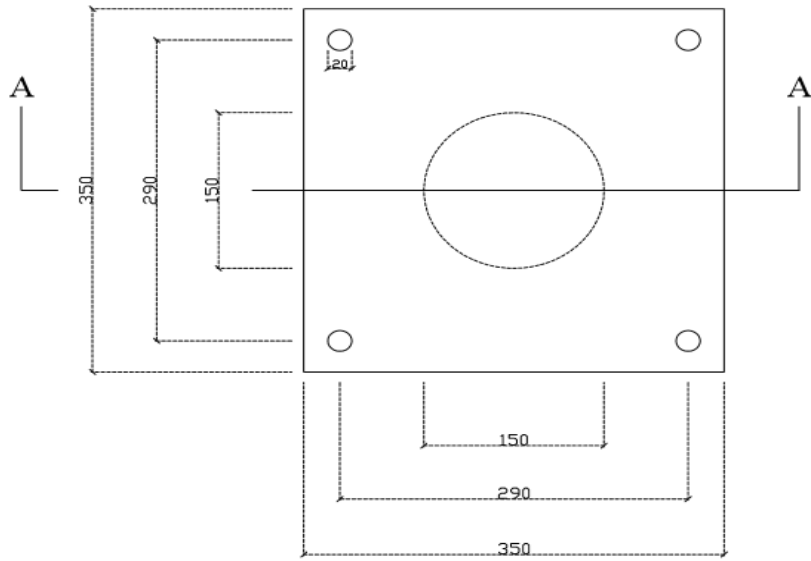
Type B-St-C150-h Bearings
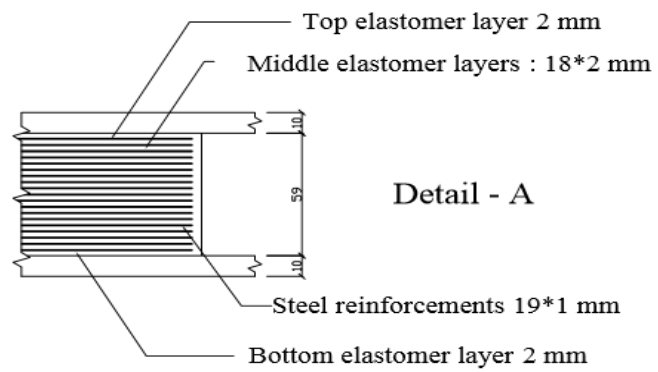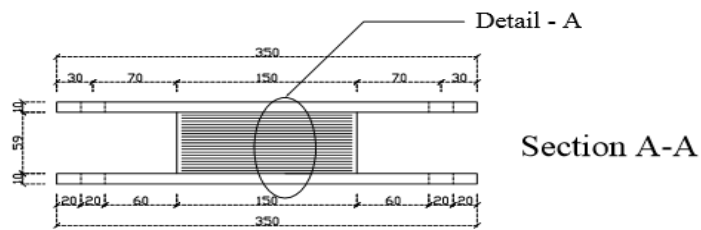
Figure A.12 Schematic view of Type B-St-C150-h bearings

160

APPENDIX B

HORIZONTAL SHEAR TEST RESULTS
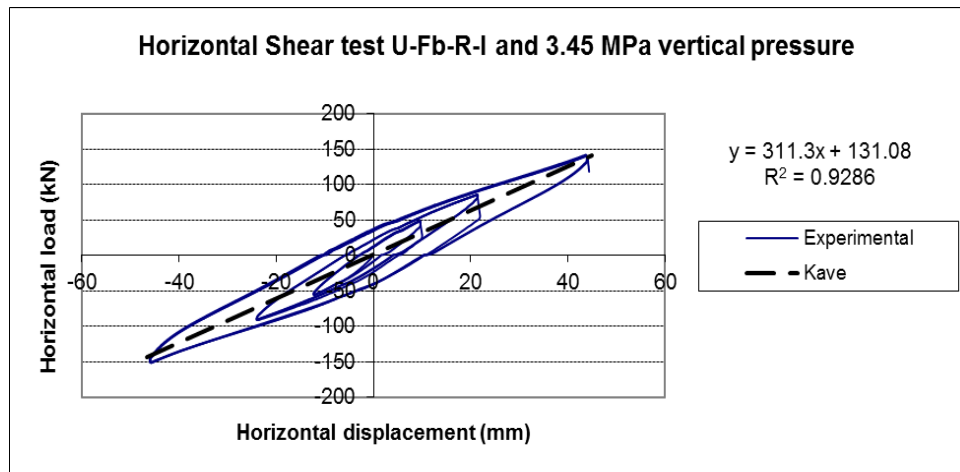
Figure B.1 Horizontal shear test for U-Fb-R-l under 3.45MPa vertical load
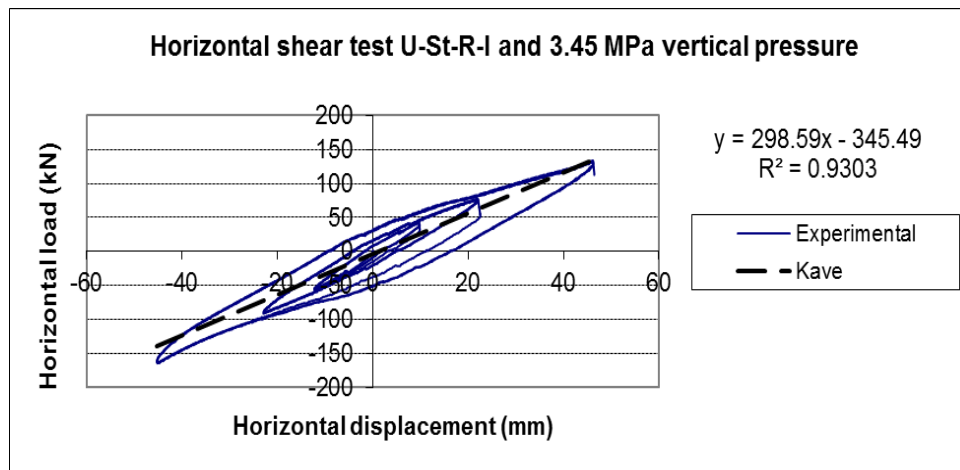
Figure B.2 Horizontal shear test for U-St-R-l under 3.45MPa vertical load
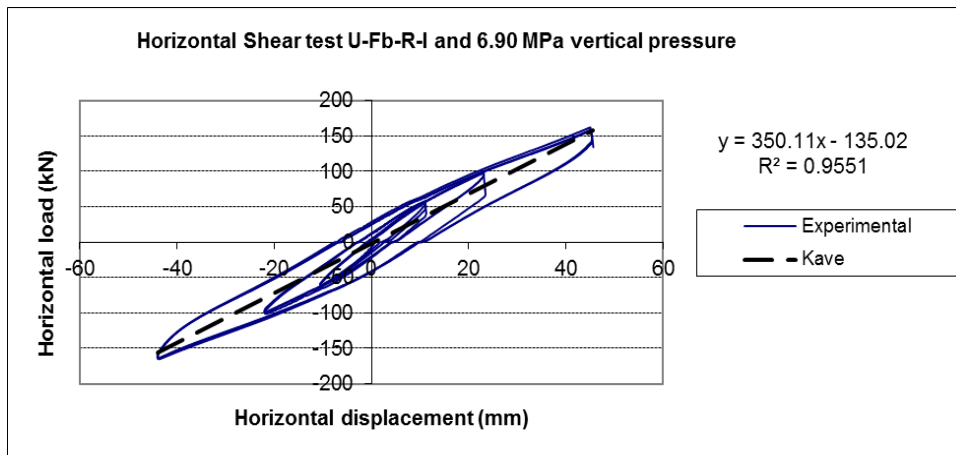
Figure B.3 Horizontal shear test for U-Fb-R-l under 6.90MPa vertical load
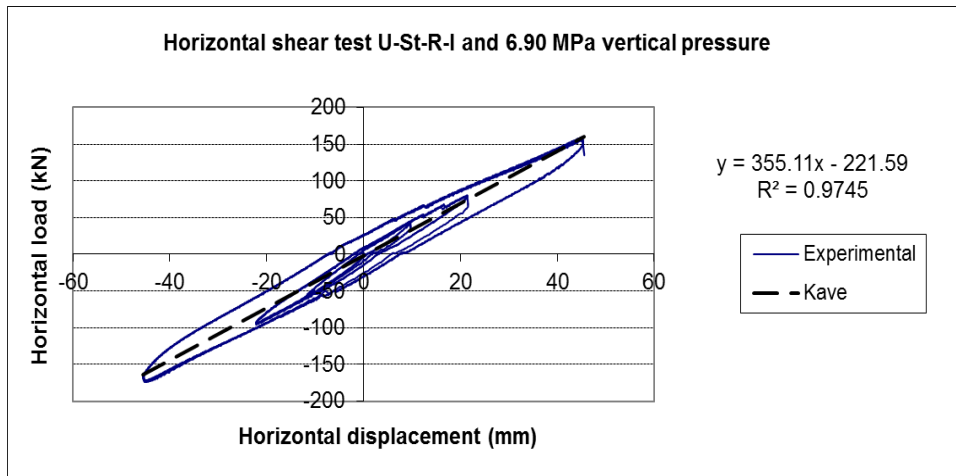
Figure B.4 Horizontal shear test for U-St-R-l under 6.90MPa vertical load
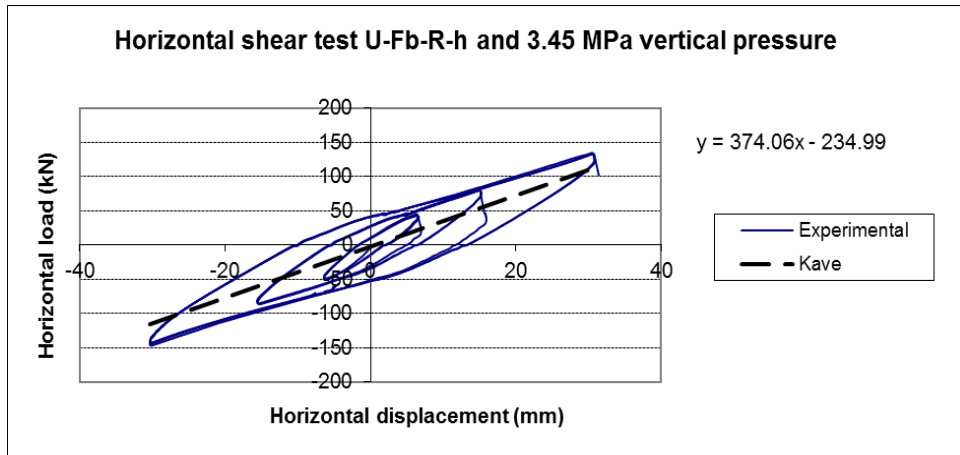
Figure B.5 Horizontal shear test for U-Fb-R-h under 3.45MPa vertical load
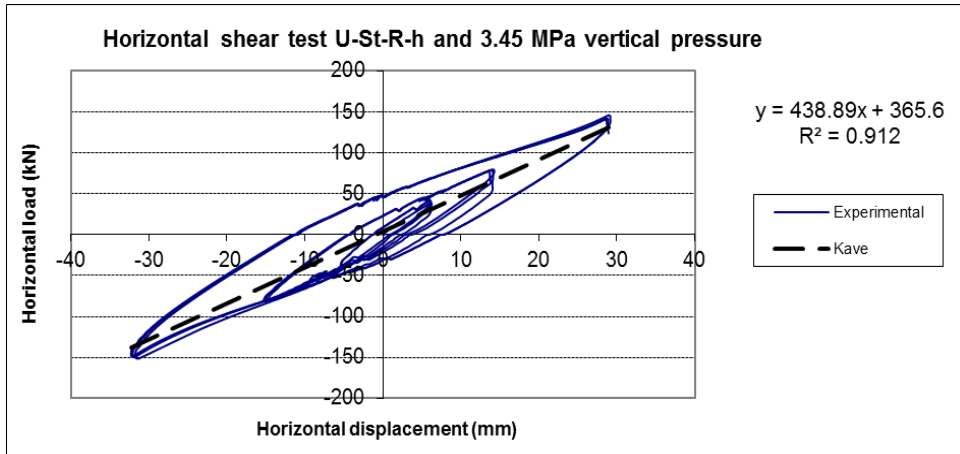
Figure B.6 Horizontal shear test for U-St-R-h under 3.45MPa vertical load

163
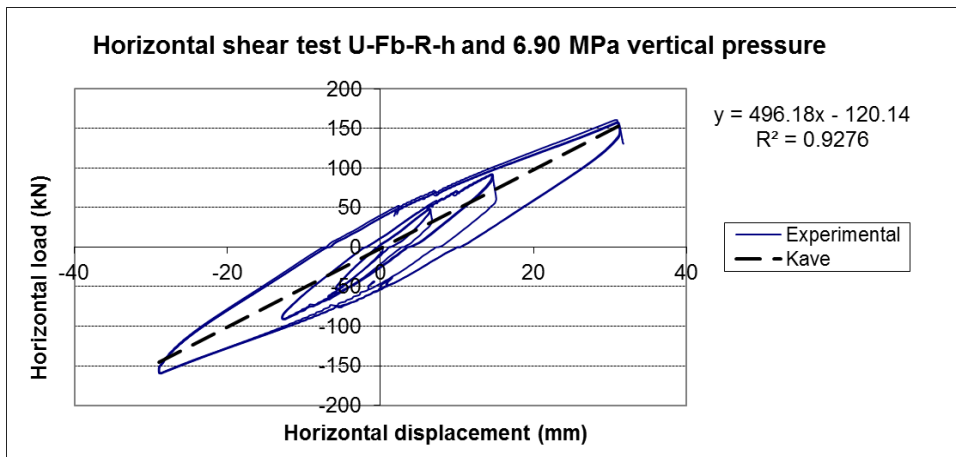
Figure B.7 Horizontal shear test for U-Fb-R-h under 6.90MPa vertical load
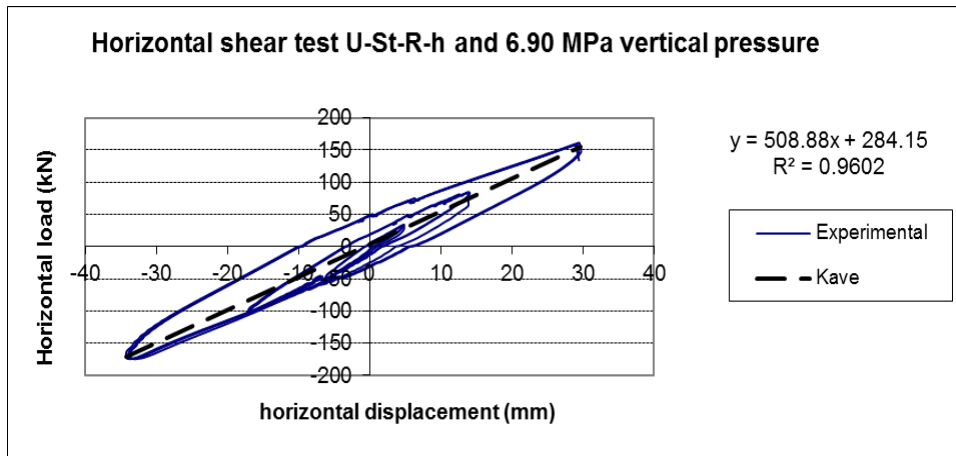
Figure B.8 Horizontal shear test for U-St-R-h under 6.90MPa vertical load

164
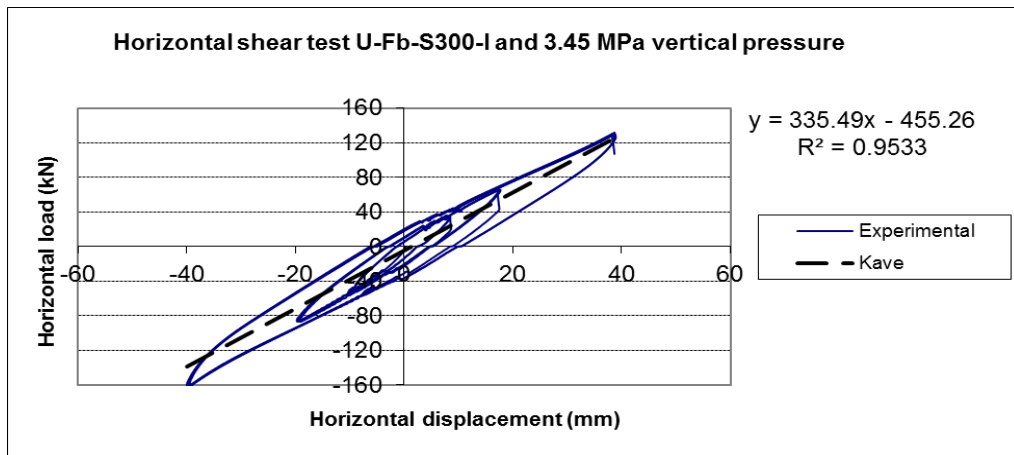
Figure B.9 Horizontal shear test for U-Fb-S300-l under 3.45MPa vertical load
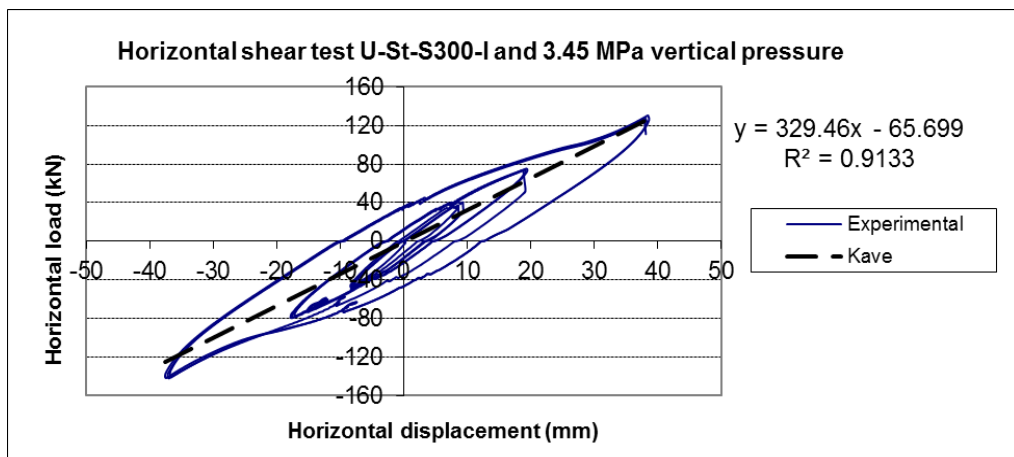
Figure B.10 Horizontal shear test for U-St-S300-l under 3.45MPa vertical load
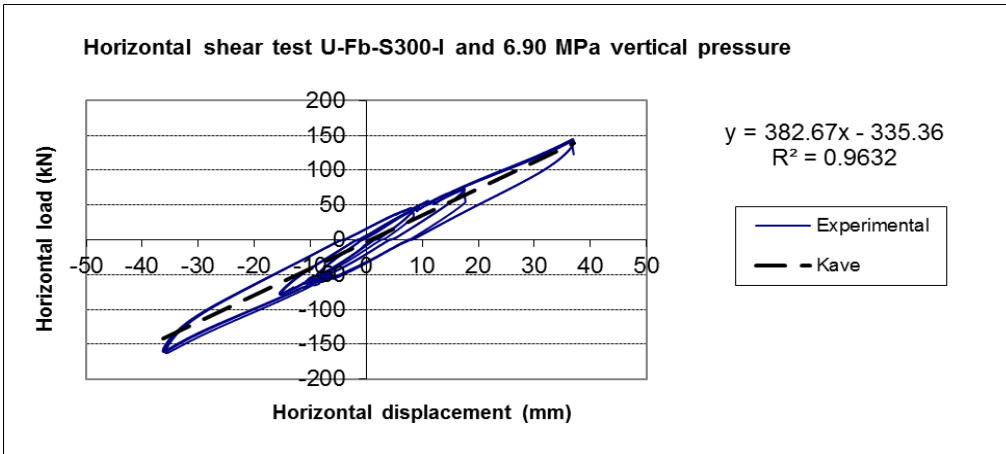
Figure B.11 Horizontal shear test for U-Fb-S300-l under 6.90MPa vertical load
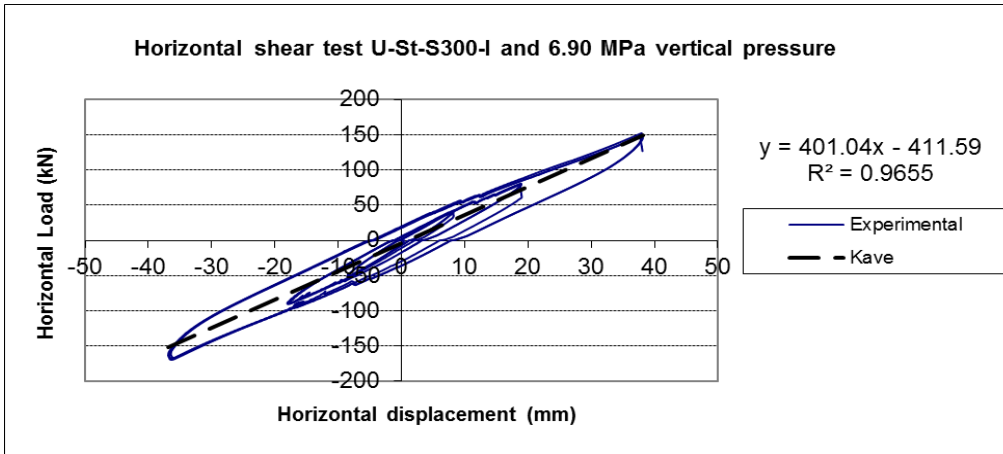
Figure B.12 Horizontal shear test for U-St-S300-l under 6.90MPa vertical load
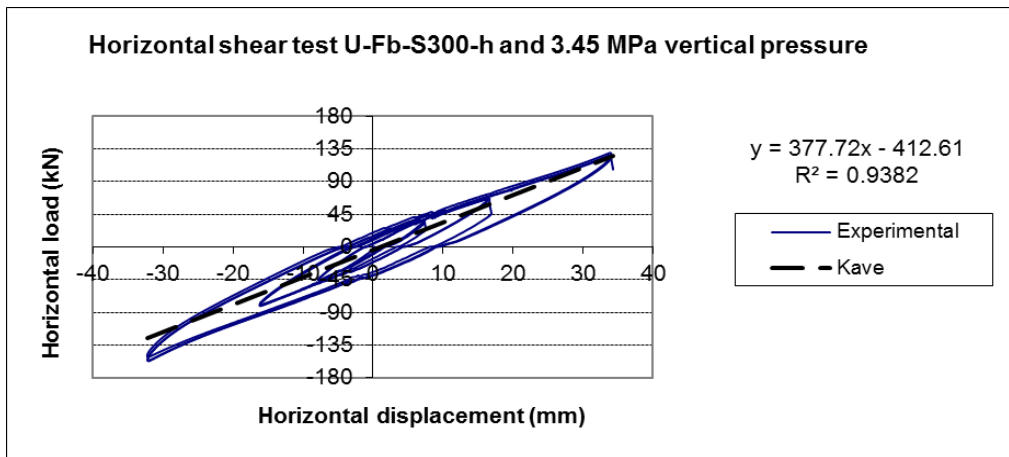
Figure B.13 Horizontal shear test for U-Fb-S300-h under 3.45MPa vertical load
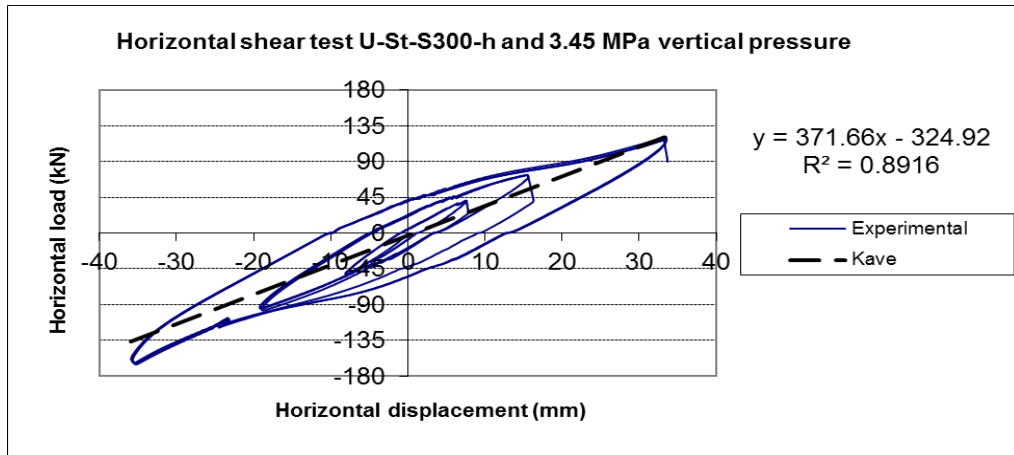
Figure B.14 Horizontal shear test for U-St-S300-h under 3.45MPa vertical load

167
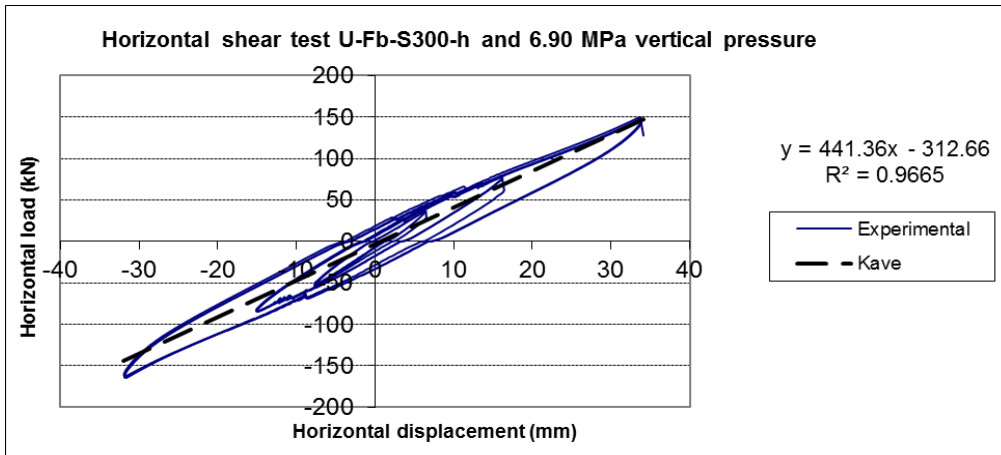
Figure B.15 Horizontal shear test for U-Fb-S300-h under 6.90MPa vertical load
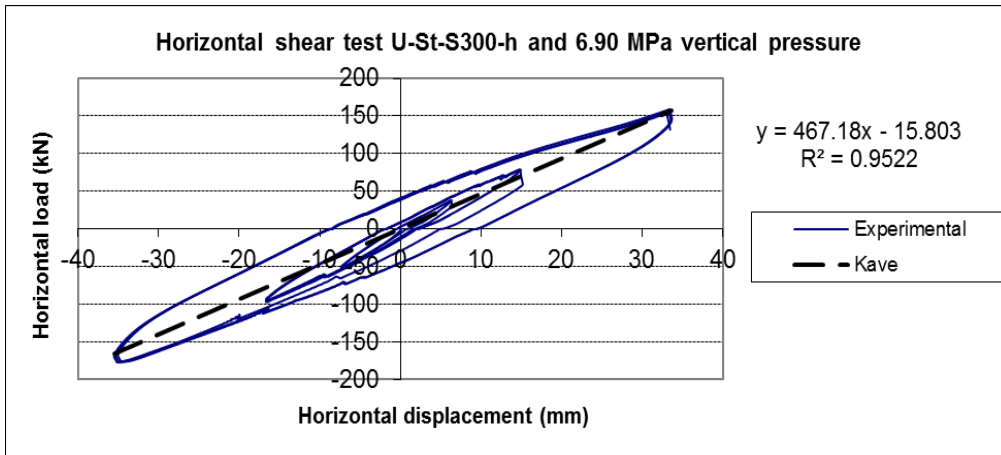
Figure B.16 Horizontal shear test for U-St-S300-h under 6.90MPa vertical load
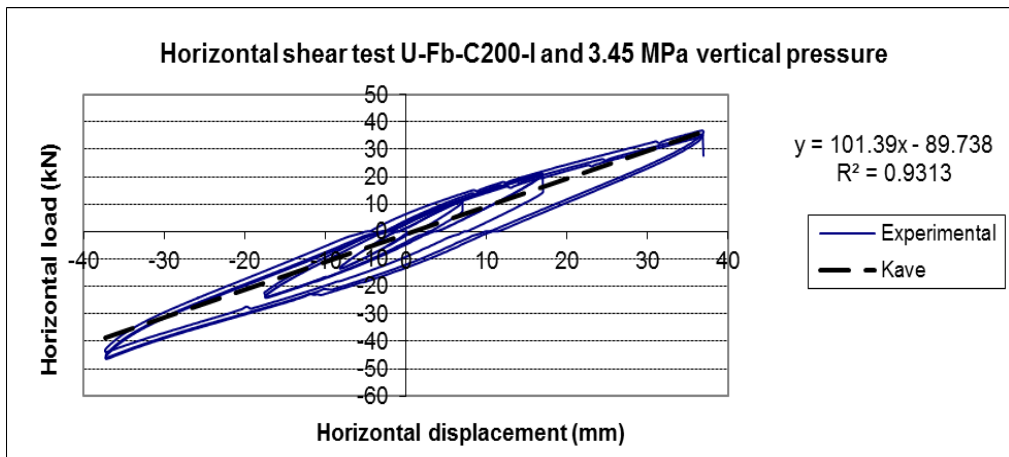
Figure B.17 Horizontal shear test for U-Fb-C200-l under 3.45MPa vertical load
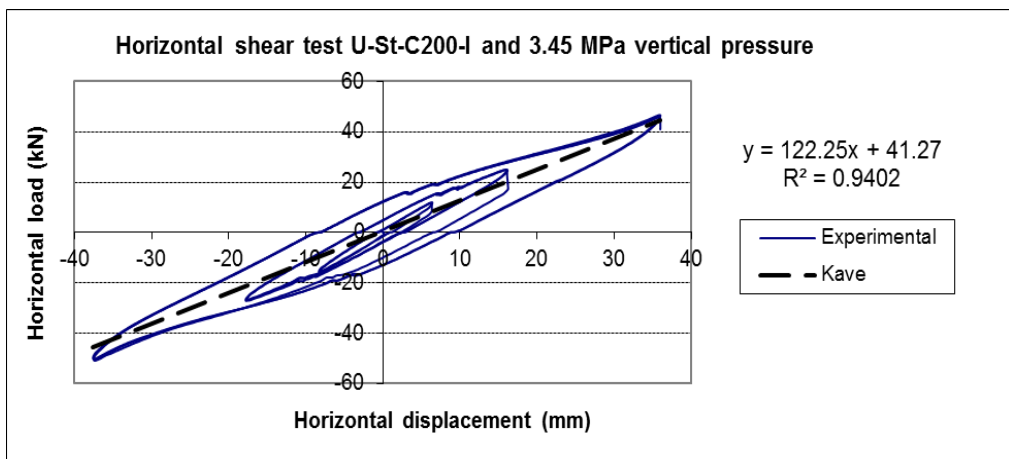
Figure B.18 Horizontal shear test for U-St-C200-l under 3.45MPa vertical load
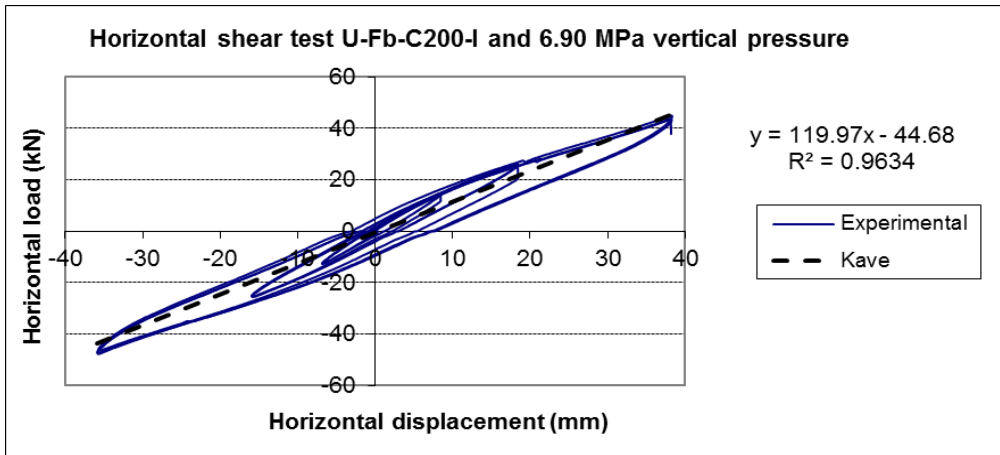
Figure B.19 Horizontal shear test for U-Fb-C200-l under 6.90MPa vertical load
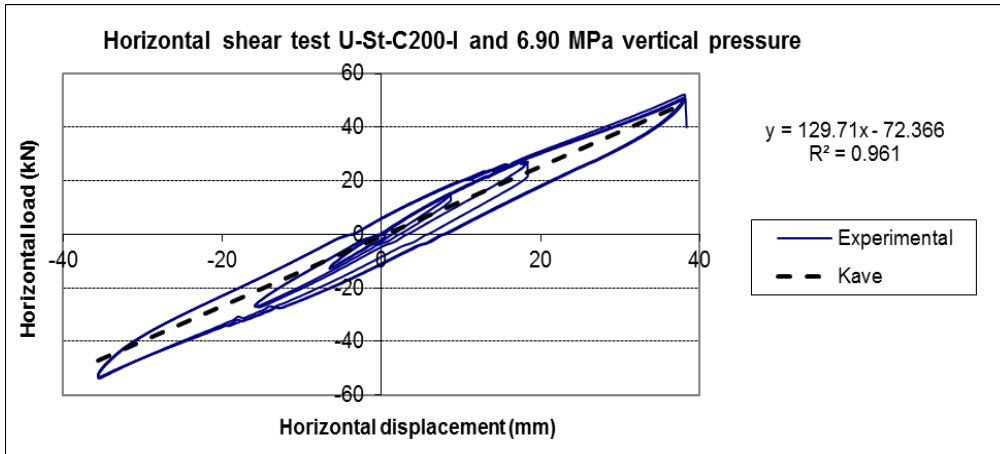
Figure B.20 Horizontal shear test for U-St-C200-l under 6.90MPa vertical load
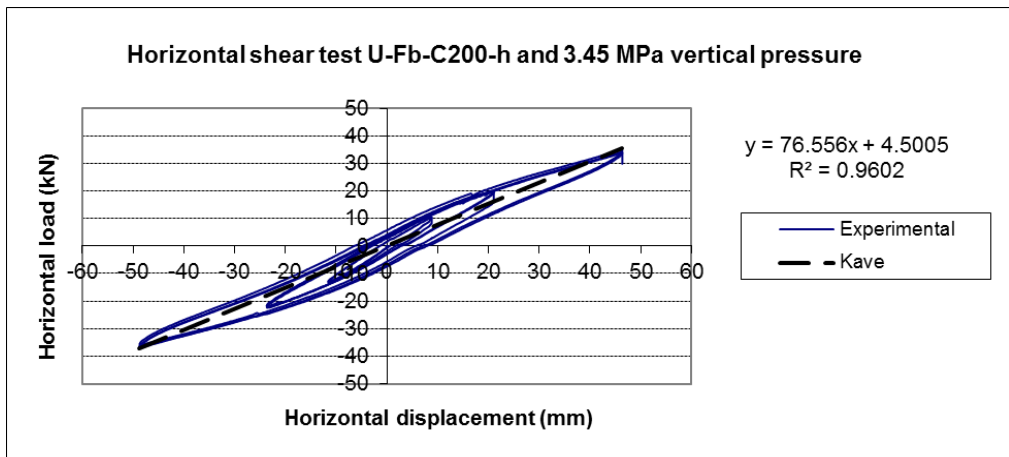
Figure B.21 Horizontal shear test for U-Fb-C200-h under 3.45MPa vertical load
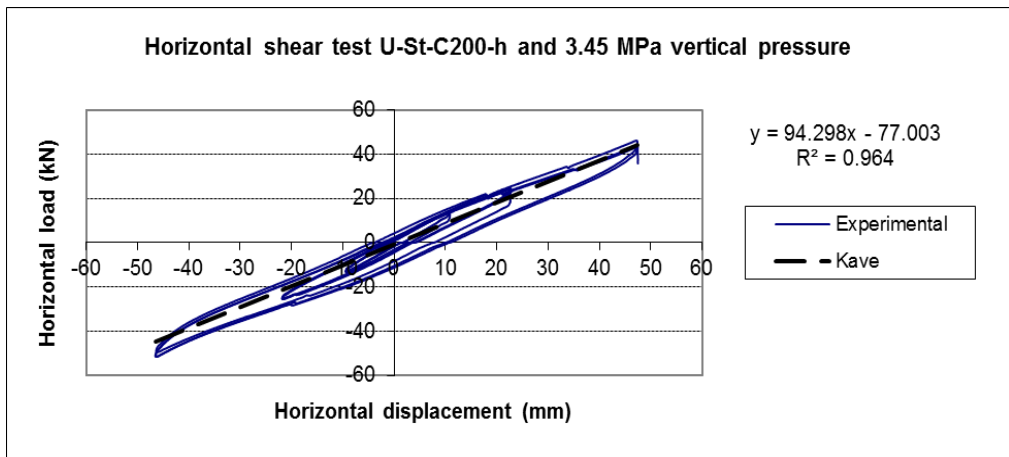
Figure B.22 Horizontal shear test for U-St-C200-h under 3.45MPa vertical load
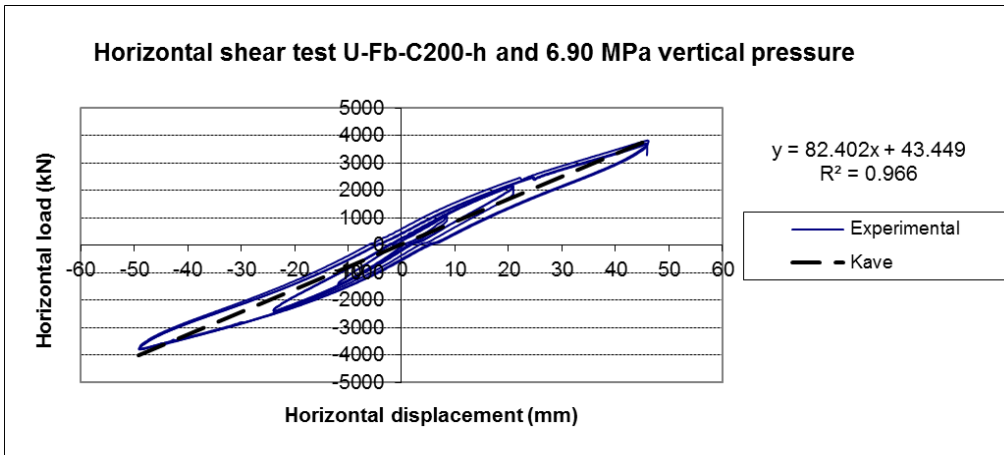
Figure B.23 Horizontal shear test for U-Fb-C200-h under 6.90MPa vertical load
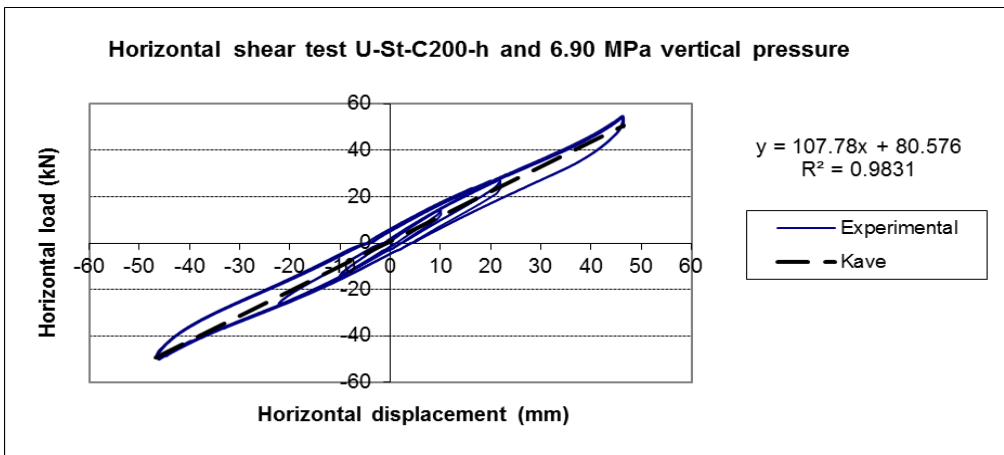
Figure B.24 Horizontal shear test for U-St-C200-h under 6.90MPa vertical load
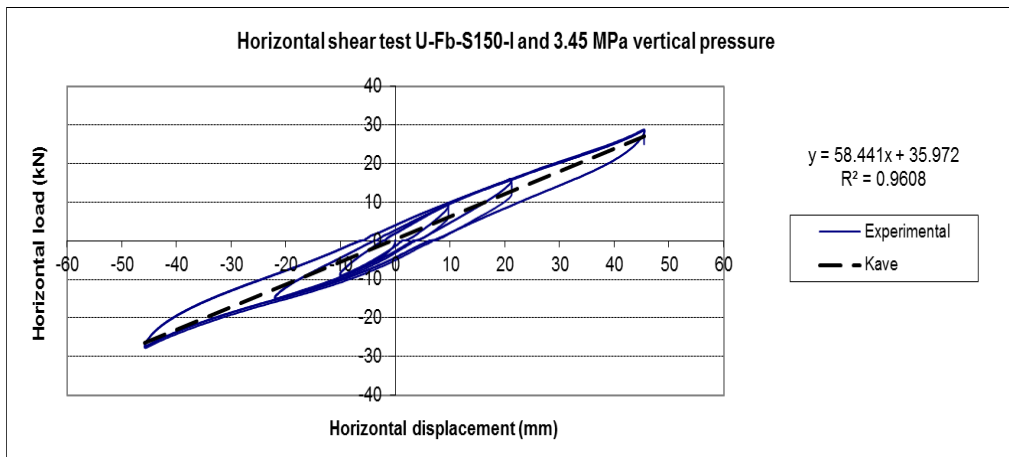
Figure B.25 Horizontal shear test for U-Fb-S150-l under 3.45MPa vertical load
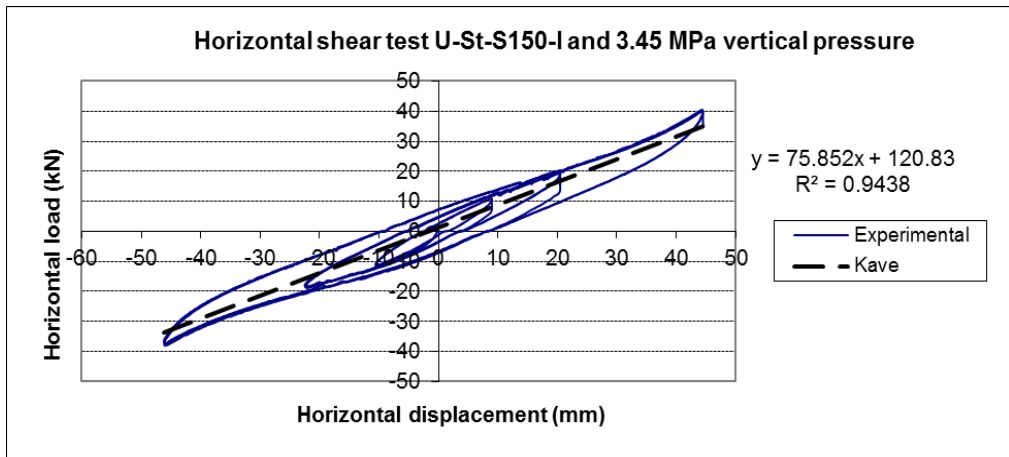
Figure B.26 Horizontal shear test for U-St-S150-l under 3.45MPa vertical load

173
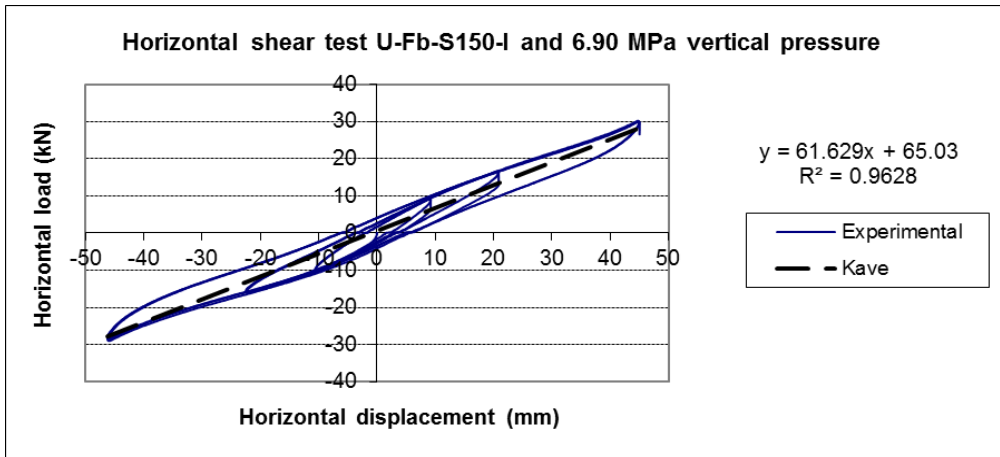
Figure B.27 Horizontal shear test for U-Fb-S150-l under 6.90MPa vertical load
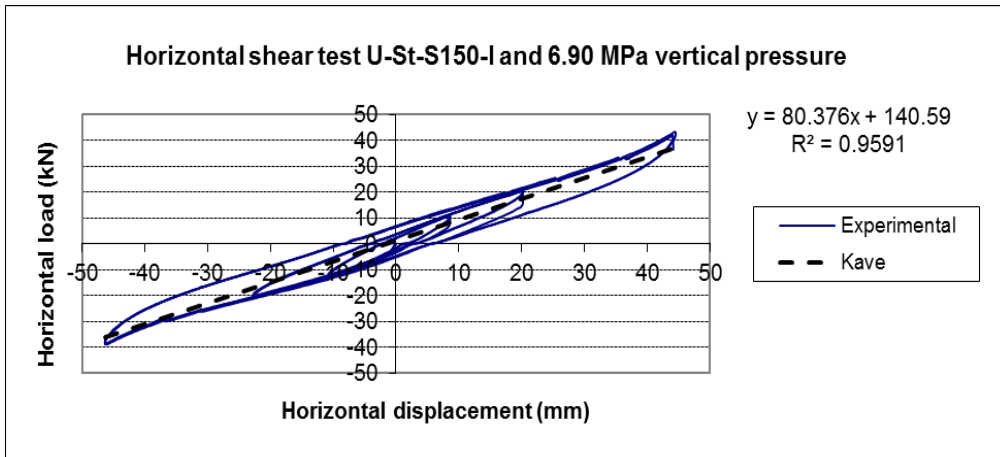
Figure B.28 Horizontal shear test for U-St-S150-l under 6.90MPa vertical load

174
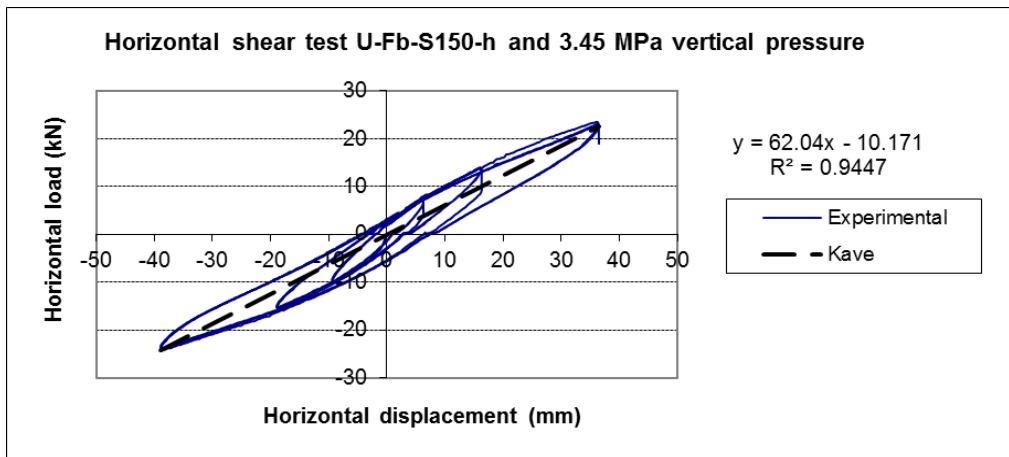
Figure B.29 Horizontal shear test for U-Fb-S150-h under 3.45MPa vertical load
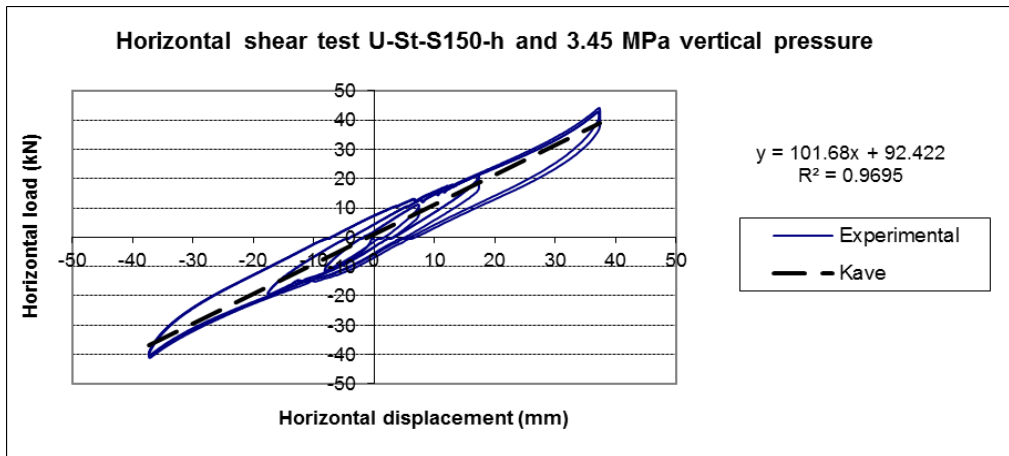
Figure B.30 Horizontal shear test for U-St-S150-h under 3.45MPa vertical load
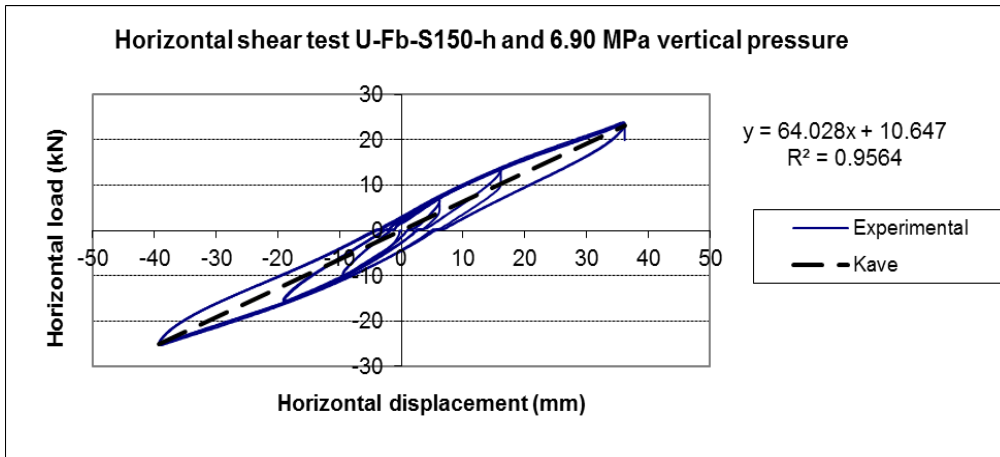
Figure B.31 Horizontal shear test for U-Fb-S150-h under 6.90MPa vertical load
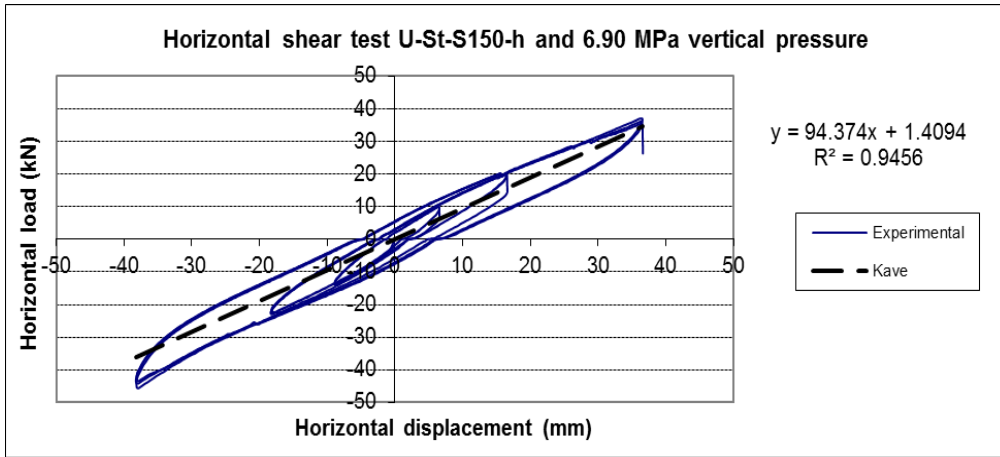
Figure B.32 Horizontal shear test for U-St-S150-h under 6.90MPa vertical load
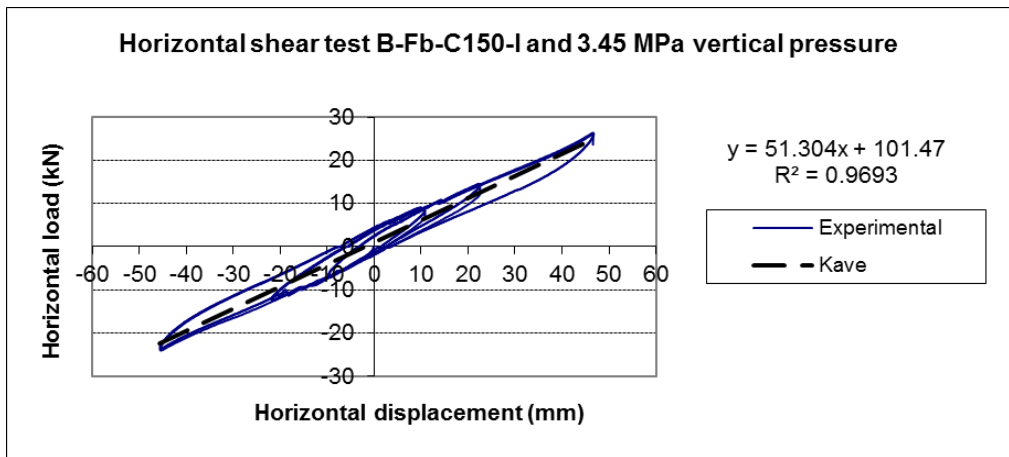
Figure B.33 Horizontal shear test for B-Fb-C150-l under 3.45MPa vertical load
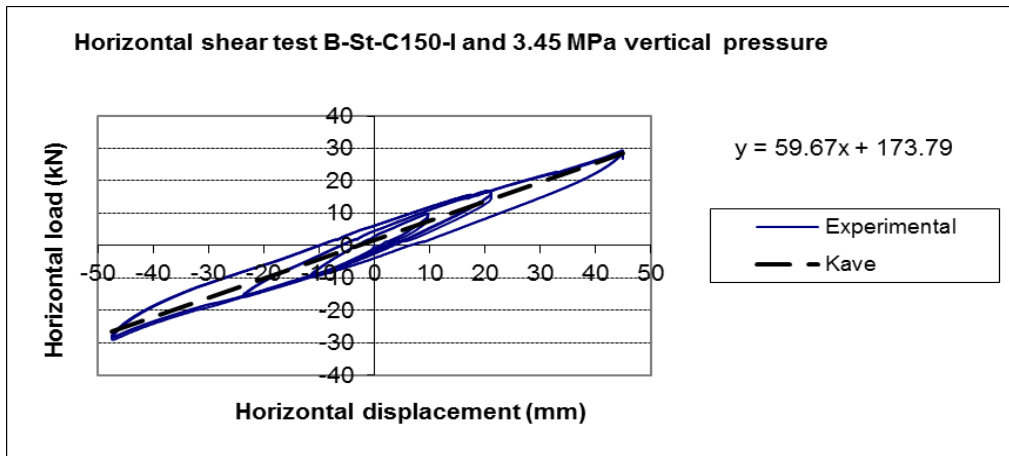
Figure B.34 Horizontal shear test for B-St-C150-l under 3.45MPa vertical load
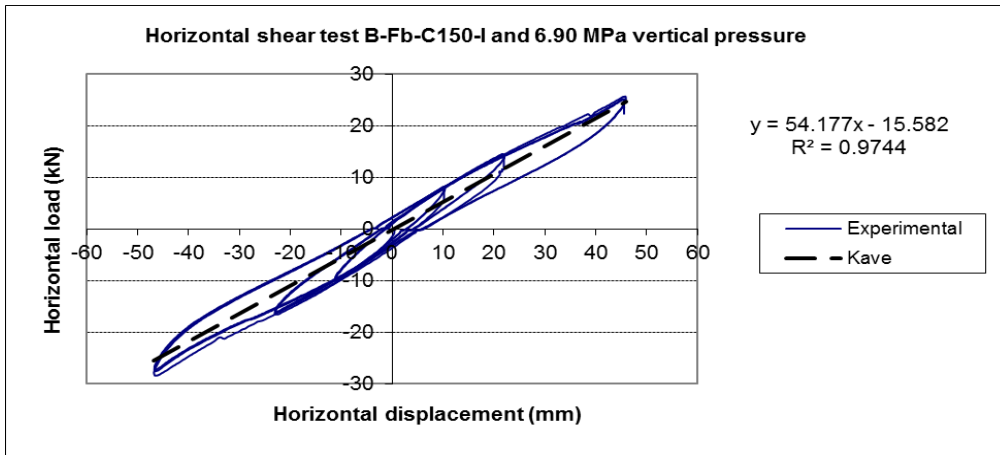
Figure B.35 Horizontal shear test for B-Fb-C150-l under 6.90MPa vertical load
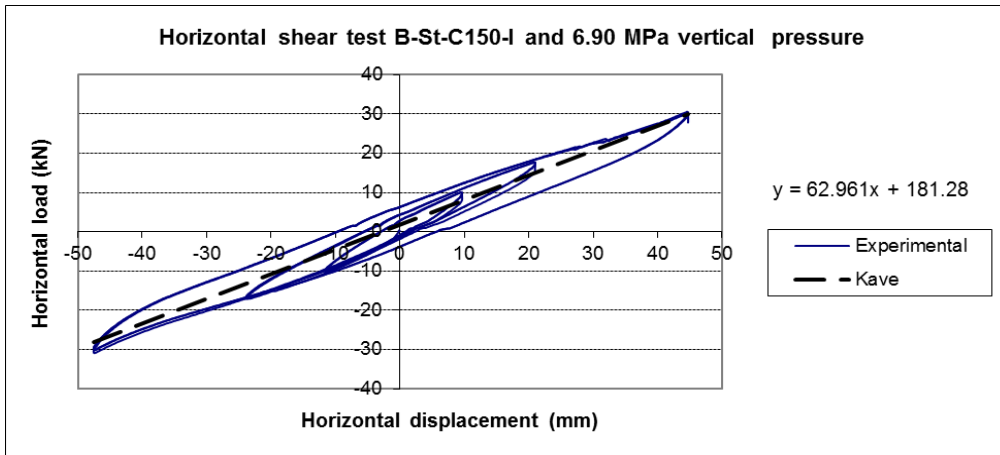
Figure B.36 Horizontal shear test for B-St-C150-l under 6.90MPa vertical load
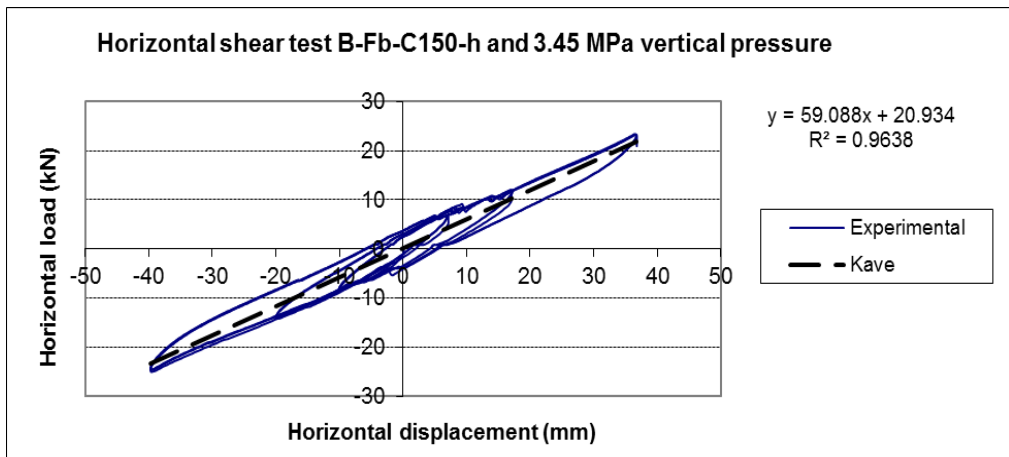
Figure B.37 Horizontal shear test for B-Fb-C150-h under 3.45MPa vertical load
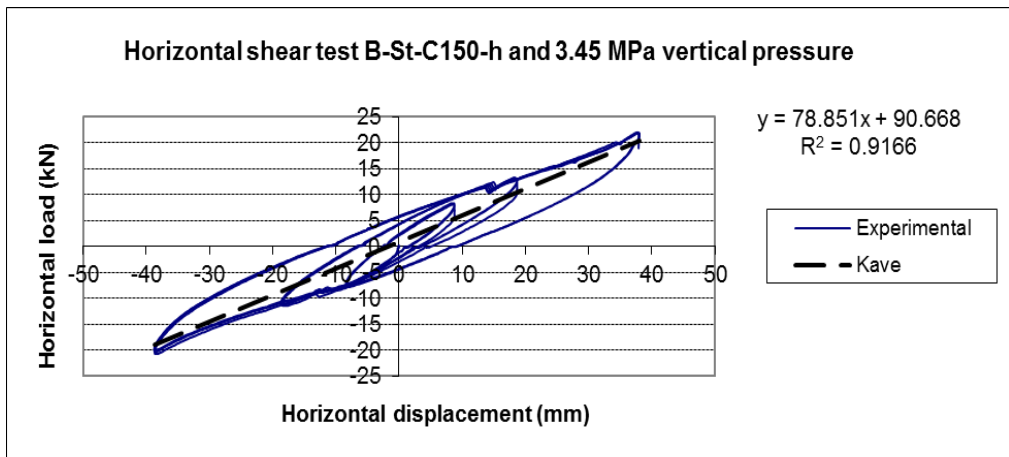
Figure B.38 Horizontal shear test for B-St-C150-h under 3.45MPa vertical load
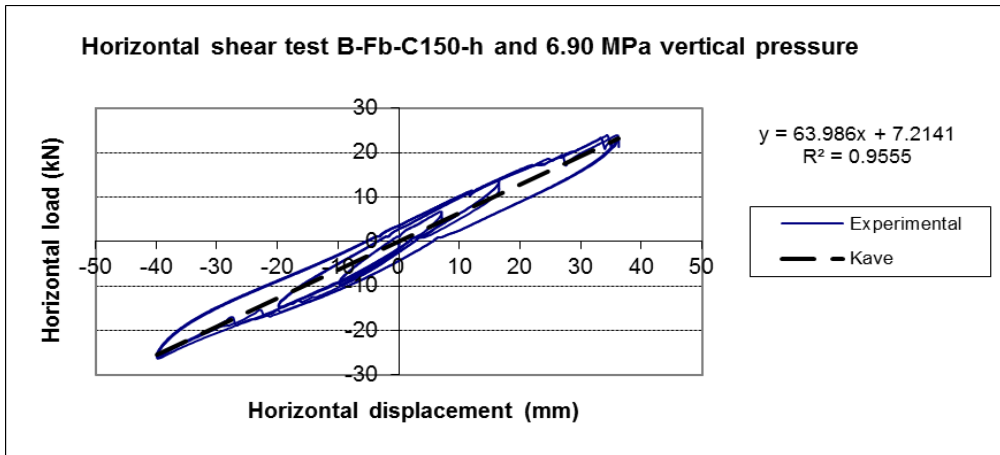
Figure B.39 Horizontal shear test for B-Fb-C150-h under 6.90MPa vertical load
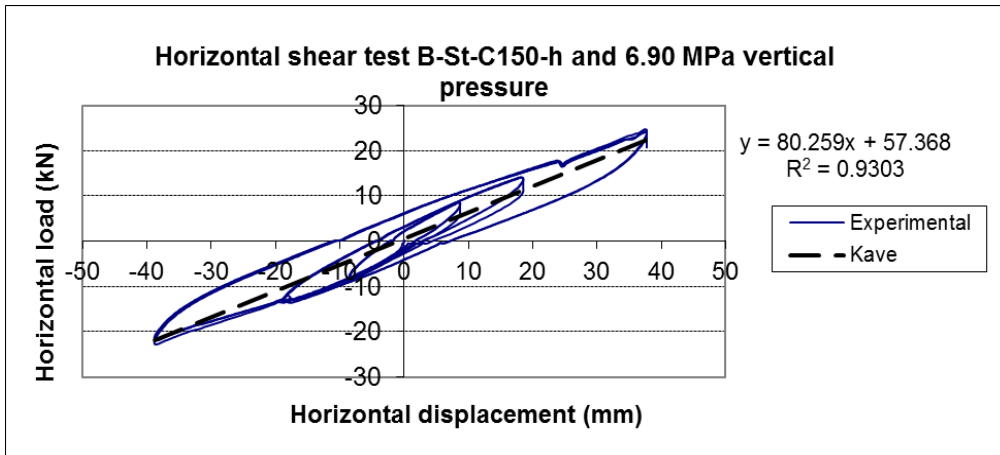
Figure B.40 Horizontal shear test for B-St-C150-h under 6.90MPa vertical load

APPENDIX C

VERTICAL COMPRESION TEST RESULT
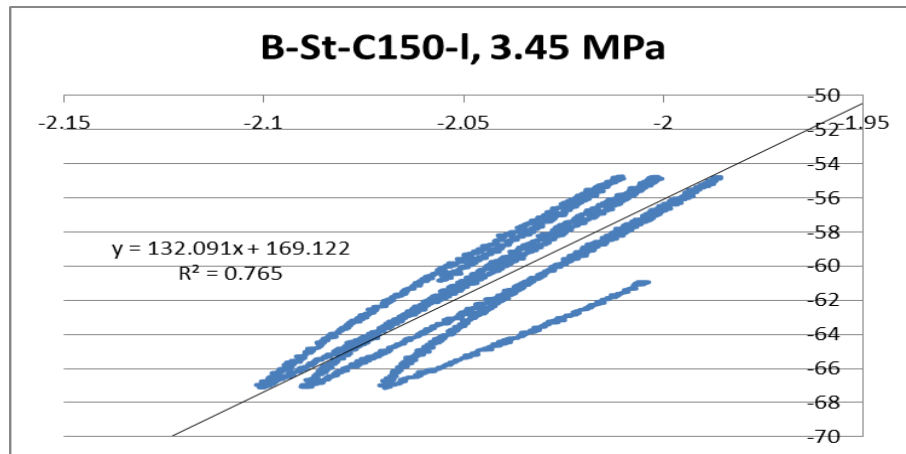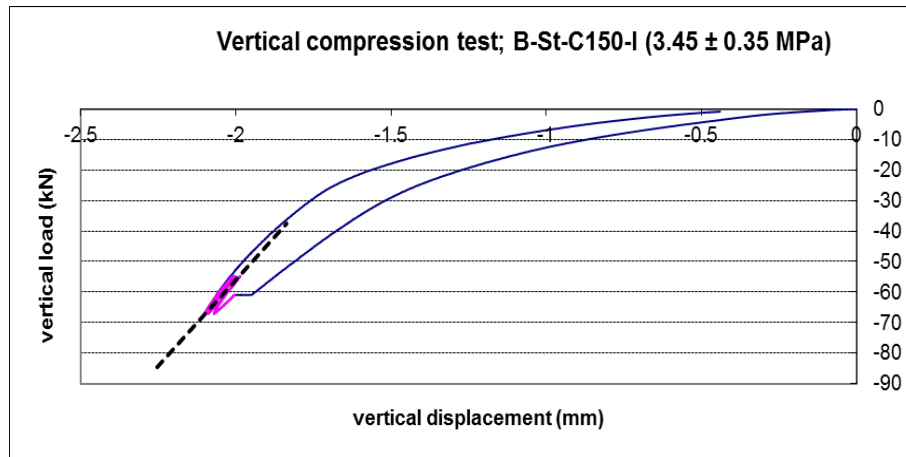
Figure C.1 Vertical load versus vertical displacement for B-St-C150-l
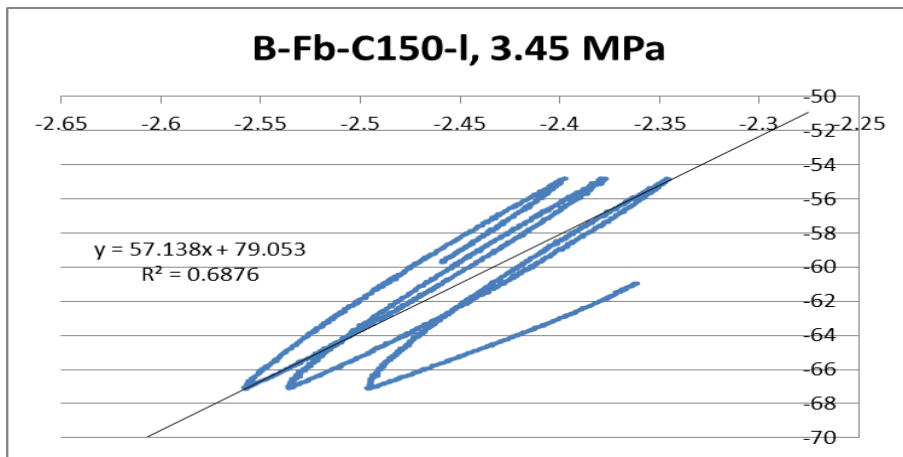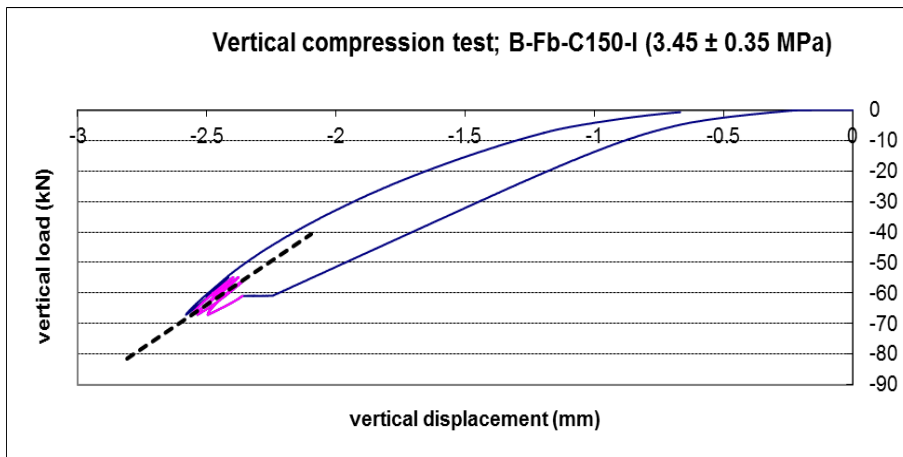
Figure C.2 Vertical load versus vertical displacement for B-Fb-C150-l
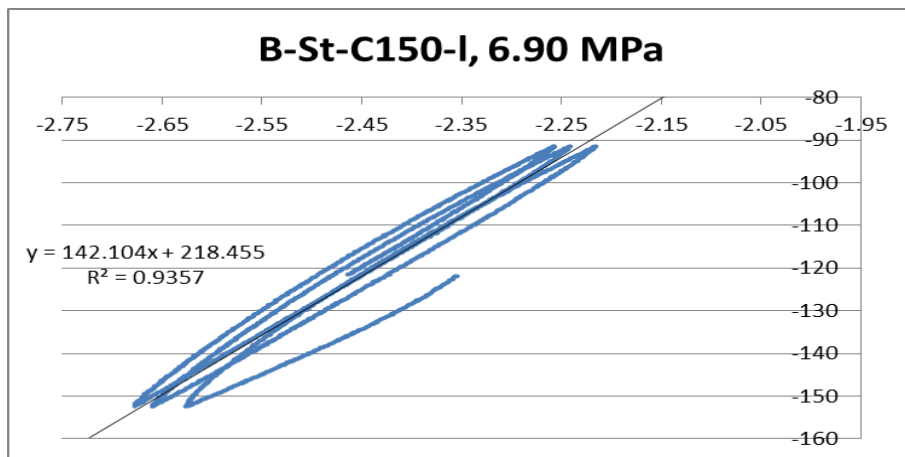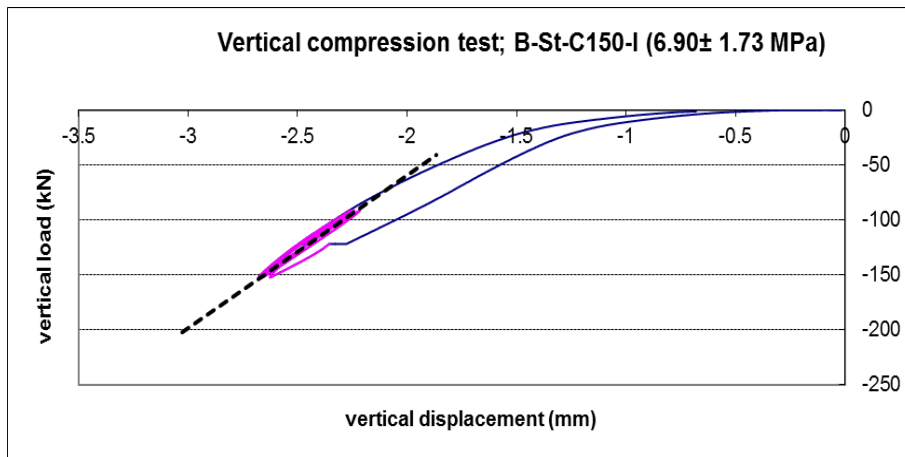
Figure C.3 Vertical load versus vertical displacement for B-St-C150-l
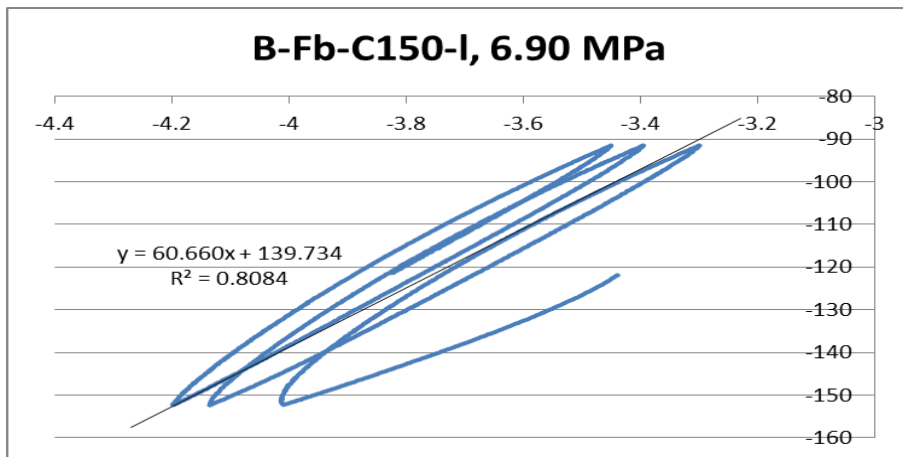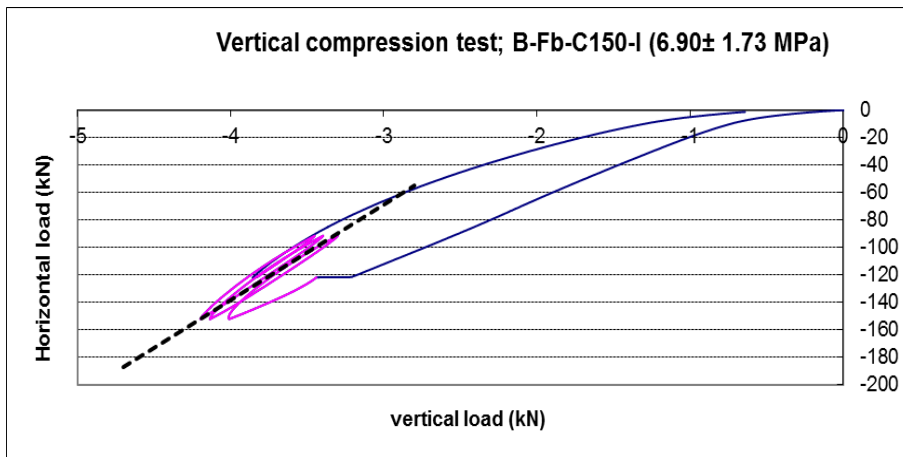
Figure C.4 Vertical load versus vertical displacement for B-Fb-C150-l
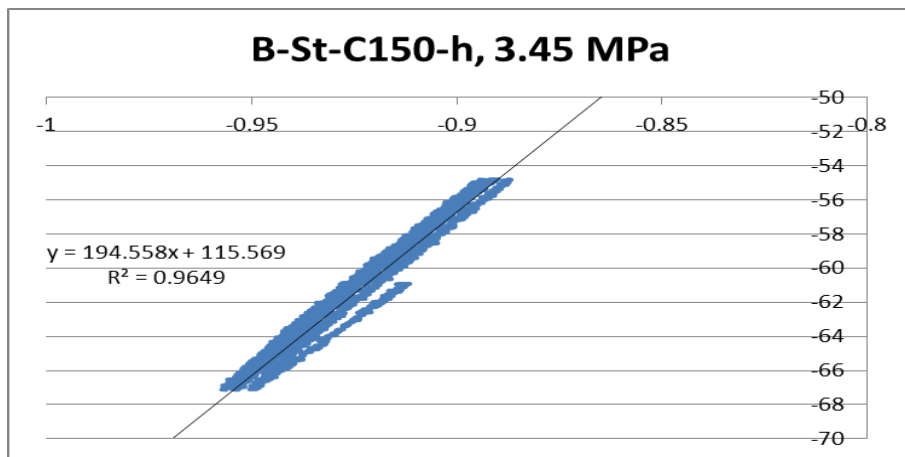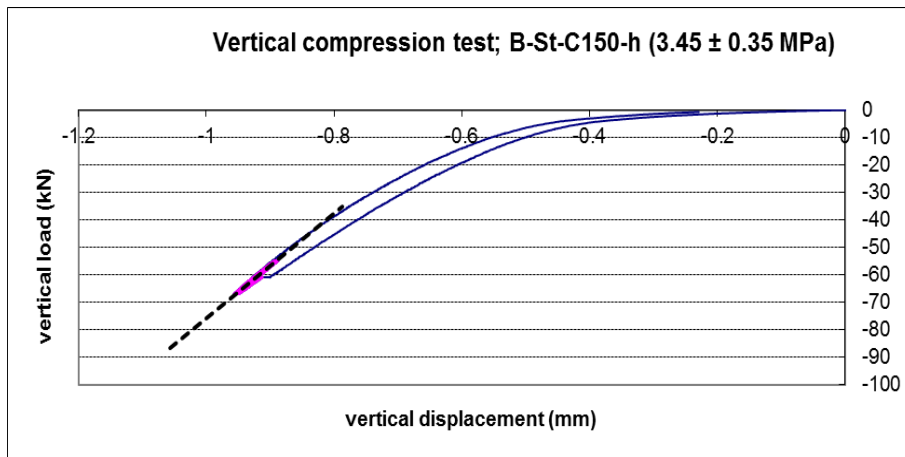
Figure C.5 Vertical load versus vertical displacement for B-St-C150-h
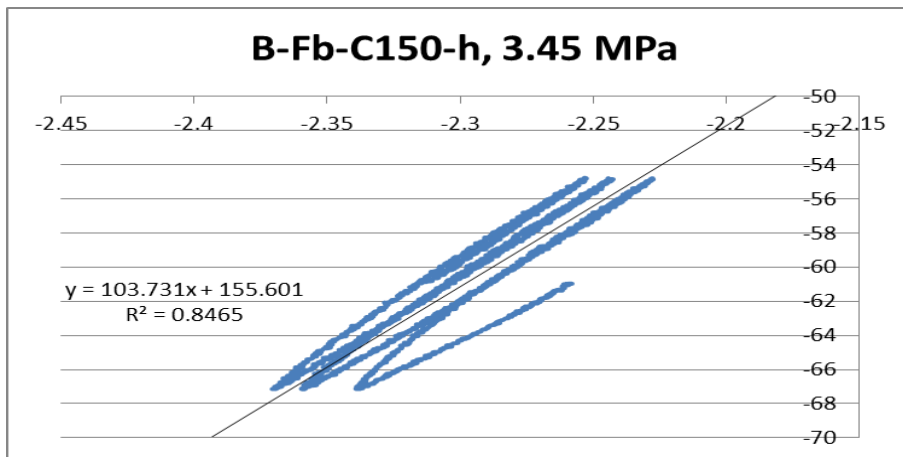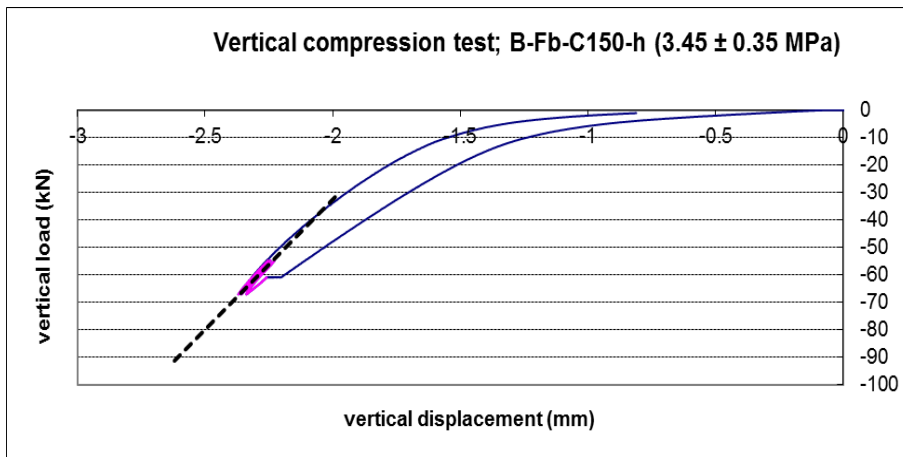
Figure C.6 Vertical load versus vertical displacement for B-Fb-C150-h
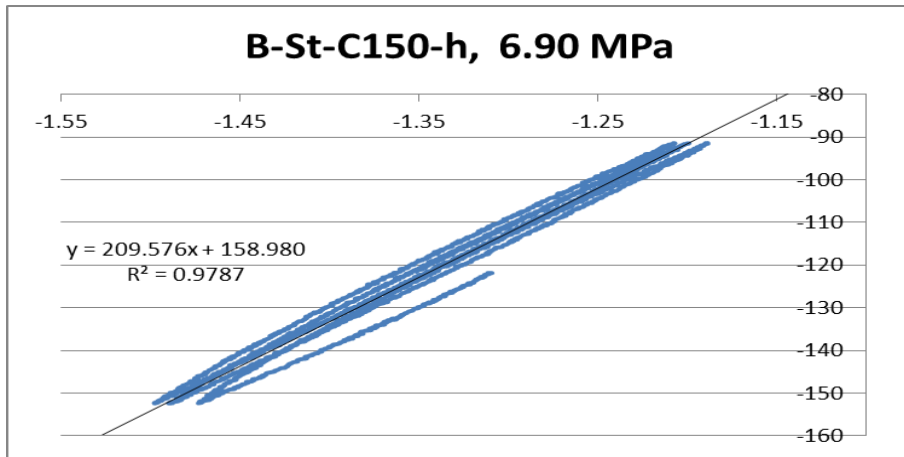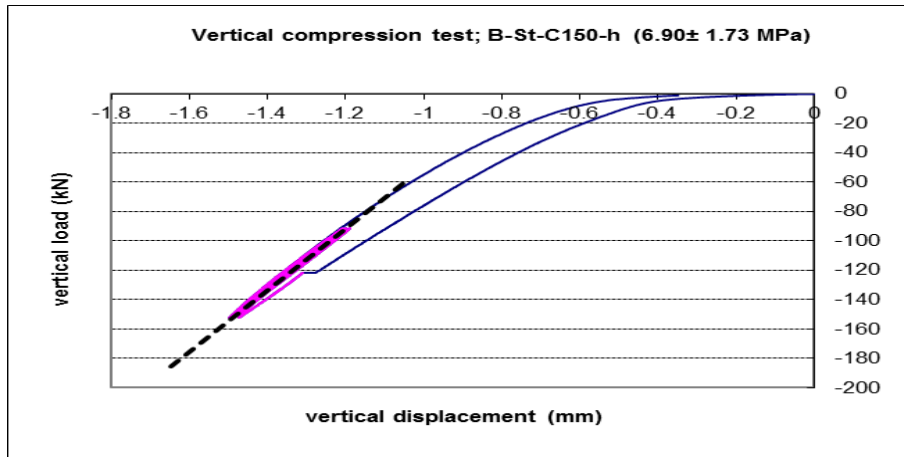
Figure C.7 Vertical load versus vertical displacement for B-St-C150-h
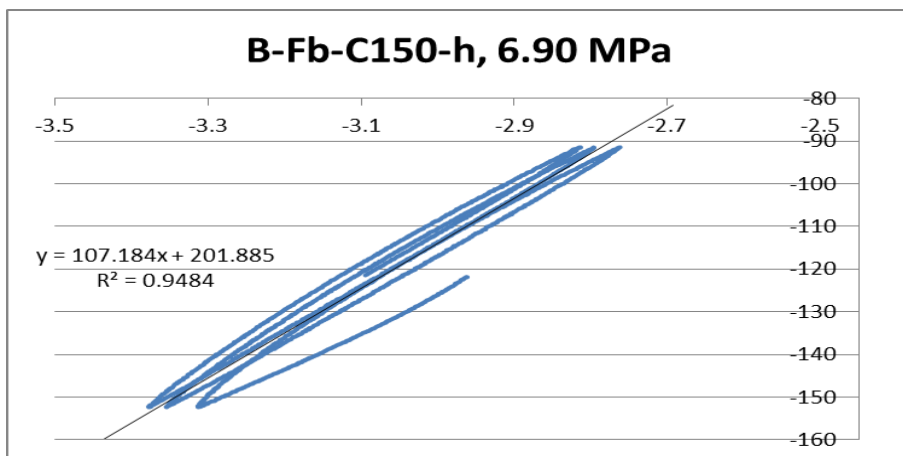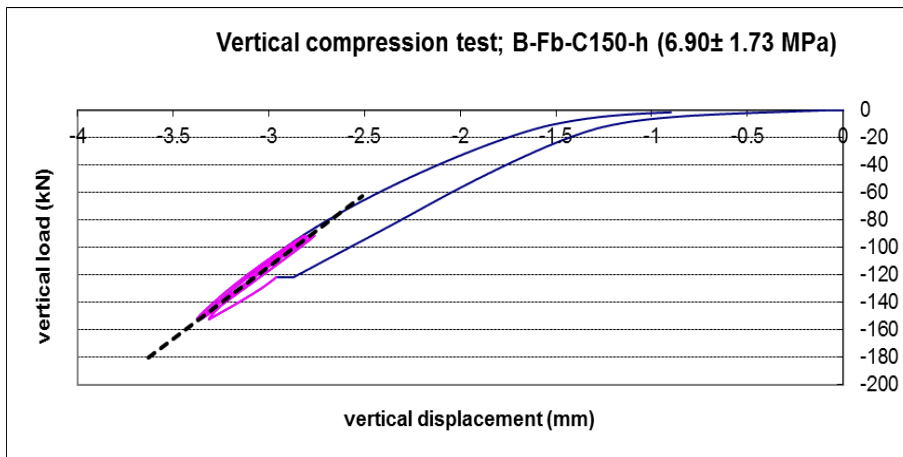
Figure C.8 Vertical load versus vertical displacement for B-Fb-C150-h

CURRICULUM VITAE

Name: Ali

Surname: Karimzadeh Naghshineh

Personal information:

Name & Surname: Ali Karimzadeh Naghshineh

Telephone(s): +905066983366

E-mail: ali_naghshine@yahoo.com

Nationality: Iranian

Date of birth: 02-05-1983

Gender: Male

Marital Status: Married

Educational Background:

Certificate Degree	Field of Specialization	Name of Institution Attended	G.P.A. OUT OF 4	Date
Ph.D.	Structural	Middle East Technical University, Ankara, Turkey	3.8	2008-2013
M.Sc.	Structural	University of Tabriz, Tabriz, Iran	3.6	2005-2007
B.Sc.	Civil Engineering	Azerbaijan Shahid Madani University, Tabriz, Iran	3.1	2001-2005

Title of Post-Graduate Thesis:

Effect of Material Hardness on the Performance of Fiber Reinforced Elastomeric Bearings

Title of Doctorate Thesis:

Experimental Studies on Fiber Mesh Reinforced Elastomeric Bearings

Work Experience:

2007–2008 Supervisor engineer in Shib-Oft Co. ,Tabriz, Iran

2013-Present Designer at Ozdwkan Rubber Industries, Ankara, Turkey

Papers:

Conference Paper:

Karimzadeh Naghshineh A., Yousefi A., and Nadimi Bavil S. (2012). **"**Analysis of the Effect of Residual Stresses on Fatigue Life of TubularMembers by Finite Element Modeling." UMTIK-15th INTERNATIONAL CONFERENCE ON MACHINE DESIGN AND PRODUCTION, Pamukkale, Denizli, Turkey.

Journal Papers:

Karimzadeh Naghshineh A., Akyüz U., and Caner A. (2013). "Comparison of Fundimental Properties of New Types of Fiber-Mesh-Reinforced Seismic Isolators with Conventional Isolators." Journal of Earthquake Engineering & Structural, in press.

Caner A., **Karimzadeh Naghshineh A.,** and Erdal S. (2013). "Performance of Ball Rubber Bearings in Low Temperature Regions." journal of Performance of Constructed Facilities (ASCE), in press.

Scholarship and Projects:

- TÜBİTAK-2215, Graduate Scholarship Programme for International Students, Turkey (2009-2012)
- BAP 03-03-2012-003, Middle East Technical University, Ankara, Turkey (2011-2012)
- TÜBİTAK KAMAG-110G093, Middle East Technical University, Ankara, Turkey (2012-2013)

Language Proficiency:

Language	Degree of Proficiency											
	Writing				Reading				Speaking			
	Native	Good	Fair	Poor	Native	Good	Fair	Poor	Native	Good	Fair	Poor
English		*			*					*		
Azeri			*			*			*			
Turkish			*			*				*		
Farsi		*			*				*			